Institut für Organische Chemie und Biochemie
der Technischen Universität München

2-Aminopurine and Pyrenylethyne-Modified Uridine as Fluorescent Probes for the Investigation of Nucleic Acids and Their Interactions

Manuela Johanna Rist

Vollständiger Abdruck der von der Fakultät für Chemie der Technischen Universität München zur Erlangung des akademischen Grades eines

Doktors der Naturwissenschaften

genehmigten Dissertation.

Vorsitzender:		Univ.-Prof. Dr. J. Buchner
Prüfer der Dissertation:	1.	Univ.-Prof. Dr. H. Kessler
	2.	Adjunct Assistant Professor J. P. Marino, PhD, University System of Maryland/USA
	3.	Univ.-Prof. Dr. M.-E. Michel-Beyerle, i. R.

Die Dissertation wurde am 22.01.2003 bei der Technischen Universität München eingereicht und durch die Fakultät für Chemie am 28.02.2003 angenommen.

dedicated to my parents and Burkhard

Thanks

The work for this PhD thesis has been carried out from October 1999 to December 2001 at the Center for Advanced Research in Biotechnology in Rockville, Maryland, in the group of Prof. Dr. J. P. Marino, and from January 2002 to January 2003 in the group of Prof. Dr. H. Kessler at the “Institut für Organische Chemie und Biochemie der Technischen Universität München” under the supervision of Dr. Hans-Achim Wagenknecht.

First and foremost, I would like to thank Prof. Dr. John P. Marino for making it possible for me to spend two years of my time as a PhD student in his group, enjoying excellent facilities and resources. I was so fortunate as to reap the benefits of his superb supervision and guidance but at the same time having the freedom I needed to perform my work.
My special thanks go to Prof. Dr. Horst Kessler for taking me up in his group so spontaneously. In Munich I enjoyed a hearty welcome and excellent working conditions.
Also, I would like to thank Dr. Hans-Achim Wagenknecht for his preeminent supervision during my time in his group and for always being available for questions and discussions.
Prof. Dr. Hannelore Daniel I thank very much for supporting my extravagant idea of spending most of my PhD time in the US.

At CARB I would like to thank

- Dr. Karen A. Lacourciere for introducing me into the secrets of fluorescence spectroscopy and biochemical lab work in real life,
- my lab colleagues Dr. Burkhard Luy, Nanda Mahashetty, Dr. Eric S. Dejong and Dr. M. Rita Mihailescu for a warm and hearty lab atmosphere and many interesting discussions,
- Prof. Dr. James T. Stivers for stimulating discussions and help with the interpretation of sometimes confusing fluorescence data,
- Dr. Fenhong Song for the synthesis of many DNA templates and labeled RNA samples,
- Nadik Abdulaev for his help with the HPLC,
- Pat Alexander, Mike Tangrea, Kathryn Fisher, Prof. Phil Bryan and Prof. John Orban for countless lunchtime discussions and insights into the American way of seeing things,
- Mariela Urrutia, Dr. Paloma Fernandez-Varela, Dr. Pia Bonander and Dr. Nicklas Bonander for the oasis in the 'other world' of CARB,

- Tom Belcher, Tim Bennett, Grace Bromfield, Cindy Denisac, Darwin Diaz, Jonathan Dill, Tom Dimsdale, Al Ledford, Davin Mackesy, Michelle Stanton and Frank Wallis for the assistance with all the 'little' things,
- and all the other wonderful people at CARB who made my stay there so interesting and unforgettable.

I would also like to thank

- Prof. Lynne Regan (Yale University) for providing us with purified Rom protein, and
- Dr. T. E. Shrader (Albert Einstein College of Medicine) for providing us with plasmid pT7-911Q

In Munich I would like to thank

- my lab colleagues Nicole Amann, Alessandro Righi, Elke Mayer, Stefan Mitschke, Peter Kaden, Clemens Wagner and Linda Valis for the great lab atmosphere, many stimulating and also entertaining discussions,
- Nicole especially for making the new start in a new lab much easier and for ceaselessly trying to turn me into a 'real' chemist,
- Georgette Thumshirn for the help with the HPLC,
- Claudia Dahmen for the occasional lift home,
- Herrn Helmut Krause for the prompt measurements of many MALDI-TOF mass spectra,
- Dr. Torsten Fiebig and his coworkers for the time-resolved transient absorption measurements,
- Dr. Rainer Häßner and Alexander Frenzel for help with all kinds of computer problems,
- Dr. Burkhard Luy and Dr. Hans-Achim Wagenknecht for the critical reading of this manuscript,
- Evelyn Bruckmaier and Marianne Machule for secretarial assistance

and all mentioned and unmentioned co-workers for the excellent working atmosphere and for being not just colleagues but also friends.

My very special thanks go to Dr. Burkhard Luy who helped me regain the fascination for science and research whenever I had doubts about my work, and without whom this work would not have been possible in this way.

Abbreviations

ε	extinction coefficient
τ	life time
λ	wavelength
°C	degree Celsius
µl	microliter
µM	micromolar
µmol	micromole
2-AP	2-aminopurine
5-I-dU	2'-deoxy-5-iodouridine
8-oxo-dG	8-oxo-deoxyguanine
A	acceptor
A	adenine/adenosine
A	electronic absorption
Å	Ångström
ACS	American chemical society
AIDS	acquired immunodeficiency syndrome
APS	ammonium peroxodisulfate
BME	β-mercaptoethanol
bp	base pair
C	cytosine/cytidine
CA	capsid protein
CD	circular dichroism
cm	centimeter(s)
CPG	controlled pore glass
CT	charge transfer
d	dimer
D	donor
dATP	deoxyadenosine triphosphate

dCTP	deoxycytidine triphosphate
ddH_2O	distilled and deionized water
DEPC	diethyl pyrocarbonate
dGTP	deoxyguanosine triphosphate
DIS	dimerization initiation site
dIz	imidazolone
DLS	dimer linkage structure
DMF	dimethylformamide
DMSO	dimethylsulfoxide
DNA	deoxyribonucleic acid
dOz	oxazolone
DTT	dithiothreitol
dTTP	deoxythymidine triphosphate
E	efficiency
E. coli	escherichia coli
e.g.	for example (exempli gratia)
EDTA	ethylene diamine tetraacetic acid
ET	electron transfer
F	fluorescence
Fapy-dG	formamidopyrimidine
FISH	fluorescence *in situ* hybridization
FRET	fluorescence resonance energy transfer
fs	femtosecond(s)
g	gram(s)
G	guanine/guanosine
h	hour(s)
HIV-1	human immunodeficiency virus type-1
HOMO	highest occupied molecular orbital
HT	hole transfer
I	intensity
I	inosine
i. e.	that is (id est)
IC	internal conversion
IN	integrase

IPTG	Isopropyl β-D-1-thiogalactopyranoside
K_D	equilibrium binding constant
l	liter(s)
LB	Luria broth
LUMO	lowest unoccupied molecular orbital
m	monomer
M	molar
MA	matrix protein
MALDI-TOF	matrix-assisted laser desorption ionization-time of flight
mg	milligram(s)
min	minute(s)
ml	milliliter(s)
mM	millimolar
mm	millimeter(s)
mRNA	messenger RNA
ms	millisecond(s)
Na-P_i	sodium phosphate
NC	nucleocapsid
NCp7	nucleocapsid protein 7
n/d	not determined
Ni-NTA	Ni-nitrilotriacetic acid
nm	nanometer(s)
nt	nucleotide
NTP	nucleoside triphosphate
OD_{260}	optical density at wavelength 260 nm
P	phosphorescence
PAGE	polyacrylamide gel electrophoresis
PBS	primer binding site
PCET	proton-coupled electron transfer
PCR	polymerase chain reaction
PEG	polyethylene glycol
PEI	polyethyleneimine
PMSF	phenylmethylsulfonyl fluoride
PR	protease

psi	punds per square inch
Py-≡-dU	5-(1-pyrenylethynyl)-2'-deoxyuridine
Py-dU	5-(pyren-1-yl)-2'-deoxyuridine
r	distance
R_0	*Förster* distance
R.T.	room temperature
RNA	ribonucleic acid
Rom	RNA one modulator
RP-HPLC	reverse-phase high performance liquid chromatography
rpm	revolutions per minute
RT	reverse transciptase
S_0	ground state
S_1	lowest excited singlet state
S_2	excited singlet state
sec	second(s)
SNP	single nucleotide polymorphism
SU	surface glycoprotein
ST	singlet-triplet intersystem crossing
T	thymin/thymidin
T_1	triplet state
TBAF	tetra-n-butyl ammonium fluoride
TBE	Tris borate EDTA buffer
TBM	Tris borate $MgCl_2$ buffer
TBCa	Tris borate $CaCl_2$ buffer
TEA	triethylamine
TEMED	N,N,N',N'-tetramethylethylenediamine
THF	tetrahydrofuran
T_m	melting temperature
TM	trans membrane protein
Tris	tris(hydroxymethyl)aminomethane
tRNA	transfer RNA
Trp	tryptophan
UV	ultra violet
V	Volt

Vis	visible
VR	vibrational relaxation
v/v	volume for volume
W	Watt
w/v	weight for volume
wt	wild-type

The nomenclature used in this work is based on the guidelines recommended by *Chemical Abstracts* (Chemical Abstracts, 'Index Guide', 77, 210) and the IUPAC-IUB commissions (IUPAC, *Eur. J. Biochem.* **1971**, *21*, 455-477; IUPAC, Pure Appl. Chem. **1996**, *68*, 1919; IUPAC Commission on Nomenclature of Organic Chemistry (CNOC) and IUPAC-IUB Joint Commission on Biochemical Nomenclature (JCBN), *Biochemistry* **1974**, *10*, 3983; IUPAC-IUB (JCBN), *Eur. J. Biochem.* **1984**, *138*, 9-37).

1 Introduction and Motivation

Nucleic acids play a central role in biology and life in general: Deoxyribonucleic acid (DNA) is the “storehouse” of genetic information. It is composed of only four different nucleosides, adenosine (A), thymidine (T), guanosine (G) and cytidine (C) that are linked covalently through phosphodiester bonds, but it is complex enough as a biopolymer to store the complete genetic information of almost every living organism. DNA has two major functions. First, it has to pass on information through replication possibly error-free, but at the same time allow evolutionary processes. Damage in the DNA sequence can lead to mutagenesis and carcinogenesis. Often, damage in DNA is caused by radical reactions as a consequence of oxidative stress. It has been observed, however, that the site of radical formation is spatially separated from the site of damage. If and how charge can migrate through DNA therefore has been discussed extensively and controversially over the past decades. Most work has focused on oxidative hole transfer, but still very little is known about the mechanism of reductive electron transfer. The second important function of DNA is to allow expression of the genetic code under defined conditions. DNA is transcribed into RNA via molecular recognition through hydrogen bonds between the DNA bases and their corresponding RNA bases. Subsequently the RNA is translated into proteins. Gene replication and expression are highly regulated processes. Usually proteins perform these regulatory functions, however in several bacteria and viruses regulation by antisense RNA was observed. The high specificity of these antisense interactions led to the promising concept of developing new antisense drugs. For reasonable drug design, though, it is useful to study native antisense interactions first.

In general, biological systems are too complex to study as a whole, so it is important to develop model systems to initially study the basic principles of biological processes. One of the most promising methods to study nucleic acid interactions and also charge transfer through DNA is fluorescence spectroscopy. The application of fluorescence methods to the study of macromolecules has seen a dramatic surge in the last few years. Fluorescence techniques are finding widespread application in biochemical and biophysical studies of macromolecules, as well as in medicinal, environmental and commercial research efforts. In studies of nucleic acids, fluorescence spectroscopy provides an important tool for the detection and probing of structure, dynamics and interactions. The intrinsic fluorescence of the naturally occurring nucleotide bases in nucleic acids is extremely weak. This drawback can be inverted into an advantage by the use of non-natural nucleotide base analogs with

optimized fluorescence properties (i.e. higher quantum yields and longer lifetimes) that can be incorporated using standard automated synthetic methods. Since no background fluorescence of the natural bases is present, site-specific structural and biophysical information in nucleic acid oligomers can be obtained.
In this thesis, fluorescence detected methods are applied to study antisense RNA interactions taken from a bacterial and a viral regulatory system and to address energy and charge transfer in DNA using two nucleoside base analogs.

The present thesis consists of two major parts. In the first part, the nucleoside base analog 2-aminopurine (2-AP) is used as a fluorescent probe for RNA-RNA interactions. In the second part, the fluorescence properties and quenching events of 2-AP are investigated in more detail, and a new fluorescent pyrene-modified nucleoside was developed for the study of reductive electron transfer in DNA.
The first part addresses the interaction of antisense RNA stem-loops derived from the strongly regulated plasmid replication system *ColE1*, and the dimerization initiation site (DIS) of the human immunodeficiency virus type 1 (HIV-1), respectively.
The *ColE1* plasmid system has been studied intensively in the past. The plasmid copy number is strongly regulated by a kinetically controlled antisense RNA strategy involving RNA I as the repressor and RNA II as the primer precursor for replication. The auxiliary protein Rom acts as an additional repressor of replication by binding to the RNA complex and stabilizing it. Thus, the following questions emerged:

- Is it possible to study the kinetics and the mechanism of antisense RNA loop-loop kissing complex formation using the 2-AP fluorescence?
- What is the importance of metal ions in this system and what kind of metal ions can induce complex formation?
- Can Rom binding be measured and quantified using the same fluorescently labeled RNA molecules?

To address these questions a concept was developed as follows:

1. Site-specific incorporation of the fluorescent nucleoside base analog 2-AP into RNA sequences derived from the *ColE1* transcripts RNA I and RNA II.
2. Determination of equilibrium binding constants as well as on- and off-rates for the RNA complex formation using steady-state and stopped-flow fluorescence spectroscopy.

3. Titration of different mono- and divalent metal ions to the RNA stem-loops to find out the metal ion dependence of the system and determine apparent binding constants for the metal ion binding to the RNA complex by steady-state fluorescence.
4. Titration of the Rom protein to RNA loop-loop complexes to determine Rom binding constants to the RNA.

Subsequently, the 2-AP assay was used for the investigation of the dimerization initiation site from HIV-1. Dimerization of the RNA genome is vital for HIV. It has been found that the dimerization is initiated at a stem-loop with a palindromic sequence by a loop-loop interaction which is followed by a structural isomerization to an extended duplex. Thus, this system can again be seen as an antisense RNA model. Based on the knowledge on this system, the questions that arose were:

- What are the kinetics of the RNA loop-loop complex formation?
- Can the loop-loop 'kissing' complex be distinguished from the mature extended duplex using fluorescence spectroscopy?
- What is the pathway of duplex maturation, does it proceed via the loop-loop complex as an intermediate, does it follow a strand exchange or a ribozyme-like mechanism as proposed by *Ennifar et al.*?[1]
- What is the role of the viral nucleocapsid protein (NCp7) in the maturation process, and how does it act on the RNA complex?

To answer these questions, the following strategy was planned:

1. Site-specific incorporation of 2-AP into the loop region of RNA sequences derived from the DIS of HIV-1.
2. Design of RNA sequences containing 2-AP that facilitate observation of loop-loop kissing complex versus mature extended duplex.
3. Application of the previously developed fluorescence assay to determine equilibrium binding constants as well as on- and off-rates for the kissing complex formation.
4. Variation of reaction conditions and/or NCp7 concentrations to determine conversion rates for the structural isomerization from kissing complex to extended duplex and the role of NCp7 in this process using fluorescence spectroscopy.
5. Titration of RNA complexes to NCp7 to determine protein binding constants by the intrinsic tryptophan fluorescence.

In the first part, changes in the fluorescence signals were exploited to study macromolecular interactions and dynamics, in the second, the electronic properties of 2-AP in DNA, and subsequently, electron transfer processes in DNA were the focus of attention.

It is known that energy transfer and charge transfer can occur in photoexcited molecules and that these processes lead to fluorescence quenching. Together with the observations from the first part of this thesis, some new questions evolve, which are:

- What happens with the energy of the photoexcited 2-AP? Is it localized on one base or can it diffuse over several bases?
- Do neighboring bases have an effect on the quenching of 2-AP fluorescence by charge transfer?

In order to address these questions, it was planned to

1. design DNA assemblies suitable for the investigation of possible excimer or exciplex formation using steady-state fluorescence and time-resolved transient absorption spectroscopy,
2. subsequently perform steady-state fluorescence and time-resolved transient absorption experiments to measure excimer or exciplex formation and determine the rates of their occurrence and decay,
3. develop a model system for the investigation of the effects of neighboring bases on the fluorescence quenching of 2-AP by charge transfer, and
4. measure the degree of quenching and the rate of charge transfer of photoexcited 2-AP using steady-state fluorescence and time-resolved transient absorption spectroscopy.

Based on the relative reduction potentials, one can assume that photoexcited 2-AP can induce both electron transfer and hole transfer in DNA. DNA-mediated hole transfer has been studied extensively, but it exists a lack of knowledge about reductive electron transfer. It was shown in previous experiments that 5-(pyren-1-yl)-2'-deoxyuridine (Py-dU) selectively initiates reductive electron transfer.[2] Concerning more details of ET in DNA the following questions were raised:

- Can pyrenylethynyl-uracil-modified DNA act as a selective electron injector similar to Py-dU?
- Can pyrenylethynyl-modified DNA be synthesized by a solid-phase strategy avoiding the elaborate phosphoramidite synthesis?

Consequently, the below-mentioned plan was pursued to answer these questions:

1. Site-specific incorporation of 5-(1-pyrenylethynyl)-2'-deoxyuridine (Py-≡-dU) into DNA using a new synthetic strategy which involves the combination of standard automated synthesis and Sonogashira-type cross-coupling reactions on the solid phase.
2. Measuring steady-state fluorescence spectra to estimate the capability of Py-≡-dU to induce reductive electron transfer in model DNA duplexes.

2 Background

2.1 Fluorescence

2.1.1 General Introduction to Fluorescence

Luminescence is the emission of light that can occur subsequent to absorption when a molecule excited to a higher order electronic state relaxes back to the ground state.[3] The absorption of light by a molecule is an electronic transition called electronic absorption or electronic excitation. The electronic transitions that are interesting for luminescence are the $n \rightarrow \pi^*$, $\pi \rightarrow \pi^*$, and intramolecular charge-transfer transitions of aromatic molecules, and they are all effected by light of 200 - 1500 nm in wavelength (near ultraviolet, visible and near-infrared regions of the electromagnetic spectrum).[4] The absorption of light leaves a molecule in one of a number of possible vibrational levels of one of its electronically excited states (Figure 2-1).

Although the absorption process is extremely rapid (10^{-15} s), the sequence of events that return the excited molecule to its ground state is considerably slower (10^{-14} to several seconds). Molecular luminescence is among the slowest of processes in electronically excited states, requiring from 10^{-10} to a few seconds, whereas thermal equilibration by loss of vibrational energy (vibrational relaxation, VR), internal conversion (IC) and singlet-triplet intersystem crossing (ST) are much faster (10^{-14} to 10^{-12} s). Consequently, luminescence usually originates from thermally equilibrated, electronically excited molecules.[3-5] The processes which occur between absorption and emission are typically illustrated by a Jablonski diagram (Figure 2-1).[4, 6]

Depending on the electronic nature of the excited state, lowest excited singlet (S_1) versus triplet (T_1), luminescence is divided into two categories, fluorescence (F) and phosphorescence (P), respectively (Figure 2-1). An important difference between these two types of luminescence is their average lifetimes. Fluorescence lifetimes are typically on the order of 10 nanoseconds and correspond to an emission rate of 10^8 s^{-1}; while phosphorescence lifetimes are typically on the order of milliseconds to seconds and correspond to emission rates that are much slower (1000 to 1 s^{-1}).[3, 4]

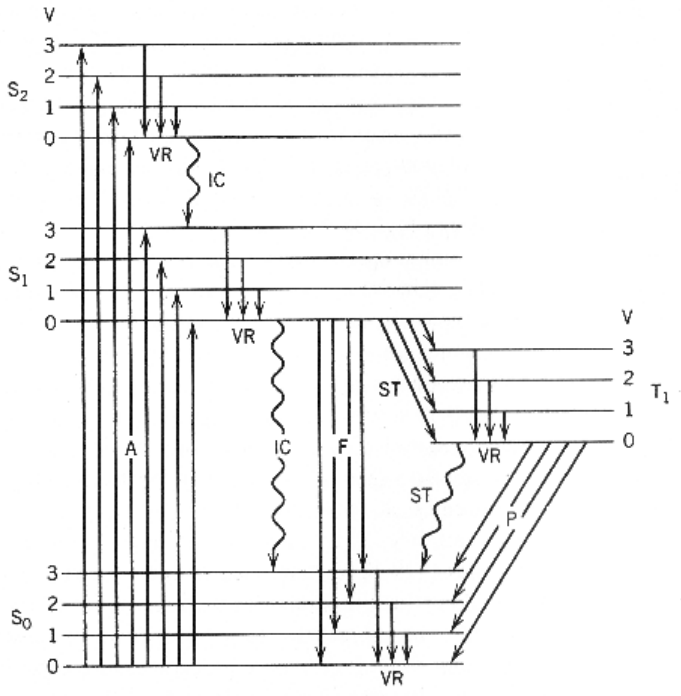

Figure 2-1. Jablonski Diagram showing photophysical processes of conjugated molecules. Electronic absorption (A) from the lowest vibrational level (v = 0) of the ground state (S_0) to the various vibrational levels (v = 0, 1, 2, 3) of the excited singlet states (S_1, S_2) is followed by rapid, radiationless internal conversion (IC) and vibrational relaxation (VR) to the lowest vibrational level of S_1. Competing for deactivation of the lowest excited singlet state S_1 are the radiatinoless internal conversion and singlet-triplet intersystem crossing (ST) as well as fluorescence (F). Fluorescence is followed by VR in the ground state. Intersystem crossing is followed by VR in the triplet state (T_1). Phosphorescence (P) and noradiative triplet-singlet intersystem crossing (ST) return the molecule from T_1 to the ground state (S_0). Vibrational relaxation in S_0 then thermalizes the 'hot' ground-state molecule. (taken from *Sharma and Shulman*[4])

The emission rates are critical for luminescence spectroscopy since they govern the time window during which a luminescent species can monitor its environment. In this work the focus will be exclusively on fluorescence processes.

An interesting observation with fluorescence is that the energy of the emitted light is usually lower than the energy of the absorbed light, i.e. emission wavelengths are longer than absorption wavelengths. This phenomenon is called "Stokes' shift", named after the scientist who first described this observation, *Sir G. G. Stokes*,[7] and it can be easily explained by examination of the Jablonski diagram in Figure 2-1. Although absorption usually occurs to a higher excited state or higher vibrational levels of excited states, emission always occurs from lowest vibrational levels of lowest excited states, and is therefore of lower energy than the absorption. This is also the explanation for the fact that emission spectra usually do not change irrespective of the excitation wavelength (Kasha's rule).[8]

Fluorescence quantum yield and lifetime

The fluorescence quantum yield and lifetime are the two most important factors that characterize a given fluorophore. Since intersystem crossing, internal conversion and various excited-state reactions (vide infra) compete with fluorescence for deactivation of the lowest excited singlet state of a molecule, not all potentially fluorescent molecules will return to the ground state by fluorescence. The fraction of excited molecules that fluoresce is called the quantum yield of fluorescence (Φ_F) or fluorescence efficiency, and under given conditions of temperature and environment is a physical constant of the excited molecular species. In terms of rates of processes competing for deactivation of the lowest excited singlet state, Φ_F is given by equation 2.1,

$$\Phi_F = \frac{\Gamma}{\Gamma + k_{nr}} \qquad (2.1)$$

where Γ is the rate of fluorescence emission, and k_{nr} is the sum of rate constants for all radiationless processes.[3, 4]

In the absence of any non-radiative pathways, an excited molecule would achieve a fluorescence quantum yield of unity. In practice, non-radiative loss is almost unavoidable in molecular systems and variations in these decay processes can be used to probe changes in the microenvironment of the fluorescent probe.

The reciprocal of Γ is called the fluorescence lifetime (τ_F) and describes the average time a molecule spends in the excited state prior to returning to the ground state. As mentioned above, excited state lifetimes for typical fluorophores are generally about 10 ns.[3, 4] The fluorescence lifetime defines the time-scale of the interaction of the fluorophore with its environment and hence governs the time window available for observing dynamic processes monitored by the fluorophore.

Solvent effects

Solvents influence electronic spectra primarily through their polarity and hydrogen bonding properties. When a solute molecule becomes more or less polar upon absorption of light, the excited state may be more or less stabilized relative to the ground state, depending on the polarity of the solvent. For example, a fluorescent species that becomes more polar upon absorption, will in a polar solvent be more stabilized in the excited state than in the ground state. The more polar the solvent, the more the fluorophore will be stabilized in the excited state, and the energy of the emitted light will therefore decrease with increasing solvent

polarity. In other words, the more polar the solvent, the more will the emission shift to longer wavelengths. Similarly, if the hydrogen bonding capacity of a solute molecule changes upon excitation, the interaction of the excited state with the hydrogen-bonding solvent may stabilize or destabilize the excited state relative to the ground state. Accordingly, incorporation of a fluorophore, such as a fluorescent nucleic acid base analog, into nucleic acids will affect the electronic spectra, since the environment in a DNA or RNA sequence is less polar than water and equals more the polarity of an organic solvent like acetonitrile. Solvent polarity and hydrogen-bonding electrostatic influences upon fluorescence spectra are qualitatively similar to those upon absorption spectra. Solvent relaxation processes, however, occur subsequent to absorption and nearly always tend to make fluorescence move to longer wavelengths with increasing solvent polarity or hydrogen-bonding capacity.[3, 4]

pH influence

Potentially fluorescent molecules have lifetimes in the lowest excited singlet state of 10^{-11} to 10^{-7} s. Although these lifetimes are extremely short, some chemical reactions are fast enough to compete with the photophysical processes that deactivate the excited molecule. Among the ultrafast reactions are those of excited acidic fluorophores with basic species and of basic excited fluorophores with acidic species in solution. Because the electron distributions are different in the excited state from those in the ground state, the degree of acidity or basicity may be very different for the same molecules in these two states. When acidity or basicity is manifested in the excited state, competition of these chemical reactions with fluorescence of the excited species often results in multiple luminescences from solutions in which only a single species is directly excited. Often the fluorescence spectra will vary with the concentration of proton acceptors or donors. The quantum yields of fluorescence and the fluorescence decay profile will then vary with pH in a way that reflects the kinetics of the reaction in the S_1 state. Consequently, fluorescence spectroscopy represents a powerful tool for the study of some of the most fundamental of chemical reactions.[4]

In this context, the proton-coupled electron transfer (PCET) should also be mentioned. PCET is an important pathway of charge transport in a variety of biochemical, electrochemical, and small-molecule organic and inorganic reactions.[9] It has been discussed, for example, for the photosystem II oxygen evolving complex, whose function is to split water,[10] for the bacterial reaction centers,[11] and for cytochrome c oxidase.[12] *Shafirovich* proposed a PCET mechanism for complexes between nucleic acid bases in DNA and aromatic fluorophores exhibiting strong fluorescence quenching of the latter by photoinduced electron transfer.[13]

The electron transfer quenching in aqueous medium is proton coupled, as inferred from isotope effects and the lack of quenching in nonaqueous solvent. The proton comes from the hydrogen bonding solvent, but the microscopic steps are difficult to elucidate, because the solvent contributes the proton.[9]

Quenching processes

Any process that decreases the fluorescence intensity of a sample (e.g. excited-state reactions, molecular rearrangements, energy transfer or charge transfer) is called quenching. Fluorescence may be quenched as a result of interaction of either the ground or excited state of the luminescing species with other species in solution. Interaction between the quencher and the potential fluorophore subsequent to excitation is called dynamic or collisional quenching - as opposed to static quenching which is characterized by complexation between the quencher and the potentially fluorescent species in the ground state. Dynamic quenching takes place during the lifetime of the excited state at a rate governed by the diffusional properties of the quencher and fluorophore, which means that the efficiency of dynamic quenching is limited by the lifetime of the excited state of the potential fluorophore and the concentration of the quenching species. The non-radiative process quenching competes directly with the parallel reaction of fluorescence emission:

$$M^* \xrightarrow{k_1} M + h\nu \qquad \text{(Fluorescence)} \qquad (2.2)$$

$$M^* + Q \xrightarrow{k_2} M + Q^* \qquad \text{(Quenching)} \qquad (2.3)$$

In these reactions, the excited molecule is defined as M* and the quencher is defined as Q. The fluorescence quantum yield in the presence of a quenching agent can be calculated from equations 2.2 and 2.3 as follows:

$$\Phi_F = \frac{k_1[M^*]}{k_1[M^*] + k_2[M^*][Q]} \qquad (2.4)$$

$$\frac{1}{\Phi_F} = \frac{k_1[M^*] + k_2[M^*][Q]}{k_1[M^*]} = 1 + \frac{k_2}{k_1}[Q] \qquad (2.5)$$

Rewriting this term as an expression of the relative fluorescence (F_0/F) gives the Stern-Volmer equation (equation 2.6),

$$\frac{F_0}{F} = 1 + k\tau_0[Q] = 1 + k_D[Q] \qquad (2.6)$$

where F defines the measured fluorescence intensity, F_0 is the initial fluorescence, k is the bimolecular quenching constant, τ_0 is the lifetime of the fluorescence and k_D is defined as the Stern-Volmer constant, with $k_D = k\,\tau_0$.[3, 4, 14]

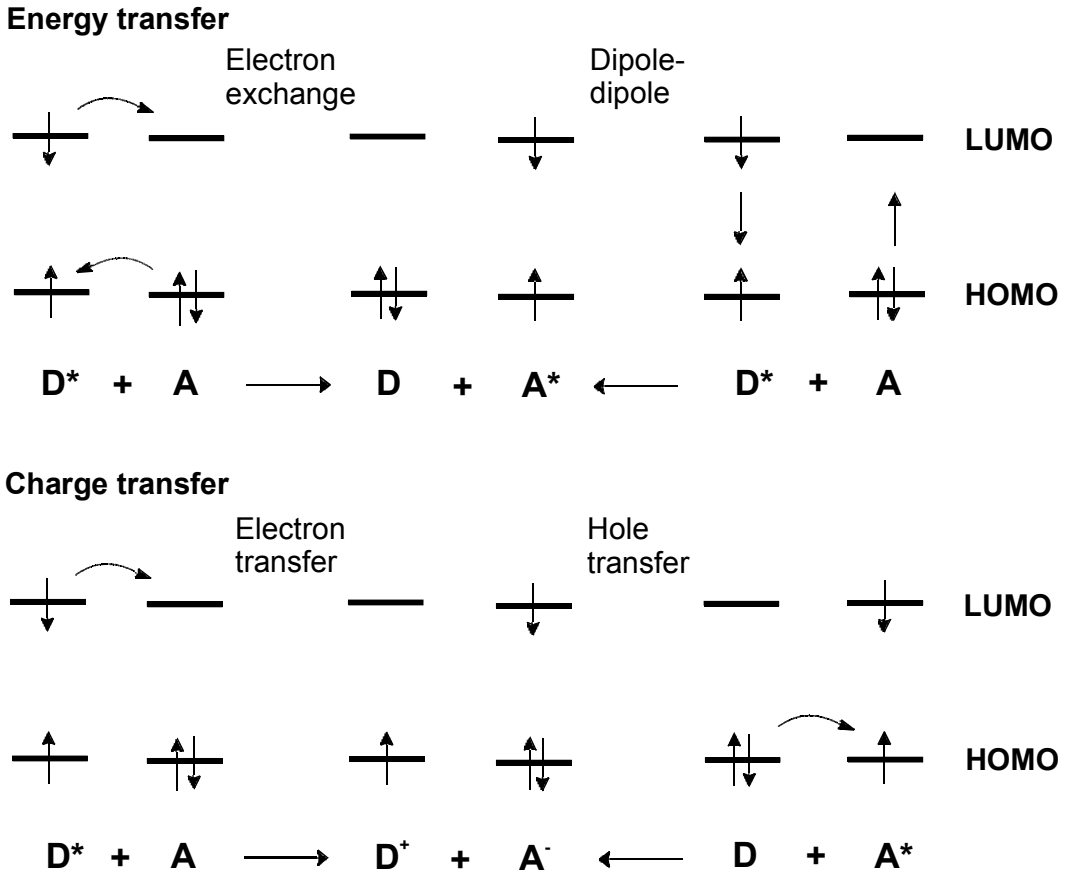

Figure 2-2. Schematic representation of energy transfer (upper panel) versus charge transfer (lower panel). In energy transfer there are two pathways for the generation of the excited state of the acceptor, **A***, energy transfer by electron exchange between the energy donor, **D** and acceptor, **A** (left), and energy transfer by dipole-dipole interactions between **D** and **A**. In charge transfer the excited state either donates or accepts an electron, and results in charge separation. Here, **D** represents the electron donor, and **A** the electron acceptor.

Quenching generates reactive intermediates that rapidly undergo transformations to stable products. In the case of energy transfer, when the quencher receives the excess energy of the excited state, the quencher itself becomes excited (equation 2.3 and Figure 2-2) and subsequently undergoes the same physical and chemical processes as if excited directly. There are two pathways for energy transfer. Energy transfer by electron exchange requires some overlap of the orbitals of the excited energy donor **D*** and the acceptor **A**. Energy transfer can also take place via a long-range dipole-dipole interaction. In this case the electronic transitions take place exclusively within **D** and **A**. In photoinduced charge transfer (Figure 2-2), the excited state either donates an electron to or receives an electron from a ground-state species, resulting in charge separation.[5]

Concentration Effects

The intensity of fluorescence does not increase linearly with absorber concentration, but rather exponentially. This becomes already very obvious at absorber concentrations of 10^{-2}M. Only in the limit of extremely low absorber concentration ($<10^{-4}$M) does the measured fluorescence signal vary linearly with absorber concentration. At higher concentrations solute-solute interactions may add to the nonlinearity of the luminescence intensity versus absorber concentration curve.[4] The aggregation of an excited-state molecule with a ground-state molecule produces an *exci*ted state com*plex* ("exciplex"). A special case of exciplexes occur if the excited-state and ground-state molecules are of the same kind, which is then called an *exci*ted state di*mer* ("excimer"). This species is an emitting charge-transfer complex that is held together by favorable orbital interactions as well as by Coulombic binding forces. The exciplex can be regarded as a charge-transfer complex in which charge and electronic excitation energy are shared by donor and acceptor molecules. Exciplexes are distinct intermediates in their own right and possess unique properties. For instance, their fluorescence is almost always at longer wavelengths (lower energy) than the fluorescence of the excited state.[5] Energy transfer from an excited donor molecule to an originally unexcited acceptor molecule becomes more probable with increasing solute concentration. There are different mechanisms of intermolecular energy transfer: The exchange mechanism of excitation energy transfer is a short range phenomenon. It is only significant, when the orbitals of donor and acceptor overlap or the donor and acceptor molecule are separated by a distance no greater than their collision diameter. When the donor and acceptor are in contact, their highest energy electrons may change places causing the unexcited acceptor to become excited and the excited donor to relax to the ground state (Figure 2-2, left). This energy

transfer is most efficient when the energy of the fluoresence of the donor lies close to the energy of the absorption spectrum of the acceptor.[4]

Fluorescence resonance energy transfer (FRET) is a comparatively long-range phenomenon and depends on: (i) the overlap of the emission spectrum of the donor chromophore with the absorption spectrum of the acceptor chromophore; (ii) the orientation of the donor and the acceptor transition dipoles; and (iii) the distance between the donor and the acceptor chromophores. In other words, FRET requires a transition dipole-dipole interaction between the two chromophores which makes the efficiency of energy transfer dependent on the distance and orientation between the two chromophores (Figure 2-2, right). The direct correlation of measurable FRET efficiency with the distance between the two chromophores has made FRET one of the most extensively used fluorescence quenching mechanisms for characterizing macromolecules. FRET efficiency is derived from Förster theory[15, 16] and is given by equation 2.7, which defines the transfer rate, k_T,

$$k_T = \frac{1}{\tau_d}\left(\frac{R_0}{r}\right)^{-6} \qquad (2.7)$$

where R_0 (the Förster distance) is the distance for 50% efficiency of energy transfer and is an inherent characteristic of the donor-acceptor pair and the medium between them, τ_d is the lifetime of the donor in the absence of the acceptor and r is the distance between the fluorophores, with the transition dipole interaction assumed to be the same for both r and R_0. At the Förster distance, the transfer rate is equal to the inverse decay rate of the donor ($k_T = \tau_d^{-1}$). FRET serves as an extremely useful measure of distances between groups in macromolecules in a range between 10 and 90 Å. FRET efficiency, E, can be described as a function of R_0 (equation 2.8) and can be monitored using a change in donor lifetime (equation 2.9) or intensity (equation 2.10),

$$E = \frac{R_0^6}{R_0^6 + r^6} \qquad (2.8)$$

$$E = 1 - \left(\frac{\tau_{da}}{\tau_d}\right) \qquad (2.9)$$

$$E = 1 - \left(\frac{I_{da}}{I_d}\right) \qquad (2.10)$$

where τ_{da} is the lifetime of the donor in the presence of the acceptor, τ_d is the lifetime of the donor in the absence of the acceptor, I_{da} is the intensity of the donor in the presence of the acceptor and I_d is the intensity of the donor in the absence of the acceptor. Similarly, FRET efficiency can be monitored as a function of acceptor lifetime or intensity.[3]

2.1.2 Investigations of Nucleic Acid Interactions Using Fluorescence Spectroscopy

Fluorophores can be divided into intrinsic and extrinsic fluorophores. Instrinsic fluorophores are those which occur naturally in a given sample, for example the aromatic amino acids tryptophan, tyrosine and phenylalanine in proteins. The intrinsic fluorescence of the naturally occurring nucleotide bases (guanine (G), adenine (A), thymine (T), uracil (U) and cytosine (C)) in DNA and RNA is extremely weak.[17] These bases exhibit very short fluorescent decay times, generally in the range of a few picoseconds, and do not provide much structural information since signals are normally averaged over all bases in the oligonucleotide sequence.[18-20] Thus, in contrast to proteins, RNA and DNA molecules in general lack naturally occurring intrinsic fluorescent reporters. An advantage of the absence of natural fluorescence from DNA and RNA molecules, however, is that fluorescent signals from unnatural nucleotide base analogs can be observed without any competing background signal. Extrinsic fluorophores are those that are added to a sample that does not display the desired spectral properties. Useful fluorescent probes should display high fluorescence intensity that is sensitive to its microenvironment, it should be stable during continued illumination and non-perturbing to the structure of the macromolecule or the process being observed.[3]

Fluorescence measurements can be typically made in two ways. Steady-state measurements are measured with constant irradiation and observation. Due to the nanosecond timescale of fluorescence most measurements are made under these conditions, and normally when a sample is photoexcited, the steady-state condition, i.e. the equilibrium situation between excitation and decay for the system is reached almost immediately. In contrast, time-resolved measurements involve the monitoring of a temporal dependence of a given fluorescence parameter, like emission intensity, lifetime or anisotropy. For these experiments the sample is exposed to a pulse of light that is shorter than the decay time of the sample and measurements are then made using a high-speed detection system capable of making discrete observations within a nanosecond time regime. Time-resolved experiments can provide novel information about the shape of the macromolecule and its flexibility or multiple conformations which may

not be observed in steady-state measurements due to averaging processes. Nevertheless, the experimental setup of time-resolved measurements is far more complex and thus experiments based on steady-state fluorescence measurements are much more widely used.

Fluorescent labeling of nucleic acids has found its use in a number of applications that previously required radioisotope labeled samples, like DNA sequencing,[21, 22] fluorescence *in situ* hybridization (FISH),[23-26] polymerase chain reaction (PCR),[27, 28] etc. Changes in the fluorescent properties (intensity, anisotropy, lifetime) of the chosen fluorophore which are observed between the fluorescent species alone versus in complexes can be used to examine macromolecular interactions. Especially nucleotide base analogs have been exploited to measure the equilibrium binding kinetics of molecular interactions involving nucleic acids,[29-38] to unravel folding pathways,[39-43] and to study the basics of energy transfer[44, 45] and charge transfer through DNA.[46-48]

2.1.3 Fluorescent and Chemical Properties of the Nucleotide Base Analogs Used in this Thesis

Since naturally occurring nucleotide bases do not display any significant fluorescence, fluorescent nucleotide base analogs were developed that can be inserted into RNA and DNA sequences as quasi-intrinsic probes. A number of nucleotide base analogs are well-characterized for incorporation into oligonucleotides for biophysical and biochemical studies.[49-61] In the present work, two nucleotide base analogs were used, namely 2-aminopurine and 5-(1-pyrenylethynyl)-2'-deoxyuridine. In the following section the properties of these fluorophores will be described.

2-aminopurine (2-AP). More than 30 years ago, *Stryer and colleagues*[49] first demonstrated that 2-AP (Figure 2-3A), a structural isomer of adenine (A), was strongly fluorescent and could be selectively excited in the presence of natural bases. Since the lowest excited single state of Ap, has a π-π^* character,[62] its absorption maximum is red-shifted compared to natural nucleotide bases and lies around 305 nm and its emission spectrum is centered at 370 nm (Figure 2-3B).

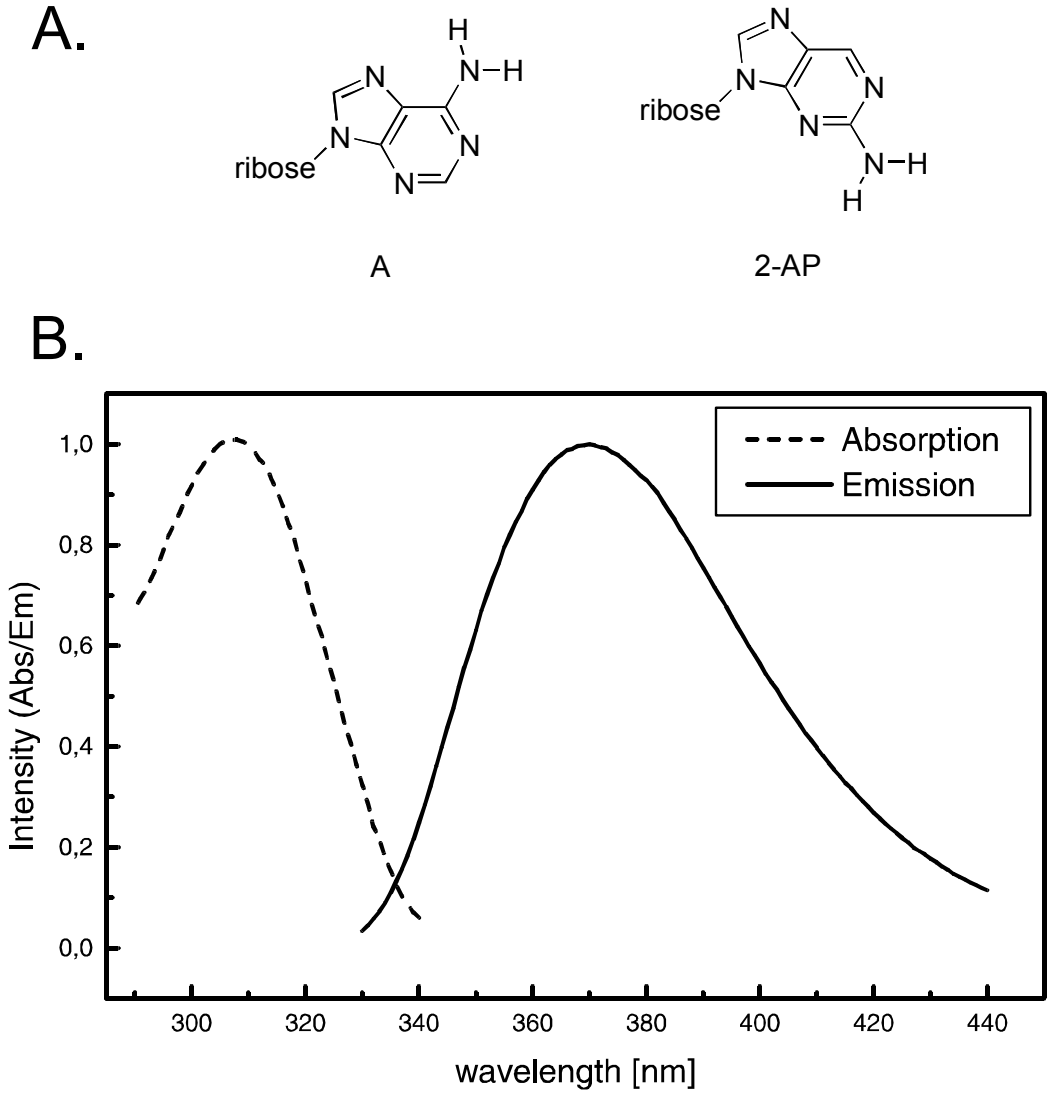

Figure 2-3. (A) Structures of adenine (A) and the highly fluorescent nucleotide base analog 2-aminopurine (2-AP). (B) Absorption (dashed line) and emission (solid line) spectra of 2-AP incorporated into DNA.

In contrast to using brilliant dyes, like fluorescein and cyanin, 2-AP is a generally non-perturbing substitution since it is structurally similar to adenine (6-aminopurine) and will form thermodynamically equivalent base pairs with thymine in DNA helices and uracil in RNA helices (Figure 2-4).[63] Thus, its substitution for adenine in canonical B- and A-form helices common to DNA and RNA structure, respectively, is almost transparent. In contrast to adenine, 2-AP is also capable of forming a base pair with cytosine (Figure 2-4C) at a substantially higher frequency, which *in vivo* can lead to mutations.[64-66] For the work presented here, however, this observation is of no importance, since in the designed RNA and DNA oligonucleotides can only form 2-AP•U/T base pairs.

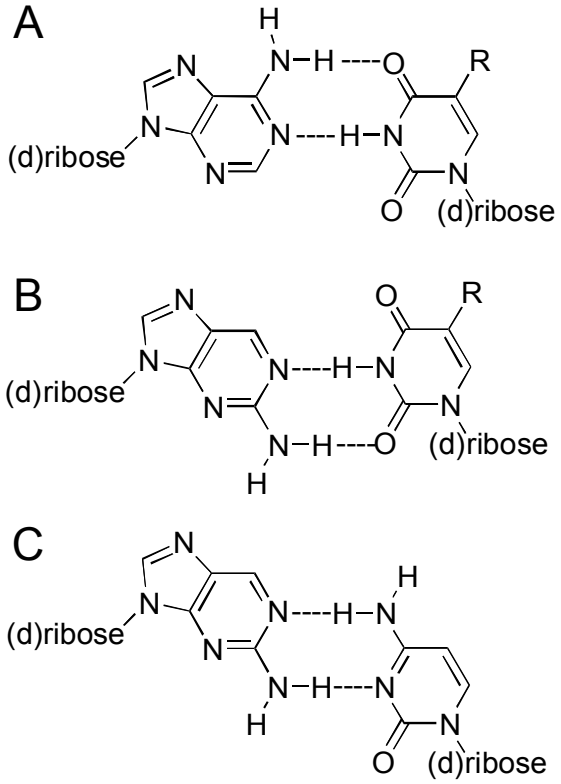

Figure 2-4. Comparison of Watson-Crick base pairs with adenine (A) and 2-aminopurine (2-AP): (A) normal A•U/T base pair, (B) thermodynamically equivalent 2-AP•U/T base pair, and (C) 2-AP•C base pair that can lead to mutations. R=H - uracil (U); R=CH_3 - thymine (T).

The introduction of 2-AP into both DNA and RNA oligonucleotide sequences in a site-specific manner is rather straightforward since it is relatively stable and available in phosphoramidite form for standard automated oligonucleotide synthesis.

The quantum yield of the free 2-AP-riboside at 25 °C, pH 7.0 is 0.68 relative to quinine sulfate, but it is highly sensitive to its microenvironment.[49] While pH in the range of 4-12 has no effect on the emission peak position or intensity, a pH < 4 will shift the emission maximum to the red and reduce the intensity.[49] With increasing temperature the quantum yield of 2-AP decreases by about 25% at 70 °C relative to 20 °C. Most importantly, the incorporation of 2-AP into single or double stranded nucleic acids can result in as much as 100-fold reduction in fluorescence intensity (Figure 2-5).[49]

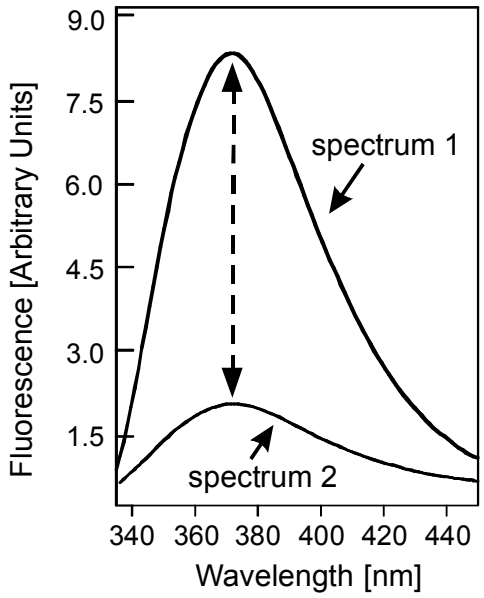

Figure 2-5. Fluorescence emission spectra of 2-AP in RNA. An example of the strong dependence of the quantum yield (Φ_F) of 2-AP fluorescence on the microenvironment of the base. If 2-AP is exposed to aqueous solvent, it is observed to be highly fluorescent (upper trace); while if 2-AP is in a hydrophobic environment (e.g. stacked in helical single or double stranded structure), its fluorescence intensity is almost completely quenched (lower trace).

Temperature and base sequence of the nucleic acid have a big influence on 2-AP fluorescence.[44, 45, 67] Investigations of the molecular interactions that cause these spectroscopic changes found the stacking and collisional quenching of neighboring bases to be the most important factors in 2-AP quenching,[68-70] which can be interpreted as energy and/or charge transfer to neighboring bases.

The sensitivity of the quantum yield of 2-AP to changes in its microenvironment allows 2-AP fluorescence intensity to be used to detect subtle conformational changes in nucleic acids. A number of experimental schemes have been devised to take advantage of this exquisite sensitivity of 2-AP quantum yield to monitor nucleic acid interactions with counter ions, proteins, other oligonucleotides or ligands, dissect RNA folding pathways and detail the mechanisms of enzymes that act on nucleic acids.[33, 38, 40, 71-78] In addition, the mechanism of 2-AP quenching has been the subject of a number of *ab initio* and theoretical analyses[68, 79-82] that have aimed to quantify the relative contributions of different relaxation pathways in the 2-AP quenching reaction.

5-(1-Pyrenylethynyl)-2'-deoxyuridine (Py-≡-dU). The use of the fluorescent nucleoside base analog 5-(1-pyrenylethynyl)-2'-deoxyuridine (Py-≡-dU) (Figure 2-6) as a reporter in nucleic acids is not well established yet, since its synthesis as phosphoramidite and use as fluorescent label in DNA has only been reported fairly recently.[83] Py-≡-dU has two absorption maxima at 378 and 402 nm in aqueous buffer solution, and its emission maximum is around 450 nm, when incorporated into DNA (Figure 2-6).

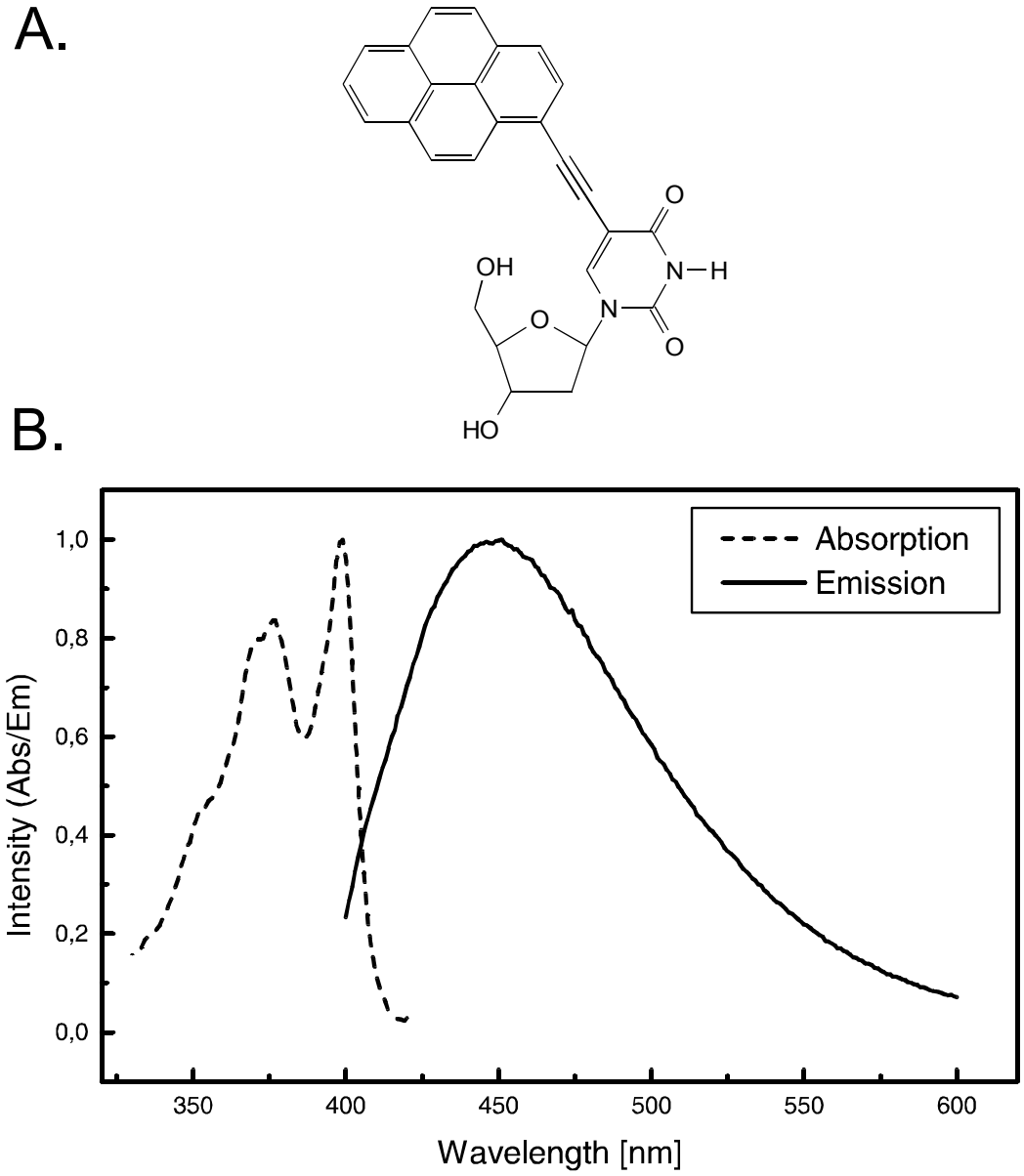

Figure 2-6. (A) Structure of the nucleoside base analog 5-(1-pyrenylethynyl)-2'-deoxyuridine (Py-≡-dU). (B) Absorption (dashed line) and emission (solid line) spectra of (Py-≡-dU) in DNA.

Fluorescence intensity of Py-≡-dU increases by several fold in double stranded DNA compared to single stranded and shows a pronounced bathochromic shift.[83] Emission also increases in single stranded oligonucleotides when a second or third Py-≡-dU unit is inserted into the sequence adjacent to the first one, which again involves a strong shift of the emission spectrum to the red. On the other hand, duplex formation of the doubly or triply labeled DNA oligomers does not induce an increase in fluorescence intensity, but rather a decrease, and the shift of the emission peak to the red is reduced compared to the mono-substituted duplex. Unfortunately, this observation is not very well understood. A possible explanation for the red shift of the fluorescence emission in the multiply labeled single stranded oligonucleotides might be the formation of excimers between the pyrene nucleoside base analogs, but this does not explain the emission increase or red shift upon duplex formation. It seems that the Py-≡-dU moiety forms exciplexes with other neighboring bases, since the fluorophore with the conjugated pyrenylethynyluracil system is partially stacked in nucleic acid duplexes and hence preorganized in a state suitable for exciplex formation.[83] Such sensitivity of the Py-≡-dU residue to the structural surroundings makes this nucleoside potentially useful in probing various interactions of nucleic acids. Also, the Watson-Crick base pairing (i.e. hydrogen bonding) properties of the uracil have not been changed by attaching the ethynylpyrene moiety, and the introduction of Py-≡-dU should not significantly perturb nucleic acid complexes, since the sterically rigid substituent at position 5 of uracil is directed into the major groove of the duplex.[84, 85] Taken together the Py-≡-dU group seems to be a promising fluorescent label for studying interactions involving nucleic acids, such as formation of nucleic acid complexes and binding to enzymes and other proteins.

It should be pointed out that a structurally very similar compound, 5-(pyren-1-yl)-2'-deoxyuracil (Py-dU), has been incorporated into DNA duplexes to study DNA-mediated electron transfer.[2] Based on these reports, it can be concluded that upon photoexcitation Py-≡-dU should also be able to act as an electron donor into the base stack and therefore might be a useful probe for the investigation of reductive electron transfer in DNA.

Py-≡-dU is not commercially available as phosphoramidite and synthesis of Py-≡-dU as phosphoramidite involves several steps with a relatively low overall yield. In the present work, a new and more efficient way of incorporating Py-≡-dU into DNA using a Pd(0)-catalyzed Sonogashira cross-coupling reaction will be described.

2.2 Time-resolved Transient Absorption Spectroscopy

Time-resolved transient absorption spectroscopy, which is also called pump-probe spectroscopy, allows observation of population and depopulation of electronic states of absorbing molecules with a time-resolution down to 50 fs, thus also allowing the observation of intermediate states. The drawback of this high time-resolution is, that a relatively large amount of sample is needed, because of the comparatively low sensitivity of the measurements.[86]

In general, in this method the fluorophore is excited by a short laser pulse (pump pulse) in the absorption band of the molecule. A second independent pulse with an arbitrary wavelength (probe pulse) is applied with different time delays, and can probe different states of the fluorophore by measuring their intermittent absorption (Figure 2-7).

1. If the probe pulse is in the wavelength range of the ground-state absorption, the rate of back charge transfer can be determined.
2. If the probe pulse is in the wavelength range of the fluorescence, stimulated emission will occur, and the depopulation of the excited state S_1 can be observed.
3. If the probe pulse is outside the fluorescence band, the probability of population of any intermediate state, such as a charge separated state, can be measured.

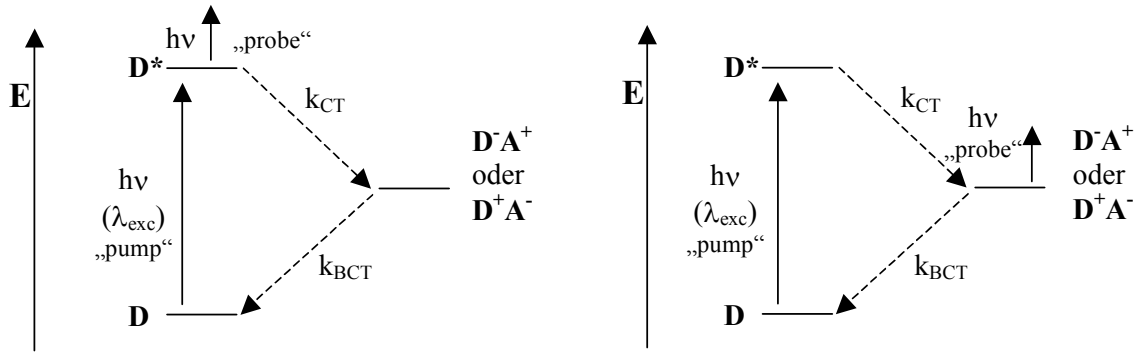

Figure 2-7. Transient absorption measurements with pump probes outside the fluorescence band.

Based on the resulting time-courses, the lifetimes of the individual states can be determined. The absorption of a sample with and without previous excitation is measured and the change of optical density is plotted against time. Depending on the observed processes, absorption, stimulated emission, bleaching and recovery of the ground-state, the values may be positive or negative. Amplitudes and time constants of the resulting spectra yield the rates of the fluorescence, charge separation and charge recombination.[86]

2.3 Antisense RNA Systems

A gene is a coded blueprint for a protein. The code is written in the precisely ordered sequence of four nucleotide bases, A, T, G, C, that make up DNA. In addition to the covalent linking of the bases in a DNA strand, A can form two hydrogen bonds with T and G can form three hydrogen bonds with C to make up the typical double helix-structure of DNA. One strand containing the 'sense' sequence (genetic code) base-pairs with an 'antisense' sequence (complementary sequence in the opposite direction) of the second strand. The high specificity of base pairing is important during DNA replication, where each of the two strands serves as a template for reconstructing its partner (Figure 2-8). Base pairing specificity is also important when genetic information is decoded to make proteins. First, DNA is transcribed into RNA, which is made of the same bases as DNA, except for T, which is replaced by a U. The RNA molecule that is assembled is antisense to the antisense DNA strand, i.e. it bears the sense sequence. From this so called messenger RNA molecules proteins are then formed on the molecular machinery of the ribosomes.[87]

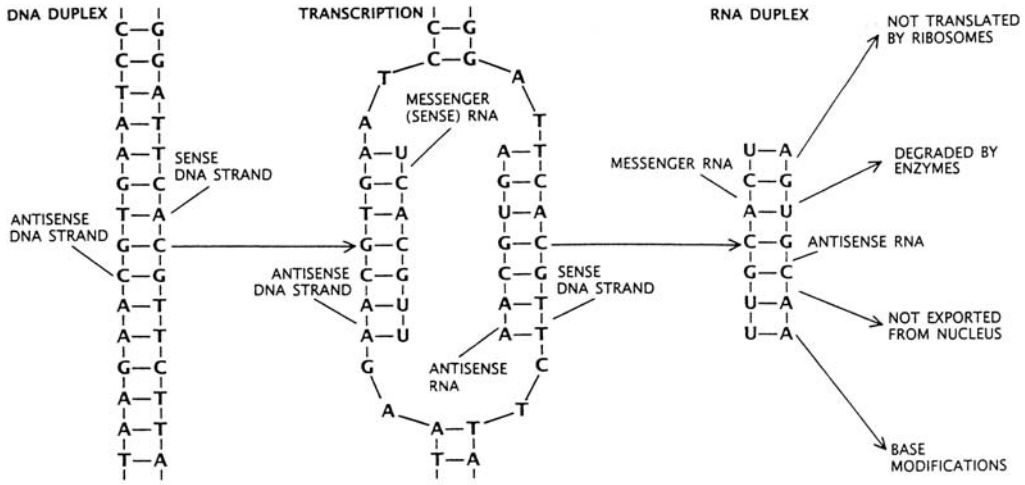

Figure 2-8. Schematic representation of the route from gene to gene product. The coding sense and the antisense strand of DNA complement each other. During the transcription of DNA into RNA, the antisense DNA strand acts as a template for assembling a complementary (sense) messenger RNA molecule. A single-stranded messenger RNA is translated into a protein in the ribosome. However, some genes are regulated by additional transcription of an antisense RNA from the sense DNA strand to prevent translation.

It has been known for a long time that gene expression in both prokaryotes and eukaryotes is controlled by proteins. In prokaryotes, however, regulatory RNA has also been found. This regulatory RNA contains a sequence that is complementary to the target RNA, usually a messenger RNA. Binding of the two RNAs occurs by base pairing, resulting in a fairly stable

complex, so that the target RNA cannot perform its function anymore. Antisense RNA has been identified in the regulation of diverse and complex phenomena in bacteria such as plasmid replication, osmoregulation of porin expression, and regulation of phage reproduction.[88]

Bacterial plasmid replication control systems have been studied in detail. In bacteria genetic information is encoded in one circular double stranded DNA molecule, the chromosome. In addition, bacteria often contain extrachromosomal elements called plasmids. They also contribute to the phenotype of their hosts, for example, by coding for antibiotic resistance, virulence factors, and catabolic functions. Plasmids control their own replication and are present at defined copy numbers (plasmid molecules per cell) that are determined by the plasmids, the host and the growth conditions.[89] Generally, this strong regulation is achieved by antisense RNA and is based on kinetics, like the rates of synthesis and decay of sense and antisense element, efficiency of replication and kinetics of the interaction between sense and antisense element. It seems that a fast rate for complex formation is more important than binding equilibria.[90]

Regulation or inhibition of gene activity with antisense RNA seems to be universal among viruses and bacteria.[87] The efficiency of the gene regulation by antisense RNA in nature led to the development of systems in which artificially constructed antisense genes regulate a cellular or viral gene of interest. This principle can be used for genetic research, for example to turn off a gene selectively to study the effects of the defect analogous to a mutation,[87] and it also led to the idea of using the antisense approach in drug design, i.e. to block the genetic code to inhibit gene expression associated with diseases. The advantage of using antisense RNA as gene regulators is the high specificity of binding. For a ligand to bind specifically to a target sequence in a nucleic acid, it has to base pair with a certain number of nucleotides depending on the size of the genome. For example, based on the assumption of a statistical distribution of base pairs in the genome and the same number of A-T and G-C base pairs, the minimal number of bases that have to be recognized is 7 in the HIV, 12 in *E. coli*, and 17 in human DNA.[91]

Studying natural antisense control systems, like the plasmid replication system *ColE1*, might help to understand the structural and kinetic basis for how nature has evolved such an efficient regulatory control system.

2.4 Energy and Charge Transfer in DNA

2.4.1 Excited State Energy Transfer

Understanding the electronic properties of DNA has been the goal of various experimental and theoretical studies over the last decades. With respect to the biological consequences, such as mutagenesis, apoptosis and carcinogenesis,[92-94] most effort by far was spent on the investigation of charge migration processes through the base stack.[95] Although photoinduced charge transfer is initiated by electronic excitation, no clear picture has yet emerged of how to describe excitation energy in duplex DNA. A key question which is crucial for the mechanism of various photoreactions in DNA is whether excited singlet states of DNA bases are localized or extended over several neighboring bases. Ever since the pioneering work of *Eisinger et al.* in 1966,[96, 97] who showed clear evidence for excimer emission between nucleosides at low temperature, excimers and exciplexes have been invoked in discussions on nucleic acid components.[17, 96-102] Very recently, *Xu and Nordlund* reported the sequence, temperature, concentration and solvent dependence of singlet energy transfer from normal bases to the base analog 2-aminopurine measured by optical spectroscopy.[44] They found that adenine was the most efficient energy donor by an order of magnitude, but conclude that energy transfer at physiological temperatures over more than a few bases is improbable. The main experimental obstacles which have so far prevented a systematic investigation of this matter at room temperature are related to the intrinsic properties of DNA:[103] a) The lowest absorption bands of all four nucleosides are very broad and overlap strongly in the UV region. Monomer and excimer emission cannot be separated because of considerable spectral overlap. b) The collective properties of duplex DNA depend on its base sequence, and therefore only studies with well-defined reference assemblies are meaningful. c) The natural nucleic acids have very low fluorescence quantum yields due to ultra short excited state lifetimes, which complicate emission band shape analysis. Only recently has femtosecond transient absorption spectroscopy been used to study the photophysical properties of bases and nucleosides.[104-107]

2.4.2 Charge Transfer

Shortly after Watson and Crick discovered the double helical structure of DNA,[108] the possibility that the one-dimensional array of π-stacked base pairs in B-form DNA might serve as a pathway for charge migration was suggested over 40 years ago.[109] Since then, many

scientists put their effort into proving this possibility, and the fundamental question if DNA serves as a medium for long-range charge transfer (CT) was discussed very controversially.

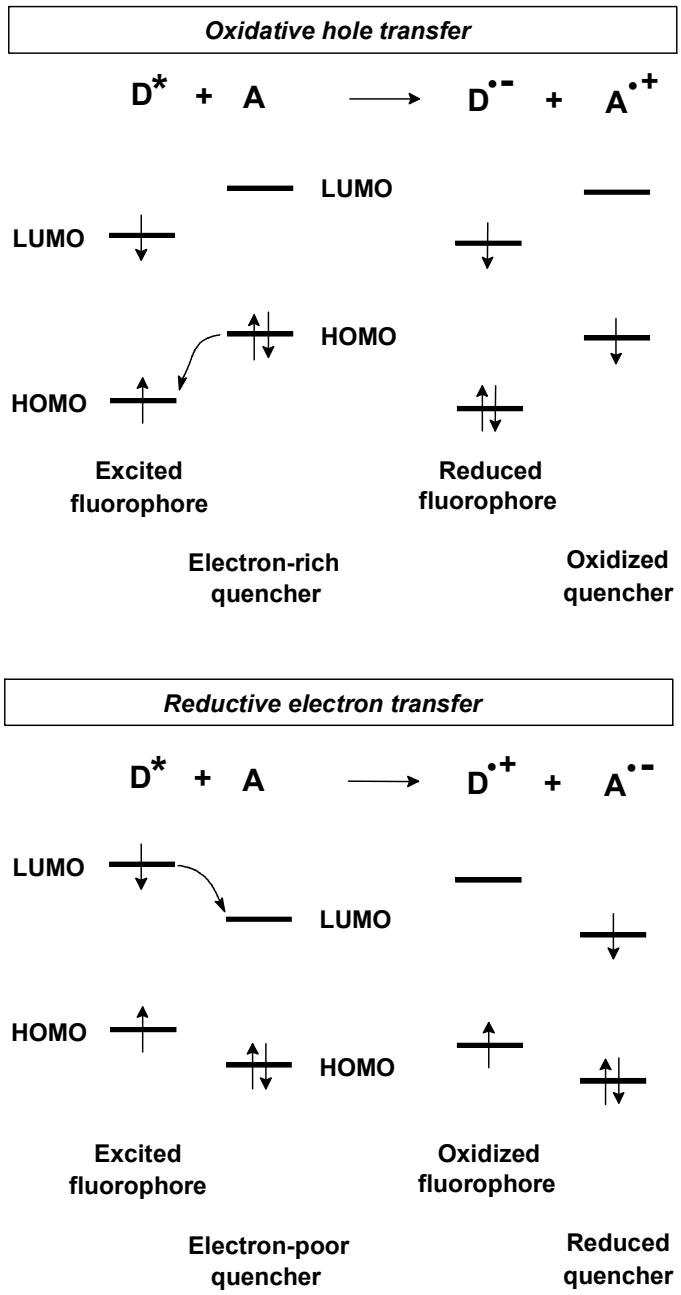

Figure 2-9. Differences of oxidative HT and reductive ET. In both cases, a photoexcited fluorophore is used in order to initiate the CT process. In case of the oxidative HT, an electron is removed from the HOMO of the charge acceptor, **A**, into the HOMO of the charge donor, **D**. In case of the reductive ET the photoexcited electron is shifted from the LUMO of **D** into the LUMO of **A**. In the first case, DNA is oxidized whereas in the latter case DNA is reduced.

The proposals ranged from DNA being a molecular wire[110] to DNA being an insulator.[111] By now, it is generally accepted that charge transfer in DNA can occur on an ultrafast timescale and over long distances.

In general there are two possibilities for CT in DNA:

1. The DNA is oxidized, i.e. an electron is abstracted from the DNA, and a radical with a positive charge (hole) is generated in the DNA strand. The charge can be transferred through the base stack. This process can be considered as an oxidative hole transfer (HT) (see Figure 2-9). This positively charged radical may also react with surrounding molecules, like water or oxygen, and result in oxidative damage to the DNA which in turn can cause mutagenesis and carcinogenesis.[92, 93, 112-114] Because of the relevance of HT to oxidative damage in DNA a large number of research groups have focused their work on the photochemically or photophysically induced oxidation of DNA, and furthermore, on the mobility of the created positively charged radical in the DNA.
2. The DNA is reduced, i.e. an excess electron is injected into the DNA, and a radical with a negative charge is generated in the DNA strand. The charge can be transferred through the DNA. This process can be considered as a reductive electron transfer (ET) (Figure 2-9). Although ET processes are currently used in DNA chip technology[115-119] and DNA nanotechnology[120-123], and despite the broad knowledge about these bioanalytical and biomedical applications, little is known about the behavior of excess electrons in DNA.

2.4.2.1 Mechanisms of Hole Transfer

Several mechanisms, such as the superexchange and the hopping mechanism, have been proposed, and experimentally verified.[95, 124-127] The two main mechanisms shall be summarized in the following section.

2.4.2.1.1 Superexchange Mechanism

The charge tunnels in one coherent step from **D** (charge donor) to **A** (charge acceptor) and never resides on the DNA bridge between them (Figure 2-10). As a consequence, no observable radicals of nucleobases in the bridge exist, and only educt and product radicals can be observed. The probability of the tunneling process depends on the energy difference of **D** and **A** and on the length of the DNA bridge between them. An exponential decrease of the charge transfer rate (k_{CT}) with the distance between **D** and **A** is characteristic for this process.

This distance dependence can be interpreted according to the Marcus theory,[128] and can be expressed by the equation

$$k_{CT} = k_0 \, e^{-\beta R}$$

where R is the distance between **D** and **A**, the exponential parameter β is a factor characteristic for each medium, which describes the charge transfer efficiency, and k_0 is an empirical constant.

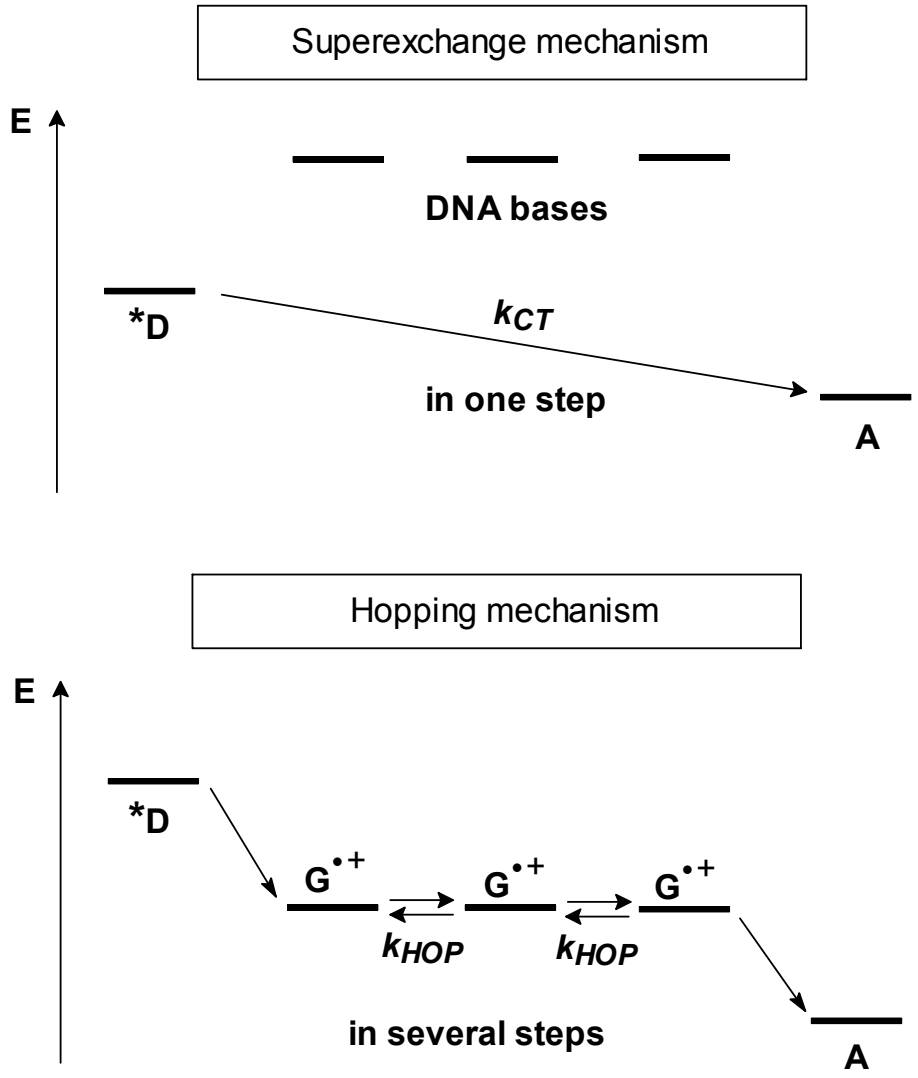

Figure 2-10. Superexchange and hopping mechanism. In the superexchange mechanism the charge does not localize on the DNA bridge between the charge donor, **D**, and charge acceptor, **A**, but tunnels through the electron cloud in one step directly from **D** to **A** with the charge transfer rate, k_{CT}. In the hopping mechanism, the charge localizes on the DNA bridge between **D** and **A**, preferentially on guanine bases (G), and migrates from **D** to **A** in several steps with the hopping rate, k_{HOP}, for every step.

The smaller the value for β, the weaker the distance dependence of the charge transfer rate. Values of β for CT through proteins lie in the range of 1.0-1.4 $Å^{-1}$.[129-131] In contrast, β values determined for CT reactions in DNA can be found in a wide range from $\beta < 0.1$ $Å^{-1}$ up to $\beta =$ 1.5 $Å^{-1}$ (Table 2-1).[95, 132] Typical values for charge transfer following a superexchange mechanism are about 0.7 $Å^{-1}$. For β-values much smaller than that, an alternative mechanism has to be considered.

2.4.2.1.2 Hopping Mechanism

The occurrence of very small β values ($\leq$ 0.1 $Å^{-1}$) exhibiting a very shallow distance dependence led to the description of an alternative mechanism which is the hopping model. In contrast to the previously described superexchange mechanism, the positive charge is transported from **D** to **A** in several steps, once it has been injected into the DNA base stack, and can finally be trapped at a suitable charge acceptor (Figure 2-10). The charge localizes on bases in the bridge, and radical cation nucleobases other than **D** and **A** can be observed as intermediates. Among the four different DNA bases, guanine can be most easily oxidized.[133, 134] Hence, the G radical cation plays the role of the intermediate charge carrier during the hopping process. Each hopping step is itself a tunneling process through the intervening A-T base pairs. In contrast to the superexchange mechanism, the rate of HT by hopping does not depend on the overall distance between **D** and **A** but is only dependent on the number of hopping steps.[135] *Lewis et al.* were able to measure the rate for a single hopping step from G to GG with a hopping rate $k_{HOP} = 5 \times 10^7$ s^{-1}.[136]

2.4.2.2 Experimental Techniques for Charge Transfer Detection

A lot of different techniques have been used to explore DNA-mediated CT processes, among these are biochemical methods and spectroscopic measurements. Most experiments were performed according to the following steps:[95]

1. Labeling of DNA with redoxactive probes through intercalation and/or covalent linkages.
2. Initiation of CT by photochemical or electrochemical techniques
3. Detection of CT processes by spectroscopic, electrochemical, or biochemical methods.

2.4.2.2.1 Oxidative Hole Transfer

For the study of oxidative HT a number of model systems have been developed using a variety of organic and inorganic intercalators or nucleic acid base analogs as charge donors and acceptors. Usually by absorption of light, the charge donor will be raised into an electronically excited state, which enables the initiation of charge transfer. According to the method of detection of the HT process, one can divide most published experiments into *spectroscopic* and *biochemical* studies.

Spectroscopic studies. Organic and inorganic intercalators which have not been covalently attached to oligonucleotides were first reported for studying CT in DNA. These experiments provide only little information because of the lack of an accurate measurement of the distance between the **D** and **A** as well as the possibility of the pairing of the intercalators. The significant experimental improvement came with the DNA assays bearing covalently linked intercalators. Using these systems, a systematic measurement of the distance dependence and the base sequence dependence was possible. The spectroscopic techniques that are applied for the measurement of charge transfer processes are usually time-resolved fluorescence spectroscopy or time-resolved transient absorption spectroscopy. The most important spectroscopic studies with a variety of charge donors and acceptors are summarized in Table 2-1.

Biochemical experiments. The G radical cation was identified to be the precursor of a variety of different oxidative G lesions which are normally described as G^{ox}. Some of these G oxidation products have been identified (Figure 2-11).[114, 137] Biochemical experiments explore HT reactions through DNA by an indirect method. As described above, after the photochemical or photophysical oxidation of DNA using a suitable intercalator, G is preferentially oxidized. The resulting G radical cation can react with H_2O and/or O_2 yielding oxidized G products G^{ox}. Such modified DNA strands can be cleaved at the site of G^{ox} by treatment using e.g. piperidine at elevated temperature, then separated by gel electrophoresis and visualized by phosphorimagery using radioactive ^{32}P-labeling.[138]

Three conclusions could be drawn from these experiments:

1. Short-range CT reactions occur on a very fast timescale ($k_{CT} = 10^9$ - 10^{12} s^{-1}).
2. The typical β-value of DNA-mediated CT is 0.6-0.8 $Å^{-1}$.
3. The intercalation of **D** and **A** is crucial for a fast and efficient CT process.

Table 2-1. Summary of important spectroscopic studies on DNA-mediated charge transfer. The rate k_{CT} and distance dependence β are given according to $k_{CT} = k_0 \bullet e^{-\beta \bullet R}$.

Charge donor / acceptor	covalently attached?	β [Å^{-1}]	k_{CT} [s^{-1}]	Research group	Year
E / MV	no	-	10^5	Fromherz[139]	1986
E / MV, Ac / DAP	no	1.0	10^8	Harriman[140]	1992
Ru(II) / Rh(III) complexes	yes	0.2	10^9	Barton[141]	1993
Ru(II) / Rh(III) complexes	yes	1.0-1.5	10^6	Meade[142]	1995
St / G	yes	0.64	10^8-10^{12}	Lewis[143]	1997
E / Rh(III) complex	yes	-	10^{10}	Barton[144]	1997
Ac / G	yes	1.4	10^5-10^{10}	Tanaka[145]	1998
E / Z	yes	-	10^{12}	Barton/Zewail[146]	1999
N / A	yes	-	10^9	Lewis[147]	1999
Ap / G	yes	0.1-1.0	10^9-10^{10}	Barton[148]	1999
Ap / G	yes	0.75	10^6-10^7	Shafirovich[149]	2000
Ap / G	yes	0.6	10^9-10^{11}	Barton/Zewail[46]	2000
Ac / G, Ac / Z	yes	-	10^7-10^{12}	Michel-Beyerle[150]	2002
Ru(II) complex / In	yes	-	$\geq 10^7$	Barton[151]	2002

Abbreviations: A = adenine, Ac = acridine, Ap = 2-aminopurine, DAP = *N*,*N*'-dimethyl-2,7-diazapyrenium, E = ethidium, G = guanine, In = 4-methyl indole, MV = methyl viologen, N = naphthaline, St = stilbenedicarboxamide, Z = 7-deazaguanine.

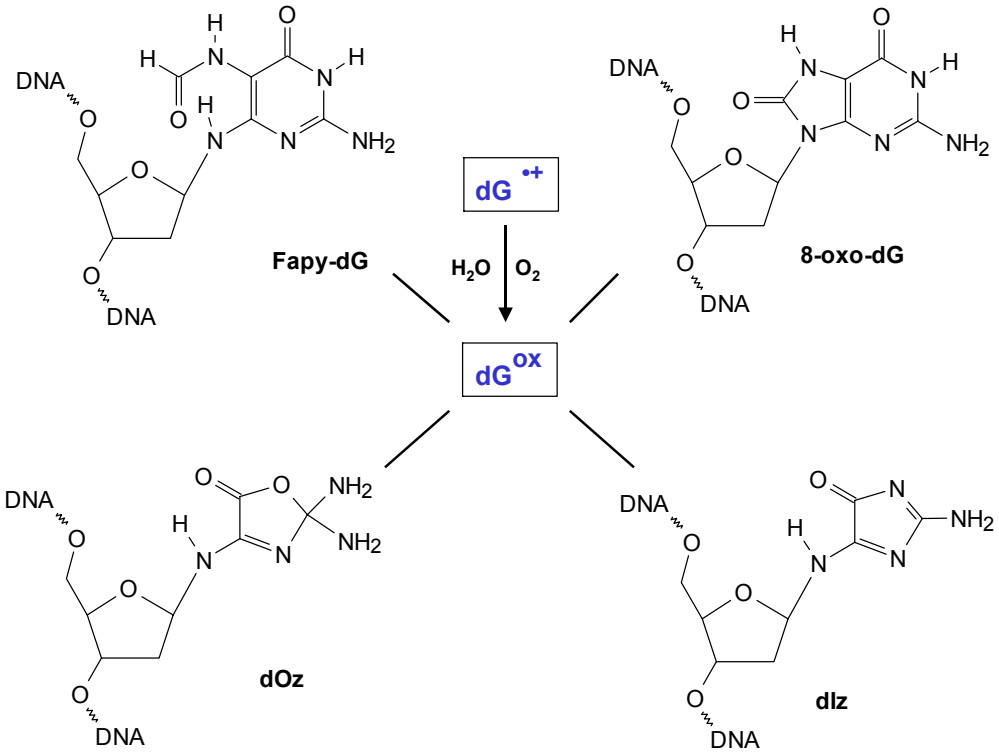

Figure 2-11. Examples of oxidative G damage (G^{ox}) with formamidopyrimidine (Fapy-dG), 8-oxo-guanine (8-oxo-dG), oxazolone (dOz) or imidazolone (dIz) structure.[114]

The most common photooxidants for DNA are metal complexes or organic intercalators (Figure 2-12). These systems differ significantly in their structural properties, their redox potentials and the absorbing wavelengths. Nevertheless, it has been observed in all systems that the positive charge can be transported with high efficiency over very long distances (up to 200 Å). The observed efficiency of HT seems to be strongly dependent on the distance and base sequence between each of the G-C pairs. It also has been shown that A can act as an intermediate charge carrier if G is not present.[152] Note that with biochemical methods in principle only relative yields of oxidative products can be measured but not rates for charge transfer.

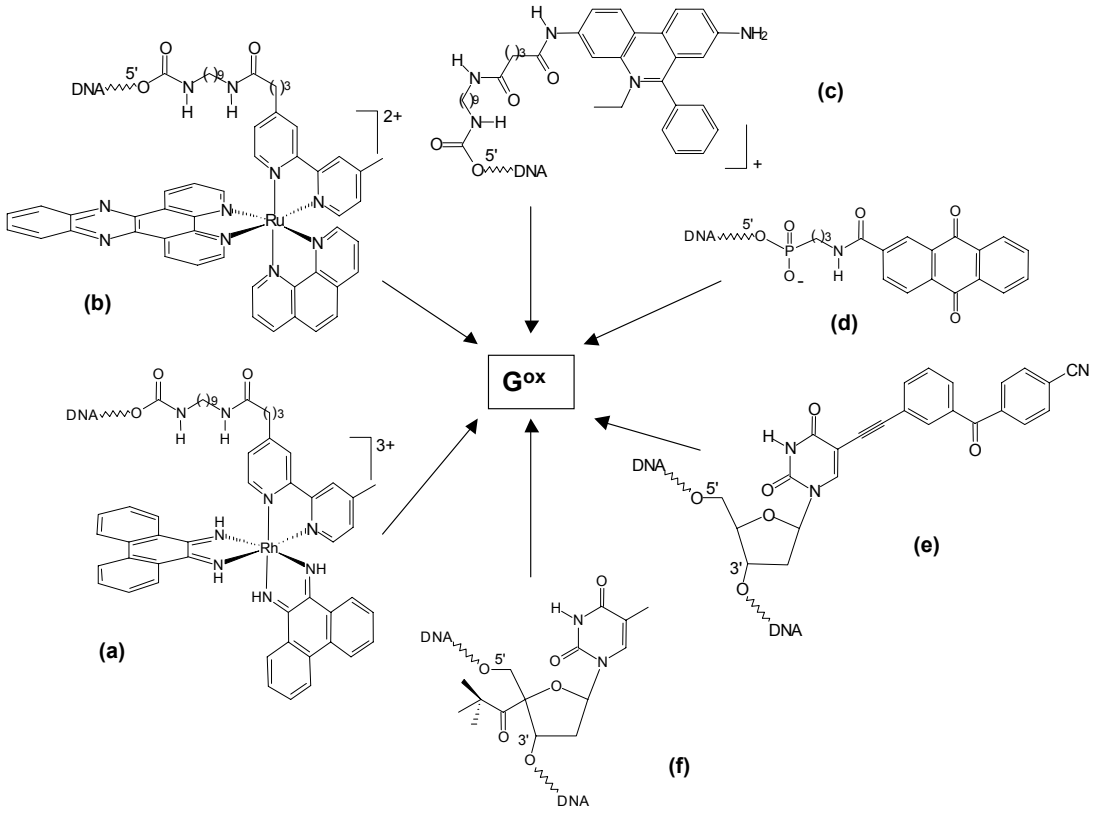

Figure 2-12. Examples of photooxidants which have been used in biochemical studies of HT in DNA. (a) Rh(III) complexes,[153] (b) Ru(II) complexes,[154] (c) ethidium derivatives,[127] (d) anthraquinone derivatives,[155] (e) uridine modified with cyanobenzoquinones,[156] and (f) modified 2'-deoxyribosides bearing a photoreactive group.[157]

2.4.2.2.2 Reductive Electron Transfer

Most studies on charge transfer in DNA have concentrated on the oxidative HT. For the investigation of reductive ET, there are not many model systems available. Most knowledge about ET comes from γ-radiolysis studies in frozen ice or glassy aqueous LiBr solutions.[158-165] The samples were irradiated to initiate the electron transfer. The DNA was doped by intercalated and randomly spaced electron traps. The intermediate radicals of the DNA bases and the acceptor were detected by ESR spectroscopy. The major disadvantage of this principle experimental setup is that the electron injection and the electron trapping does not occur site-selectively. Nevertheless, a few remarkable and principle conclusions and implication can be drawn from these studies. They suggest that below 77 K, ET in DNA occurs via a superexchange mechanism with an average β-value of 0.9 $Å^{-1}$.[159-162] At

temperatures above 170 K an electron transfer over longer distances follows an activated hopping process.[158, 160, 161, 165]

The trend for the reducibility of DNA bases has been established to be T ~ C > A > G.[134, 166] The DNA bases that are most easily reduced are T and C, whose reduction potentials are very similar.[134] Thus, it is expected that the excess electron migration through DNA occurs via a hopping mechanism involving all base pairs (C-G and T-A) and the pyrimidine radicals $C^{\bullet-}$ and $T^{\bullet-}$ as intermediate charge carriers.[157]

Recently, a new DNA assay was published by *Carell et al.* which allows the photoinduced cleavage of T-T dimers by a flavine derivative from the distance (Figure 2-13).[167, 168] The flavine moiety was synthetically incorporated as an artificial nucleobase into oligonucleotides.[169] Despite the fact that spectroscopic measurements with these systems have not been published, the T-T dimer splitting was interpreted as the chemical result of a reductive ET through the DNA base stack. This interpretation is mainly based (i) on the known redox properties of the flavin intercalator in its reduced and deprotonated state,[170] and (ii) on the absence of a typical DNA base sequence dependence which would be observed in case of a hole hopping process.

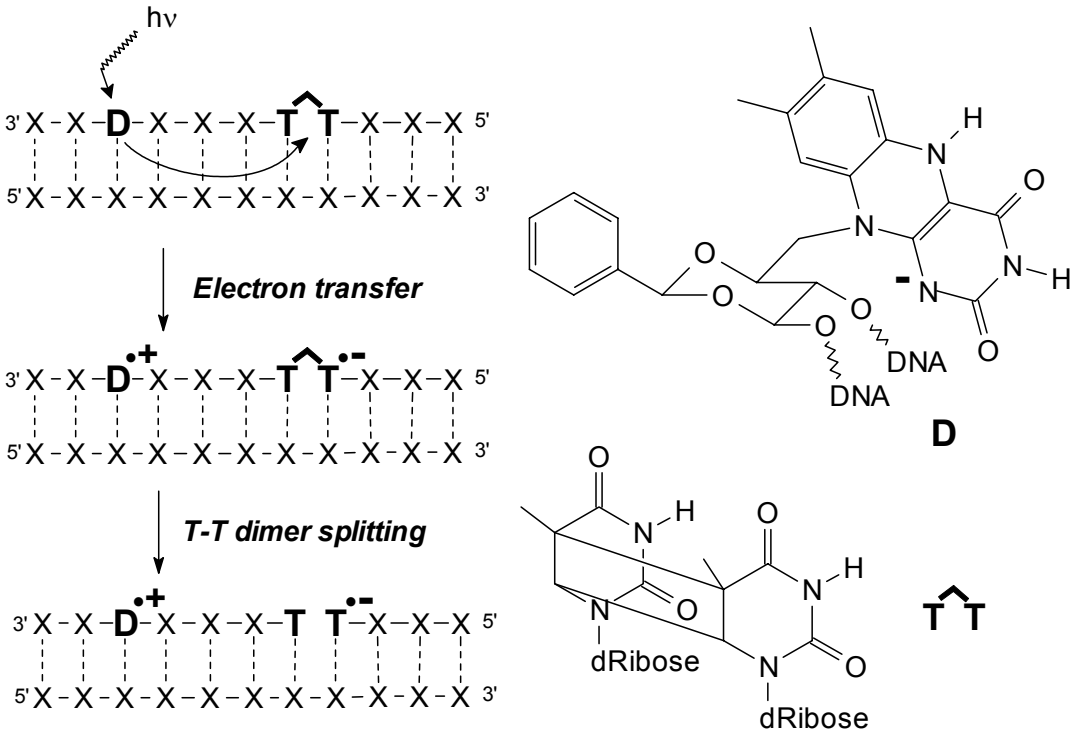

Figure 2-13. Chemical assay for the investigation of reductive ET in DNA. The T-T dimer (T^T) splitting is the chemical result of a photoinduced ET from a distant flavine derivative as the charge donor (**D**).

Most recently, *Zewail et al.* reported femtosecond time-resolved studies on the reduction of T by photoexcited 2-aminopurine (Ap*) in DNA duplexes.[46] They found that Ap* can induce both reductive ET by injecting an electron into a neighboring T, and oxidative HT by injecting a hole into a neighboring G. The rates of these processes are very similar with 20 ps and 19 ps, respectively.

Lewis et al. investigated the dynamics of photoinduced electron transfer in DNA hairpins which have been synthetically capped by a stilbenediether derivative serving as an electron donor (Figure 2-14).[171] The electron injection rates are larger using T ($>2\times10^{12}$ s^{-1}) as the electron acceptor in comparison to C (3.3×10^{11} s^{-1}). This indicates that the reduction potential is lower for T versus C in double-helical B-DNA. Interestingly, a small difference of the electron injection rate was detected using C as the electron acceptor which is base-paired to G versus inosine (I). The C-G base pair has stronger hydrogen bonding compared to the C-I base pair. As a result, the electron injection rate into the C-G base pair is slower (3.3×10^{11} s^{-1}) than into the C-I base pair (1.4×10^{12} s^{-1}) indicating the differences in reduction potentials of C as a result of different base-pairing.

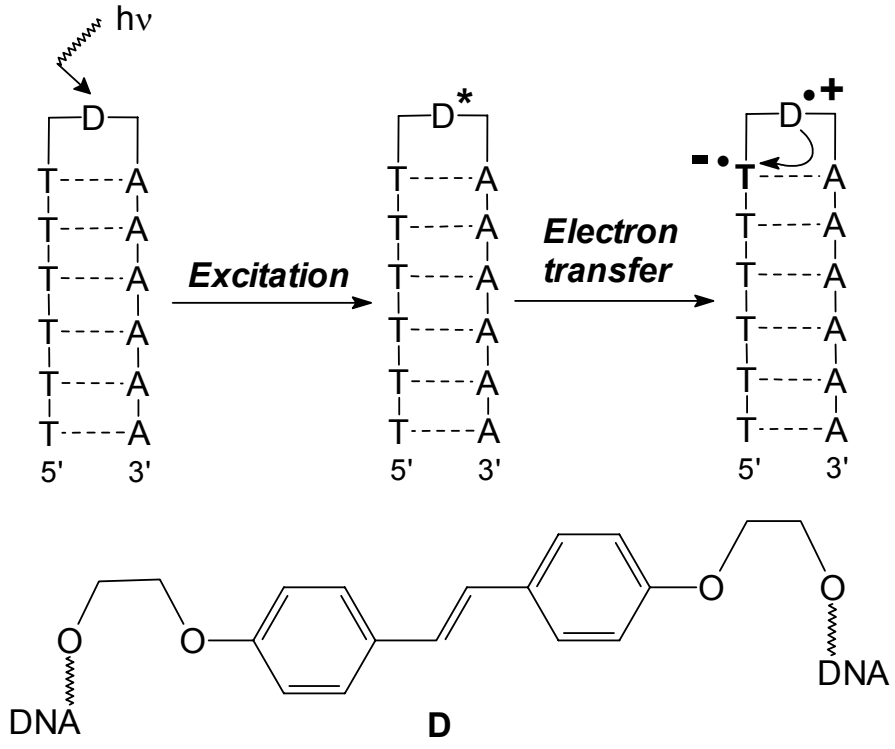

Figure 2-14. Electron transfer in DNA hairpins which are capped with a stilbene diether derivative as the charge donor (**D**).

Another recent approach to investigate reductive ET in DNA with spectroscopic methods is the use of the fluorescent nucleoside analogs 5-pyrenyl-2'-deoxyuridine (Py-dU) and 5-(pyren-1-yl)-2'-deoxycytidine (Py-dC) as electron injectors into DNA.[172] Photoexcitation of the pyrenyl group results in an intramolecular ET yielding the corresponding U or C radical anion and the pyrenyl radical cation ($Py^{\bullet+}$-$dU^{\bullet-}$/ $Py^{\bullet+}$-$dC^{\bullet-}$). This CT assignment has been proven previously by *Netzel et al.* based on nanosecond fluorescence lifetime measurements and by *Amann et al.* using transient absorption spectroscopy.[173, 174]

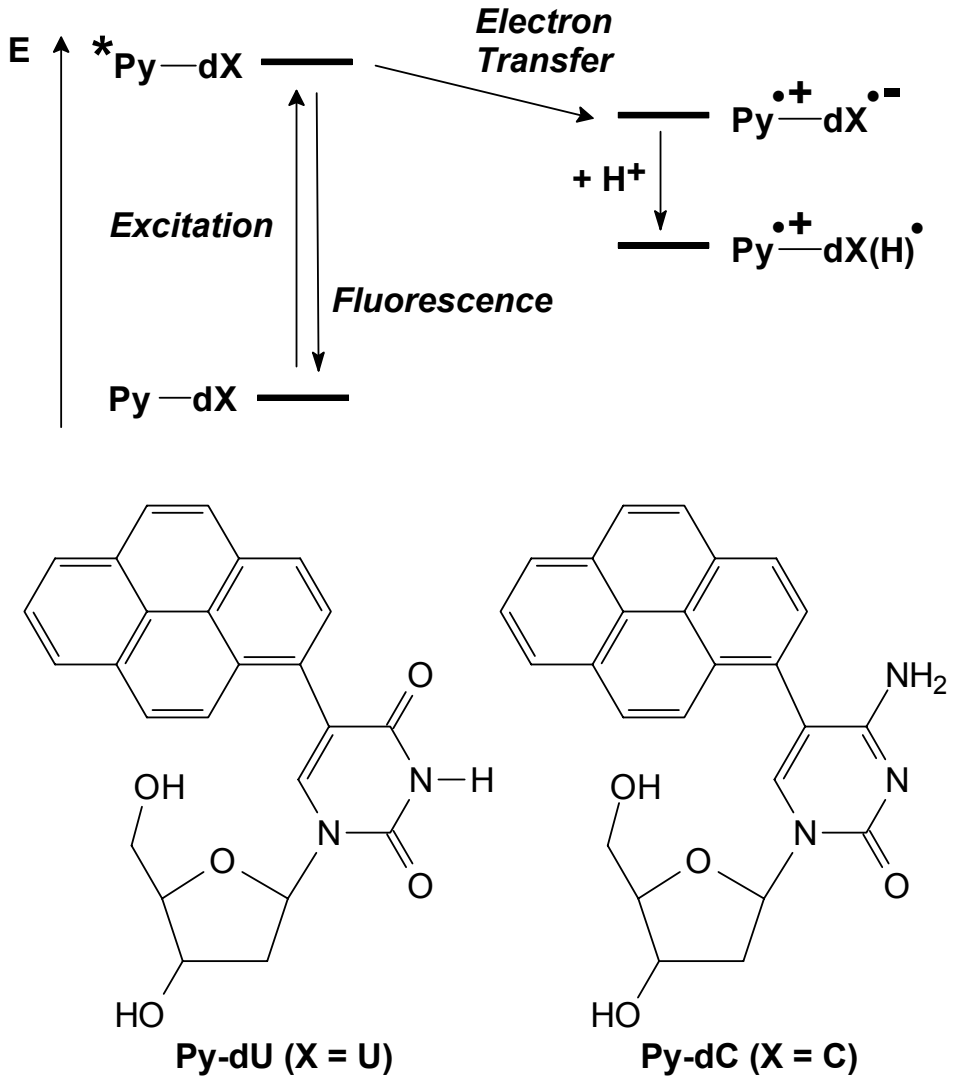

Figure 2-15. Intramolecular electron transfer in Py-dX as described in *Amann et al.*[175] Upon excitation Py-dX may either return to the ground state by fluorescence or undergo an intramolecular electron transfer. The radical anion $X^{\bullet-}$ can be protonated and thus be removed from the equilibrium between excited state and charge separated state.

The properties and dynamics of the intramolecular electron transfer in Py-dU and Py-dC have been characterized by steady-state fluorescence spectroscopy and femtosecond transient absorption spectroscopy in water at different pH values (Figure 2-15).[174, 175] By comparing PydC and PydU as nucleoside models for electron transfer in DNA, it was found that a small energy difference exists between $U^{\bullet-}$ and $C^{\bullet-}$, which is in agreement with several calculations and experiments.[47, 134, 160, 176] Most importantly, it was shown that there is a difference of the basicity of the generated pyrimidine radical anions which implies significance for the understanding of electron migration in DNA (Figure 2-16). The non-protonated radical anion of C ($C^{\bullet-}$) could not be observed in aqueous solution, which provides strong evidence that protonation of $C^{\bullet-}$ by the complementary DNA base G or the surrounding water molecules will occur rapidly. Thus it was conlcuded that $C^{\bullet-}$ cannot play a major role as an intermediate charge carrier. In contrast, $U^{\bullet-}$ or $T^{\bullet-}$, respectively, can act as stepping stones for electron hopping in DNA since protonation of these radical anions does not occur.

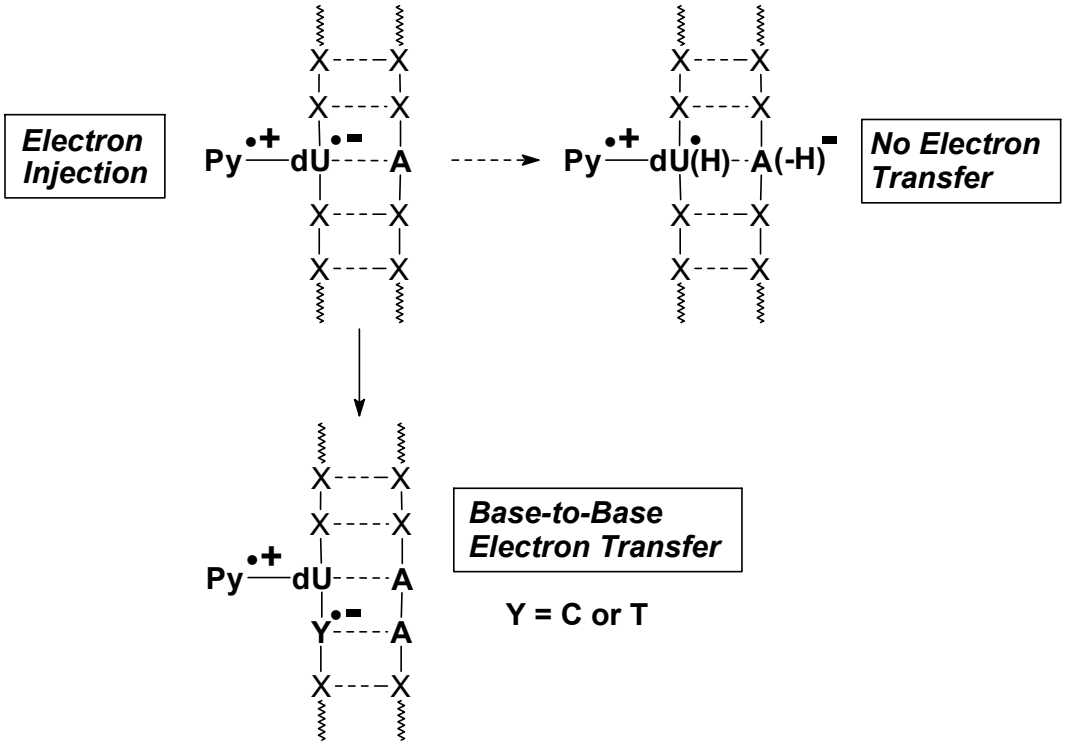

Figure 2-16. After electron injection by excitation of Py-dU and subsequent charge separation, the generated U radical anion $U^{\bullet-}$ can either be protonated by its base pairing partner of transfer an electron to a neighboring base X. This electron transfer only takes place, if X = T or C.

Using the nucleoside Py-dU, a range of pyrene-modified duplexes was prepared which differ mainly in the bases located next to the Py-dU group.[2] The covalently attached pyrene group is located outside the DNA base stack. Upon excitation, an intramolecular electron transfer in the Py-dU group represents the injection of an excess electron into the DNA base stack. A significant quenching of the Py* emission was only detected, if a T or a C was placed adjacent to the Py-dU group. This observation can be assigned to a base-to-base electron transfer process (Figure 2-16), which is supported by femtosecond time-resolved pump-probe laser spectroscopy measurements.

Despite these efforts in understanding reductive ET in DNA, future experiments have to focus on (i) the dynamics of the electron injection process in a more detailed way, (ii) the base sequence dependence of ET, (iii) the rate of base-to-base ET in terms of the hopping model, and (iv) the chemical reactivity of the radical anions in DNA such as cross-linking.

2.4.2.2.3 Biotechnological Applications of Electron Transfer in DNA

From the various studies of charge transfer in DNA it became clear that these processes show an extreme sensitivity towards perturbation and interruptions of the base-stacking which are caused by base mismatches or DNA lesions.[46, 135, 150, 176-178] Thus, charge transfer in DNA should be suitable to obtain an electrochemical readout of DNA chips. The basic idea is that the subsets of a critical gene are immobilized as single stranded oligonucleotides on an electrode or chip and contain a redoxactive probe which is intercalated and/or covalently attached (Figure 2-17). Intact DNA material which is added to the chip forms perfect DNA duplexes leading to an efficient electron transfer between the chip surface and the distant redoxactive probe. Base mismatches and DNA lesions significantly interrupt charge transfer in DNA, and as a result, the electrochemical response is missing. This is a very promising technique for a reliable detection of genomic sequence variations, like point mutations (single nucleotide polymorphism, SNP), which is critical for the study of population genetics, for the clinical diagnostics of cancer, for the diagnosis, and treatment of genetic or viral diseases, and most recently, for the concept of pharmacogenetics.

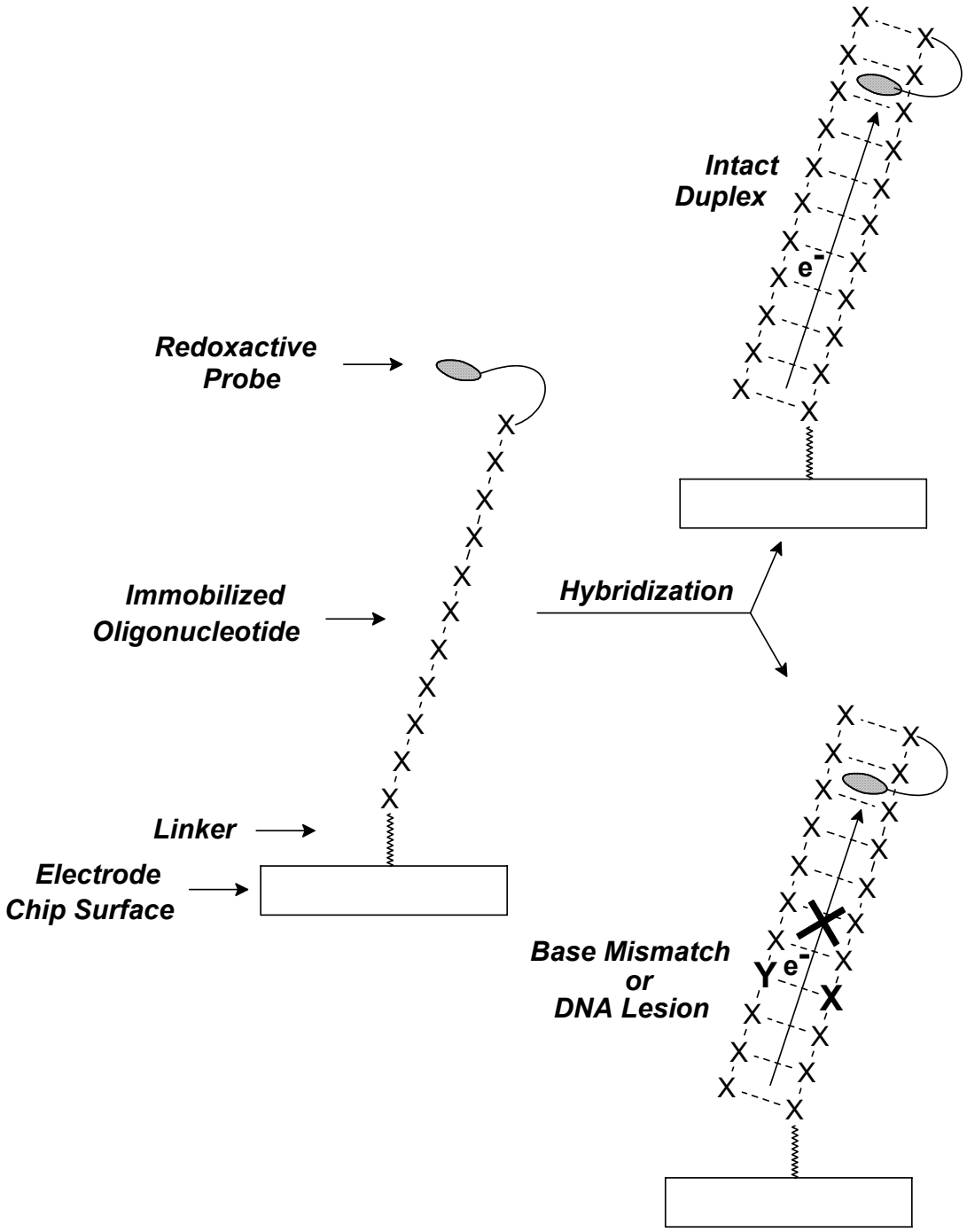

Figure 2-17. Electron transfer in DNA chip technology. The oligonucleotide is immobilized on the chip surface or an electrode and modified with a redoxactive probe. After hybridization, an efficient electron transfer can only take place in intact DNA duplexes. Single-base mismatches or DNA lesions interrupt the electron transfer efficiency significantly.

3 Quantitative Analysis of an Antisense RNA Loop-Loop Complex from the *ColE1* Plasmid Replication System

3.1 Biochemical Background

Replication of the Escherichia coli plasmid *ColE1* is regulated by two RNA transcripts. RNA II, which originates 555 bp upstream of the origin of replication, is transcribed through the origin of replication and forms a persistant RNA-DNA hybrid that is cleaved by RNase H. The short RNA-DNA duplex then acts as the primer for replication by DNA polymerase I. The 108 nt long RNA I is transcribed from 447 nt upstream of the origin of replication in opposite direction to RNA II, and is therefore complementary to the 5'-end of RNA II. Hybridization between RNA I and RNA II alters the conformation of RNA II that is required for formation of the persistant DNA-RNA duplex, and results in failure of RNAseH processing at the replication origin, thus preventing initiation of plasmid replication (Figure 3-1).[179, 180] Both RNA I and RNA II form several stem loops. In the multi-step folding pathway proposed for binding of RNA I to RNA II, a loop-loop kissing interaction between the two RNAs forms as a critical folding intermediate that holds the RNA molecules in close proximity to allow complete hybridization of RNA I to the 5'-terminus of RNA II (Figure 3-2).[181-184] The 63 residue, plasmid encoded RNA one modulator (Rom) protein enhances the stability of the intermediate RNA I and RNA II loop-loop complex, and thereby acts as an auxiliary repressor of replication (Figure 3-1).[185, 186] The *ColE1* plasmid replication is strongly controlled by this antisense RNA regulatory system. It is intriguing to think about using the same antisense principle to regulate gene expression in other cells or organisms, for example to study gene functions or to block a defective gene. The study of natural antisense control systems like *ColE1* will help to understand the structural and kinetic basis for how nature has evolved such efficient regulatory control systems.

Previous studies have demonstrated that individual hairpins derived from the RNA I and RNA II transcripts can interact with remarkable stability, with dissociation constants as low as 10^{-10} M.[185, 187, 188] It has also been demonstrated that the addition of Rom protein stabilizes the loop-loop complex to dissociation and thereby increases the RNA complex lifetime by about two orders of magnitude.[185-187] Footprinting, as well as chemical protection

experiments, indicate that Rom binds specifically to the loop-loop complex, but not the duplex, with a stoichiometry of one Rom per RNA complex.[185, 187]

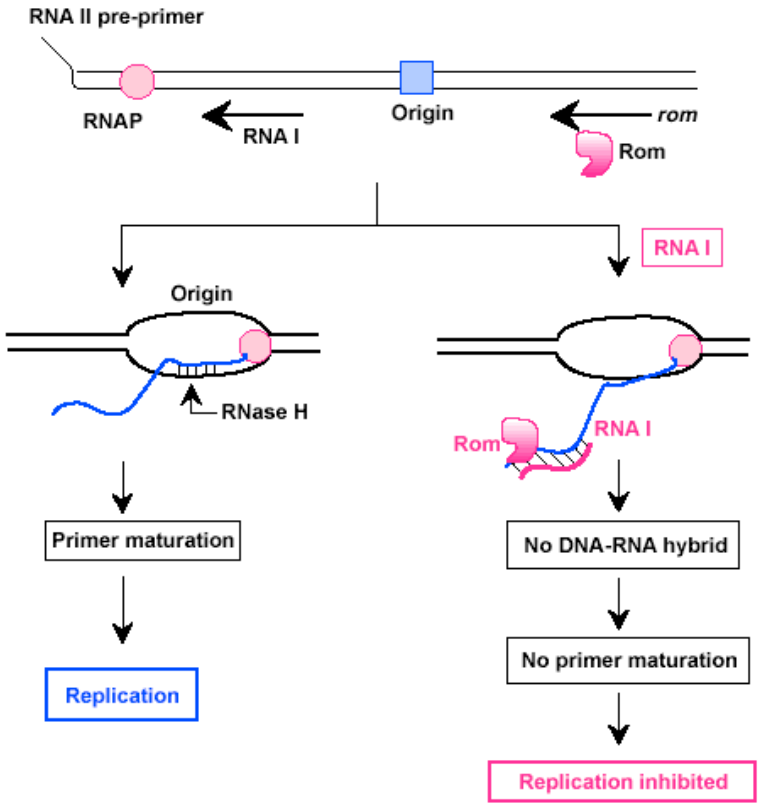

Figure 3-1. Copy number control in *ColE1*. Synthesis of the preprimer RNA II by RNA polymerase (RNAP, stippled circle) is essential for replication. In the absence of interaction with the RNA I (left), the RNA II forms a stable hybrid with the template DNA at the origin of replication. This hybrid is cleaved by RNase H to generate the 3'-OH end of the RNA primer, from which replication starts. Interaction between the inhibitor RNA I and the complementary region in the RNA II preprimer (right) is aided by Rom protein (ellipse). RNA I-RNA II interaction inhibits the formation of the DNA-RNA II hybrid at the origin region, preventing maturation of the RNA II into the replication primer. (taken from [189])

The high-resolution solution structure of an enhanced stability loop-loop complex formed by hairpins derived from RNA I and RNA II with inverted loop sequences (so called R1inv and R2inv) has been determined using NMR spectroscopy.[190, 191] The NMR structure revealed that the complex formed via Watson-Crick base pairing of all seven complementary loop nucleotides thereby making a loop-loop helix which was 3'-stacked between the two stem helices (Figure 3-3). The resulting pseudo-contiguously stacked helical structure showed a pronounced bend towards a compressed major groove of the loop-loop helix.

In this study, the fluorescent probe, 2-aminopurine-2'-O-methyl riboside (2-AP) has been selectively incorporated at adenosine positions in the sequence of stem-loops R1inv and

R2inv (Figure 3-3), such that fluorescence-detected stopped-flow and equilibrium methods could be used to study the mechanism of this RNA kissing interaction. Using these constructs, the detailed kinetics of the RNA-RNA interaction, the divalent metal ion requirement for formation of stable RNA loop-loop complexes and the interaction of Rom with the RNA complex have been analyzed.

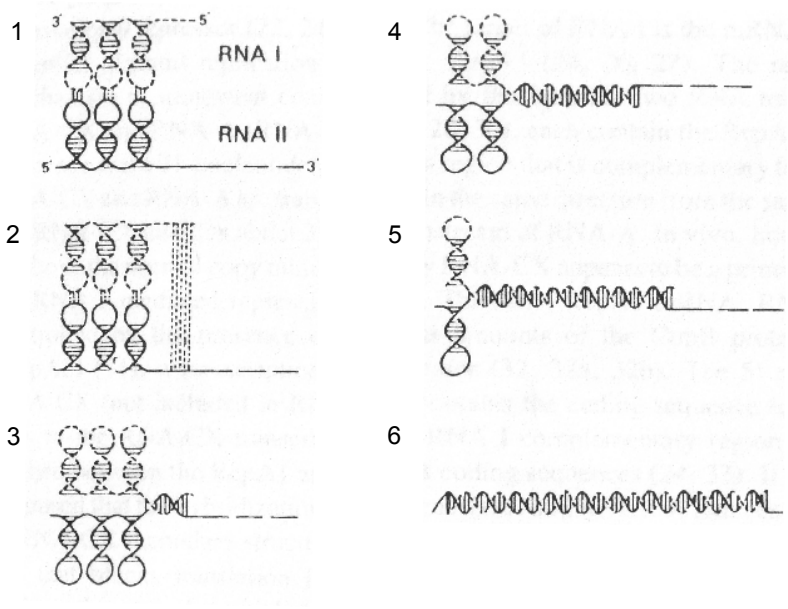

Figure 3-2. Model for the stepwise binding of *ColE1* RNA I to RNA II. In step 1 RNA I and RNA II interact at the loops of their folded structures. This interaction facilitates pairing (step 2) that starts at the 5'-end of RNA I (step 3). At this stage, the loop-loop contacts may be broken. Progressive pairing continues as the stem-and-loop structures unfold (steps 4 and 5). It should be noted that the three pairs of loops do not necessarily interact simultaneously, and RNA II may interact in an alternative folded structure. (taken from [88])

3.2 Sample Preparation and Characterization

3.2.1 RNA Oligonucleotide Preparation

Unlabeled RNA hairpins were synthesized by T7 polymerase run-off transcription using overexpressed and purified T7 polymerase and chemically synthesized DNA templates and primers according to the method of *Milligan and Uhlenbeck*.[192] 2-AP labeled RNA hairpins were chemically synthesized using standard phosphoramidite chemistry. All RNA samples were purified by preparative scale denaturing polyacrylamide gel electrophoresis (PAGE), electroeluted, lyophilized, and dialyzed into the standard buffer.

For details see Materials and Methods.

Rom protein was a kind gift from Lynne Regan (Yale University).

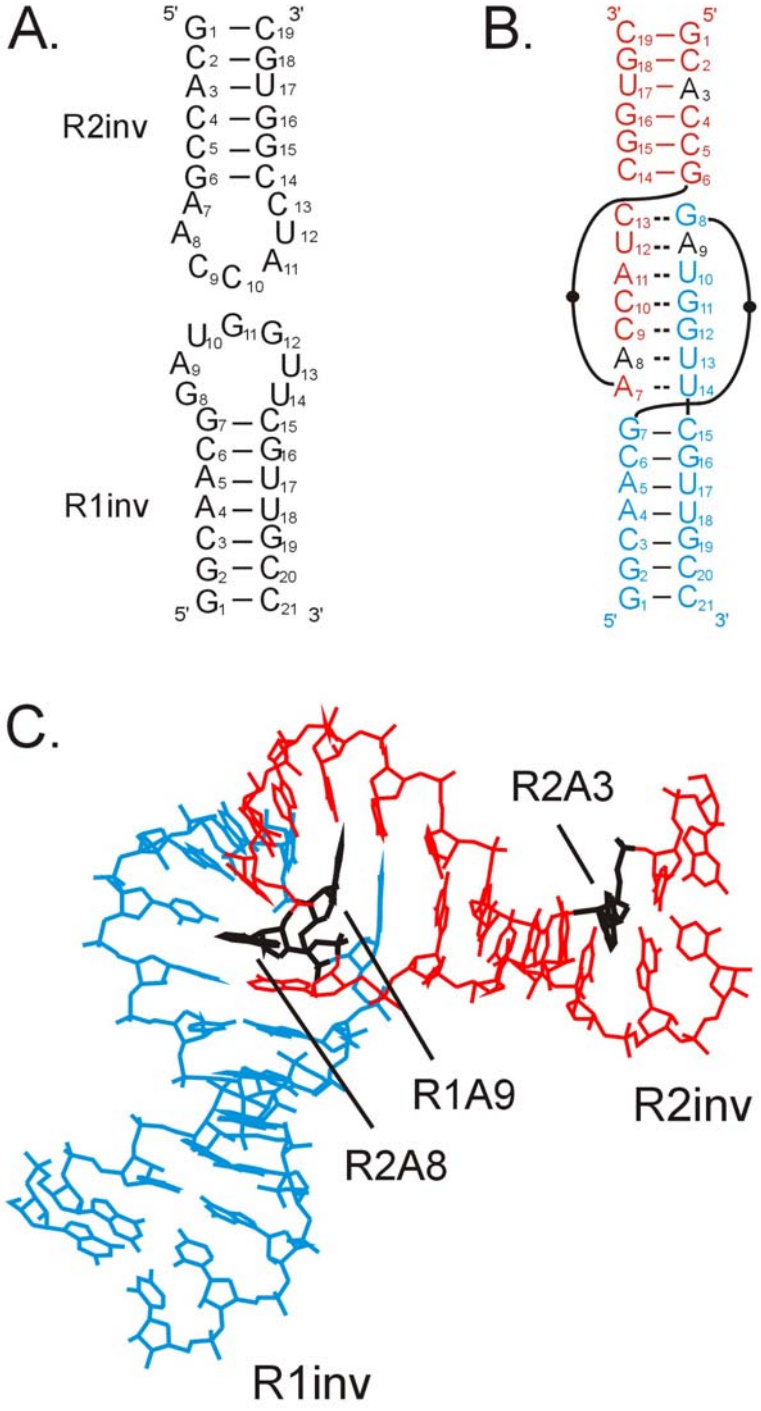

Figure 3-3. (A) RNA sequences of the stem-loop hairpins derived from the *ColE1* plasmid encoded RNA I and RNA II transcripts (so called R1inv and R2inv). (B) Base pairing found in the antisense R1inv-R2inv loop-loop complex formed by these hairpins. The R2inv sequence is shown in red letters and the R1inv sequence in blue letters. Intramolecular base pairs are indicated by solid lines and intermolecular base pairs are indicated by dashed lines. Nucleotide positions in R2inv (A3 and A8) and in R1inv (A9) that were substituted with the fluorescent probe 2-aminopurine-2'-O-methyl riboside (2-AP) in this study are shown in black. (C) Stick representation of the NMR determined structure of the R1inv-R2inv loop-loop complex, with the sequence of R1inv in blue, the sequence of R2inv in red and the 2-AP substituted residues in black.

3.2.2 Samples Used

The RNA oligonucleotide sequences used for this study are shown in Figure 3-3. They are hairpins derived from RNA I and RNA II. The loops were inverted compared to the wild-type sequence to enhance the stability of the complex,[188] which is indicated by an 'inv' after the stem-loop name. Also, the stem sequence of R1inv was altered slightly compared to the wild-type sequence by exchanging the third C-G base pair from the loop with an A-U base pair to prevent complete hybridization of the two oligonucleotides.[187] To facilitate the fluorescence experiments, 2-aminopurine was placed at naturally occurring adenine positions in the loop (to observe complex formation) and in the stem (as a control): at position A9 in R1inv to give R1inv-9ap, at position A8 in R2inv to give R2inv-8ap, and at position A3 in R2inv to give R2inv-3ap (Figure 3-3).

The Rom protein is a four-helix-bundle protein with two identical subunits, each consisting of 63 amino acids forming two antiparallel α-helices of approximately the same length, connected by a short linker segment (Figure 3-4).[193, 194]

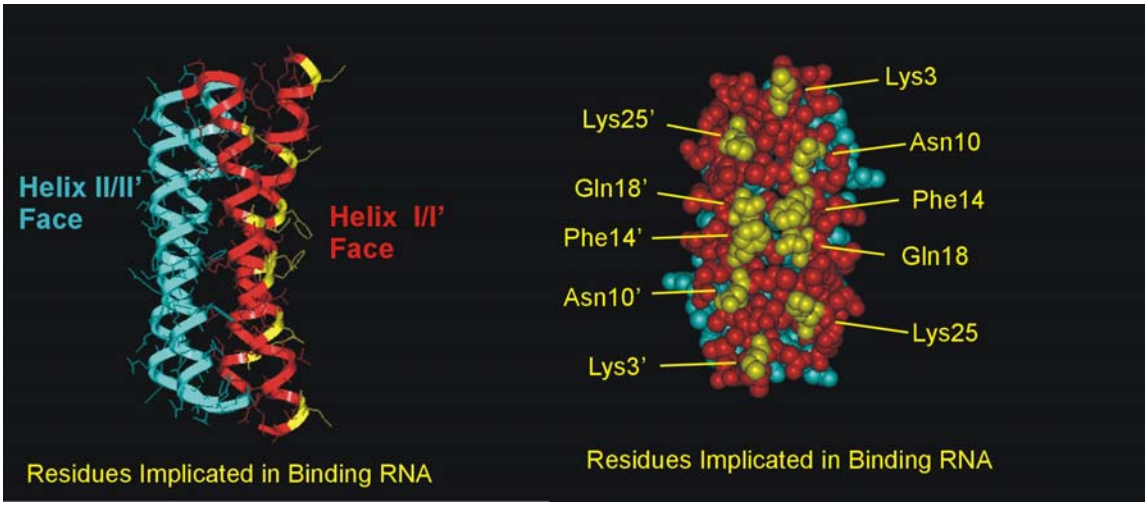

Figure 3-4. Structure of Rom protein. Residues that are implicated in binding RNA are indicated in yellow.

3.2.3 Native Gel Electrophoresis and UV Melt

To confirm independently of the fluorescence measurements that no structural perturbation resulted from substitution of 2-AP probes in R1inv and R2inv, native gel electrophoresis and UV-melting analysis were performed using the 2-AP constructs.

For all 2-AP RNA constructs used in this study, stable complexes could be observed, that were super-shifted by Rom protein, under identical native gel conditions as were used to observe RNA complex formation and Rom binding of the unlabeled hairpins (Figure 3-5).

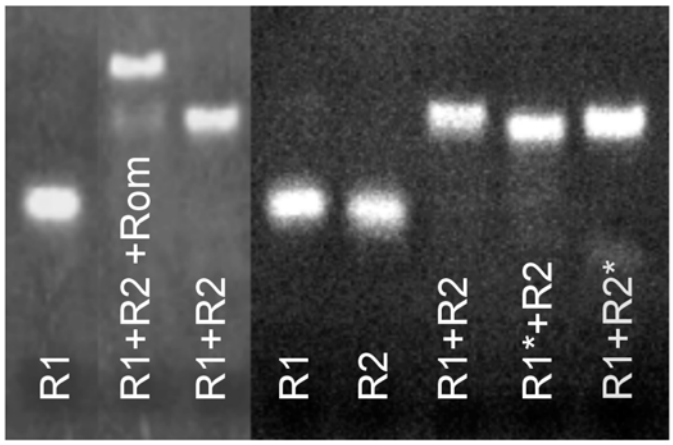

Figure 3-5. Polyacrylamide assay used to detect the Rom-RNA interaction. The gel was stained with ethidium bromide and visualized on a UV transilluminator. Free R1inv is shown in lanes 1 and 4, R2inv in lane 5. Lanes 6, 7 and 8 show the complexes formed by R1inv + R2inv, R1inv-9ap + R2inv, and R1inv + R2inv-8ap, respectively. Rom binds to these complexes to form a ternary complex, which migrates with even lower mobility, lane 2.

UV-melting curves measured for loop-loop complexes formed by the 2-AP RNA constructs were practically indistinguishable from melts of unlabeled complexes, with approximately the same melting temperatures (T_m) observed for loop-loop ($T_m \sim 62$ °C) and hairpin ($T_m > 85$ °C) helix melting transitions in all cases (Figure 3-6).

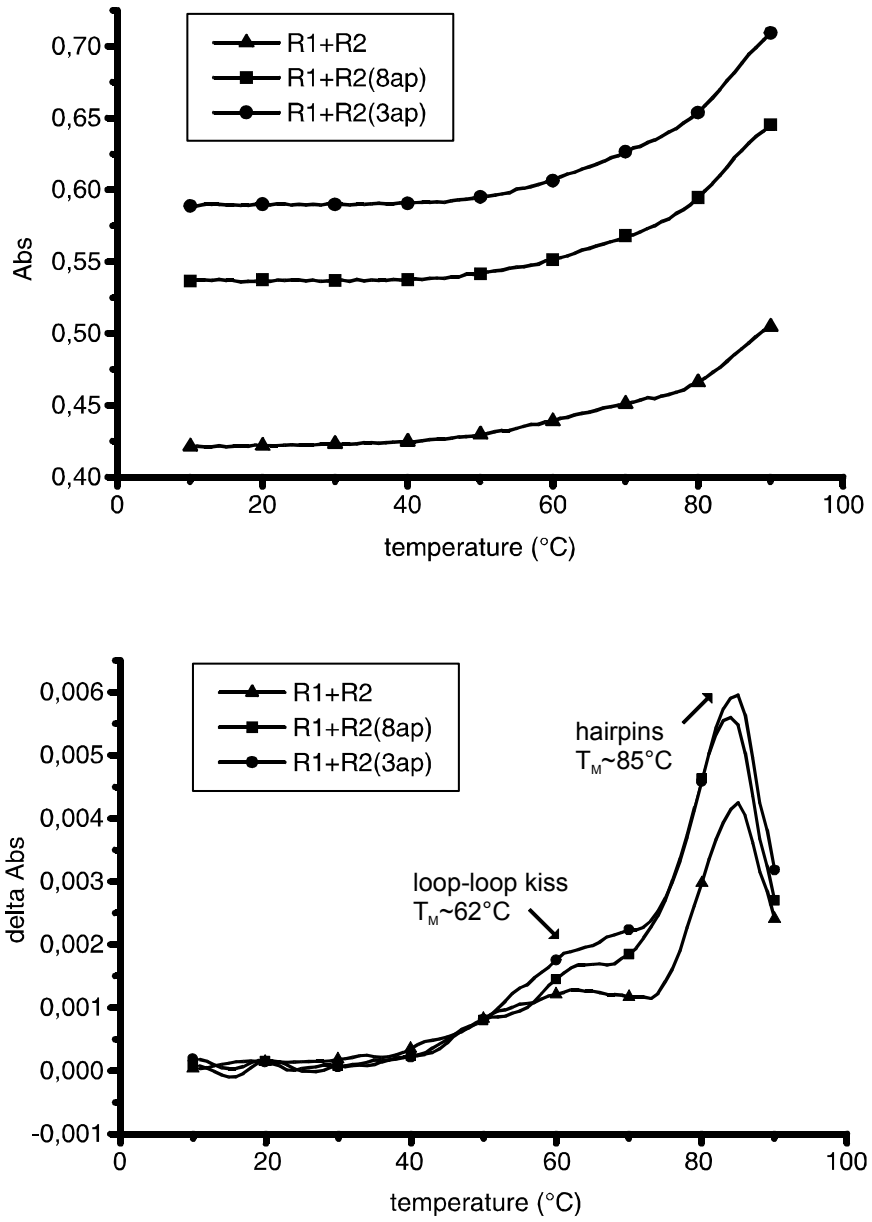

Figure 3-6. (A) UV-melting curves of kissing complexes with and without 2-AP labels. UV melts were recorded in melting buffer with 5 mM Mg^{2+}, at a heating rate of 0.25°C/min. (B) Derivatives of melting curves with local maxima showing melting temperatures of the loop-loop kissing interaction (T_m~62°C) and hairpins (T_m~85°C), respectively.

3.3 Fluorescence Experiments

3.3.1 Kinetics of Kiss Formation with Mg^{2+}

Incorporation of single 2-AP probes at naturally occurring adenosine positions of the R1inv and R2inv hairpins (Figure 3-3) provided sensitive probes for measurement of RNA loop-loop complex equilibrium binding and real time kinetic measurements by fluorescence quenching.

To determine the equilibrium binding constants, K_D, of the R1inv and R2inv hairpins, a fixed concentration of one sample with a 2-AP label was titrated with increasing amounts of unlabeled complement in standard buffer in the presence of 5 mM Mg^{2+}.

In Figure 3-7, it is shown that the intensity of the 2-AP emission spectrum of R1inv-9ap construct is initially relatively high and decreases in a saturable fashion as the concentration of R2inv is increased, with a maximal decrease of about five-fold. The direction of the fluorescence change indicates that the 9ap substituted base becomes stacked upon binding to R2inv, which is consistent with the formation of a R1A9-R2U12 base pair as observed in the NMR structure of the inverted loop-loop complex (Figure 3-3).[190, 191] By fitting the data shown in Figure 3-7B to equation 9.2, a K_D = 0.23 ± 0.19 nM for RNA loop-loop complex formation at 25 °C was calculated. In additional measurements in which the R1inv-9ap concentration was varied from 25 to 100 nM (n = 2), an average K_D value of 1.6 ± 1.1 nM for RNA loop-loop complex formation was determined. (Note that the precision of determined K_Ds was lower for certain experiments due to the fact that reactions were measured at concentrations that approximated stoichiometric binding conditions).

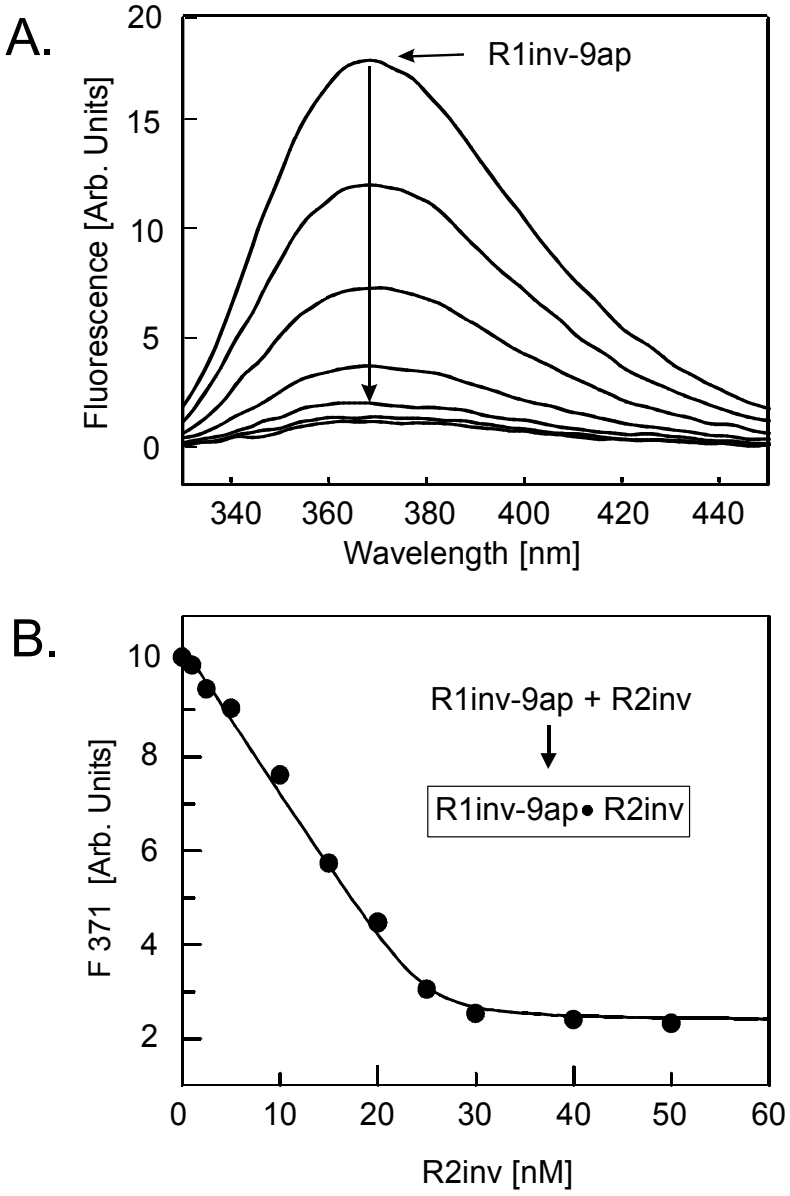

Figure 3-7. Fluorescence changes accompanying titration of 2-AP labeled R1inv-9ap with R2inv. (A) Fluorescence emission spectra from 330 to 450 nm as a function of titration of 100 nM R1inv-9ap with increasing concentrations of R2inv in standard buffer [25 mM NaCl, 1 mM cacodylate (pH 6.5)] with 5 mM $MgCl_2$ at 25 °C. (B) Plot of the relative fluorescence decrease at 371 nm as a function of total R2inv concentration for a titration using 25 nM R1inv-9ap. The solid curve is a fit to equation 9.2 ($K_D = 0.23 \pm 0.19$ nM). The species that is directly detected in the experiment is marked with a box in the panel.

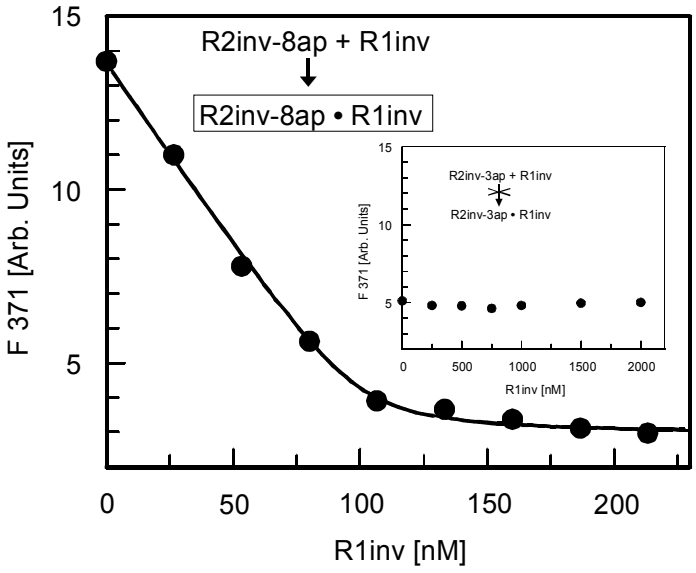

Figure 3-8. Plot of the relative fluorescence decrease at 371 nm as a function of total R1inv concentration for a titration using 100 nM R2inv-8ap. The solid curve is a fit to equation 9.2 (K_D = 3.6 ± 2.2 nM). The species that is directly detected in the experiment is marked with a box in the panel. inset: Fluorescence at 371 nm as a function of total R2inv concentration for a titration using 500 nM R2inv-3ap. Fluorescence of the free R2inv-3ap is initially quenched and shows no appreciable change upon titration with R1inv.

The formation of the RNA loop-loop complex could also be monitored using the intensity of the 2-AP emission spectrum of the R2inv-8ap RNA hairpin construct as a function of R1inv concentration. For the R2inv-8ap hairpin, the 2-AP emission spectrum is also initially relatively high and decreases in a saturable fashion as the concentration of R1inv is increased (Figure 3-8). As observed for the R1inv-9ap construct, the direction of the fluorescence change indicates that 2-AP probes become stacked upon binding to R1inv, which is again consistent with the NMR structure of the loop-loop complex. By fitting the data in Figure 3-8 to equation 9.2, a K_D = 3.6 ± 2.2 nM for RNA loop-loop complex formation at 25 °C was calculated. In contrast to these two 2-AP RNA hairpin constructs, a control hairpin with the 2-AP label placed in the stem (R2inv-3ap) showed an initially highly quenched state in the hairpin alone and produced no appreciable fluorescence change upon titration with R1inv (Figure 3-8, inset). This confirms that the principle reason for quenching of the 2-AP probes placed in the complementary loops is the formation of the loop-loop helix upon RNA-RNA association and that stacking of the stem base pairs is not significantly perturbed when the complex forms.

The average K_D measured here using 2-AP fluorescence for the inverted RNA loop-loop complex (K_{Dav} = 2.6 ± 1.7 nM) is consistent with the K_D = 0.57 nM that was previously

measured at 25 °C by following the formation of enzymatic cleavage products using denaturing gel electrophoresis.[185, 187] The results obtained using the fluorescence measurements, together with the results of native PAGE and UV-melting analysis, therefore demonstrate that 2-AP probes do not significantly affect RNA complex formation and can act as sensitive reporters for complex formation. The K_Ds determined using the different 2-AP RNA constructs are summarized in Table 3-1.

Using these 2-AP labeled RNA hairpins, the off-rate, k_{off}, of the kissing complex could also be determined with steady-state fluorescence by following the increase in 2-AP fluorescence of either R2inv-8ap • R1inv or R1inv-9ap • R2inv as the RNA complex dissociates. To a preformed loop-loop complex of, for example, R1inv-9ap and R2inv a 20-fold excess of unlabeled R1inv was added, making the dissociation of the complex irreversible by trapping free R2inv and thereby preventing rebinding of the dissociated hairpin to the 2-AP labeled complement, and the increase in fluorescence from the free R1inv-9ap could be observed. The same experiment was also performed using R2inv-8ap and R1inv as the preformed complex, and adding an excess amount of unlabeled R2inv. From these experiments an average k_{off} = 8.9 x 10^{-5} s^{-1} can be determined (Figure 3-9, Table 3-1).

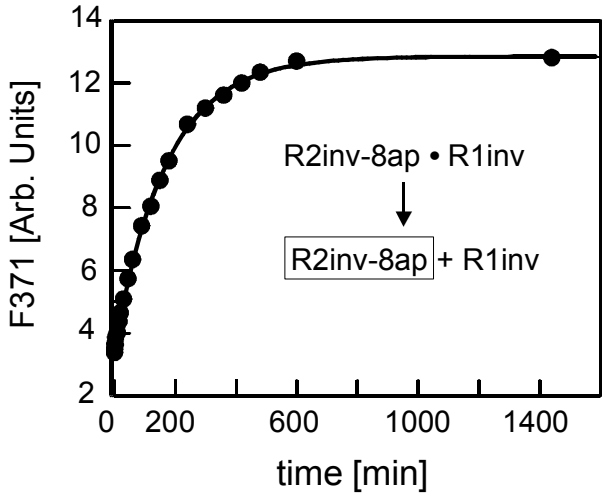

Figure 3-9. Determination of the R1inv off-rate from R2inv-8ap using unlabeled R2inv as an irreversible trap for the free R1inv. A complex consisting of 100 nM each R2inv-8ap and R1inv was rapidly mixed by hand with a solution of 2 μM R2inv. A k_{off} of 9.7 x 10^{-5} s^{-1} for R2inv-8ap•R1inv complex was determined from this experiment.

Table 3-1. Kinetic Rates and Thermodynamic Binding Constants

RNA Constructs	K_D [RNA• RNA] (nM)	K_D [RNA•Rom] (nM)	k_{off} (s^{-1})	k_1 ($\mu M^{-1} s^{-1}$)	k_2 (s^{-1})	$k_{-1} k_{-2}$ (s^{-2})	K_D^{calc} (nM)
R1inv-9AP + R2inv	1.6 ± 1.1	56 ± 26	$8.2 \times 10^{-5} \pm 0.03$	0.12 ± 0.12	0.09 ± 0.03	7.3×10^{-6}	0.68
R2inv-8AP + R1inv	3.6 ± 2.2	64 ± 22	$9.7 \times 10^{-5} \pm 0.01$	0.14 ± 0.08	0.09 ± 0.04	7.7×10^{-6}	0.61

Measurements were made in the standard buffer at 25°C. The thermodynamic parameters represent average values from different experiments, and the errors are standard uncertainties. The kinetic constants correspond to the two-step binding mechanism in equation 9.5. The equilibrium constant K_D for the RNA loop-loop complex formation was calculated from the kinetic constants (i.e. $K_D^{calc} = k_{-1}k_{-2}/k_1k_2$).

To determine the association kinetics of RNA inverted loop complex formation, stopped-flow fluorescence experiments were performed at 25 °C in standard buffer solution with 5 mM $MgCl_2$.

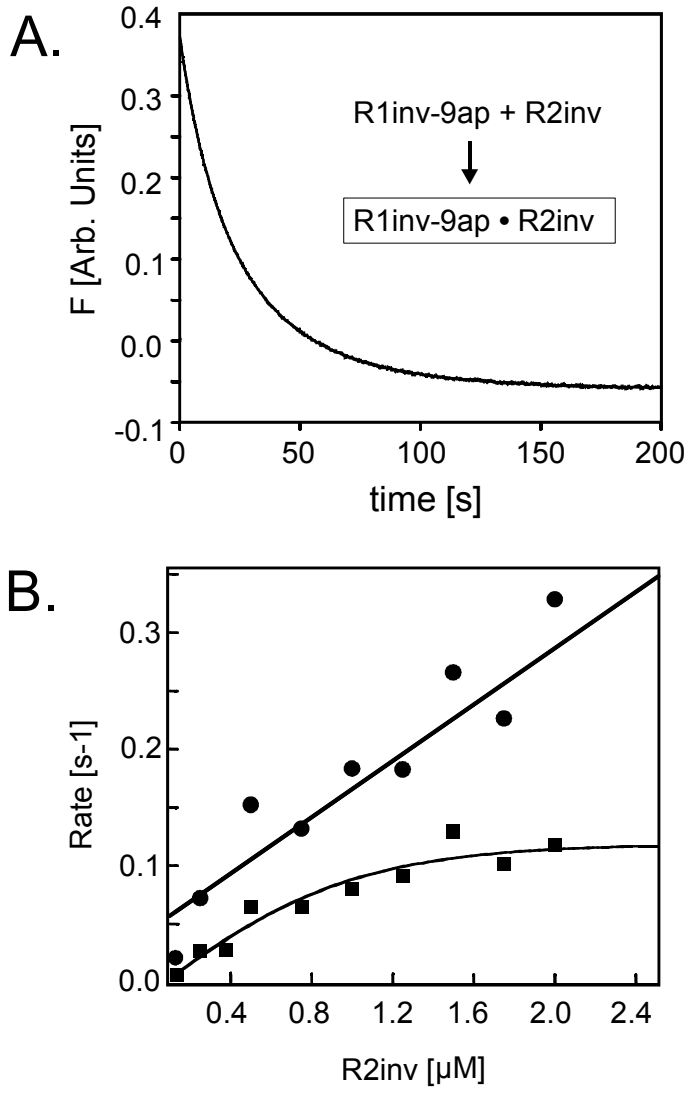

Figure 3-10. Kinetic measurements of RNA complex formation between R1inv and R2inv hairpins. (A) Stopped-flow measurement of the association rate by monitoring the fluorescence change at $\lambda >$ 335 nm upon rapid mixing of R1inv-9ap with R2inv. The representative trace was obtained at 100 nM R1inv-9ap and 500 nM R1inv concentration and fit to a double exponential equation (k_1 = 0.013 s^{-1}, k_2 = 0.0049 s^{-1}). (B) Concentration dependence of the two kinetic phases of the R1inv • R2inv complex formation. The linear dependent rates are plotted as filled circles and the hyperbolic dependent rates as filled squares.

The kinetics of RNA complex formation was followed using pseudo-first order conditions, where the unlabeled hairpin was present at concentrations 20-fold greater than the labeled one. The time course of the decrease in 2-AP fluorescence (F_t) as a result of loop-loop complex formation showed two kinetic phases (Figure 3-10) which suggests a two-step binding mechanism. Rate constants measured using observed fluorescence changes for the 2-AP probes placed in the complementary loops of either R1inv or R2inv hairpin were found, within the error of the measurements, to be the same. Thus, the 2-AP probes appear to report on similar global folding events associated with RNA binding that are manifested in changes in the local 2-AP microenvironment.

In experiments using R1inv-9ap as the labeled hairpin and R2inv in concentrations ranging from 5- to 25-fold R1inv-9ap concentration, one kinetic phase is found to be linearly dependent on complementary unlabeled RNA hairpin concentration, while a second phase follows approximately a hyperbolic dependence on unlabeled RNA hairpin concentration (Figure 3-10).

The concentration dependence of the observed rates of binding was fit using the simple two-step binding mechanism of equation 3.1:

$$\text{R1inv} + \text{R2inv} \underset{k_{-1}}{\overset{k_1}{\rightleftharpoons}} \text{R1inv•R2inv} \underset{k_{-2}}{\overset{k_2}{\rightleftharpoons}} \text{R1inv•R2inv*} \qquad (3.1)$$

The linearly dependent rate was fit to the equation $k_{obs} = k_1[\text{R2inv}] + (k_{-1} + k_2 + k_{-2})$. For a kinetic mechanism as described in equation 3.1, the slope of the linear phase is equal to the observed on-rate, k_1, and the *y*-intercept is equal to the sum of $k_{-1} + k_{-2} + k_2$.[195] An average $k_1 = 0.13\ \mu M^{-1}\ s^{-1}$ has been determined based on the slope of the linear phase. For the hyperbolically dependent phase, the asymptotic rate is equal to the sum $k_2 + k_{-2}$, and the *y*-intercept provides a crude estimate of the off-rate k_{-2}. The maximal rate ($k_{max} = k_2 + k_{-2}$) was estimated from the maximum of the hyperbolic dependent rate. Since $(k_{-1} + k_{-2}) << k_2$, an average k_2 of $0.09\ s^{-1}$ was estimated by assuming k_{-1} and k_{-2} were equal to zero in these equations. Due to the extremely slow rates, k_{-1} and k_{-2} could not be determined explicitly from fitting the curves in Figure 3-10B and only an approximate upper limit of $10^{-2}\ s^{-1}$ can be assigned for k_{-1} and k_{-2}. However, using the measured k_{off}, the product of the rate constants $k_{-2}k_{-1}$ could be determined by fitting the equation $k_{off} = (k_{-1}k_{-2})/k_2$ to be 7.5×10^{-6}. The equilibrium binding constant K_D was calculated from the measured microscopic rate constants, $K_D^{calc} = k_{-1}k_{-2}/k_1k_2$, to be on average 0.65 nM, which is in good agreement with the

measured average K_D of 2.6 ± 1.7 nM. Thus, the two-step mechanism is consistent with the thermodynamic measurements on this RNA system. Rate constants for the two-step mechanism are reported in Table 3-1.

3.3.2 Proposed Model: a Two-Step Mechanism for RNA Kissing

In *ColE1*, plasmid copy number is controlled kinetically and depends on the rate by which the antisense(RNA I) - target(RNA II) complex is formed rather than on binding equilibrium. A kissing interaction is the critical first step in the formation of this antisense (RNA I) - target (RNA II) complex. Understanding the details of the mechanism for how the antisense RNA I molecules targets its cognate RNA II target is therefore critical to understanding how these molecules work *in vivo*. In this study, the 2-AP fluorescence detected fast kinetic measurements of the RNA I – RNA II kissing interaction provide the first insight into the details of this important binding reaction on a millisecond to second time scale. From the stopped-flow experiments, 2-AP probes substituted in the complementary loops of the R1inv and R2inv hairpins have been shown to experience at least three different microenvironments during association of the RNA complex (Figure 3-10). The simplest explanation for this observation is that the RNA kissing reaction occurs via a two-step mechanism, with a single kinetic intermediate state. The two-step mechanism for RNA loop-loop complex formation can be described as an initial encounter of the RNA hairpins in which the complementary loops of R1inv and R2inv first base pair to form the loop-loop helix (average k_1 = 1.3 x 10^5 M^{-1} s^{-1}), and then a subsequent isomerization of the RNA complex to the final tertiary fold in a second slower step (average k_2 = 0.09 s^{-1}), where the helical stacking around the junctions is optimized. This three-state model for the folding trajectory for the kissing interaction is shown schematically in Figure 3-11. The second-order rate constant measured for the initial encounter step of the kissing interaction is in the range of values expected for formation of this type of an antisense complex and is consistent with previous estimates.[185, 187] Since (k_{-1} + k_{-2}) is estimated to be much less than k_2, the folding pathway for the kissing interaction (Figure 3-11A) shows energetic barriers to the backward k_{-1} and k_{-2} rates, which are significantly higher than the barrier to the forward rate, k_2. As a consequence of the relative values of k_{-1}, k_2 and k_{-2} and the observation that k_{off} can be fit to a single first order rate, the on-rate can be estimated by k_1 (average k_1 = 1.3 x 10^5 M^{-1} s^{-1}, Table 3-1) and the off-rate by $k_{-1}k_{-2}/k_2$ (average k_{off} = 8.6 x 10^{-5} s^{-1}, Table 3-1). Overall, the low K_D value measured and calculated for the kissing complex formation is therefore largely the result of the slow off-rate.

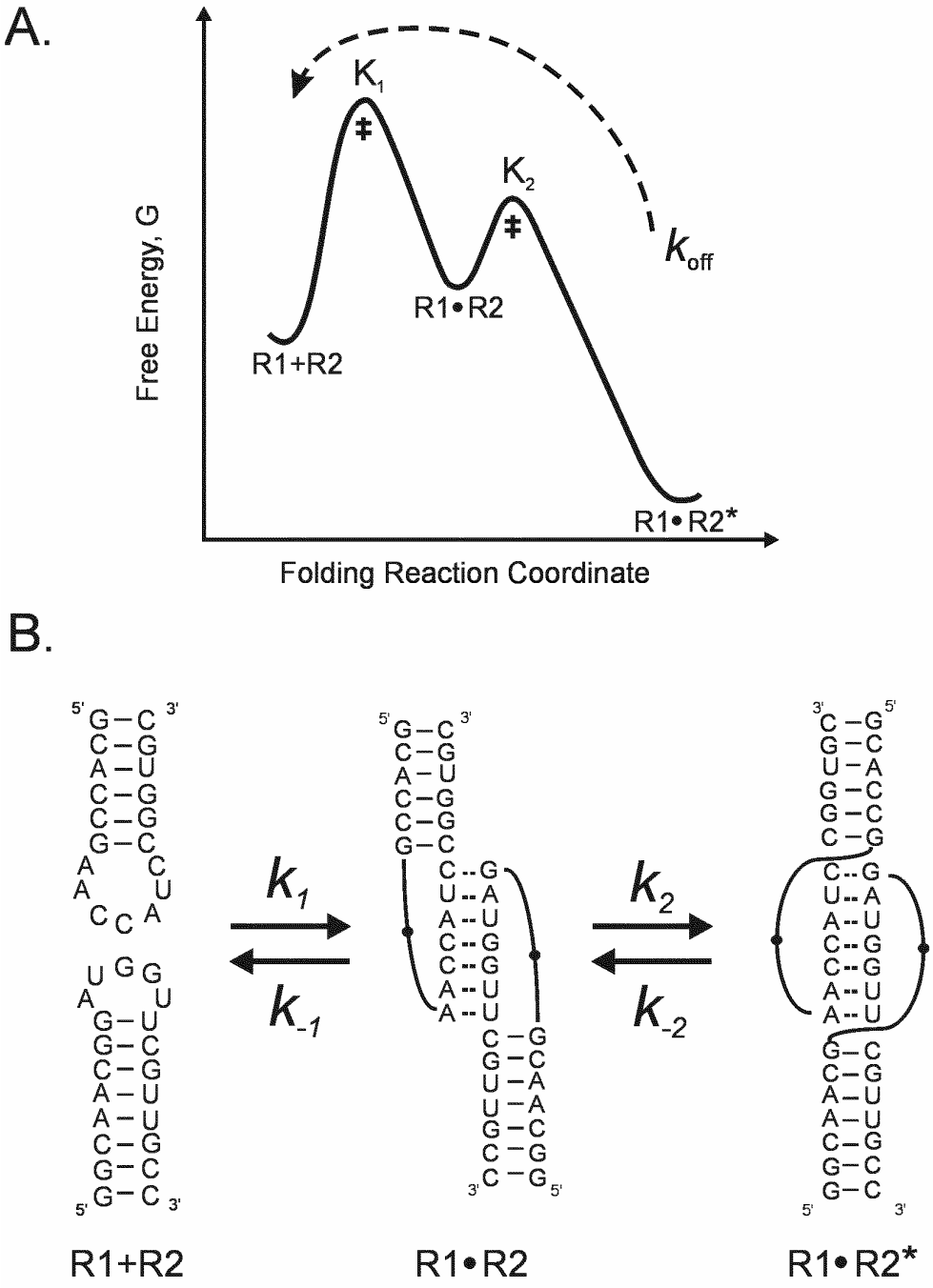

Figure 3-11. (A) Three-state model for the association of the R1inv-R2inv loop-loop kissing complex. A collision complex (R1•R2) initially forms via loop-loop helix formation between the two individual hairpins (R1+R2), which is then followed by a much slower isomerization to the final tertiary fold (R1•R2*). (B) Proposed model for the folding states in the association of the RNA loop-loop complex. In the initial step, the two hairpins (R1+R2) associated to form the loop-loop helix through Watson-Crick base-pairing (R1•R2). In the second step, the complex isomerizes to a more stable tertiary fold (R1•R2*) in which the loop-loop helix is optimally stacked between the two stem helices.

The significant decrease in fluorescence that occurs upon forming the initial encounter complex is consistent with 2-AP-U base pairing and stacking in the initial binding event of loop-loop helix formation (Figure 3-11B). The second slower kinetic transient, which has a smaller amplitude, may represent a final isomerization step in which the RNA complex assumes its final folded conformation. Such an isomerization step may contribute significantly to the total free energy of binding of the complex since it would involve rearrangement to the optimal stacking geometry, especially at the junctions between the stem helices and the loop-loop helix. This idea is consistent with previous findings that base stacking contributes most significantly to the thermodynamic stability of RNA kissing complexes[188] and also suggests that the rate k_{-2} is likely to be significantly slower than k_{-1} in the unfolding pathway.

3.3.3 Metal Ion Requirement for the RNA Loop-Loop Complex Formation

The RNA inverted loop-loop complex investigated here has an extremely stringent divalent metal ion requirement for formation of a stable interaction. The NMR spectra of the imino proton region show remarkably that formation of the RNA loop-loop complex absolutely requires divalent metal ion cofactors even at millimolar concentration of RNA (Figure 3-12). This contrasts other studied RNA antisense loop-loop complexes that can form at higher concentrations without a divalent ion cofactor or can form in the presence of monovalent cations at an approximately 10-fold higher concentration than required for divalent cations.[196-198]

To further explore the stringency of the requirement of the divalent metal ion cofactor for RNA complex formation, apparent binding constants for a series of divalent cations binding to the RNA inverted loop-loop complex were determined (Table 3-2). In this experiment the decrease in fluorescence (F) at 371 nm was monitored as a fixed concentration of R1inv-9ap and R2inv, mixed in 1:1 stoichiometry in standard buffer, was titrated with increasing amounts of the divalent metal ion. Metal binding, which induces RNA complex formation, was monitored indirectly by measuring 2-AP quenching associated with RNA loop-loop complex formation, from which apparent binding constants were calculated.

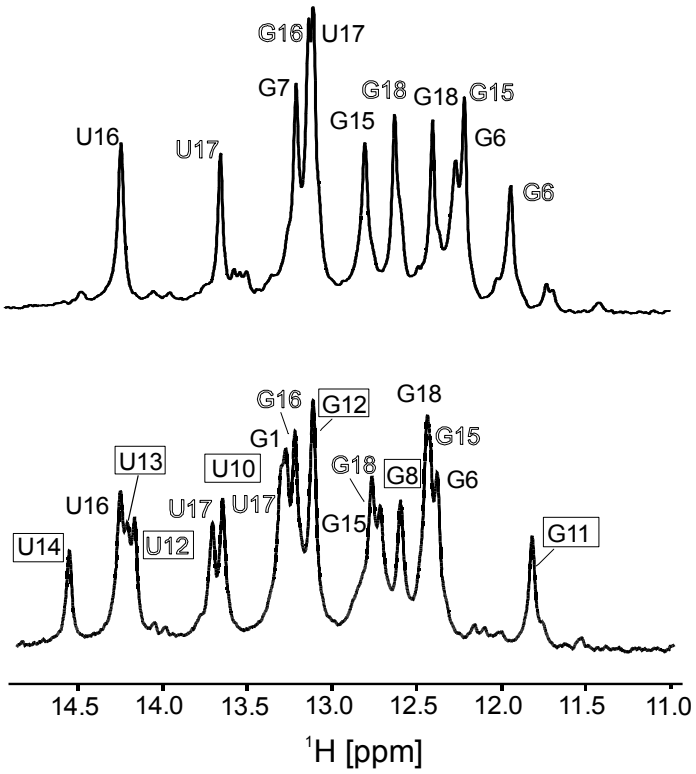

Figure 3-12. 1D proton spectra of the imino region of a 1:1 stoichiometric mixture of the R1inv and R2inv hairpins in standard buffer [upper trace] and in standard buffer with the addition of 5 mM $MgCl_2$ [lower trace]. In both traces, imino proton resonances are labeled as edged letters for those assigned to the R2inv sequence and as solid letters for those assigned to the R1inv sequence. In the lower trace, additional imino proton resonances observed upon formation of the loop-loop complex are boxed. (spectra acquired by J.P. Marino)

Table 3-2. Apparent metal ion binding constants to R1inv-9ap + R2inv

metal ions	$K_{D\ app}$	ΔF
Mg^{2+}	618 µM	83%
Ca^{2+}	738 µM	89%
Sr^{2+}	2289 µM	74%
Ba^{2+}	2575 µM	66%
Zn^{2+}	163 µM	85%
Mn^{2+}	358 µM	90%
Cd^{2+}	766 µM	82%

Solutions of divalent metal ions were titrated to a 1:1 mixture of R1inv-9ap and R2inv, and decrease in fluorescence intensity observed. Data was fit to an equilibrium binding equation assuming a single class of metal binding sites. ΔF is the relative change in fluorescence upon metal ion titration.

In contrast to the observed fluorescence decrease at 371 nm associated with the titration of R1inv and R2inv with divalent cations, titration of the RNA hairpins with monovalent cations resulted in no significant change in fluorescence emission at 371 nm up to a concentration of 1.0 M (Figure 3-13A), indicating that the loop-loop complex formation can not be induced by monovalent cations.

For all divalent metal ions investigated (Table 3-2), binding of the metal, as detected as a function of loop-loop complex formation, is saturable (Figure 3-13B). However, the extent of the 2-AP quench upon RNA complex formation observed with different metals varied by up to a factor of 0.25. For example, titration with strontium resulted in only about 75% of the 2-AP quench observed in the magnesium experiment (Figure 3-13B). This suggests that for larger metals to be accommodated into the metal binding pocket, the loop-loop helix in the RNA complexes are slightly destacked and hence the fluorescence quench is only a fraction of that observed for smaller metals, like magnesium.

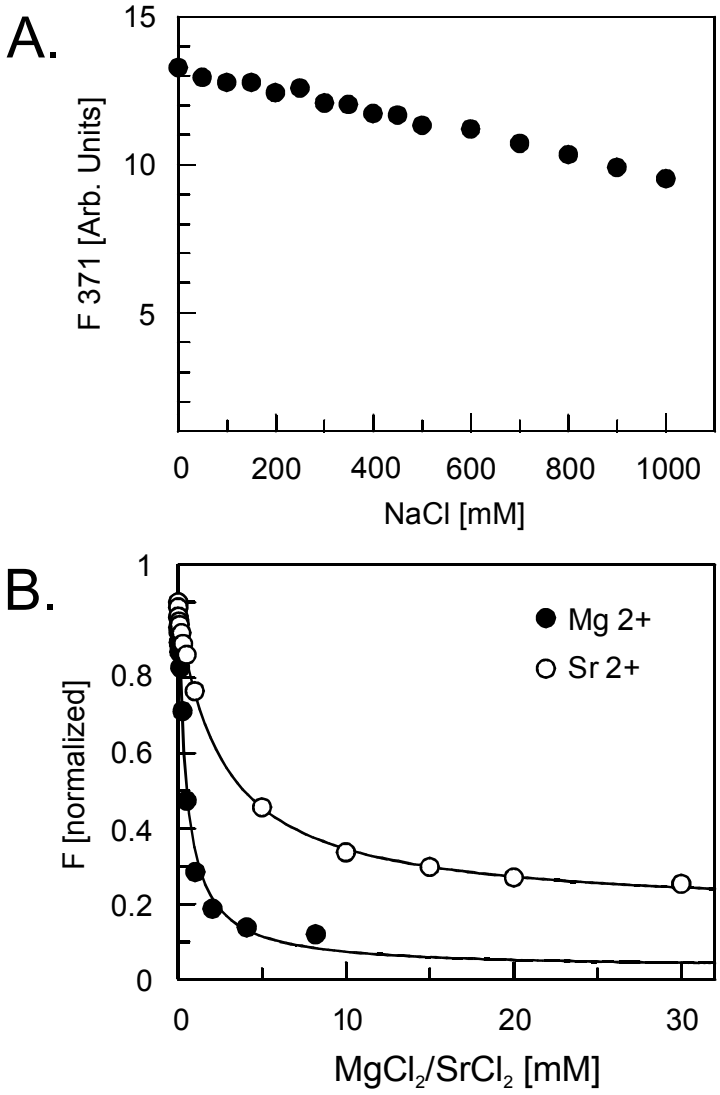

Figure 3-13. (A) Titration of 100nM R2inv-8ap + 100nM R1inv with NaCl. No significant or saturable change in fluorescence is observed up to a NaCl concentration of 1M. (B) Fluorescence changes accompanying titration of a 1:1 stoichiometric mixture of R1inv-9ap and R2inv with $MgCl_2$ (solid circles) and $SrCl_2$ (hollow circles). The relative fluorescence decrease at 371 nm as a function of total metal ion concentration is plotted.

These results, together with the fact that monovalent cations can not be substituted for divalent cations in binding and stabilizing the loop-loop complex, strongly suggest that the binding site for the required metal ion cofactor must accommodate two positive charges in a sterically restricted, although somewhat flexible, cavity.

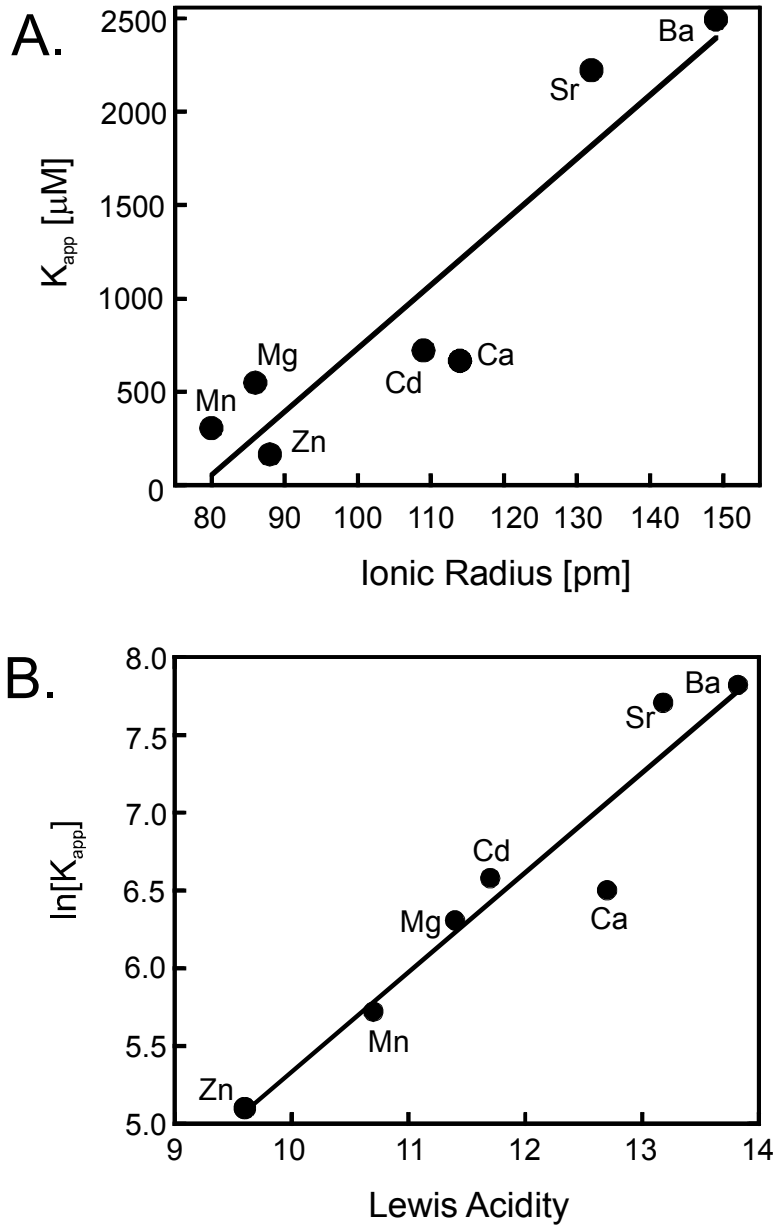

Figure 3-14. (A) The apparent binding constants K_{app} for a series of divalent cations plotted as a function of ionic radius. (B) The natural logarithm of the K_{app}, ln[K_{app}], for a series of divalent cations plotted as a function of Lewis acidity.

The high degree of specificity of the divalent metal requirement for stable loop-loop complex formation is further demonstrated by the dependence of the apparent binding constants K_{app} of different metal ions for promoting RNA complex formation on cationic radius and Lewis acidity, as shown in Figure 3-14. The linear dependence of the K_{app} on the cation radius shows that the specific metal binding pocket for the divalent metal ion cofactor is very sensitive to the size of the hydrated cation, with smaller divalent cations showing higher affinities. A dependence of the ln[K_{app}] on Lewis acidity was also found to be quite remarkable, with more

acidic ions binding more tightly to the specific site(s) that stabilize the RNA complex. The linear correlation between $\ln[K_{app}]$, which is proportional to the free energy of metal binding to the loop-loop complex stabilizing site(s), and the Lewis acidity suggests that deprotonation of the hydration sphere of the metal ion may be associated with complex formation. This conclusion is consistent with earlier results that showed a pK_a and ionic radius dependence to the thermal stability of the RNA complex.[188] In summary, the ionic dependence shows clearly that smaller, more acidic cations bind and stabilize the loop-loop complex with higher apparent affinity than larger, more basic cations.

3.3.4 Rom Binding Kinetics

As discussed above, the observed variation of the degree of 2-AP quenching indicates that RNA complexes formed by larger more basic metals, such as Sr^{2+}, are not as well stacked as those complexes formed with smaller more acidic metals. The binding of Rom to RNA complexes formed with these larger metals, resulted in a further decrease of 2-AP fluorescence. This offered an elegant way of determining the equilibrium binding constant of Rom to the RNA loop-loop complex by observing the decrease in 2-AP fluorescence as a complex of R1inv-9ap and R2inv, preformed in a buffer containing 30 mM Sr^{2+}, was titrated with Rom. Figure 3-15 shows a trace of the 2-AP emission spectrum of R1inv-9ap mixed with R2inv in the absence of any divalent metal ion, in the presence of 30 mM $SrCl_2$, where 100 % RNA loop-loop complex was observed, and after titration with Rom protein. The addition of Rom protein to the RNA complex formed in the presence of 30 mM $SrCl_2$ resulted in a further decrease in the 2-AP fluorescence of R2inv • R1inv-9ap in a saturable fashion, with a maximal decrease of about 25% of the original fluorescence.

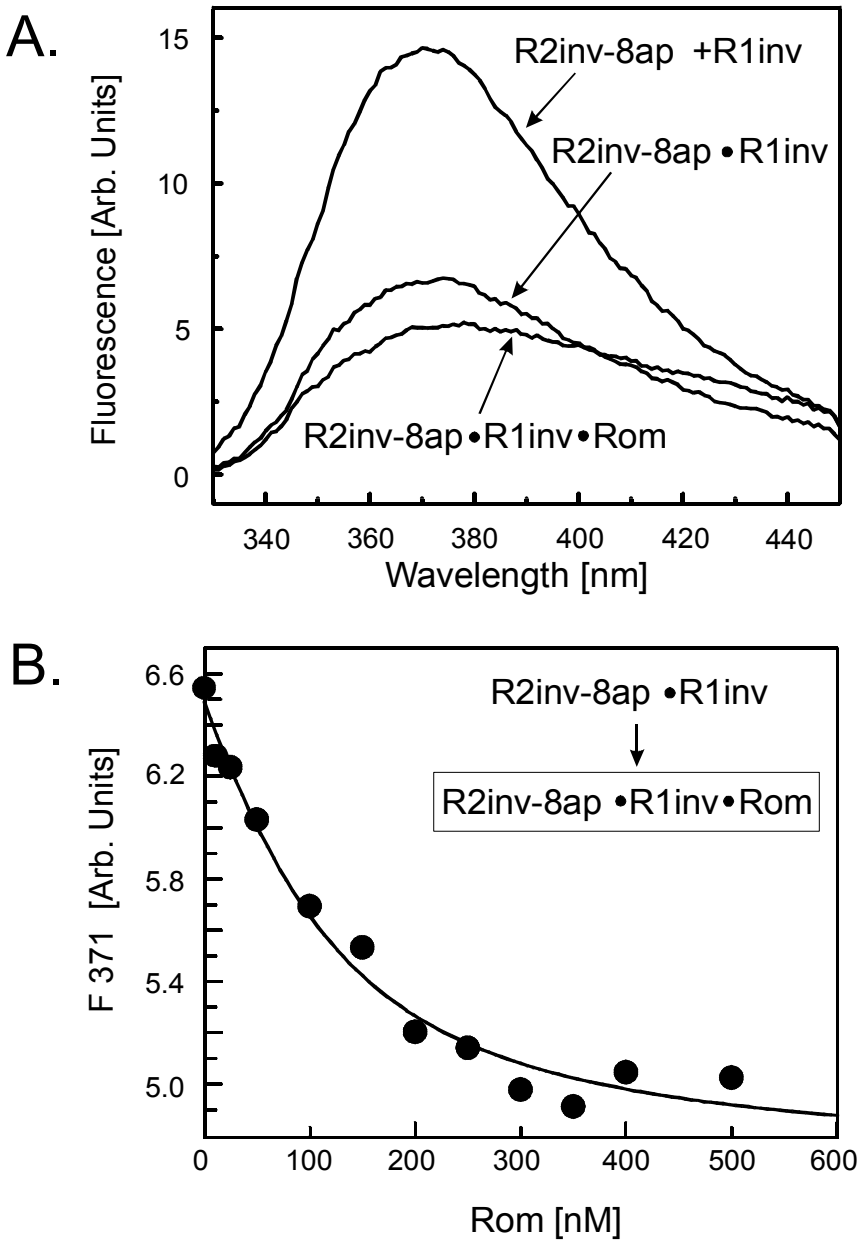

Figure 3-15. Fluorescence changes accompanying titration of the RNA loop-loop complex formed between R1inv and R2inv in the presence of 30 mM $SrCl_2$ with Rom. (A) Fluorescence emission spectra from 330 to 450 nm of the 1:1 stoichiometric mixture of R1inv-9ap and R2inv in standard buffer (R1inv-9ap + R2inv), with 30 mM $SrCl_2$ added (R1inv-9ap•R2inv), and after titration with Rom is completed (R1inv-9ap•R2inv•Rom). Note that at this concentration of Sr^{+2}, 100 % RNA loop-loop complex was observed so that the binding data could be fitted using a single-site binding mode for Rom according to equation 9.4. (B) Plot of the relative fluorescence decrease at 371 nm accompanying titration of 100 nM R1inv•R2inv-8ap complex with increasing concentrations of Rom protein. The solid curve is a fit to equation 9.4 (K_D = 64 ± 22 nM). The species that is directly detected in the experiment is marked with a box in the panel.

By fitting the data shown in Figure 3-15B to equation 9.4, a K_D = 64 ± 22 nM for Rom binding to the RNA loop-loop complex at 25 °C was calculated. These results (Table 3-1) indicate that RNA complexes formed with the 2-AP construct are also still able to bind specifically to the Rom protein with native-like affinity.[185, 199]

The fluorescence decrease associated with Rom binding to these complexes indicates that Rom can induce more ideal stacking of the loop-loop helix so that 2-AP becomes more stacked, and these complexes display the same degree of fluorescence quench as observed for smaller ideal metals.

The effect of Rom binding on the fluorescence of these loop-loop complexes thus suggests a possible structural mechanism, involving optimization of base stacking in the loop-loop helix, for how Rom might stabilize the RNA complex. This mechanism is consistent with previous studies that indicate that Rom binding induces bending in the RNA loop-loop complex towards the major groove, which may result from a compression of base pairs in the loop-loop helix.[190]

3.4 Summary

2-Aminopurine (2-AP) has been shown in previous studies to be a useful probe of the structure and dynamics of specific sites in DNA,[74, 200] as a monitor for enzyme-DNA[33, 200-202] and RNA-ligand interactions,[76, 203] and to study Mg^{2+}-dependent conformational changes in the hammerhead ribozyme.[72, 204] In this study, a general quantitative method is presented for studying RNA kissing complexes that uses changes in the quantum yield of 2-AP fluorescence emission. It is shown that substitution of 2-AP at positions in the complementary loops of the RNA hairpins that form kissing complexes yields constructs that retain the ability to form native-like interactions, e.g. RNA-RNA kissing and Rom binding, while acting as extremely sensitive reporters for the RNA-RNA binding reaction.

Using the 2-AP fluorescence quenching assay it was possible to determine not only the equilibrium binding constants for kissing complex formation of R1inv and R2inv (K_{Dav} = 2.6 ± 1.7 nM), that are in good agreement with previous measurements,[185, 187, 199] but also the detailed kinetics of the complex formation. In equilibrium experiments the dissociation constant of the kissing complex could be determined, whereas the association kinetics were measured using stopped flow. From these results a two step binding model could be developed. In addition, the stringent divalent metal ion requirement of this system could be

investigated further, and Rom binding to the kissing complex was measured in real-time in an elegant way using the presented method.

In contrast to other binding assays, like native gel electrophoresis and filter binding, the 2-AP fluorescence assay is in general more sensitive and less prone to artifacts that could produce inaccurate binding constant measurements, since 2-AP probe incorporation is non-perturbing and binding measurement can be made under native solution conditions. For example, K_Ds measured using 2-AP fluorescence for Rom protein binding to the RNA kissing complex are in good agreement with previous measurements made indirectly by quantification of the products of RNAse cleavage reactions;[187] while, direct measurements made using native gel electrophoresis underestimate the K_D by approximately an order of magnitude.[199]

4 Investigation of the Dimerization and Structural Isomerization of the Dimerization Initiation Site (DIS) Stem-Loop from HIV-1

4.1 Introduction

Since the discovery of the human immunodeficiency virus (HIV) as the causative agent for the acquired immunodeficiency syndrome (AIDS) in 1983[205-207], much effort has gone into the development of antiviral drugs against it. Research has focused primarily on studies of the biology, biochemistry and structural biology of HIV, and on the interaction between viral components and potential new drug candidates. Several drugs have successfully been developed and are currently in use in the clinic that inhibit either the viral enzyme reverse transcriptase (RT) or protease (PR). Unfortunately, the virus has been able to quickly develop resistance against most of these drugs. In addition, the current use of multidrug 'cocktails' is expensive and compliance with treatment regimens is difficult. It is therefore prudent to continue to pursue new antiviral therapies that are based on targeting novel viral components.[208, 209]

Although the past 20 years of research has produced a fairly detailed picture of HIV-1 biology, basic research continues to expand our understanding of how the virus works at the molecular level and helps to identify new strategies for antiviral therapy. The morphology of a mature human immunodeficiency virus type-1 (HIV-1) virion is shown in Figure 4-1. The viral particle is enveloped by a lipid bilayer that is derived from the membrane of the host cell. The lipid bilayer contains the transmembrane protein (TM, gp41) to which exposed surface glycoproteins (SU, gp120), responsible for cell recognition, are anchored. The inner surface of the membrane is lined by a matrix shell composed of approximately 2000 copies of the matrix protein (MA, p17). In the center of the viral particle a conical capsid core comprising about 2000 copies of the capsid protein (CA, p24) is located. The capsid contains two copies of the unspliced viral RNA genome, which is stabilized as a ribonucleoprotein complex with circa 2000 copies of the nucleocapsid protein (NC, p7), three enzymes, namely protease (PR), reverse transcriptase (RT), and integrase (IN), and three accessory proteins (Nef, Vif and Vpr). The viral genome also encodes for three additional accessory proteins

(Rev, Tat, Vpu) that function in the host cell but appear not to be packaged into the viral particle.[208, 209]

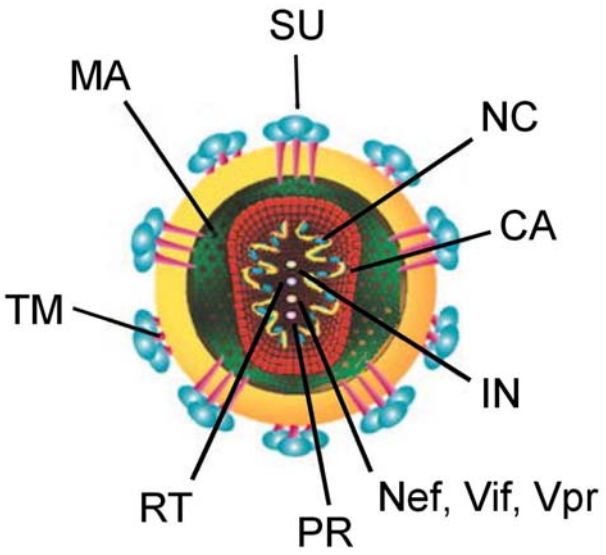

Figure 4-1. Morphology of a mature HIV particle. SU = surface protein, NC = nucleocapsid protein, CA = capsid protein, IN = integrase, PR = protease, RT = reverse transcriptase, TM = transmembrane protein, MA = matrix protein, Nef, Vif, Vpr = accessory proteins. (adapted from [209])

In the early phase of the HIV-1 life cycle (Figure 4-2), recognition of the host cell is achieved by the binding of SU specifically to CD4 receptors. Unlike other retroviruses, in HIV-1 only the interaction with additional cell surface proteins, like the CCR5 chemokine receptor, triggers the fusion of virus and cell membranes. After membrane fusion, the virion core enters the host cell where it is uncoated to expose the ribonucleoprotein complex. RT catalyzes the reverse transcription of genomic RNA into DNA, which is then transported as part of a preintegration complex that includes IN, MA, RT and Vpr into the host cell nucleus and integrated into the host genome by IN. The late phase of the HIV-1 replication cycle starts with the synthesis of spliced and unspliced viral mRNA transcripts, which are transported out of the nucleus with the aid of Rev. In the cytosol, the mRNA is translated into the viral envelope, structural and accessory proteins. The Env precursor polyprotein is synthesized in the endoplasmatic reticulum, where it is also glycosylated, and is later cleaved to form a TM-SU complex that localizes at the cell membrane.

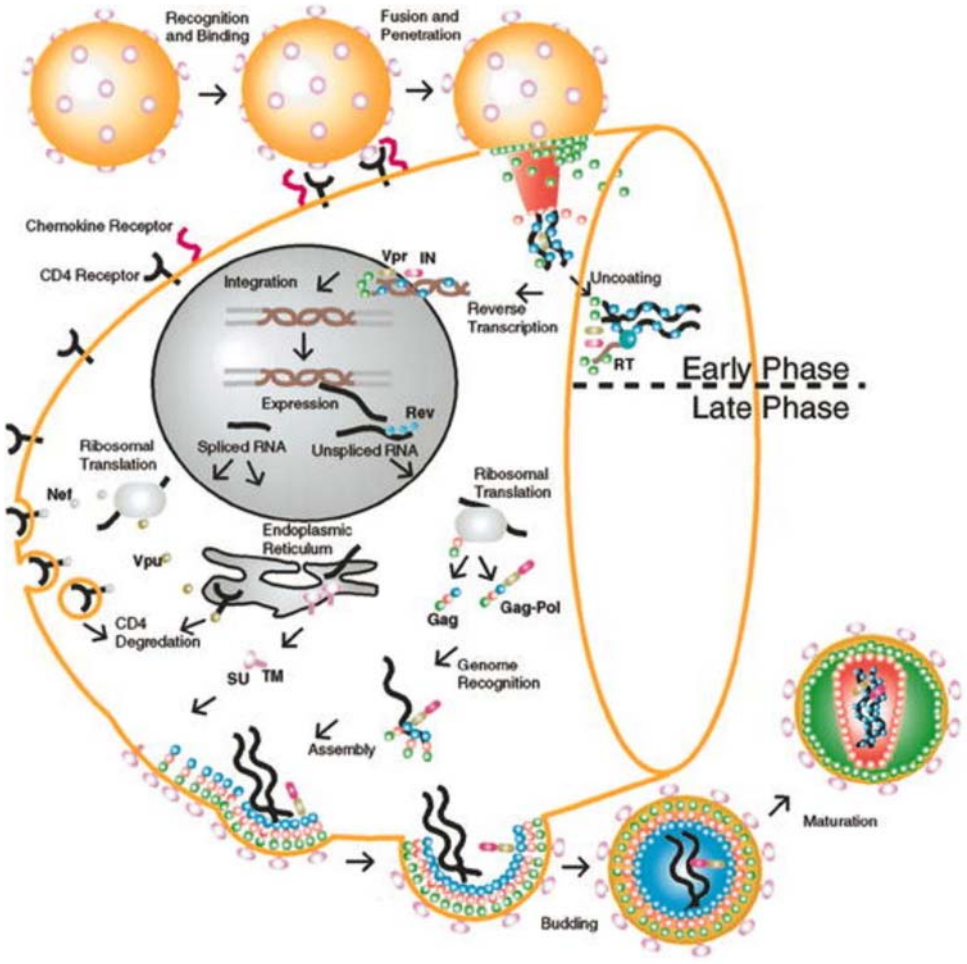

Figure 4-2. General Features of the HIV retroviral life-cycle (Abbreviations as in Figure 4-1) (taken from [209])

At the same time, the accessory proteins Vpu and Nef target CD4 molecules in the endoplasmatic reticulum, and at the cell surface, respectively, to signal their degradation to prevent binding of the newly formed SU to CD4 receptors in the host cell. The *gag* polyprotein is synthesized in the cytoplasm and also transported to the cell surface. Approximately 1200 - 2000 copies of *gag* are incorporated into the budding immature viral particle, which encapsidates two copies of the unspliced RNA genome. Subsequent to budding, the viral PR cleaves the *gag* polyproteins to produce the three viral enzymes PR, RT, IN and the three structural proteins MA, CA, and NC. The post-budded virion then undergoes a morphological change to form the infectious viral particle termed 'maturation'. During this process, the structural proteins rearrange and the RNA genome dimer undergoes

conformational changes which result in the formation of a more compact, thermodynamically stable dimer.[208-210]

All known retroviruses package two identical positive copies of their RNA genomes in budding viral particles.[211, 212] The packaged RNAs form homodimers that are linked non-covalently through a leader sequence at the 5'-end of the RNA genomic sequence called the dimer linkage structure (DLS).[213, 214] In HIV-1, dimerization is initiated by a highly conserved 35-nucleotide stem-loop, called the dimerization initiation site (DIS), which is located within the DLS.[197, 215, 216] RNA genome dimerization is proposed to be involved in a number of important events in the retroviral life cycle, including recombination and reverse transcription,[211] translation of the *gag* gene,[217] and selective encapsidation and packaging of genomic RNA.[213, 215, 218-220] Deletion or mutations of the DIS sequence that prevent dimerization have been found to reduce packaging efficiency 2- to 6-fold,[211, 212] dramatically decrease viral replication rates[215, 221] and reduce infectivity by as much as a 1,000 fold.[211, 215, 216, 219-222] The apparently critical role of DIS in proper viral packaging and maturation makes it a potential target for novel antiviral drugs that can inhibit dimerization. For clever drug design, the kinetics and mechanism of the DIS dimerization need to be studied at first.

The DIS loop contains an auto-complementary hexanucleotide sequence, which is found most often to be either GUGCAC (subtype A or Mal variant) or GCGCGC (subtype B or Lai variant), together with highly conserved 5'- and 3'-flanking purine nucleotides (Figure 4-3A). *In vitro* experiments have shown that sequences derived from the DLS can spontaneously form homodimers through a loop-loop kissing interaction[198, 216, 222-226] and that isolated DIS stem-loops will also self-associate to form homodimer kissing complexes (Figure 4-3B).[198, 211, 223-226] It was demonstrated *in vitro* that NCp7 activates conversion of metastable homodimers, formed between short retroviral RNA transcripts either from the 5'-end of Harvey sarcoma virus or from the Lai subtype of HIV-1, to more stable mature dimer forms.[227, 228] In further *in vitro* studies with the Lai sequence variant of HIV-1, the DIS kissing dimer has been shown to be converted under certain ionic conditions by incubation either at 55 ºC or with the addition of NCp7 at 37 ºC to a more thermodynamically stable extended duplex dimer form as shown in Figure 4-3B.[216, 229-231] However, this two-step dimerization from kiss to duplex dimer was only observed with full length 39mer DIS stem-loops containing native trinucleotide stem bulges. In these studies, the shorter 23mer DIS hairpins were observed only in the extended duplex form and 39mer DIS stem-loops lacking the stem bulge could not be converted by addition of NCp7.[230] Further studies have indicated that NCp7 can still function as a chaperone in catalyzing the DIS isomerization

reaction even when Zn^{2+} was not present in the buffer, indicating that properly folded NCp7 is not critical to function.[230] In addition, short basic peptides derived from NCp7 were also found to promote DIS isomerization.

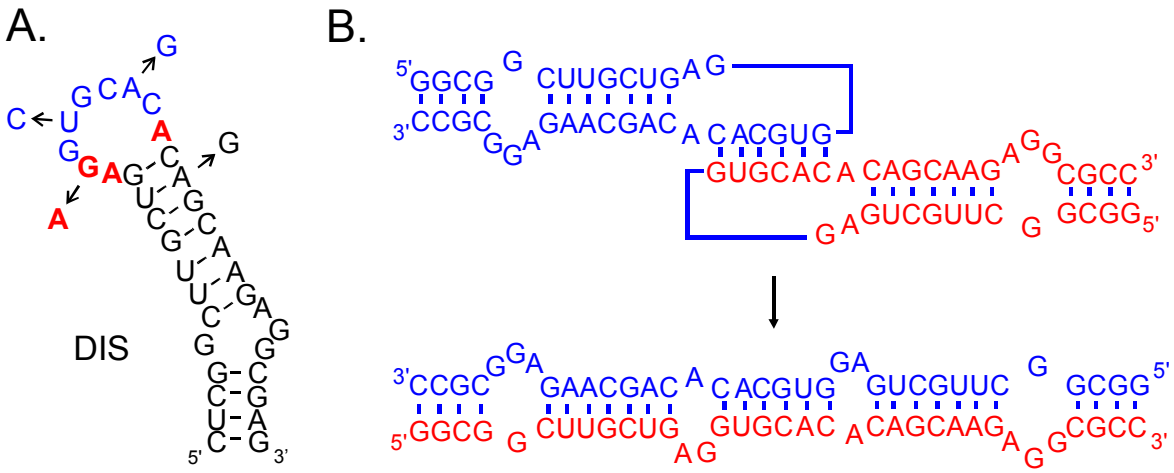

Figure 4-3. (A) RNA sequence and secondary structure of the DIS stem-loop from subtype-A of HIV-1. In the DIS loop, the hexanucleotide palindromic sequence is highlighted in blue and conserved flanking purine nucleotides bolded in red. Positions in the sequences which differ for the subtype-B strain of HIV-1 are indicated by arrows and substituted nucleotides. (B) Schematic of the structural conversion of the DIS homodimer from loop-loop kissing to extended duplex conformations. In each of the two dimers, one of the two identical hairpin sequences is shown in red and the other in blue.

Since maturation of post-budded HIV-1 retroviral particles requires active viral PR and appears to correlate with cleavage of NCp7 from the *gag* protein, it has been hypothesized that NCp7 activated RNA isomerization of DIS observed *in vitro* may be related to maturation of dimeric genomic RNA observed *in vivo*.[210, 227, 228, 230, 232] Taken together, the *in vivo* and *in vitro* data suggests that the released NCp7 acts as a nucleic acid chaperone[232] by activating RNA refolding events associated with genomic RNA maturation. NCp7 has also been shown to act as a nucleic acid chaperone in promoting a number of other nucleic acid annealing and strand transfer processes involved in HIV-1 replication, such as $tRNA^{Lys}$ hybridization to the primer binding site (PBS) on genomic RNA[233, 234] and strand transfer and renaturation reactions subsequent to the initiation of reverse transcription.[235-240]

High-resolution structures of the DIS kissing and mature duplex dimer isoforms from both the HIV-1 Mal and Lai variants have been determined through solution NMR[241-243] and crystallographic[1, 244] methods. To date, however, a number of unresolved discrepancies exist between the solution and X-ray determined structures. In addition, mechanisms for the DIS dimer structural isomerization and the specific role of NCp7 in this reaction, that have been proposed based on these structural studies have only been speculative. In this study, an *in*

vitro model system has been designed to allow the unambiguous and direct detection of kissing versus extended duplex DIS dimer formation through incorporation of the highly fluorescent nucleotide base analog 2-aminopurine (2-AP) as a structural probe at specific positions in stem-loop sequences derived from the wild-type DIS_{Mal} sequence. Fluorescence-detected methods have been used to determine the equilibrium and kinetic binding constants for DIS dimerization, as well as the molecular mechanism of HIV-1 DIS structural isomerization from kissing complex to extended duplex, and to address the specific role of NCp7 in the process.

4.2 Preliminary Experiments

4.2.1 Homodimers

In an attempt to measure equilibrium binding constants for DIS dimerization and the kinetics of NCp7 mediated structural isomerization, initial experiments were performed with wild-type (wt) DIS sequences derived from the Mal variant of HIV-1. One full size 35mer DIS stem-loop with the adenosine at position 16 exchanged for a 2-AP [DIS 35-16ap], and two shortened 21 nt hairpins, that were truncated just above the stem bulge, with the adenosines at positions 13 (to observe complex formation) and 17 (as a control), respectively, exchanged for a 2-AP [DIS 21-13ap and DIS 21-17ap] and corresponding unlabeled 35mer and 21mer hairpins (Figure 4-4) were synthesized.

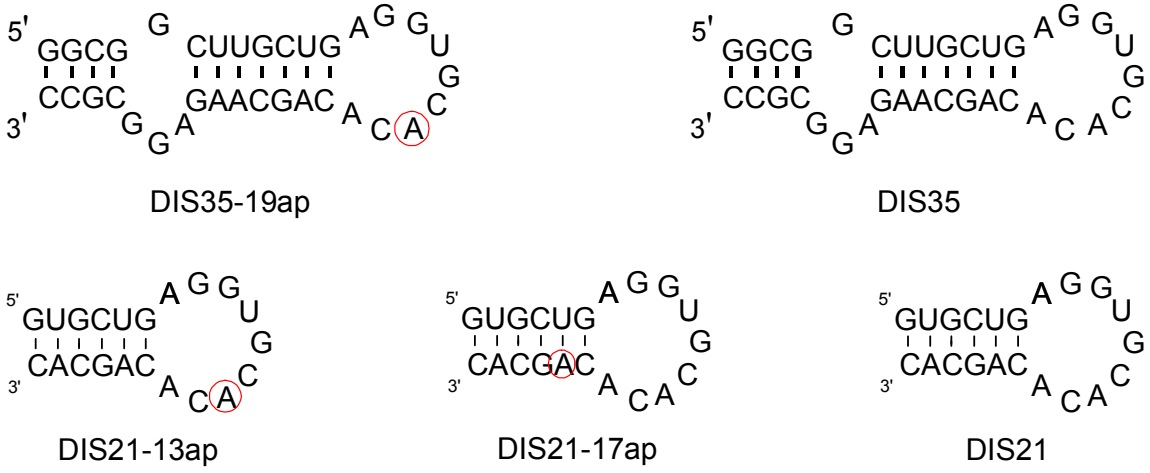

Figure 4-4. RNA sequence and secondary structure of the wt DIS stem-loops that form homodimer complexes. 2-AP positions are circled in red.

Since these DIS samples could form homodimers, and evidence for an equilibrium mixture of dimer and monomer states was observed even at nanomolar concentrations, it was not possible to collect well controlled 2-AP fluorescence-detected binding and kinetic data using these samples. The two major problems encountered with these samples were:

(1) Since the binding constants of these RNA hairpins were in a range of 1 to 5 nM, it was not possible to prepare samples containing 100 % of the monomeric species in the nanomolar concentration ranges required for the fluorescence experiments, even after snap cooling the RNA samples to kinetically force them into the monomeric hairpin state. At concentrations of 500 nM RNA, the 2-AP label in the loop was already somewhat quenched, with DIS35-19ap appearing more quenched than the DIS21-13ap. By comparison to DIS21-13ap, the 2-AP label in the stem in DIS21-17ap showed about 20 % of the fluorescence intensity at the same concentration. Since base-paired and stacked 2-AP probes are expected to show similar degrees of quenching whether in the stem or loop-loop helix of the dimer, the differences in fluorescence intensities suggest that in the absence of Mg^{2+} these hairpins are in an equilibrium between monomer and dimer states. In addition, non-denaturing polyacrylamide gels demonstrated that at higher micromolar concentrations the short RNA hairpins existed almost exclusively as dimers. Since this dimer state was observed using native PAGE in the absence of Mg^{2+}, it was further concluded that the dimer state was mainly in the mature duplex form, that had isomerized spontaneously from the kissing dimer.
(2) In the fluorescence experiments, it was not possible with these samples to distinguish between the kissing complex and extended duplex dimer. In both dimers, the 2-AP labels incorporated into the loop and stem are base-paired and well stacked. Hence, in both dimers the 2-AP probe is expected to be in a highly quenched state and therefore no detectable change in fluorescence of the 2-AP fluorescence would be expected between the kissing complex and extended duplex dimer (Figure 4-3B).

This first set of samples thus turned out to be impractical for the study of the DIS loop-loop kissing complex formation and maturation to extended duplex using fluorescence detected methods. As a consequence, the DIS hairpin samples were modified as described below to promote the formation of exclusively heterodimer complexes, and 2-AP probes were selectively incorporated into these samples to allow unambiguous distinction between the two dimer states.

4.2.2 Heterodimers

In previous *in vitro* studies, it had been found that 5'-leader sequences from the HIV-1 RNA genome can still dimerize even if the autocomplementary sequence in the DIS loop has been disrupted so long as a complementary mutation is introduced into a second RNA sequence species.[221, 245, 246] Based on these results and a philosophy of introducing as few changes as possible, a second set of samples was synthesized for these studies in which the autocomplementary sequence in the loop was disrupted to prevent homodimer formation by alteration of a single base in the loop sequence. A series of complementary RNA hairpins was made as follows: In the labeled RNA hairpins, the fourth position in the loop was changed from U to a C, and 2-AP was incorporated at the naturally occurring adenosine at the seventh position in the loop [DIS35C16-19ap and DIS21C10-13ap], and unlabeled complementary hairpins with the corresponding A to G mutation in the seventh position in the loop were designed [DIS35G19 and DIS21G13] (Figure 4-5). In addition, to facilitate direct observation of the extended duplex dimer formation, hairpins with a 2-AP label added in an extended two-base 'overhang' at the 5'-end of the stem and not in the loop [DIS35C16e-36ap and DIS21C10e-22ap], and their respective complements [DIS35G19c and DIS21G13c] were synthesized (Figure 4-5). As controls, DIS hairpin samples were also designed with loops complementary to the labeled samples but with stem sequences modified such that only kissing complexes could form and not extended duplexes [DIS35HxG16 and DIS21HxG13] (Figure 4-5).

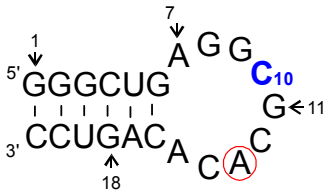

DIS21 C10-13ap

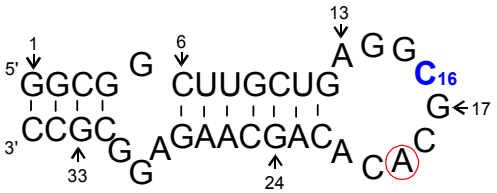

DIS35 C16-19ap

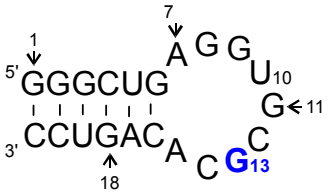

DIS21 G13

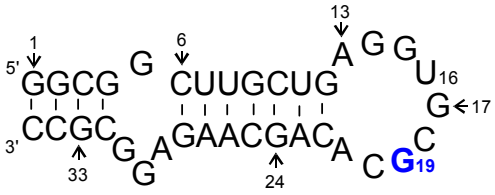

DIS35 G19

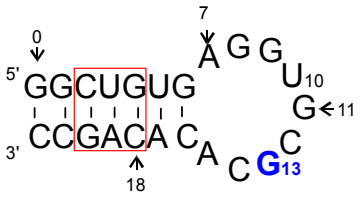

DIS21 HxG13

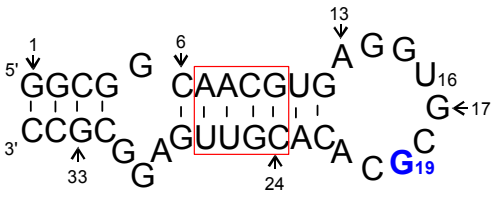

DIS35 HxG19

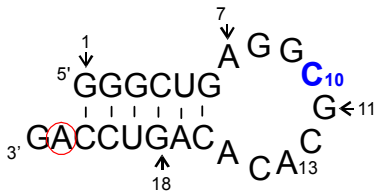

DIS21 C10e-22ap

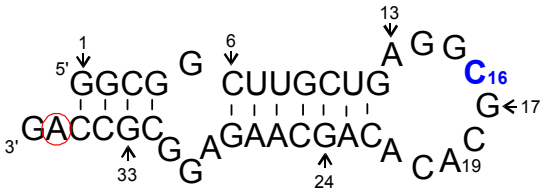

DIS35 C16e-36ap

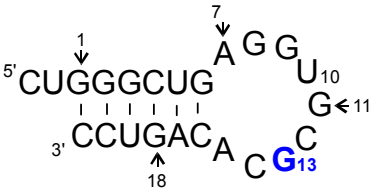

DIS21 G13c

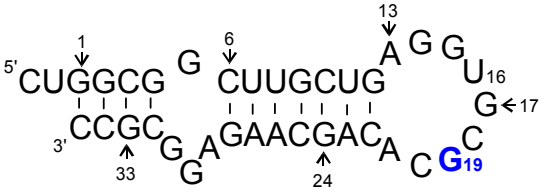

DIS35 G19c

Figure 4-5. RNA sequences and secondary structures of the first set of DIS stem-loop constructs designed to form heterodimer complexes. Point mutations in the hexanucleotide sequence [U10 to C10 and U16 to C16 to form the DIS 21 C10 and DIS 35 C16 stem-loops and A13 to G13 and A19 to G19 to form the complementary DIS 21 G13 and DIS 35 G19 stem-loops] which destroy the palindromic nature of the sequence and promote heterodimer formation are bolded in blue. Nucleotide positions in the DIS 21 C10 and DIS 35 C16 stem-loops that were substituted with the fluorescent probe 2-AP are circled in red. The exchanged stem helices of DIS 21 and DIS 35 (HxUC) are boxed in red.

Using these DIS samples, it was possible to measure equilibrium binding constants for kiss formation by titration of DIS21C10-13ap or DIS35C16-19ap with the respective unlabeled complements in the presence of 5 mM Mg^{2+}. For both the 21 and 35 nt RNA hairpins, the average K_Ds were found to be approximately 3 nM with the fully complementary sequence as well as with the exchanged stem sequence. This lead to the conclusion that the stem structure does not have a significant effect on the DIS kissing dimer association and that the presence of a stem bulge found in wild-type DIS is not required for stable kissing dimer formation. Although apparent stoichiometries of 1:1 between the complementary heterodimeric DIS hairpins was observed in most of the fluorescence binding assays, native gel electrophoresis showed unexpectedly that some of the RNA hairpins with disrupted palidromic sequences still formed homodimers. Although snap cooling could be used to force the RNA sequences into the monomeric hairpin form in the absence of Mg^{2+}, in the presence of 1 mM Mg^{2+} some of the designed RNA samples appear to exist almost 100 % in homodimer form as observed on native gel (Figure 4-6).

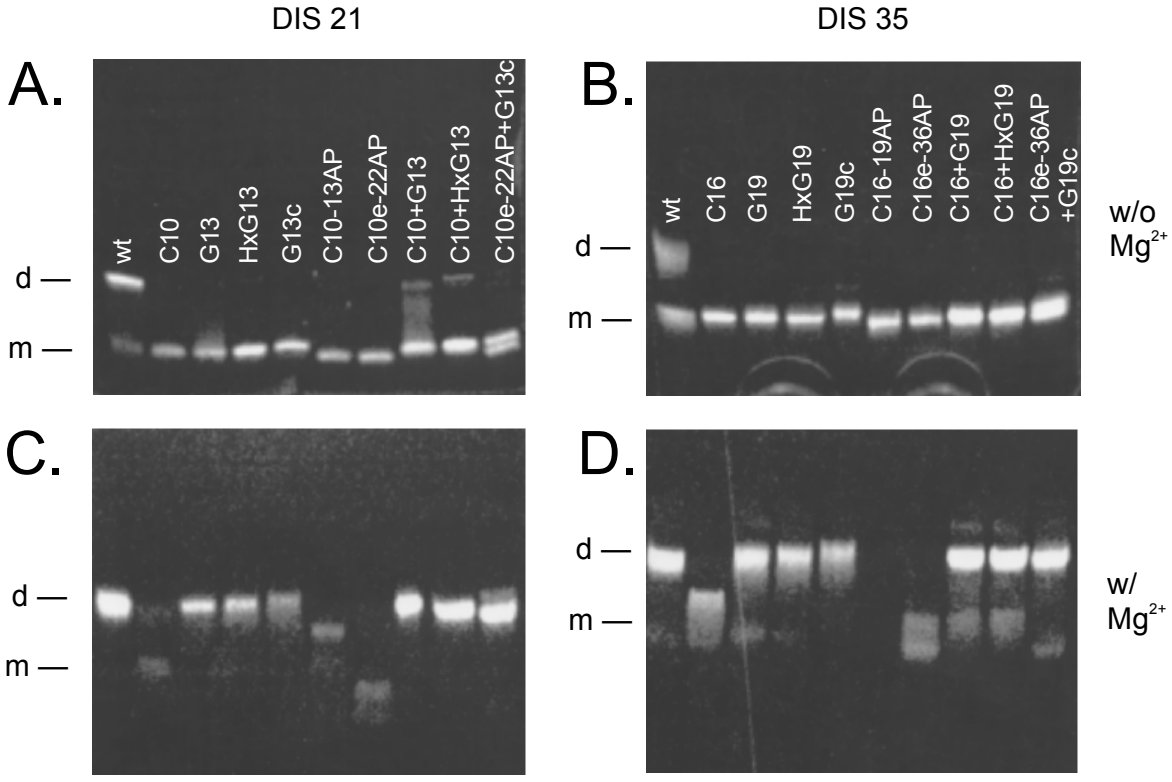

Figure 4-6. Non-denaturing polyacrylamide gels on first set of DIS heterodimers showing ability of A to G mutants to form homodimers in the presence of Mg^{2+}. (A) and (C) show DIS21 hairpins without and with 1 mM Mg^{2+}, respectively. (B) and (D) show DIS35 stem-loop without and with 1 mM Mg^{2+}, respectively. All RNAs have been snap cooled before loading on the gel. wt = wild-type sequence; d = dimer; m = monomer.

The most likely explanation for this observation is that the DIS21 hairpin with the A13→G13 mutation and DIS 35 hairpins with A19→G19 mutations can tolerate two non-canonical G13-U10 and G19-U16 wobble mismatched base pairs within the loop-loop helix of homodimers formed by these hairpins. These DIS mutant sequences demonstrated the high degree of tolerance of the DIS loop sequence to modification that were originally expected to be more significantly disruptive of homodimer formation. Another drawback found with this set of samples was the lack of a significant fluorescence change for the 2-AP probe inserted into the 3'-extended single stranded sequences, DIS21C10e-22ap and DIS35C16e-36ap, that was anticipated to accompany the structural isomerization to mature duplex. The 2-AP fluorescence in both DIS21C10e-22ap and DIS35C16e-36ap samples was found to be highly quenched even in monomeric hairpins, indicating that the 2-AP probe in the single stranded tail at the 5'-end of the stem is already well stacked. Thus, upon strand exchange and base pair formation with the complementary DIS stem-loops, no significant fluorescence emission change can be observed. In hindsight this result was not so surprising since single stranded overhanging sequences of RNA, as well as DNA, are often expected to be well stacked even in the absence of base pairing and therefore would be expected to be highly quenched. In light of later studies on charge transfer in DNA (chapter 6), it seems that the G next to 2-AP at the 3'-end of the RNA sequence, was not a good choice, since it can quench 2-AP fluorescence by hole transfer.

In summary, although fluorescence detection of kissing complex formation was achieved for the first time with this set of mutated DIS stem-loops, homodimer binding reactions were still observed that might contaminate the analysis of the equilibrium binding curves and more likely complicate any kinetic analysis. Moreover, the use of differences in fluorescence intensity of a 2-AP probe inserted into a 3'-extension of a DIS stem helix as mode for the detection of kissing complex versus extended duplex also did not prove successful. These DIS hairpin were therefore not used further and a second set of heterodimeric DIS hairpins was designed and synthesized.

4.3 Fluorescence Experiments with Second Set of Heterodimers

4.3.1 Sample Design

Based on the results from the preliminary experiments, a third set of DIS RNA samples was designed. Again, the palindromic nature of the hexanucleotide sequence of DIS loop was altered. Two bases in the autocomplementary sequence were exchanged to create two unique DIS stem-loops (Figure 4-7), so called DIS(GA) and DIS(UC), that associate at nanomolar concentrations with each other as hetero- rather than homodimers, as has previously been demonstrated.[218, 230] 2-AP labels were inserted at two specific positions in the DIS24(GA) stem-loop: one construct with 2-AP substituted at the A12 loop position [DIS24(GA)-12ap], and a second with 2-AP inserted as a single bulged nucleotide in the stem [DIS24(GA)-4ap]. These two constructs were designed to probe kissing versus mature duplex dimer formation, respectively. Two unlabeled DIS(UC) constructs, with loop sequences complementary to the DIS24(GA) stem-loops, were also designed: one construct with a stem sequence complementary to DIS24(GA)-4ap, that can specifically probe the DIS structural isomerization [DIS24(UC)] and a second construct with an exchanged stem sequence that is capable of forming only the kissing dimer [DIS23(HxUC)].

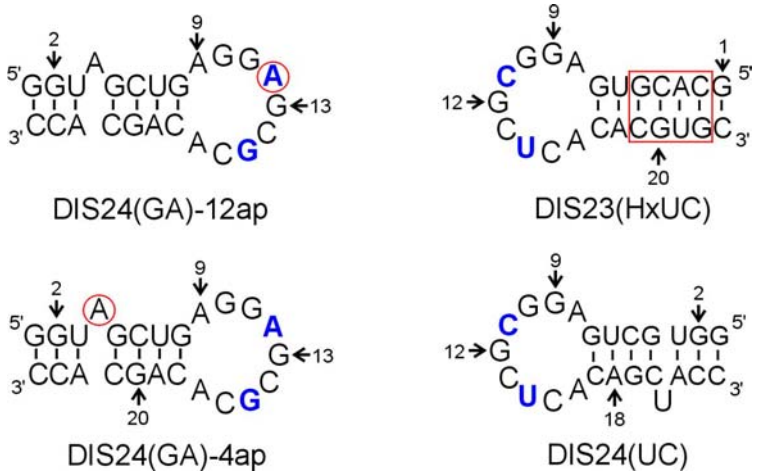

Figure 4-7. RNA sequences and secondary structures of the second set of DIS stem-loop constructs designed to form heterodimer complexes. Point mutations in the hexanucleotide sequence [U12 to A12 and A15 to G15 to form the DIS(GA) stem-loop and U11 to C11 and A14 to U14 to form the complementary DIS-UC stem-loop] which destroy the palindromic nature of the sequence and promote heterodimer formation are bolded in blue. Nucleotide positions in the DIS(GA) stem-loop that were substituted with the fluorescent probe 2-AP are circled in red. The exchanged stem helix of DIS23(HxUC) is boxed in red.

These samples finally provided an *in vitro* model system with reliable, unambiguous, and sensitive fluorescent probes for monitoring kissing complex, as well as NCp7 activated duplex formation.

The NCp7 protein is a 72 amino acid protein, common to all HIV-1 variants, containing two Zn-knuckles of the CCHC-motif with a basic linker. The protein sequence used in these studies is essentially wild-type (wt), but consists of only the first 55 amino acids. The truncated 55 amino acid NCp7 sequence contains only a single tryptophan in the C-terminal Zn-knuckle. Sequence and secondary structure are shown in **Figure** 4-11.

4.3.2 Results

4.3.2.1 DIS Kissing Dimer Kinetics

Using this new set of heterodimer forming samples, equilibrium and kinetic binding constants for the DIS loop-loop kissing interaction were determined. Titration of the DIS_{Mal} derived hairpin, DIS24(GA)-12ap, substituted with 2-AP at position A12 in the loop (Figure 4-7) with either of the complementary DIS(UC) stem-loops [DIS24(UC) or DIS23(HxUC)] in the presence of 5 mM Mg^{2+} at 25 °C, results in an approximately 6-fold decrease in 2-AP fluorescence emission (Figure 4-8). The direction and magnitude of this fluorescence change indicates that the 2-AP substituted base becomes significantly stacked upon binding, which is consistent with 2-AP•U base pairing that would accompany the formation of the DIS kissing complex loop-loop helix. From the fluorescence detected equilibrium binding experiments, these heterodimeric DIS kissing complexes were found to have an average equilibrium binding constant $K_D = 3 \pm 1$ nM. This result is consistent with previous measurements made using other techniques,[223-226] and is in the same range as was determined for the entire 35-nucleotide DIS stem-loop in chapter 4.2.2. These truncated DIS stem-loops therefore faithfully mimic the kissing association of the wild-type 35-nucleotide DIS stem-loop and provide a useful *in vitro* system for modeling this interaction.

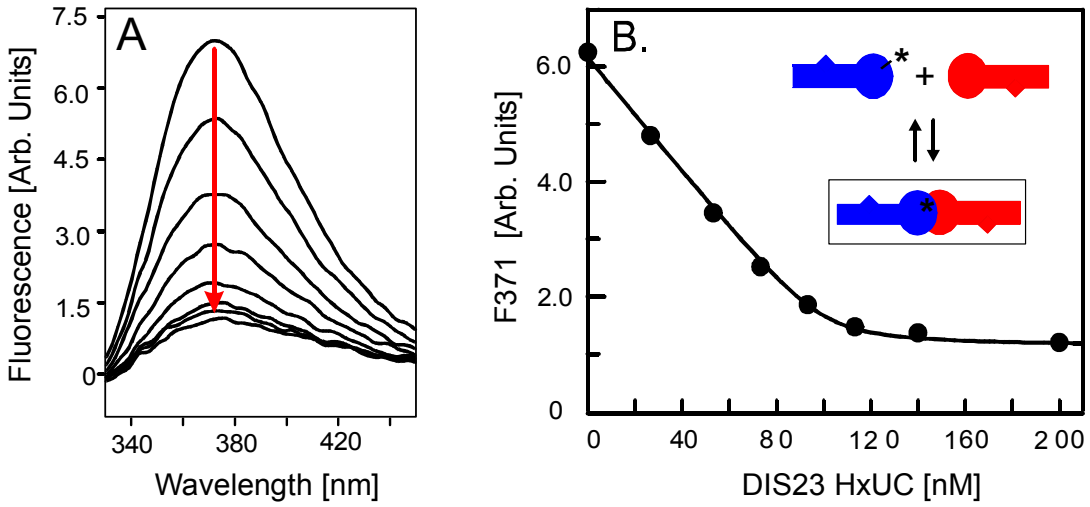

Figure 4-8. (A) Fluorescence changes accompanying titration of 100 nM DIS24(GA)-12ap with increasing concentrations of DIS23(HxUC) in standard buffer with 5 mM $MgCl_2$ at 25 °C. Emission spectra are plotted from 330 to 450 nm. (B) Plot of the fluorescence decrease at 371 nm as a function of total DIS23(HxUC) concentration for a titration using 100 nM DIS24(GA)-12ap. The location of the 2-AP probe on the DIS-GA stem-loop is indicated by an asterisk and the species that is directly detected in the experiment is marked with a box in the panel. The solid curve is fit to equation 9.6, yielding a $K_D = 1.3 \pm 0.7$ nM.

The dissociation kinetics of the DIS loop-loop kissing dimer was measured at both 25 and 35 °C by following the time-dependent increase in 2-AP fluorescence of DIS24(GA)-12ap as the DIS24(GA)-12ap•DIS23(HxUC) complex dissociates. The free DIS23(HxUC) was trapped with a 20-fold excess of unlabeled DIS24(GA) stem-loop to achieve pseudo first-order conditions and make the dissociation irreversible. Fitting the data from this experiment to a first order rate constant equation, yields off-rates $k_{d(25°C)} = 0.0019$ min^{-1} and $k_{d(35°C)} = 0.0063$ min^{-1}, respectively (Figure 4-9). An apparent on-rate for DIS kissing complex formation was determined at 25 °C again using pseudo first-order conditions, where a 20-fold greater concentration of DIS23(HxUC) was added to DIS24(GA)-12ap in the presence of 5 mM Mg^{2+} and the decrease in fluorescence was monitored over time. Fitting the data from this experiment to a single exponential equation yields an on-rate $k_a = 0.8912$ min^{-1} (Figure 4-9) under these experimental conditions.

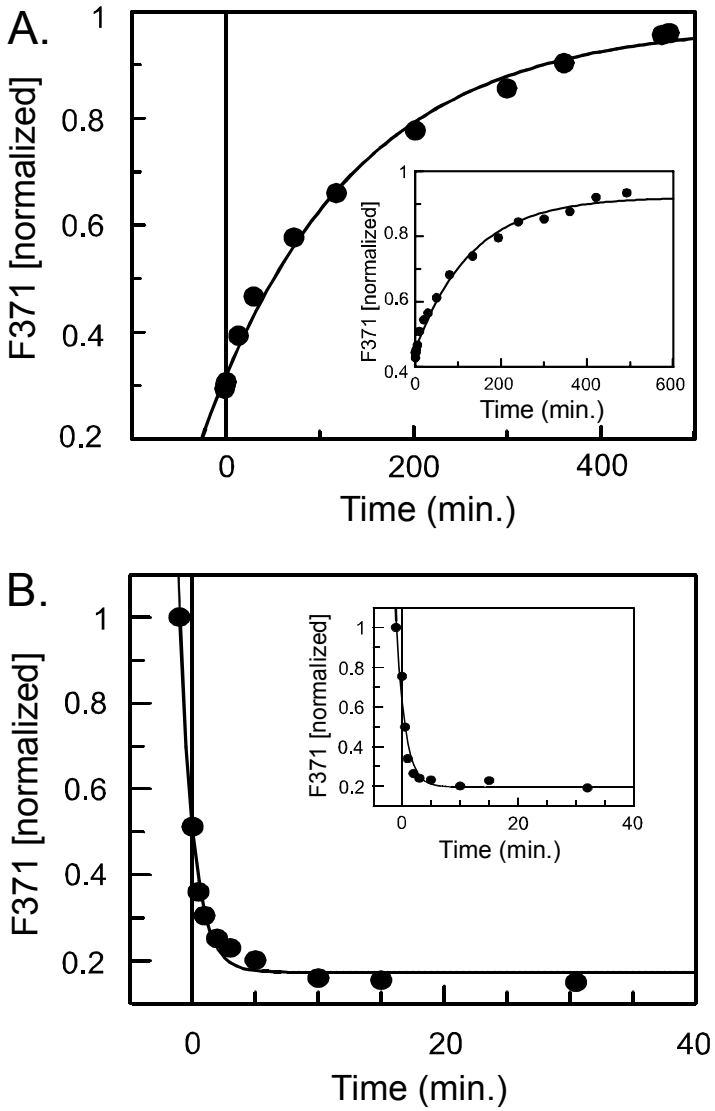

Figure 4-9. (A) Kinetic measurement of the DIS loop-loop 'kissing' complex dissociation at 35°C. Fluorescence change upon rapid mixing of 100 nM DIS24(GA)-12ap•DIS23(HxUC) with excess (2 μM) unlabeled DIS24(GA) acting as an irreversible trap for the free DIS23(HxUC). The data was fit using a first order rate constant equation (k_{off} = 1.05 x 10^{-4} s^{-1}). In a similar experiment that is plotted in the inset, the k_{off} for DIS24(GA)-12ap from DIS23(HxUC) was determined with 500 nM NCp7 present in the buffer (k_{off} = 1.08 x 10^{-4} s^{-1}). (B) Plot of the fluorescence decrease at 371 nm as a function of time after a 20-fold excess of DIS24(HxUC) is added to 100 nM DIS24(GA)-12ap in the presence of 5 mM $MgCl_2$. The data was fit (k_{on} = 0.91 min^{-1}) to a single exponential equation. In the inset the same experiment is shown in the presence of 250 nM NCp7 (k_{on} = 0.67 min^{-1}).

As previously described for the bacterial antisense RNA hairpins from the *ColE1* system, the metal ion requirement of DIS kissing complex formation was also investigated. To a 1:1 mixture of DIS24(GA)-12ap and DIS23(HxUC), different mono- and divalent cations were titrated and the decrease of the fluorescence emission at 371 nm monitored. Note that no fluorescence changes were observed over time in a 1:1 mixture of the two complementary hairpins in the absence of cations. The mutations in the autocomplementary sequence made DIS kissing dimer formation cation dependent at the concentrations used in the fluorescence

experiments (100 nM RNA). From these experiments, it was found that DIS kissing complexes could be formed with all divalent cations tested and apparent binding constants could be determined as before (see **chapter** 3 and **equation** 7.7).

Table 4-1. Apparent Equilibrium Binding Constants for Metal Ions to RNA

metal ions	K_{Dapp}
Mg^{2+}	262μM
Ca^{2+}	200μM
Sr^{2+}	209μM
Mn^{2+}	62μM
Na^{+}	119mM
K^{+}	143mM

Solutions of divalent metal ions were titrated to a 1:1 mixture of DIS24 (GA)-12ap and DIS 23 HxUC and decrease in fluorescence intensity observed. Data was fit to an equilibrium binding equation assuming a single class of metal binding sites.

As shown in Table 4-1, the calculated apparent binding constants of the tested divalent metal ions to the RNA kissing complex are all more or less in the same range. Unlike in the bacterial system investigated in chapter 3, ionic radius or Lewis acidity do not seem to affect cation binding associated with DIS kissing complex formation. Positive charge alone seems to be effective enough to promote kissing complex formation. In contrast, NCp7 does not appear capable of promoting kiss formation since addition of 500 nM NCp7 to a 1:1 mixture of complementary RNA hairpins does not result in quenching of 2-AP fluorescence in the loop (data not shown). In addition and in contrast to the bacterial RNA systems, the DIS stem-loops were also observed to associate as kissing dimers in the presence of monovalent cations, such as Na^+ or K^+ in concentrations of 100 to 300 mM (Table 4-1), or with sufficiently high RNA concentrations (> μM) under standard buffer conditions as observed by NMR measurements (unpublished data from M. R. Mihailescu). DIS kissing dimers, formed under these conditions, however, have been found to be metastable and capable of spontaneously converting to the mature duplex form at an appreciable rate over time (vide infra).

4.3.2.2 DIS Conversion

To unambiguously detect the DIS structural isomerization and to determine the role of NCp7 in this process, the stem-loop DIS24(GA)-4ap capable of forming heterodimeric DIS24(GA)•DIS24(UC) complexes was constructed with a 2-AP probe inserted into the stem sequence such that it formed a single nucleotide bulge (Figure 4-7). The fluorescence of the 2-AP probe at this position in the free DIS24(GA) stem-loop was found to be relatively high and confirmed that the 2-AP is indeed in an unpaired bulged state. Upon formation of a DIS kissing dimer with the DIS24(UC) stem-loop in standard buffer containing 5 mM $MgCl_2$, the fluorescence intensity of the 2-AP probe of DIS24(GA)-4ap was found to initially increase slightly (~ 25%) but then remained constant. The Mg^{2+}-stabilized DIS kissing dimers are therefore kinetically trapped, as has been observed for kissing complexes associated with regulatory RNAs involved in regulation of plasmid replication in bacteria.[180, 247]

Addition of NCp7 to Mg^{2+}-stabilized DIS kissing complexes preformed between the DIS24(GA)-4ap and the complementary DIS24(UC) stem-loop results in a time-dependent 5-fold decrease in 2-AP fluorescence emission (Figure 4-10A). The DIS24(UC) stem-loop contains a single stem bulge uridine that can form a 2-AP•U base pair in the mature duplex dimer with the 2-AP base from DIS24(GA)-4ap if the stem strands are exchanged. The direction and magnitude of the observed fluorescence change indicates that the 2-AP substituted base becomes significantly stacked with time, which is consistent with 2-AP•U base-pairing and stacking that would accompany exchange of the stem strands during the isomerization process.

To confirm that the change in fluorescence observed is due to DIS structural conversion and exchange of stem strands, the fluorescence response of NCp7 addition to a kissing complex formed between DIS24(GA)-4ap and DIS23(HxUC), which contains a mismatched stem sequence incapable of forming proper Watson-Crick base pairs in the mature duplex dimer, was measured. Although the DIS23(HxUC) stem-loop efficiently forms a kinetically stable kissing dimer with DIS24(GA)-4ap in the presence of 5 mM Mg^{2+}, time-dependent quenching of the stem 2-AP probe was not observed when NCp7 was added to catalyze conversion of this DIS kissing dimer (Figure 4-10A). Instead, only an initial static decrease (~ 10%) in the fluorescence of the 2-AP probe was observed. Addition of Mg^{2+} directly to the individual DIS24(GA)-4ap stem-loop also resulted in only a slight static increase in the 2-AP fluorescence emission (25 %), further confirming that direct interaction of neither NCp7 nor Mg^{2+} with the 2-AP label is responsible for the observed temporal changes in the 2-AP fluorescence emission. Thus, it is clearly strand exchange of the stem helices associated with

DIS structural isomerization that is responsible for the quenching of 2-AP fluorescence in the experiment.

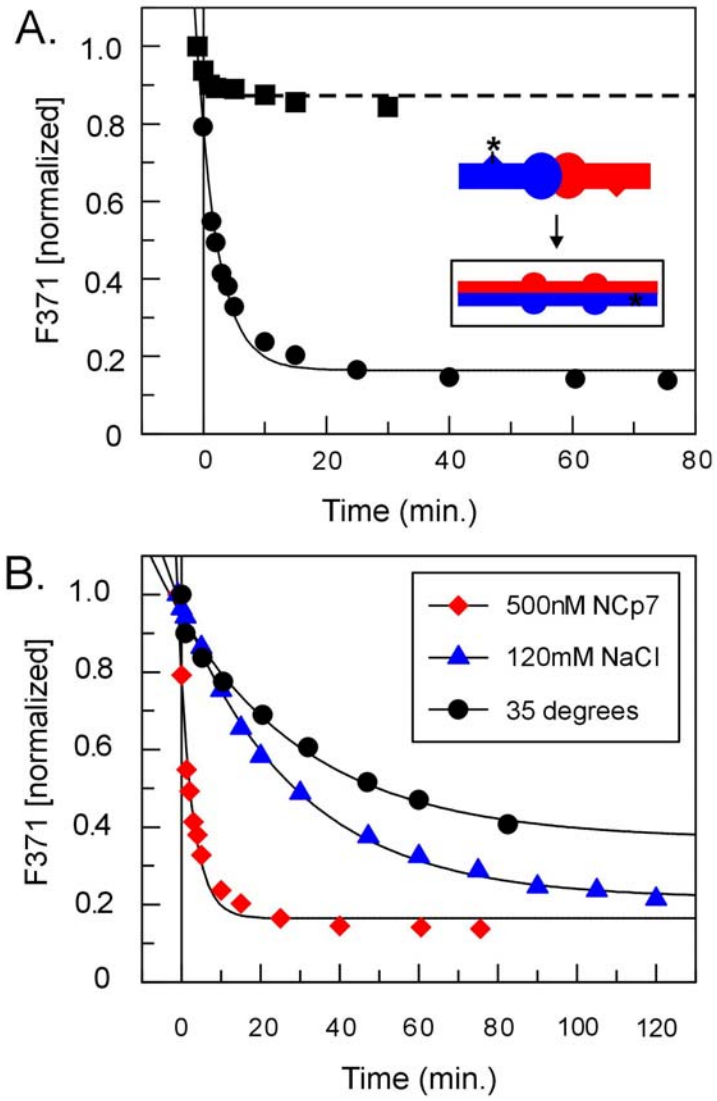

Figure 4-10. (A) Plot of the fluorescence decrease at 371 nm as a function of time after a 2.5-fold excess of NCp7 protein is added to 100 nM DIS24(GA)-4ap•DIS24(UC) kissing complex preformed in the presence of 5 mM $MgCl_2$ (filled circles). The location of the 2-AP probe on the DIS(GA) stem-loop is indicated by an asterisk and the species that is directly detected in the experiment is marked with a box in the panel. The structural isomerization rate was fit using a single exponential equation (k_{conv} = 0.46 min^{-1}). A similar experiment with the preformed DIS24(GA)-4ap•DIS23(HxUC) complex resulted in only a 10% initial decrease in fluorescence (filled squares and dashed line). (B) Plot of fluorescence decrease at 371 nm as a function of time using different 'maturation agents' to induce conversion.

Several research groups have found that maturation of DIS can be achieved using other conditions that do not include NCp7. Other co-factors and conditions that seem to be able to

accelerate the DIS structural isomerization include temperature, high salt concentration and basic peptides.[248-251] Since the 2-AP label incorporated into the samples used for this study allows direct measurement of conversion in real-time, measurement of the conversion rates could be used to test if temperature and positive charge can substitute for NCp7 as the isomerization catalyst, or if the NCp7 plays a specific role in maturation.

Table 4-2. Conversion Rates with different 'maturation agents'

	rate constant [min^{-1}]	
'maturation agent'	at 25°C	at 35°C
none	-	0.0283
500nM NCp7	0.2901	0.7943
120mM Na^+	0.0340	0.1283
5mM Mg^{2+} + 500nM NCp7	1.4691	2.3302
120mM Na^+ + 500nM NCp7	0.0449	0.1316
500nM denatured NCp7	0.2484	n/d
1.66µM Rev peptide	0.0621	n/d

Decrease in fluorescence intensity was observed over time as the 'maturation agent' was added to a 1:1 mixture of DIS 24 (GA)-4ap and DIS 24 UC in standard buffer. Data was fit to a single exponential equation.
n/d = not determined

From these experiments, it appears that native NCp7 can convert DIS hairpins to the mature duplex under all conditions tested, but that conversion rates are fastest at higher temperature (35 °C) and if the kissing complex is preformed by addition of Mg^{2+} (Table 4-2, Figure 4-10B). Simply increasing the temperature to 35 °C promotes mature duplex formation of the DIS hairpins, however at an extremely slow relative rate. As mentioned above, addition of 5 mM Mg^{2+} locks the DIS hairpins in the kissing conformation. By increasing the Mg^{2+} concentrations to 50 mM, or increasing the temperature to 35 °C no significant change in fluorescence can be observed, which indicates that no appreciable conversion is observed for the divalent metal ion stabilized DIS kissing dimer. On the other hand, high concentrations of NaCl (100 - 300 mM) appear to promote duplex formation, at 25 °C or 35 °C, and can also act in converting the divalent metal ion stabilized DIS kissing complexes, but the rates are very slow. Addition of NCp7 to monovalent metal ion stabilized DIS kissing complexes does not significantly accelerate the conversion, which leads to the conclusion that conversion in the presence of monovalent ions follows a different mechanism from that followed by NCp7

acting on the divalent metal ion stabilized DIS kissing complexes. The 22 amino acid Rev peptide, derived from the 116 residue HIV viral protein Rev, was also assayed for its ability to promote DIS conversion. Rev contains 10 arginines and is a highly basic peptide, which has little structure in solution. Using the fluorescence assay, it was demonstrated that Rev can also act in converting DIS, but that a much higher concentration is needed to catalyze the reaction in comparison to NCp7 and the rates are again significantly slower than with NCp7.

To test if the folded state of NCp7 is important for is activity as a RNA folding chaperone, the protein structure was disrupted through removal of the Zn^{2+} ions by treatment with the aromatic nitroso-compound, 3-Nitrosobenzamide. Removal of the zinc is expected to disrupt the native Zn-knuckle structures of NCp7. Performing the conversion experiment with denatured NCp7 showed that this form of NCp7 could still convert DIS kiss to duplex, but not quite as effectively as the native NCp7. This result is in agreement with an earlier study with the DIS Lai sequence.[230] Thus, the catalytic function of NCp7 in DIS maturation can not be reduced solely to its positive charge. Of all the conditions tested, folded NCp7 is the agent with the most effective conversion rates when added to the divalent metal ion stabilized DIS kissing dimer (Table 4-2). These conditions most likely reflect those *in vivo* and lead to the possibility that protease activated NCp7 could be a mechanism for temporal control of maturation of the packaged immature genomic RNA dimer in the post budded viral particle. Newly transcribed copies of HIV-1 genomic RNA might first associate in cells via a kissing dimer since these types of dimers form with relatively fast kinetic association rates and are quite stable under native cell conditions where Mg^{2+}, as well as other divalent metal ions are present. Proteolytic release of NCp7 in the post-budded immature viral particle would then allow absolute temporal control over DIS refolding and associated viral maturation.

4.3.2.3 NCp7 Mechanism

To further elucidate the role of NCp7 in the DIS dimer isomerization, the importance of preformation of the DIS kissing dimer structure in specific NCp7 binding and activity was examined using antisense oligonucleotide probes (Figure 4-11). DIS conversion rates were measured essentially as described above in the presence of a 10-fold excess of 6mer and 7mer antisense DNA oligonucleotides complementary to the central loop sequence, which compete with the DIS(UC) for binding to the DIS(GA) loop and thereby slow down the DIS(GA)•DIS(UC) kissing association rate.[224] At a 10-fold excess concentration, saturated binding of the oligonucleotides to the DIS(GA) loop is observed (data not shown). If preformation of the DIS kissing dimer structure is important for NCp7 activated

isomerization, the addition of the antisense DNA oligonucleotide competitors directed at the DIS loop sequence would be expected to also slow down the rate of conversion. Indeed, in the presence of these antisense oligonucleotides, the rate of the NCp7 catalyzed conversion of the DIS kissing complex to mature duplex is reduced as would be expected based on this model of competitive inhibition of kissing association (Figure 4-11). Thus, it can be concluded that preformation of the DIS kissing dimer is required for rapid, NCp7 catalyzed structural isomerization.

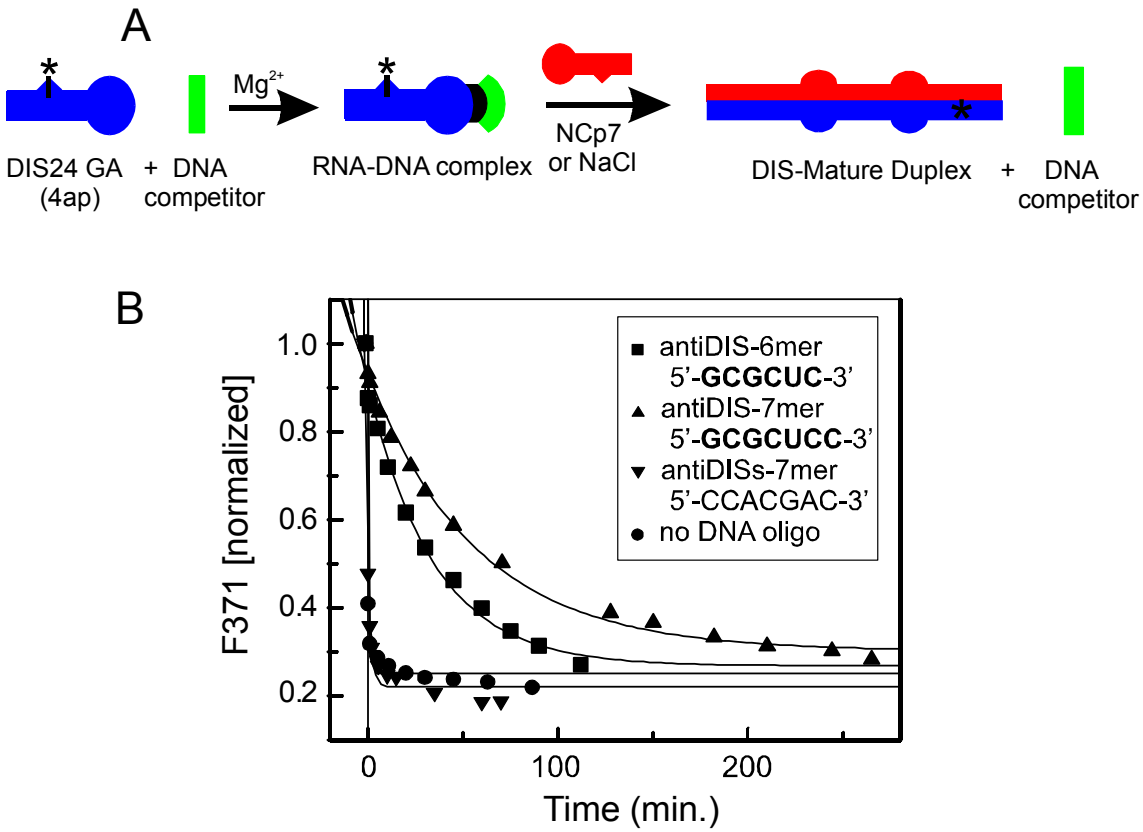

Figure 4-11. (A) Scheme of competitive inhibition of conversion with DNA oligonucleotides. (B) Plot of the rate of structural isomerization of the kissing complex to mature duplex with NCp7 in presence of antisense 7mer (filled triangles) and 6mer (filled squares) DNA oligonucleotides complementary to the DIS loop sequence, in presence of a 7mer DNA oligonucleotide (filled inverted triangles) complementary to a strand of the DIS stem and in the absence of any DNA competitors (filled circles). Solid lines show the rates for the structural isomerization that were fit using a single exponential equation [antisense-6mer: k_{conv} = 0.029 ± 0.004 min^{-1}; antisense-7mer: k_{conv} = 0.018 ± 0.002 min^{-1}; stem-7mer and no DNA competitor: $k_{conv} \geq 0.55 \pm 0.04$ min^{-1}].

In contrast, a 10-fold excess of a 7mer DNA oligonucleotide designed to bind competitively to the stem of DIS(GA), did not significantly slow down the rate of conversion (Figure 4-11). This result indicates that although the stem strands are exchanged during the conversion

reaction, the lifetime of any single stranded species is not long enough to allow capture by the antisense competitor. It also demonstrates that, although NCp7 is known to bind both single stranded RNA and DNA oligonucleotides with micromolar affinity, the reduction in rate of isomerization by the antisense DNA competitors is most likely not related to inhibition due to direct competitive binding of the DNA oligonucleotides with NCp7.

The effect of NCp7 on the dissociation and association rates of the DIS kissing dimer has also been examined (Figure 4-9). The experiments were essentially performed as above, but with 500 nM NCp7 present in the reaction solution. It was found that NCp7 did not significantly affect the rate of either the association or dissociation of the DIS kissing dimer. In addition, an experiment was performed with a DIS kissing complex, preformed between DIS24(GA)-12ap and DIS24(UC) in the presence of 5 mM Mg^{2+}, and NCp7. It was known that conversion will take place under the experimental conditions, but observation of the 2-AP label in the loop showed no significant increase in the intensity of the fluorescence emission as a function of DIS conversion. This indicates that the 2-AP base remains well-stacked during the DIS structural isomerization and suggests that the integrity of the loop-loop kissing helix is not significantly perturbed during the process. Taken together, these results indicate that NCp7 recognizes and binds to a preformed DIS kissing dimer and catalyzes isomerization, while the dimeric nature of DIS complex is maintained throughout the process.

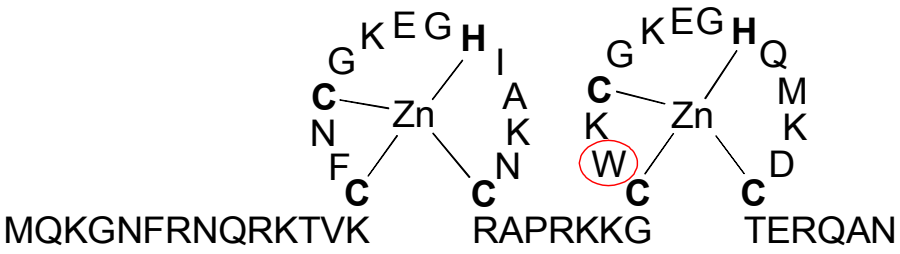

Figure 4-12. Sequence and secondary structure of the NCp7 protein. The cystein (C) and histidine (H) residues that complex the Zn^{2+} ion are printed in bold. The tryptophan used for the fluorescence experiments is circled in red.

In addition to probing the RNA structural rearrangement with 2-AP fluorescence, the interaction of NCp7 with the DIS stem-loops could also be monitored directly using tryptophan fluorescence, since the 55 amino acid NCp7 protein used in this study contains a single tryptophan residue in the C-terminal Zn-knuckle (Figure 4-12).[252-254] Titration of a fixed concentration of NCp7 with DIS kissing dimers, preformed between unlabeled DIS24(GA) and DIS24(HxUC) in the presence of 5 mM Mg^{2+}, results in approximately a 3-fold tryptophan fluorescence emission decrease (Figure 4-13), which provides a sensitive

measure for the binding reaction. Using tryptophan fluorescence quenching, NCp7 is observed to bind the DIS stem-loop kissing dimer with high affinity (K_D = 61 ± 12 nM) and in a saturated fashion (Figure 4-13). An approximate stoichiometry of two NCp7s per one RNA dimer can also be estimated from the fluorescence binding curves, which is consistent with the C2-symmetry of the DIS dimer. While tryptophan fluorescence clearly monitors one high-affinity class of NCp7 interaction with the DIS kissing dimer, this does not exclude the possibility that additional NCp7 binding event(s) might be undetected when using tryptophan as a reporter. This could be a potential reason for why a second lower affinity 'catalytic' NCp7 binding class, which is implied by the NCp7 catalyzed DIS isomerization experiments described below, may not be detected by the tryptophan fluorescence measurements.

NCp7 tryptophan fluorescence intensity could also be monitored as a function of DIS conversion. In this experiment, where a DIS kissing complex, preformed between unlabeled DIS24(GA) and DIS24(UC) in the presence of 5 mM Mg^{2+}, was added to 500 nM NCp7, the tryptophan fluorescence was observed to remain highly quenched during the entire course of the DIS structural isomerization, suggesting that the high-affinity sites for NCp7 binding to the DIS kissing dimer remain occupied during the course of the structural conversion and even in the mature extended duplex form.

To further examine the ability of NCp7 to act catalytically in the DIS structural isomerization reaction, conversion rates were monitored using 2-AP fluorescence as a function of NCp7 concentration. Under the conditions used in this experiment, DIS conversion was not observed in the absence of NCp7. Figure 4-13 shows fits for the rates of conversion of 100 nM DIS24(GA)-4ap•DIS24(UC) kissing dimer as a function of increasing NCp7 concentrations over a range of 75 to 500 nM. In all cases where NCp7 is added, the structural isomerization is observed to go to completion as evidenced by the common plateau of final fluorescence emission intensity. However, two distinct ranges of conversion rates are observed which correspond to ratios of NCp7 to DIS kissing dimer that are either above or below the estimated 2:1 NCp7:DIS stoichiometry of binding. An apparently maximal rate of conversion is observed when the NCp7 concentration is above the 2:1 NCp7:DIS stoichiometry for high-affinity binding, while a slower average rate is observed at substoichiometric ratios of protein to DIS kissing dimer.

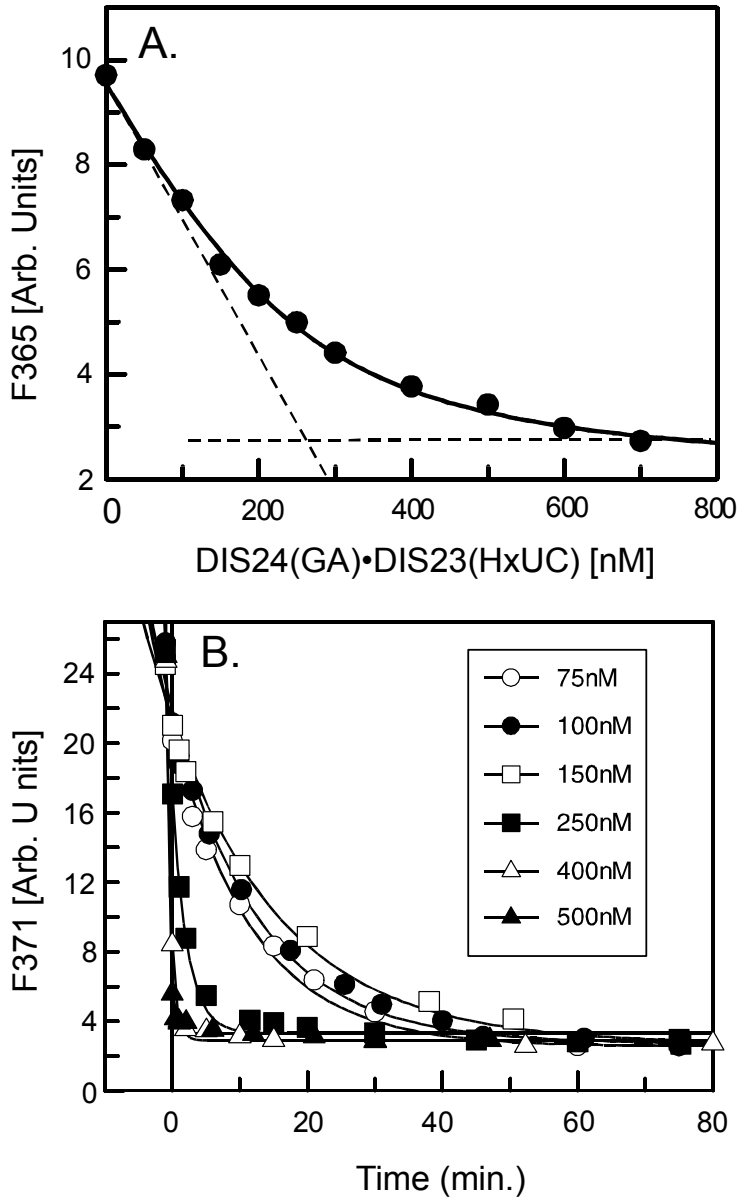

Figure 4-13. (A) Plot of the decrease in fluorescence at 365 nm as a result of titration of 500 nM NCp7 with a preformed DIS24(GA)•DIS23(HxUC) complex [RNA complex was in standard buffer containing 5 mM $MgCl_2$]. The solid curve is fit (K_D = 61 ± 12 nM) using an equilibrium binding equation and assuming two equivalent binding sites for NCp7. A linear extrapolation of the first few points and the plateau of fluorescence emission intensity are shown as dashed lines. The intercept of these two lines gives an estimated binding stoichiometry of 2:1 (NCp7:DIS dimer). Binding data were collected at 25 °C. (B) Plots of the rate of structural isomerization of 100 nM DIS24(GA)-4ap•DIS24(UC) kissing complex as a function of NCp7 concentration. Symbols indicating the curves for concentrations of NCp7 ranging from 75 nM to 500 nM are given in an inserted box. The structural isomerization rates (75 nM NCp7: k_{conv} = 0.084 ± 0.008 min^{-1}; 100 nM NCp7: k_{conv} = 0.077 ± 0.007 min^{-1}; 150 nM NCp7: k_{conv} = 0.06 ± 0.006 min^{-1}; 250 nM NCp7: k_{conv} = 0.460 ± 0.024 min^{-1}; 400 nM NCp7: k_{conv} = 1.39 ± 0.06 min^{-1}; 500 nM NCp7: k_{conv} = 2.2 ± 0.15 min^{-1}) were fit using an exponential equation. Two ranges of conversion rates are clearly observed which correspond to reactions carried out with ratios of NCp7 to DIS dimer that were either less or greater than the estimated 2:1 stoichiometry of binding.

4.3.2.4 Junction Mutants

With the determined stoichiometry of two high-affinity NCp7 proteins bound to one RNA kissing complex, the question arises as to where the proteins might bind to the RNA dimer. The RNA kissing dimer complex is C2-symmetric, and NCp7 is known to bind preferentially to purine-rich single stranded and bulged nucleic acid structures.[253, 255, 256] Based on this information, one might postulate that NCp7 might bind at the two 'junction' regions between the stem and the loop, where there are highly conserved unpaired purine bases. A recent NMR structure of the NCp7 bound to stem-loop 3 (SL3) of the DLS (Figure 4-14) supports this hypothesis, since the NCp7 is shown to bind to a GAG sequence in the loop of SL3,[257] and the same motif can be found in the junction region of DIS (Figure 4-14). These purines flanking the autocomplementary sequence in the loop are highly conserved among all known HIV-1 sequence classes.[258-260]

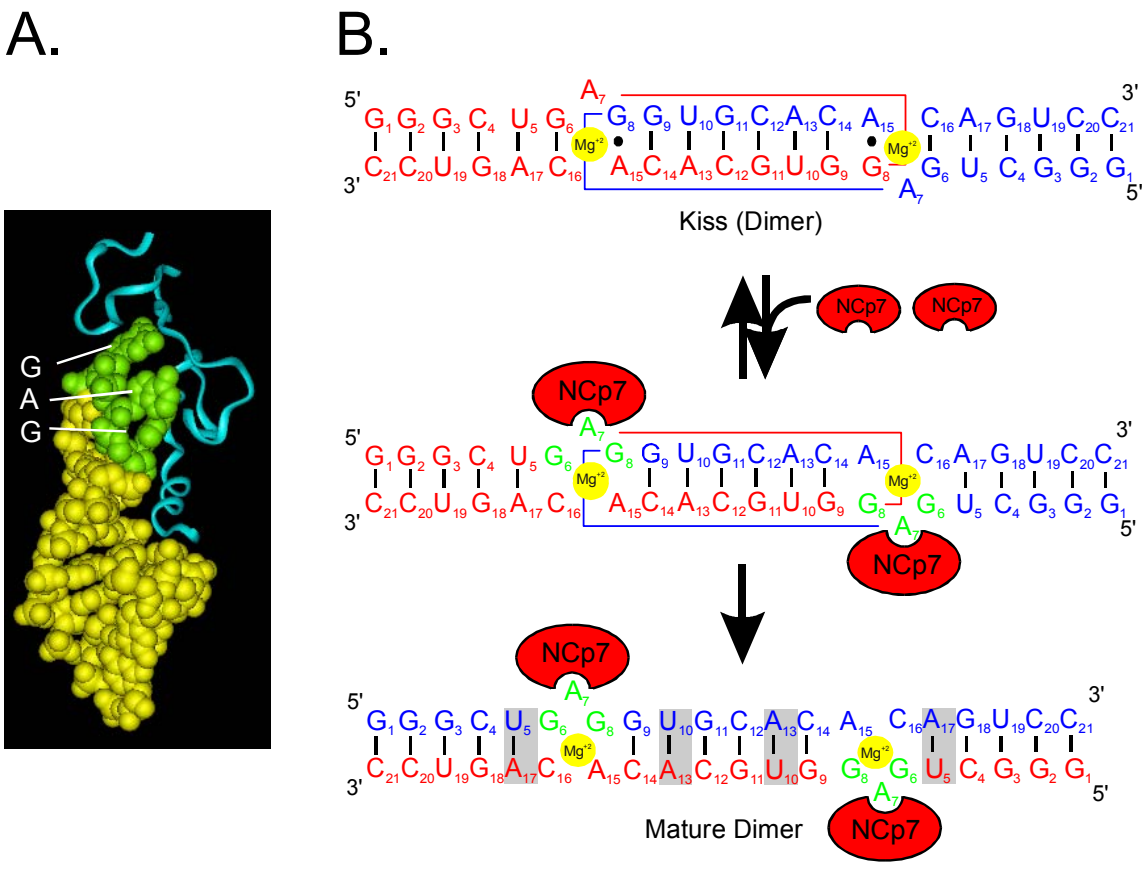

Figure 4-14. (A) Structure of NCp7 bound to stem-loop 3 of the HIV-1 DLS as determined by solution NMR.[257] The bases GAG that the protein binds to are marked in green. (B) Possible NCp7 binding site and model for NCp7 activated DIS maturation. GAG bases at the junction region that might be recognized by NCp7 are highlighted in green.

To investigate the potential role of the conserved purines in NCp7 binding, DIS kissing complex stability and structural conversion, point mutations were made at these base positions in the model DIS hairpins. The resulting so called 'junction mutant' DIS RNA oligonucleotide samples are only slightly modified as compared to the previously described samples, where the two mutations in the hexanucleotide sequence and the single nucleotide stem bulge were maintained, and the nucleotides 1, 2 and 9 in the loop were systematically mutated one by one or in pairs, while at the same time not introducing the possibility for any new base pairs in the mutant sequences that would extend either the stem or loop helix. (Figure 4-15).

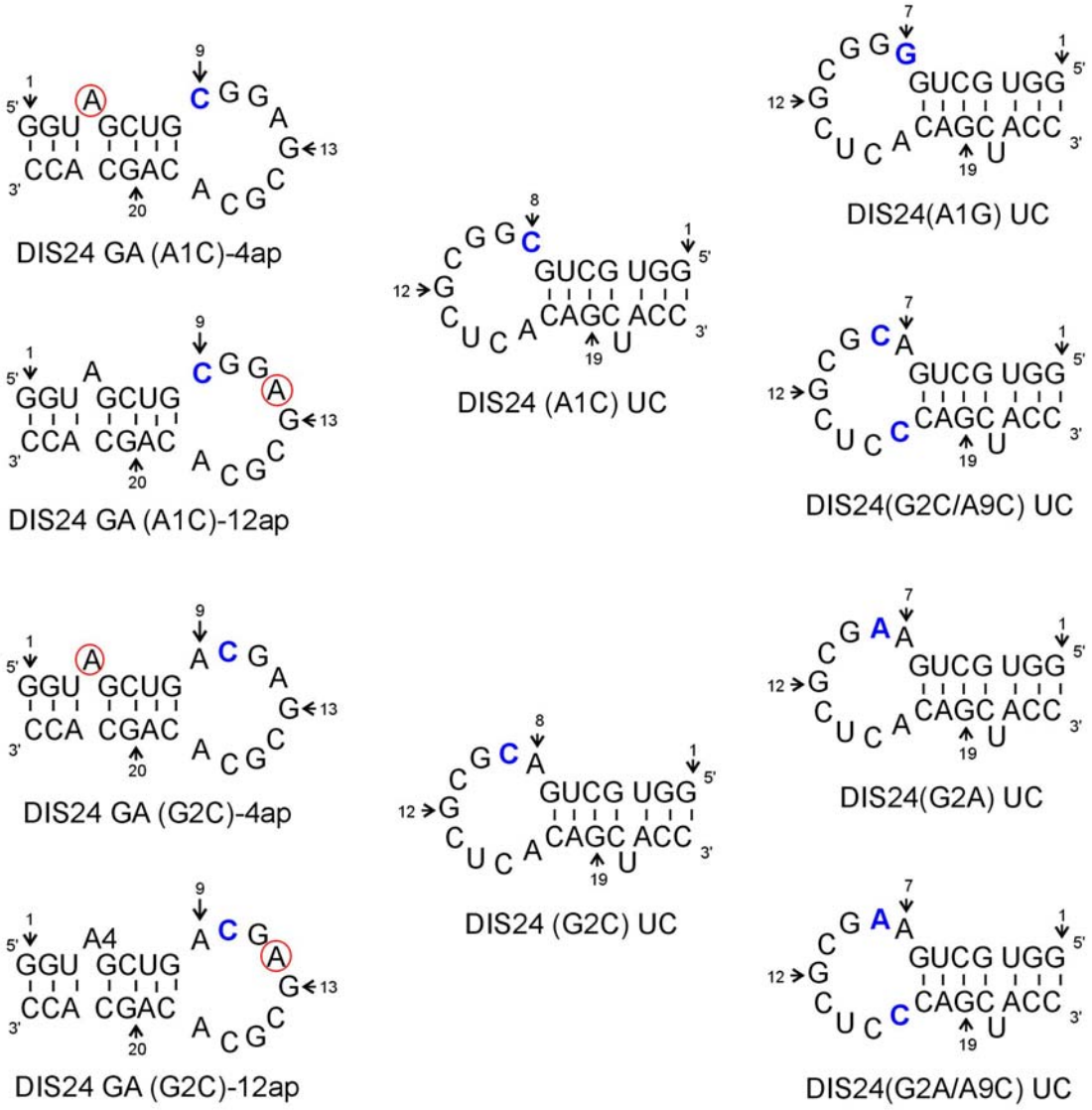

Figure 4-15. RNA sequences and secondary structures of the DIS 'junction mutant' stem-loop constructs designed to form heterodimer complexes. Point mutations in the loop sequence in addition to the GA and UC are bolded in blue, positions substituted with 2-AP are circled in red.

Using the junction mutant samples, it was first tested if the kinetics of the kiss formation were affected. Titration of unlabeled complement (DIS24(A1C)UC or DIS24 (G2C)UC) to a fixed concentration of 2-AP loop-labeled hairpin (DIS24GA (A1C)-12ap or DIS24GA (G2C)-12ap) in the presence of Mg^{2+}, and fitting of the data to equation 9.6, yielded equilibrium binding constants of $K_{Daverage}$ = 1.6 nM that were not significantly different from the previous results. Thus, it was concluded that the kissing dimer stability is not affected by the mutations. In contrast to what was expected based on a model of NCp7 binding to the junction, the apparent binding affinity of NCp7 to DIS kisses formed with junction mutants did not change dramatically. Titration of a fixed concentration of NCp7 with a kissing complex preformed between unlabeled DIS24GA and DIS24(A1C)UC or DIS24(G2C)UC in the presence of 5 mM Mg^{2+} yielded binding constants of ~50 nM. NCp7 binding was therefore not affected by the mutations, which means either that NCp7 does not bind in the junction region as predicted, or that it does not recognize a specific sequence but rather the tertiary structure at the junctions of the kissing complex.

The effect of the junction mutations on the rates of conversion of the DIS hairpins from kissing to mature duplex was investigated. In these experiments, the kissing complexes were preformed in the presence of 5 mM Mg^{2+}, before adding NCp7 to promote conversion at 20 °C. It seemed that kissing complexes that contained one or two (G2C) mutants converted faster than GA•UC kisses, and that (A1C) mutants showed slower isomerization rates (Figure 4-16), whereas the (G2A/A9C) and (G2A) mutants were not significantly different from the GA•UC kisses.

Surprisingly, the double mutant samples, DIS24(G2C/A9C)UC and DIS24(A1G)UC showed a spontaneous pronounced decrease in fluorescence emission intensity of the DIS24(GA)-4ap sample upon addition of only Mg^{2+}. These results suggested that the double junction mutant DIS samples can convert to duplex with divalent cations as maturation agents. Since spontaneous conversion is apparently occurring for these mutant samples, the conversion rates with NCp7 were not determined.

In summary, the results obtained from the junction mutant experiments suggest a possible role for the conserved purine nucleotides (especially adenosine at position 1 of the loop) in the conversion potential of the DIS kissing dimer, more experiments clearly need to be performed to confirm the results on the Mg^{2+}-dependent conversion and to find out the specific role of each of the three mutated nucleotides.

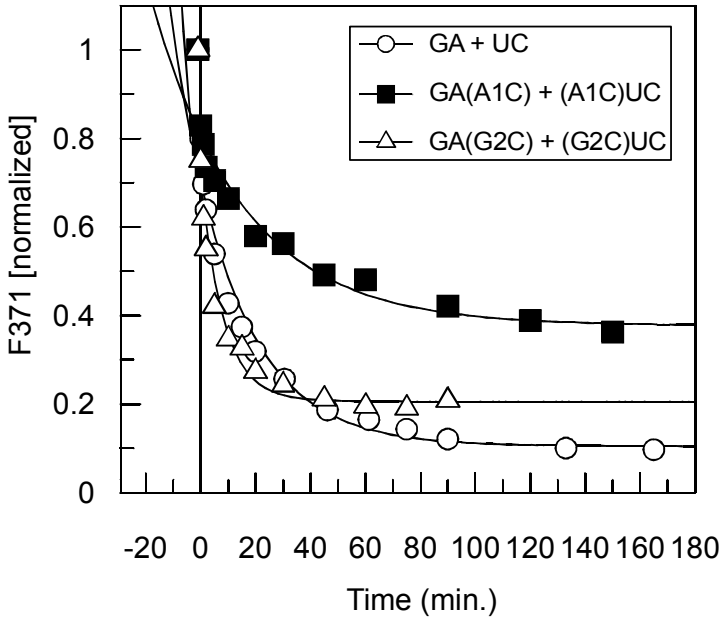

Figure 4-16. Conversion of 'junction mutants'. Plot of the decrease in fluorescence at 371 nm after adding 250 nM Ncp7 to 100 nM DIS kissing complex, preformed with 5 mM $MgCl_2$. Open circle: DIS24(GA)-4ap + DIS24(UC); filled square: DIS24(A1C)GA-4ap + DIS24(A1C)UC; open triangle: DIS24(G2C)GA-4ap + DIS24(G2C)UC.

4.3.2.5 Proposed Model for DIS Conversion

Under all conditions tested for *in vitro* isomerization, the results indicate a secondary structure rearrangement mechanism for isomerization that involves melting of intramolecular stem base pairs and reformation of intermolecular base pairing between the two stem helices of the DIS stem-loops. This observed mechanism is consistent with the initial proposal for *in vitro* DIS maturation[216, 227, 228, 257] and results from other recent studies;[230, 231, 261, 262] however, it contradicts a recently proposed autocatalytic mechanism.[244] Based on crystal structures of both the kissing and extended duplex DIS dimers,[1, 244] *Ennifar et al.* argued that the nucleotides directly flanking the DIS palindromic sequence in the kissing dimer are favorably oriented for symmetrical cleavage and subsequent cross religation to produce the mature DIS dimer.[244] If maturation proceeded through such a ribozyme-like mechanism, without melting and exchange of the stem helical strands, the stem inserted 2-AP fluorescent probe used here would not have reported on the maturation process.

The rate enhancement observed for NCp7 activated isomerization can be rationalized in terms of the extent to which this refolding catalyst either destabilizes the kissing dimer or conversely stabilizes the transition-state folding intermediate (Figure 4-17). Either type of

interaction would decrease the activation energy and accelerate the rate of the DIS conversion reaction. Such a role for NCp7 would be analogous to the classic transition state theory for how enzymes accelerate chemical reactions, and suggests an enzyme-like mechanism for how this RNA chaperone functions. NCp7 is also able to turn over and affect multiple DIS conversion reactions, reinforcing the description of this RNA chaperone as a true refolding enzyme in this *in vitro* system. However, two ranges of conversion rates are observed which correspond to ratios of NCp7 to DIS kissing dimer that are either above or below the estimated 2:1 NCp7:DIS stoichiometry for high-affinity binding of NCp7 (Figure 4-13).

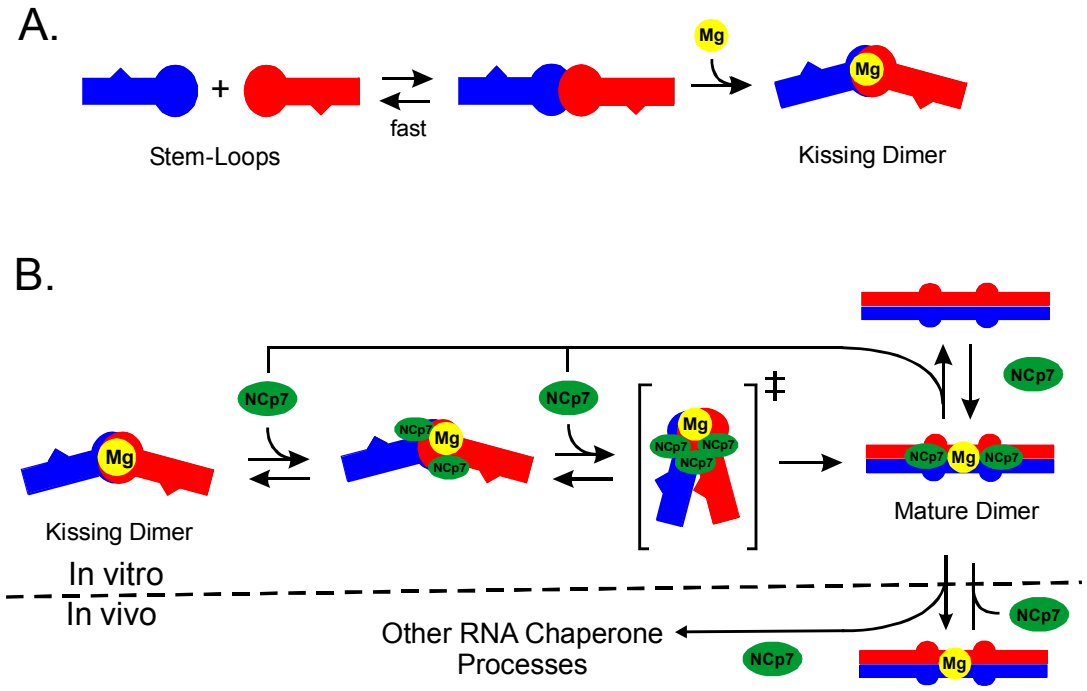

Figure 4-17. Binding pathway and proposed catalytic role of NCp7 in the structural isomerization of the DIS homodimer *in vitro*. (A) A collision complex initially forms via a loop-loop interaction between two individual DIS stem-loops which is stabilized by divalent metal ions. The DIS stem-loops are shown schematically in blue and red to allow them to be distinguishable from each other in the dimer complexes. The intermediate loop-loop kissing complex is kinetically trapped in the presence of Mg^{+2} (represented by a yellow sphere) and does not spontaneously convert to the mature extended duplex form. (B) NCp7 (represented by a green sphere) acts by binding to the intermediate loop-loop kissing complex in an excess of the stoichiometry of two NCp7 molecules to one DIS dimer. Binding of NCp7 decreases the energy difference between the kissing intermediate and the transition state in the refolding pathway, thereby lowering the activation energy and increasing the rate of structural isomerization. Dissociation of NCp7 from the mature extended duplex form of DIS allows it to act catalytically by rebinding and converting another intermediate kissing dimer. Since there is only one DIS interaction to act on *in vivo*, the biological significance of the observed recycling of NCp7 activity *in vitro* could be related to chaperone activities of NCp7 at different sites on the genomic RNA.

Furthermore, the apparent maximal rate for DIS isomerization is only observed when the NCp7 concentration is above the estimated 2:1 NCp7:DIS stoichiometry. These results suggest that the high-affinity sites for NCp7 binding must first be saturated before the full catalytic effect of NCp7 is observed and implies the two NCp7 molecules that occupy the high-affinity sites on DIS may be inactive in catalyzing the refolding reaction. Instead, excess 'free' NCp7 may act either independently or together with the high-affinity bound NCp7 molecules in capturing and stabilizing the transition state and thereby producing the catalytic effect. Accordingly, the rate of conversion would be limited by the concentration of the 'free' NCp7, which would depend on the off-rate of the NCp7 protein from the DIS dimers at concentrations of NCp7 that are less than the 2:1 NCp7:DIS stoichiometry of the high-affinity binding class. The off-rate of NCp7 for the DIS dimers has not been explicitly determined here, however, it can be inferred to be relatively fast from the conversion rates observed at substoichiometric ratios of NCp7 to DIS 'kissing dimer.

The two apparent classes of interactions of NCp7 represented by the binding and kinetic data may indicate two unique functional roles for how NCp7 interacts with the DIS kissing dimer. NCp7's first role could involve a high-affinity interaction with the DIS kissing dimer which results in the formation of a specific RNA-protein complex that may both facilitate DIS maturation, as well as packaging of the genomic RNA. The second role for NCp7 would involve a transient chaperone-type interaction with the DIS kissing dimer resulting in the destabilization of the DIS stem helices and the promotion of stem strand exchange. The description of two classes of NCp7 interaction with DIS is in some ways consistent with previous observations that a threshold binding ratio of approximately one NCp7 molecule per seven nucleotides of RNA is required for NCp7 to exhibit chaperone activity.[228, 240, 263] This has been shown to be the approximate ratio at which nucleic acids become saturated with NCp7.[256, 264, 265] The requirement of a threshold concentration for the observation of a demonstrable NCp7 nucleic acid chaperone activity suggests that there may be no turn over in the NCp7 catalysis of conformation changes. The need for threshold concentrations of NCp7 might also indicate that interactions between NCp7 molecules bound to RNA play a role in the chaperone effect.[266]

Similarly, the results of the present study also indicate a threshold concentration requirement for the most rapid NCp7 catalytic activity and correlate this threshold concentration to the need to first fully occupy two high-affinity NCp7 structural binding sites on the DIS kissing dimer. Only after these binding sites are saturated is full catalytic chaperone activity observed for the excess 'free' NCp7 protein, as is also suggested by previous studies.[228, 240, 263, 267] The

ability of NCp7 to turn over in the DIS conversion reaction may simply reflect the availability of only two high-affinity NCp7 structural binding sites on the DIS dimer, with moderate off-rate rates, in this minimal system. In contrast with the isolated DIS kissing dimer, NCp7 may be continually trapped in multiple binding sites of moderate to high-affinity in the larger RNA systems and thereby be significantly inhibited from binding and functioning in its role as a chaperone. The interpretation that the catalytic interaction(s) of NCp7 with DIS may involve a lower-affinity, transiently bound class of molecules is also consistent with previous observations that the chaperone activity of NCp7 is non-sequence specific and driven primarily through non-specific electrostatic and intercalative interactions. It is also consistent with the absence of a measurable tryptophan fluorescence change for this class of NCp7 interaction.

Observation of NCp7 turnover in the *in vitro* refolding reaction (Figure 4-17) may not have specific relevance to the *in vivo* genome maturation process, where only a single RNA dimer exists on which NCp7 could act. Instead, the observed recycling ability of the catalytic NCp7 may function *in vivo* by promoting other nucleic acid structural rearrangements or transient structural binding events at other locations on the RNA strand within the budded viral particle. Alternatively, the observed turnover of NCp7 could be related to chaperone functions it may carry out as a domain within the intact *gag* protein. Since *gag* is abundant in HIV-1 infected cells and has been shown to potentate similar chaperone activities as the isolated NCp7 *in vitro*,[268, 269] the observed recycling could possibly be related to an *in vivo* nucleic acid chaperone function of *gag* that either requires or is made more effective by multiple turnovers in activity.

Since DIS structural isomerization can occur under different experimental conditions and requires preformation of the DIS kissing dimer, the conversion process is clearly related to the structure and dynamics of the DIS kissing dimer and is likely to involve a common transient-state RNA folding intermediate (Figure 4-17). Furthermore, the structure of the Mg^{2+}-stabilized DIS kissing dimer may be pre-organized to facilitate NCp7 binding and fast conversion rates. In its specific catalytic role, NCp7 accelerates the rate of strand exchange between the two hairpin stem helices, without destabilization of the loop-loop helix. Under these structural constraints, NCp7 might act to facilitate the exchange of stem helices by distorting or stressing the DIS kissing conformation. One possible mode of structural distortion would be through helical bending centered on the loop-loop kissing helix, which could bring the two stem helices into close proximity and proper alignment to facilitate the isomerization process. Although not observed in the crystal structures,[1, 244] such a helical

distortion of a kissing complex structure has precedent from previous structural studies in solution[190, 191, 196] and in this instance might uniquely involve the highly conserved purine nucleotides that flank the palindromic DIS loop sequence. These nucleotides may assume a unique conformation in the transient-state folding intermediate that both distort the DIS kissing dimer conformation and concomitantly destabilize the stem helices. In this model for DIS conformational isomerization, the observed spontaneous conversion of the metastable DIS kissing dimers could be the result of the inherent structural plasticity in these dimers. Unlike the divalent metal ion stabilized kissing dimer, the metastable kissing dimers might be sufficiently close in energy to the transition-state conformation such that this intermediate state is accessible through simple thermal fluctuations and consequently spontaneous structural isomerization is possible.

4.4 Summary

In this study the highly fluorescent adenosine base analog 2-AP has been selectively incorporated into RNA constructs derived from the HIV-1 DIS_{Mal} sequence to provide unambiguous and unique probes for *in vitro* formation of the two isoforms of the DIS_{Mal} dimer. Using 2-AP fluorescence detected methods, equilibrium and kinetic binding constants for the DIS kissing dimer interaction have been determined. In addition, real-time 2-AP fluorescence measurements have been employed to gain a detailed kinetic view of the process of DIS isomerization. The 2-AP fluorescence detected equilibrium binding experiments demonstrate that the truncated DIS stem-loops used in this study, which lack the wild-type stem bulge and have been altered in the loop palindromic sequence, associate under a number of experimental conditions to form kissing dimers with wild-type affinities. The formation of a kinetically stable intermediate DIS kissing dimer, however, requires the addition of divalent metal ions. Thus, two different classes of the DIS kissing dimer, with distinct isomerization potentials, could be distinguished using the 2-AP fluorescence methods. The divalent metal ion stabilized DIS kissing dimer class, which is kinetically stable, required the addition of NCp7 to activate fast-rates structural isomerization; while the metastable DIS kissing dimer class, which forms with monovalent cations or at higher concentration (> μM), converted spontaneously to the mature duplex form at an appreciable, but 10-20 fold slower rate than observed for NCp7.

The data also clearly demonstrate a secondary structure rearrangement model for *in vitro* DIS stem-loop isomerization and provide insight into the role of NCp7 in catalyzing this process.

How DIS structural isomerization could similarly be accomplished *in vivo* and how it relates to retroviral maturation and packaging still remain open questions. An isomerization mechanism involving DIS stem strand exchange, as described here for the isolated DIS hairpins, would potentially involve large-scale movements of the entire 5'-ends of the two copies of the HIV-1 RNA genome relative to each other, within the budded viral particle. Determining if and how this associated structural rearrangement could be achieved will require further studies into the molecular basis underlying the *in vivo* process.

5 Excimer Formation in DNA Studied with 2-AP Fluorescent Markers

5.1 Introduction

In the previous two chapters of this thesis, the quenching of 2-AP fluorescence upon a change in its environment was exploited to study RNA-RNA and RNA-protein interactions. But, in fact, it is unclear if the 2-AP fluorescence only comprises the 2-aminopurine base itself or if adjacent bases are also affected by the energy absorbed during the fluorescence experiments. It is a key question which is crucial for the mechanism of various photoreactions in DNA, whether excited singlet states of DNA bases are localized or extended over several neighboring bases. As already discussed in section 2.4.1, evidence for excimer emission between nucleosides at low temperature was given by *Eisinger et al.* in 1966,[96, 97] but experimental obstacles like overlapping spectra of natural DNA bases hampered spectroscopic studies at room temperature. In this work, a novel experimental approach to study excitonic coupling, excitation energy transfer, and excimer formation in DNA with optical spectroscopic methods at room temperature is presented using the distinct photophysical properties of 2-AP.

5.2 Sample Design and Control Experiments

Figure 5-1 shows the sequences of the two DNA assemblies **A1** and **A2** used in this study. The design of the sequences was based on the following considerations: At least two 2-AP units next to each other are needed to be able to observe potential excimer formation. It is assumed that the signal intensity of the recorded spectra will improve significantly when several 2-AP dimers are present in the duplex. At the same time it is important that the excimers experience the same environment. These considerations led to the design of the palindromic sequence of the "excimer strand" **A1**. The two G-C base pairs on either end are required to prevent higher order aggregates of the regular $(Ap\text{-}Ap\text{-}T\text{-}T)_n$ sequence. The reference strand **A2** was designed to resemble the excimer sequence **A1** as closely as possible

without the 2-AP pairs. Hence, **A2** contains only single 2-AP units with adenines replacing every other 2-AP.

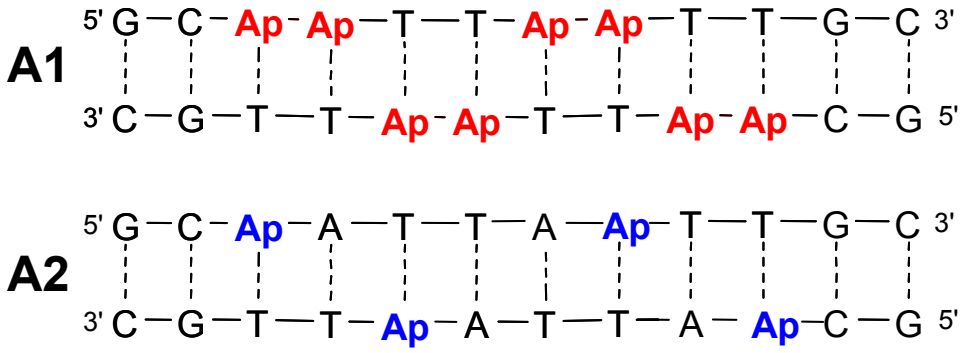

Figure 5-1. The two DNA assemblies used in this study. Sequence **A1** is designed to explore excimer formation between two adjacent 2-aminopurine bases (Ap) while sequence **A2** serves as the reference sequence with isolated fluorescent markers but similar DNA sequence.

To confirm that incorporation of 2-AP units does not significantly perturb the B-conformation of the DNA duplexes used here, UV-melting curves and CD spectra of the two assemblies were recorded.

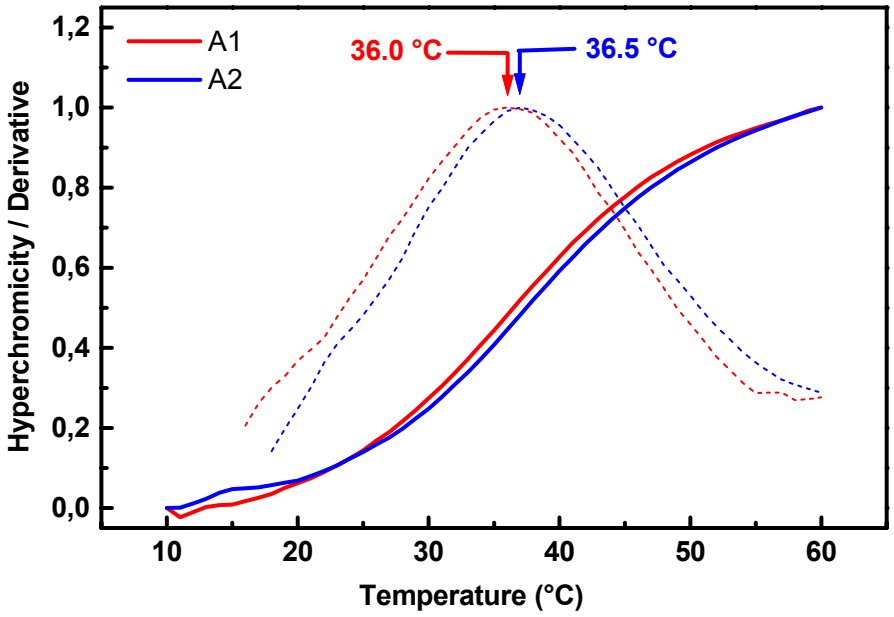

Figure 5-2. UV melting curves (solid lines) and their derivatives (dashed lines) of the two DNA sequences **A1** (red) and **A2** (blue). The derivatives of the melting curves show a melting temperature (T_m) of 36 °C for **A1** and 36.5 °C for **A2**, corresponding very well with the calculated value of T_m = 36 °C for a reference duplex containing adenines in all positions of 2-AP.

The UV melting curves and their derivatives are shown in Figure 5-2. The resulting melting temperatures were 36.0 °C for **A1** and 36.5 °C for **A2**, corresponding perfectly with the calculated value of T_m = 36 °C for a reference duplex containing only adenines in the positions of 2-AP.

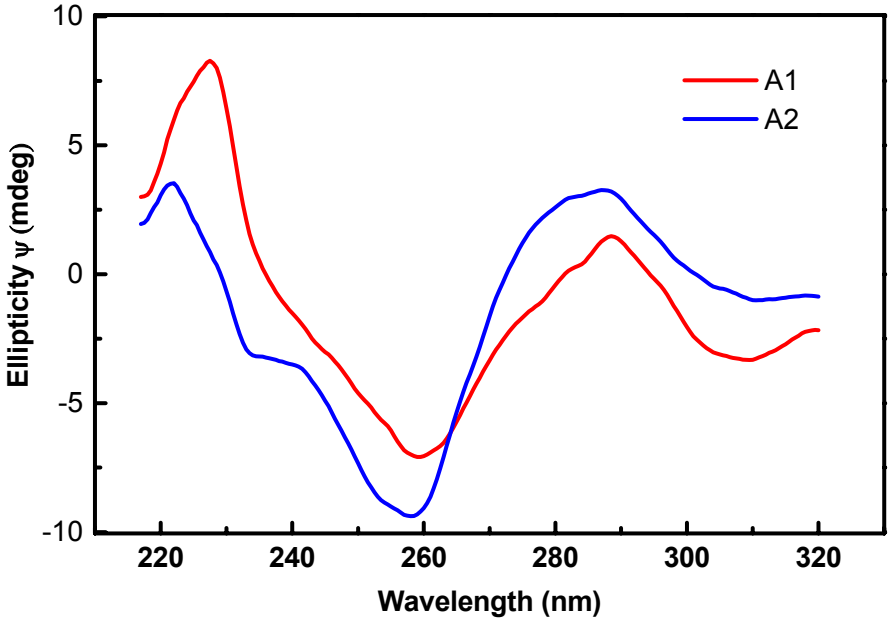

Figure 5-3. CD spectra of the two assemblies from Figure 5-1. Both spectra are indicative for B-form DNA.

The CD spectra of **A1** and **A2** are shown in Figure 5-3. Both spectra show a minimum around 260 nm and a maximum around 280 nm which is indicative for a B-form helix of the DNA-duplex. In summary, it can be concluded that the 2-AP incorporation does not perturb the overall structure or stability of the employed DNA assemblies relative to a duplex of the same DNA sequence with all natural bases.

5.3 Results and Discussion

5.3.1 Steady-State Fluorescence Spectroscopy

Figure 5-4 shows the absorption spectra of the two DNA assemblies **A1** and **A2** in the range of the long-wavelength absorption of 2-AP. Note that in **A1** there are four pairs of adjacent 2-AP bases, whereas in **A2** all 2-AP bases are adjacent to either A, T, or C. By comparing the spectroscopic properties of **A1** and **A2** one can characterize the interaction between the two 2-AP units in the base stack. Figure 5-4 reveals a small but distinct difference (~ 3 nm) between the absorption maxima of **A1** and **A2**. This is already the first indication of a specific ground state interaction between the adjacent 2-AP nucleotides in **A1**.

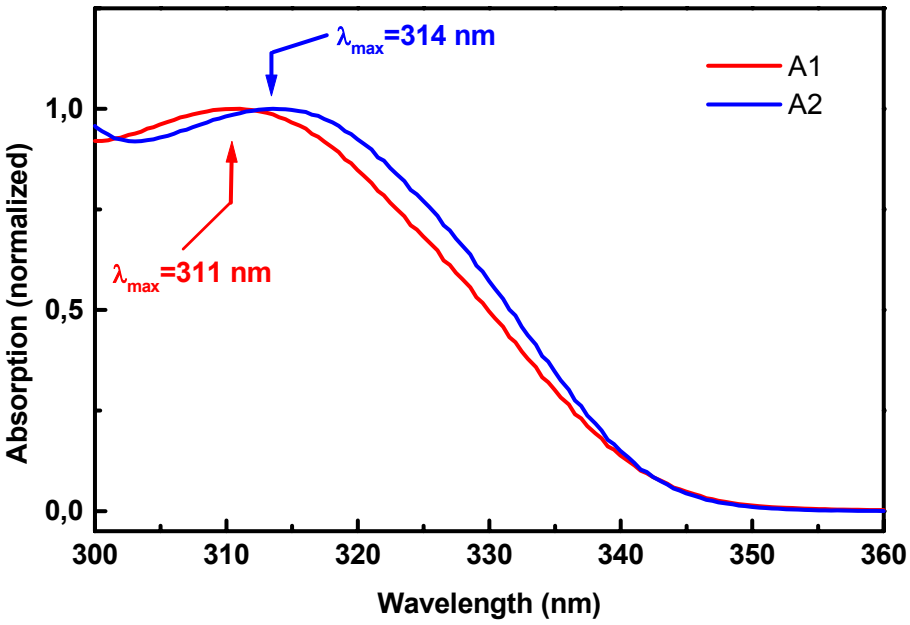

Figure 5-4. Absorption spectra of the assemblies **A1** and **A2** in the wavelength range of 2-AP, normalized to their respective absorption maxima. A small but distinct difference of the position of maximum absorbance can be observed.

The fluorescence spectra of the two assemblies **A1** and **A2** which were obtained at two different excitation wavelengths, are displayed in Figure 5-5. When the excitation occurs at 320 nm (Figure 5-5 top), near the maximum of the absorption, one observes the typical 2-AP fluorescence with a maximum emission around 370 nm. It is remarkable that the fluorescence

quantum yield of **A2** is significantly larger than that of **A1**, although **A2** contains only half as many 2-AP units. When excitation is set to 343 nm (Figure 5-5 bottom), an additional red-shifted fluorescence band around 440 nm is observed, which is present in both systems, although its magnitude is almost three times larger in **A1** than in **A2**.

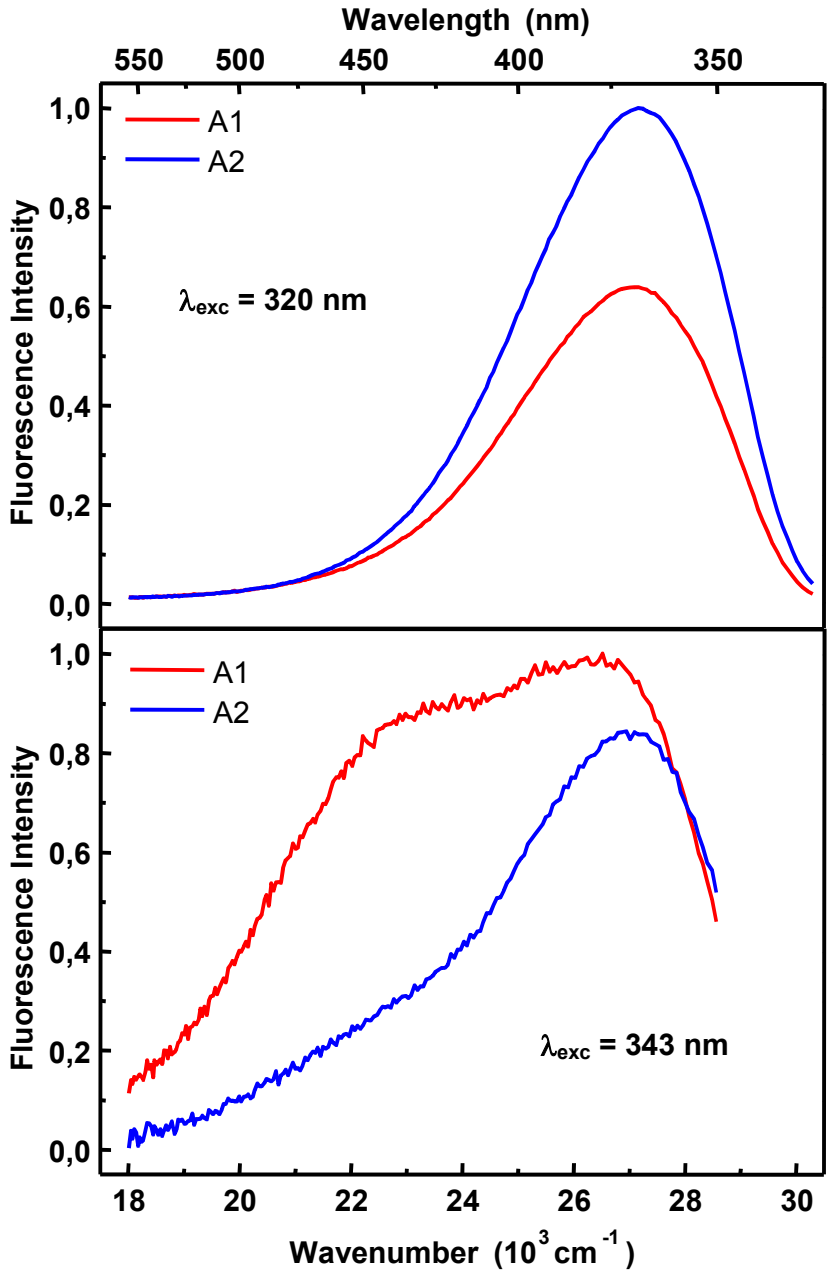

Figure 5-5. Emission spectra of the assemblies **A1** and **A2** at two different excitation wavelengths of 320 and 343 nm, normalized to the absorption maximum of the stronger signal. As clearly visible, the fluorescence spectra show a strong dependence on the excitation wavelengths.

To further investigate the fluorescence properties of **A1**, the excitation wavelength was varied from 310 to 350 nm (Figure 5-6). Two distinct peaks at 370 nm and at 440 nm could clearly be observed with amplitudes depending on the excitation wavelength.

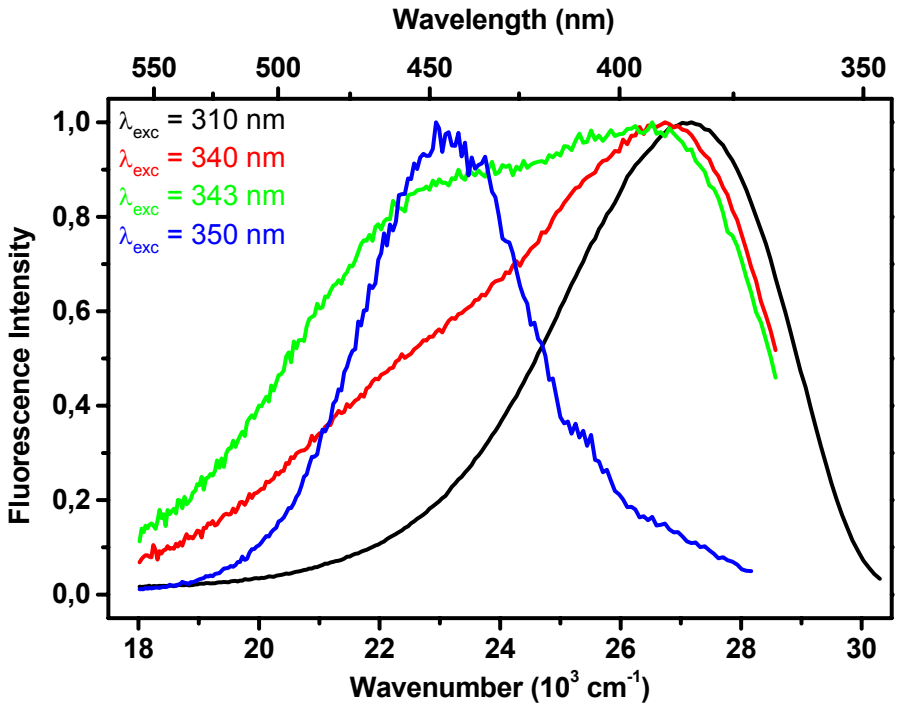

Figure 5-6. Fluorescence emission spectra of **A1** at excitation wavelengths of 310, 340, 343, and 350 nm, normalized to the maximum intensity of each spectrum. Note that when the sample is excited at 350 nm the typical fluorescence of 2-AP at 370 nm almost vanishes.

Finally, the fluorescence excitation spectra of both assemblies are presented in Figure 5-7. Recording the emission intensities at 430 and 470 nm one could expect that both systems follow their absorption spectra. However, two important differences need to be noted. First, there are additional bands at lower excitation energies (360 to 380 nm), which are not visible in the absorption spectra. They imply that emission, especially in the case of **A1**, originates from (at least) two electronic states which involve 2-AP. It is important to note that the spectral position of the low-energy bands are different for **A1** and **A2**, indicating that the electronic states involved in the optical transition are of a different nature in **A1** and **A2**. Furthermore, there is a small spectral shift in the second bands (around 320 nm) of the excitation spectra, compared to the maxima of the absorption spectra (Figure 5-4).

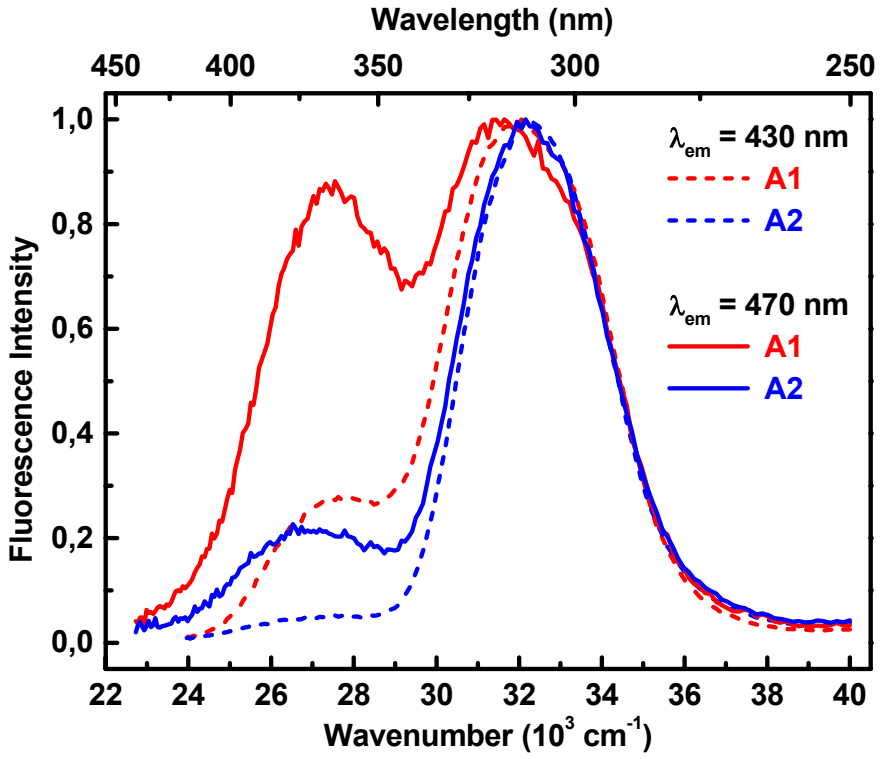

Figure 5-7. Fluorescence excitation spectra of **A1** and **A2** at emission wavelengths of 430 (dashed lines) and 470 nm (solid lines) normalized to the maximum intensity of each spectrum. Both DNA assemblies show two peaks, however, the low energy peaks in **A1** are several times larger than in **A2** and appear at slightly higher excitation energy (~ 730 cm^{-1}) than the peaks of **A2**.

From the results presented here the following picture emerges (Figure 5-8). The data reveal a significant ground-state interaction between two adjacent 2-AP bases in duplex DNA. As a result, the local transition dipole moments (S_0-S_1) of the individual 2-AP units are strongly coupled and the excitation becomes delocalized. Exciton theory[270] predicts the formation of two exciton states (Ψ_1 and Ψ_2). In **A1** the extinction coefficient for the transition to the stacked 2-AP-2-AP state (Ψ_1) is so small ($\varepsilon_{370} < 100$ $M^{-1}cm^{-1}$) that it can only be observed in the excitation spectrum (compare Figures 5-4 and 5-7). The optical excitation of Ψ_1 leads to a broad fluorescence band around 440 nm.

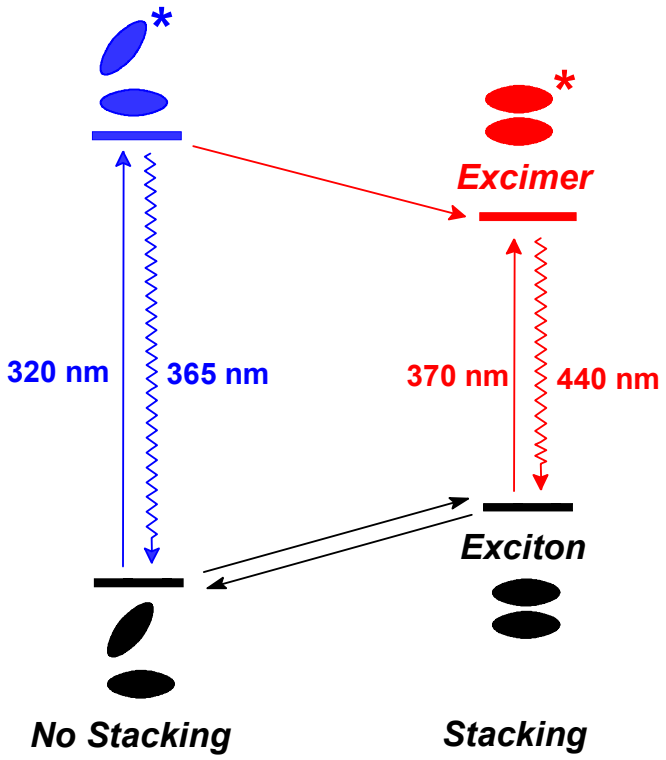

Figure 5-8. Model for the excited-state base alignment. Non-stacked bases are shown on the left with an absorption at 320 nm and fluorescence emission at 365 nm. The corresponding wavelengths for the stacked bases are 370 and 440 nm, respectively. For a subensemble of molecules, a single non-stacked and therefore uncoupled 2-AP base is excited which transfers its energy to its adjacent neighbor as soon as the coupling is established again.

The discrepancies between excitation and absorption spectra above 340 nm can be rationalized by taking into account that the DNA assemblies are characterized by a certain degree of structural inhomogeneity. Thus there will be a subensemble of molecules where a single ("uncoupled") 2-AP base is excited and can subsequently transfer energy to its adjacent neighbor (excimer formation). Note that in this case the ground-state interaction between adjacent 2-AP bases (left side in Figure 5-8) is very weak or completely absent. Therefore the red-shifted emission of **A1** (especially at 470 nm) may originate from both statically excited exciton states and dynamically formed excimers (right side in Figure 5-8).

The spectroscopic properties of **A2** indicate that 2-AP also interacts with other adjacent DNA bases. This follows from the shoulder in the fluorescence spectrum (Figure 5-5) and from the weak band in the excitation spectrum around 375 nm (Figure 5-7). Hence, it can be concluded that excitonic interaction leads to exciplex-type emission in **A2**. Such interaction between 2-AP and other bases includes additional charge transfer contributions which have been reported in previous work on 2-AP-containing DNA assemblies.[46] However, the

delocalization of excitation energy is enhanced by resonance interaction and should be more pronounced for identical bases. It should be noted, however, that despite the formal inversion symmetry of the sequences **A1** and **A2** there is no geometrical symmetry in the base stack and hence, no symmetrical exciton level splitting should be expected.

Further evidence for exciton coupling arises from the fact that the fluorescence quantum yield of **A1** is significantly smaller than the one of **A2** when excited at 320 nm (Figure 5-5), which suggests the presence of additional nonradiative channels from the exciton state Ψ_2.

The results presented here may also be relevant for the ongoing discussion about the short excited state lifetimes of the DNA bases.[62, 271-273] *Georghiou et al.*[100] proposed that the formation of excimers (or exciplexes) between adjacent bases are responsible for ultrafast quenching of DNA base singlet states. However, these authors exclude ground state interaction between bases. The results from this study, especially the fluorescence excitation spectra, demonstrate that there are indeed ground-state interactions which lead to partially delocalized excitations. Note that this information is profound regarding the base-to-base coupling in DNA and its dependence on structural fluctuations, expecially at room temperature.[274]

5.3.2 Time-Resolved Transient Absorption Spectroscopy

Femtosecond time-resolved pump-probe spectroscopy investigations addressing the dynamics for electronic energy migration in DNA were performed in collaboration with the group of Dr. T. Fiebig at the Institute for Physical Chemistry at the Technical University of Munich. The time-resolved transient absorption spectra of **A2** in Figure 5-9 show a peak around 550 nm representing the excited state of 2-AP (Ap*), which decreases over the time course of the experiment (20 ps). In other words, Ap* is formed immediately upon excitation (within the time-resolution of this experiment of 150 fs) and decays exponentially over 20 ps. The spectra of **A1** show the same peak at 550 nm at the beginning of the measurement. However, this signal does not only decay within the experiment time, but also undergoes a dynamic spectral shift from 550 to 510 nm which cannot be found in **A2**. This shift is attributed to the 2-AP excimer formation. Additionally, one observes the rise of an absorption band at 360 nm, which cannot be found in the reference system **A2**, and which is assigned to the wavelength range of the exciton ground state of the 2-AP dimer (Figure 5-9).

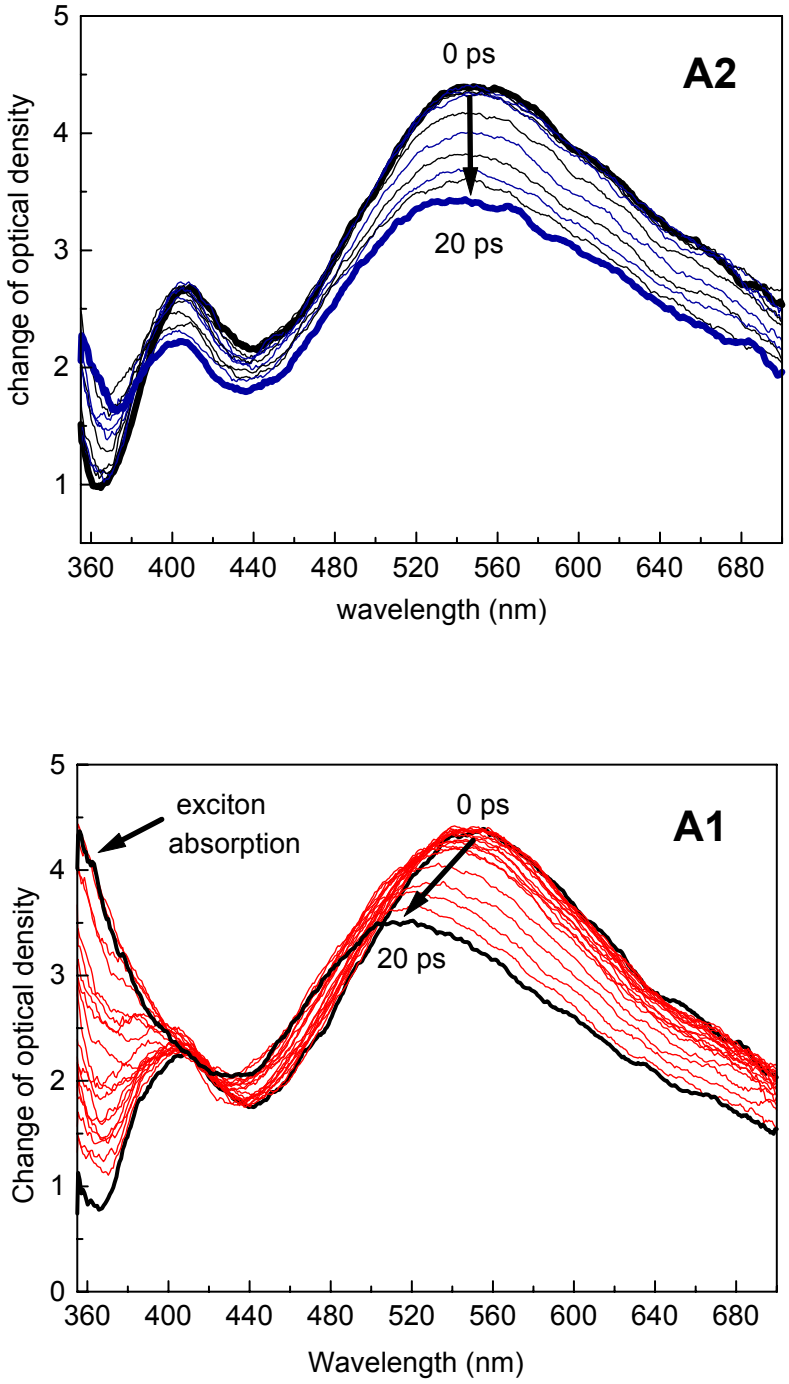

Figure 5-9. Time-resolved transient absorption spectra of **A2** and **A1**. Spectra with probe-pulse delays varying between close to 0 and 20 ps were recorded. In **A2** a distinct maximum at 550 nm representing the excited state of 2-AP can be observed that decays over time. The same distinct maximum at 550 nm can be observed for **A1**, but in addition to the decay, a shift to about 510 nm at 20 ps is observed, which represents excimer formation. The strongly increasing signal at 360 nm wavelength can be attributed to exciton formation.

To further explain the ground-state exciton formation, the change of optical density at 360 nm is depicted against time in Figure 5-10. It shows that the exciton absorption develops within 5 ps and subsequently decays with a lifetime of 80 ps.

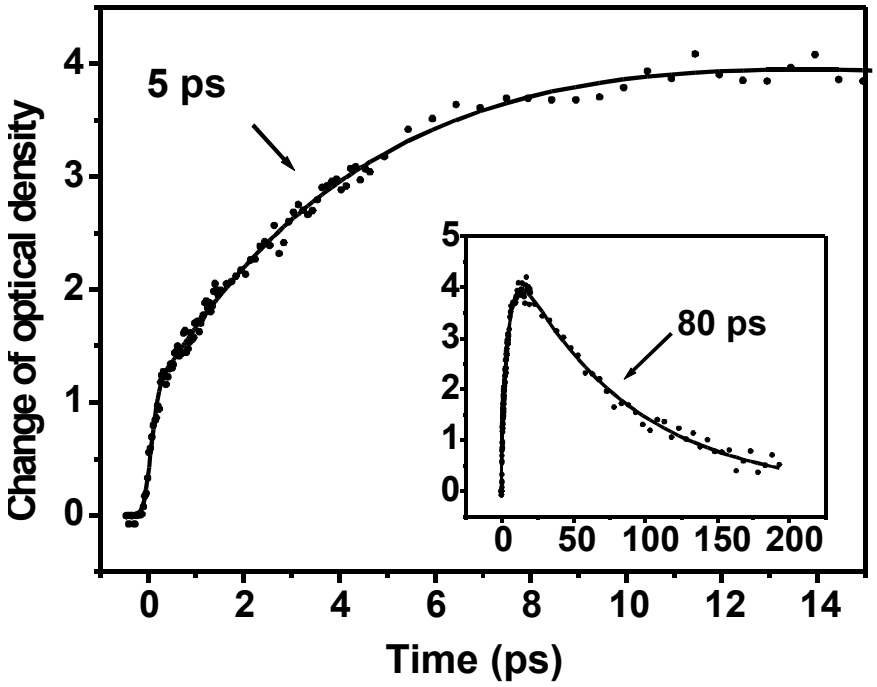

Figure 5-10. Temporal evolution of the transient absorption of the exciton coupled 2-AP at λ = 360 nm. After a fast exponential increase, an exponential decay with a decay time of 80 ps can be observed.

5.4 Conclusion

In conclusion, two specifically functionalized DNA assemblies, **A1** and **A2**, have been presented here, which make it possible to address the important issue of electronic energy migration in DNA by applying optical spectroscopic methods. The study shows that excitonic coupling between adjacent bases leads to a delocalized excitation between identical bases, even at room temperature. As a result, a new, weakly allowed emission band was observed, which is red shifted with respect to the typical 2-AP fluorescence. Excitonic interaction (with partial charge transfer character) between nonidentical bases leads to exciplex emission, however, this interaction is substantially weaker. The confirmation of the delocalized excitation energy is an important step toward the understanding of the mechanism of various photoreactions in DNA. In addition, it was found that the stacking and destacking of bases in duplex DNA occurs on the order of 5 ps. This number is of biological importance, since it reveals information about the stacking dynamics in DNA.

6 Studies of Charge Transfer in 2-Aminopurine Containing Dinucleotides

6.1 Introduction

The fluorescent nucleotide base analog 2-AP has been used in many studies to investigate macromolecular interactions and nucleic acid structure and dynamics[40, 74, 76, 200, 275, 276] as well as in chapters 3 and 4 of this work. It serves as a sensitive fluorescent probe by changing its spectral features depending on the environment. These features are usually interpreted phenomenologically without considering the electronic context dependence of the 2-AP fluorescence. On the other hand, it has been shown that 2-AP can undergo charge transfer reactions that can be exploited to investigate different aspects, such as the mechanism of DNA-mediated charge transfer. *Kelley and Barton*, for instance, used 2-AP to measure the distance dependence of charge transfer and the influence of stacking.[148] *Zewail and co-workers* tried to determine distance and sequence dependence of the 2-AP induced charge transfer.[46] It was again the group of Barton who first realized that 2-AP can act as a dual reporter probing both structural dynamics and charge transfer processes in the same nucleic acid assemblies. It was concluded that the efficiency of charge transfer depends on the structural dynamics.[48, 277]

Thus it seemed promising to look at how the base sequence influences the efficiency and the rate of 2-AP fluorescence quenching due to charge transfer. Dinucleotides represent the smallest possible units of nucleic acids for the investigation of interactions between two nucleobases. Therefore, in this study it was investigated how each of the natural DNA bases and inosine influence the fluorescence of 2-AP.

6.2 Sample Design and Control Experiments

Five dinucleotides containing 2-AP (Figure 6-1) were synthesized using standard phosphoramidite chemistry.

5’-Ap-A-3’ 5’-Ap-G-3’

5’-Ap-T-3’ 5’-Ap-I-3’

5’-Ap-C-3’

Figure 6-1. Dinucleotide sequences synthesized for the charge transfer studies.

Absorption spectra for all five dinucleotides were recorded and are shown in Figure 6-2, normalized to the maximum absorption of 2-AP. They all exhibit the characteristic 2-AP absorption with a maximum around 305 nm, but strongly varying absorption at shorter wavelengths.

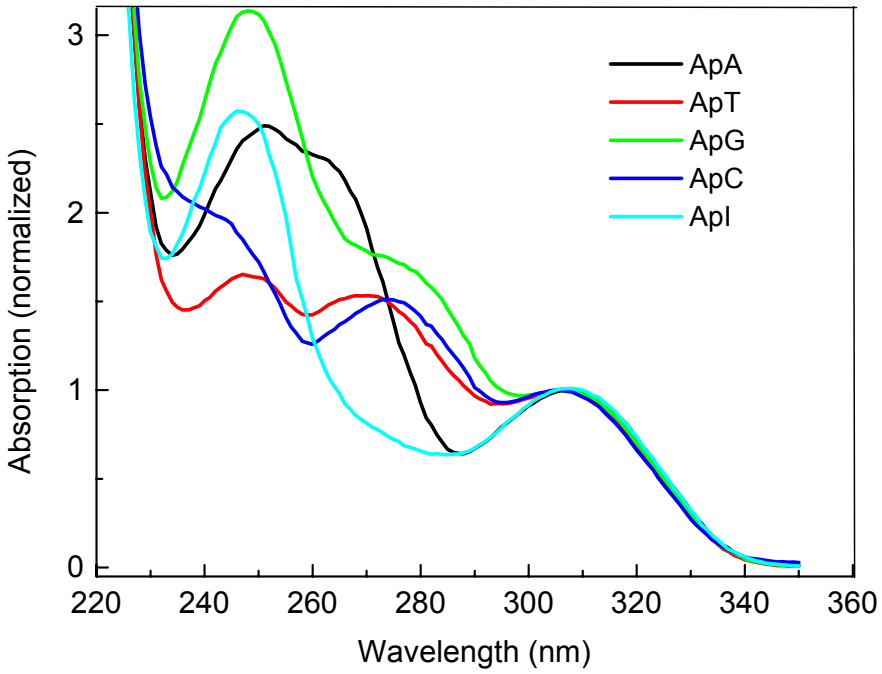

Figure 6-2. Absorption spectra of the five synthesized dinucleotides containing 2-AP bases (Ap) in the 5’-position.

In an attempt to confirm that these dinucleotides are stacked at room temperature and in a right-handed helical conformation as reported by *Kang et al.* and *Cantor et al.*,[278, 279] CD spectra were recorded at ambient temperature for all samples. A cotton effect is observed in all five dinucleotides (Figure 6-3). However, the wavelength range of these cotton effects vary significantly between 230 and 290 nm. This result is due to the fact that the absorption

maxima of the five dinucleotides are different (Figure 6-2). The observed cotton effect of ApC and ApG is rather weak since the extinction coefficients between 230 and 290 nm of these two nucleotides are very low according to the absorption spectra. At longer wavelengths between 300 and 330 nm a weak signal can be observed for ApA, ApT, and ApC that can be attributed to 2-AP. Again, the signal is very faint due to the low extinction coefficient of 2-AP.

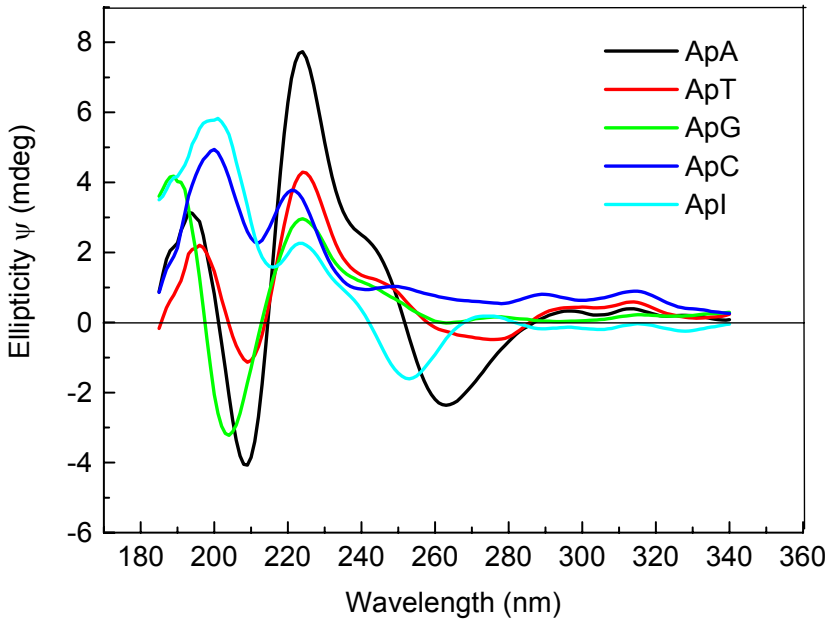

Figure 6-3. CD spectra of the five dinucleotides shown in Figure 6-1. Clearly visible is the Cotton effect on all nucleotides at wavelengths between 230 and 290 nm for the natural bases and between 300 and 330 nm for 2-AP.

6.3 Results and Discussion

Fluorescence emission spectra of the dinucleotides ApX show significant differences in the quantum yields depending on the neighboring nucleobase (Figure 6-4). Using samples with the same optical density at the excitation wavelength of 310 nm, the fluorescence intensities decrease in the following order of the neighboring DNA bases: I > C > T ~ A > G. This behavior cannot directly be assigned to the established trend for either the oxidation (G > A > I > C, T,[133, 134, 280]) or the reduction (T ~ C > A > G,[134]) potentials of the nucleotides.

The driving force for charge transfer is determined by the difference of the reversible redox potentials of the donor and acceptor. Although there is no complete set of reversible potentials

of the DNA bases and 2-AP, some information is already available in the literature. The peak potential for one-electron reduction of the excited state of 2-AP (Ap*) has been determined to be +1.5 V (versus normal hydrogen electrode (NHE)).[148] According to this value, Ap* should be able to oxidize G (+1.29 V),[133] and maybe even A (+1.42 V).[133] The reverse process, ET from Ap* to a DNA base requires knowledge of the oxidation potential of Ap, which has not yet been obtained as a reversible signal in cyclic voltammetry. *Shafirovich et al.* have estimated a value of +1.34 V for $E(Ap^{\bullet+}/Ap)$.[281] Given an excited-state energy for Ap* of E_{00} = 3.74 eV, it becomes apparent that Ap* can reduce any base with a reduction potential of about -2.5 V or higher (i. e. a smaller absolute value). However, the error of this potential due to irreversible electrochemical follow-up reactions has been estimated to be ± 300 mV.[47] Finally, there have been at least two different values reported for the oxidation potential of I (+1.5[148] and 1.39 V[282]) but no values for the reduction potential. Therefore, it is not possible to obtain accurate and conclusive ΔG values for either the reduction (ET) or the oxidation (HT) processes of the nucleobases. Moreover, in the case of I it can only be speculated whether HT or ET operates.[47]

Despite the uncertainties related to irreversible electrochemistry, a trend for the oxidizability of the nucleobases has been established: G > A >> C > T.[133, 134] This trend is supported by correlation of peak potentials with measured ionization potentials in the gas phase[280] and by high-level DFT calculations of the adiabatic ionization potentials.[283] Therefore it is concluded that both reaction types (HT and ET), namely reduction and oxidation of nucleotides by Ap*, are present in this series of dinucleotides.

The direction of charge transfer for ApG, ApT, and ApC is the following: G is oxidized, whereas T and C are reduced. It is expected that A and I will be positioned somewhere in between these two limits, maybe even undergo both HT and ET. It is noteworthy that this interpretation is also supported by a recent theoretical study. *Jean et al.* have carried out *ab initio* calculations on the stacked complexes of 2-AP with nucleobases.[68] Although these calculations neglect environmental effects, such as the solvent or neighboring bases, they clearly revealed the existence of excited states with charge transfer character for all four DNA bases. In particular for ApT complexes, a distinct energetically low-lying charge transfer state was obtained when an electron was transferred from 2-AP to T.

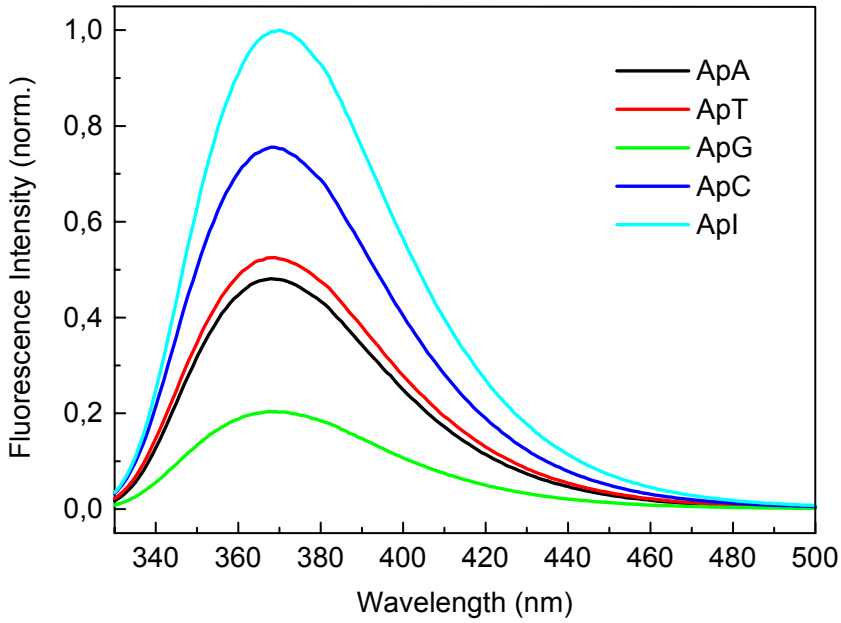

Figure 6-4. Fluorescence emission spectra of the five dinucleotides ApX in 10 mM Na-P_i, pH 7.0 with an excitation wavelength of 310 nm.

To further investigate the dynamics of the charge transfer process in the synthesized dinucleotides ApA, ApT, ApC, and ApG, time-resolved transient absorption spectra were recorded in collaboration with the group of Dr. T. Fiebig. The decay of the transient absorption of photoexcited 2-AP (Ap*) at 550 nm is depicted in Figure 6-5.

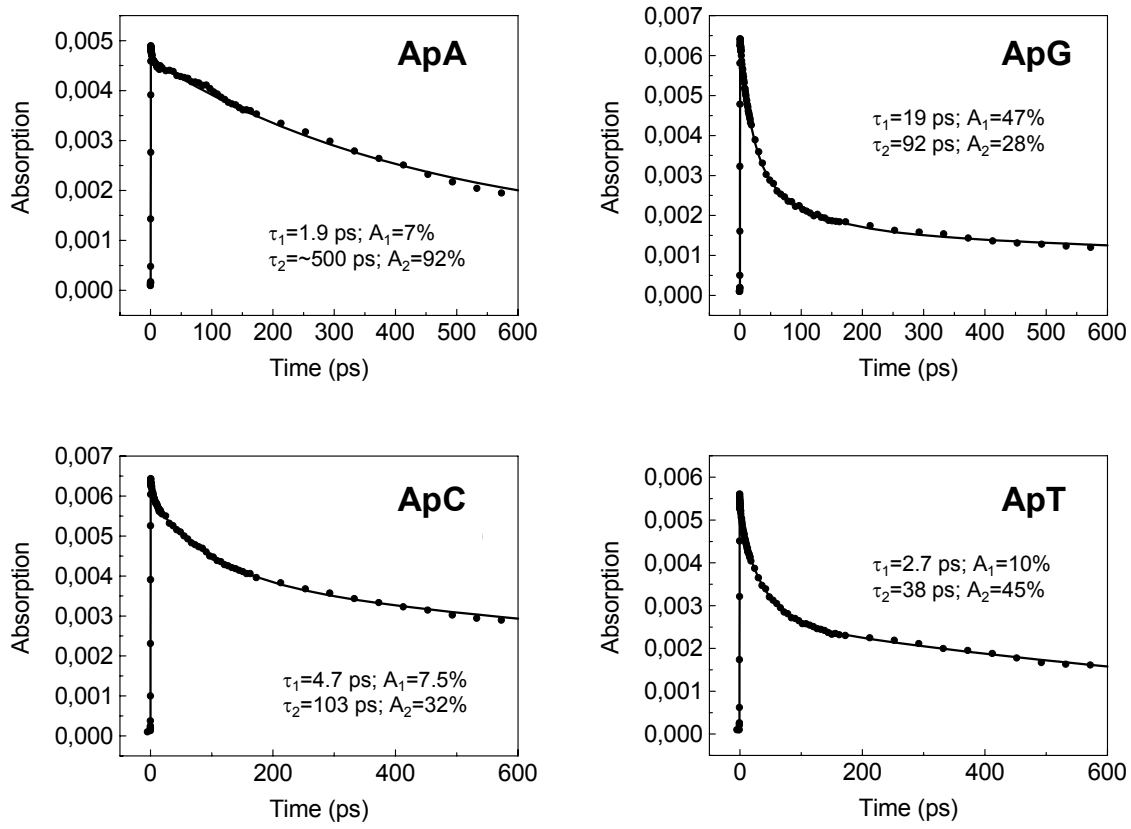

Figure 6-5 Transient absorption decays of the four dinucleotides ApA, ApC, ApG, and ApT recorded at 550 nm. Each of the experiments shows a significant biexponential decay with rates τ_1 and τ_2. Relative amplitudes of the two decays are given as A_1 and A_2 in percent.

All transients clearly exhibit a biexponential decay. This is in agreement with earlier reports by *Fiebig et al.*[47], where mixtures of all DNA nucleotides with 2-AP were observed to follow basically the same trends. Although superficially the curves look very similar, the rates obtained by the biexponential fitting are slightly different. In the work of *Fiebig et al.*[47] the slow decay components, τ_2, were all longer that 1 ns and were attributed to free (uncomplexed) Ap*, including any dynamic quenching, and the fast rates, τ_1, were between 19 and 350 ps. The fast decay components were attributed to an excited state complex of two nucleotides, since they were not dependent on the concentration of the added nucleotide, instead only the amplitude of the fast decay rate increased with increasing concentration.[47] Internal conversion and energy transfer are excluded as the cause for the measured decay rates, whereas all results point to a charge transfer from the excited 2-AP to the complexed

nucleotide, where a hole transfer takes place to G and A, and electron transfer takes place to T and C.[47]

In the present work, no nanosecond component could be observed, since the two nucleotides here are covalently linked and there is no uncomplexed 2-AP. The slow decay components range here from 38 ps (ApT) to ~ 500 ps (ApA), and the fast rates are between 1.9 and 19 ps, which are - except for ApG - much faster than reported by *Fiebig et al.*[47]

If one calculates an average decay rate $\langle\tau\rangle$ according to the equation

$$\langle\tau\rangle = A_1*\tau_1 + A_2*\tau_2,$$

where A_1 and A_2 are the amplitudes of the fast and slow decay components, respectively, the data correspond fairly well with the fast rates from *Fiebig et al.*[47] (Table 6-1).

A comparison of the fast rates τ_1 obtained by *Fiebig et al.* and the fast rates τ_1 and average decay rates $\langle\tau\rangle$ from this study is summarized in Table 6-1.

Table 6-1. Comparison of the fast components of biexponential decay of nucleoside mixtures Ap + X of *Fiebig et al.*[47] and dinucleotides ApX investigated in this study.

X	τ_1 of nucleoside mixture (ps)[47]	τ_1 of dinucleotide ApX (ps)	$\langle\tau\rangle$ of dinucleotide ApX (ps)
A	350	1.9	460
G	19	19	34.7
C	47	4.7	33
T	20	2.7	17.4

Comparing the amplitudes of the transients of the dinucleotides with the degree of quenching in the steady-state fluorescence data shows that the larger the sum of amplitudes of fast and slow components the stronger the quenching of 2-AP fluorescence in the steady-state experiments. The exception is ApA, where one would have to look at the amplitude of the fast decay rate only to fit to the model. Preliminary results by time-resolved fluorescence measurements indicate an excitation energy transfer in ApA.

In summary, one can say that a G next to 2-AP quenches the fluorescence the most, so there must be a strong interaction between the two bases, and since G is the base with the lowest oxidation potential of the nucleobases, the quenching is probably caused by a HT from 2-AP to G. Inosine, however, is the base which quenches the 2-AP fluorescence the least. Hence, the oxidation and reduction potential of inosine must lie in a range so that the excited 2-AP can neither oxidize nor reduce the neighboring inosine. The bases C and T show intermediate effects on 2-AP. They are able to quench the fluorescence emission of 2-AP more than A, but not as efficiently as G. ApA seems to be a special dinucleotide in a sense that it shows stacking in the CD spectra, but 2-AP emission is hardly quenched in the steady-state fluorescence experiments, and the transient absorption spectroscopy shows a very fast and a very slow decay of the excited state of 2-AP that cannot be explained at this stage. Since the results from neither the steady-state fluorescence nor the time-resolved transient absorption experiments follow the established trends for the oxidizability or the reducibility of DNA bases, this study proves the conclusion by *Fiebig et al.*[47], that 2-AP can oxidize and reduce neighboring bases.

7 Reductive Electron Transfer Studied with 5-(1-pyrenylethynyl)-2' deoxyuridine (Py-≡-dU)

7.1 Introduction

Oxidative hole transfer has been studied intensely in the past 20 years using a variety of methods and model systems, but not many studies have been published yet on reductive electron transfer using spectroscopic methods. It was intended with this work to contribute to the knowledge on the mechanism of reductive electron transfer in DNA. As shown in the previous chapter, 2-AP is suitable to photoinitiate charge transfer in DNA, but it can both oxidize and reduce neighboring bases. Therefore it does not seem to be particularly useful for systematic investigations of pure reductive ET. A more suitable candidate for an electron donor is pyrene when it is covalently attached to a deoxyuracil in DNA as shown by *Amann et al*.[2, 172, 174]

5-(Pyren-1-yl)-2'-deoxyuridine (Py-dU) and 5-(Pyren-1-yl)-2'-deoxycytidine (Py-dC) were synthesized and used for charge transfer studies by *Amann et al*.[2, 172, 174] In Py-dU, the deoxyuracil is attached to the pyrene group via a single C-C bond. Therefore, it cannot be excluded that the pyrene moiety directly interacts with bases in the DNA duplex adjacent to the Py-dU group. As a result, the CT process could follow this shortcut, which implies that experimental results might not be unambiguous. In an attempt to reduce these structural concerns, the aim of this study was to prepare DNA duplexes containing the nucleoside base analog 5-(1-pyrenylethynyl)-2'-deoxyuridine (Py-≡-dU) (Figure 2-6), which has been reported to be a promising new base analog that is sensitive to its environment,[83, 284] while the greater distance of pyrene from the base stack should allow fully controllable electron injection into DNA. Additionally, a new synthetic approach has the advantage that the preparation of pyrenylethynyl-modified oligonucleotides is not limited by the "bottleneck" of a phosphoramidite synthesis. Instead, a modified protocol from *Khan and Grinstaff*[285] was followed.

7.2 Sample Preparation and Control Experiments

Using the nucleoside Py-≡-dU, a range of pyrene-modified duplexes were prepared, that mainly differ by the bases flanking the Py-≡-dU unit (Figure 7-1). The sequences were based on the ones previously used in the experiments of *Amann et al.*[2]

Figure 7-1. DNA sequences of pyrenylethyne-modified strands **P1** to **P6** and their respective complementary strands **C1** to **C6** synthesized to investigate electron transfer to bases next to Py-≡-dU.

Py-≡-dU was incorporated by a combination of standard phosphoramidite chemistry and Pd(0)-catalyzed Sonogashira cross coupling reactions using a protocol analogous to *Khan and Grinstaff*.[285] Figure 7-2 shows a schematic representation of the synthetic strategy: DNA is synthesized following standard protocols on a commercial DNA synthesizer up to the position of the pyrene-modified unit. The 2'-deoxy-5-iodouridine (5-I-U) is inserted without deprotection of the terminal 5'-OH group. Subsequently, the CPG vials are removed from the

synthesizer and a Sonogashira-coupling reagent containing $Pd(Ph_3)_4$, 1-ethynylpyrene and CuI in DMF:TEA (3.5:1.5) is added to the CPGs via syringes. After a coupling time of 3 hours at room temperature, the CPGs are washed and dried. After the coupling, the synthesis is continued in the DNA synthesizer. The standard procedures for deprotection and cleavage of the DNA strands from the solid phase have not been modified.

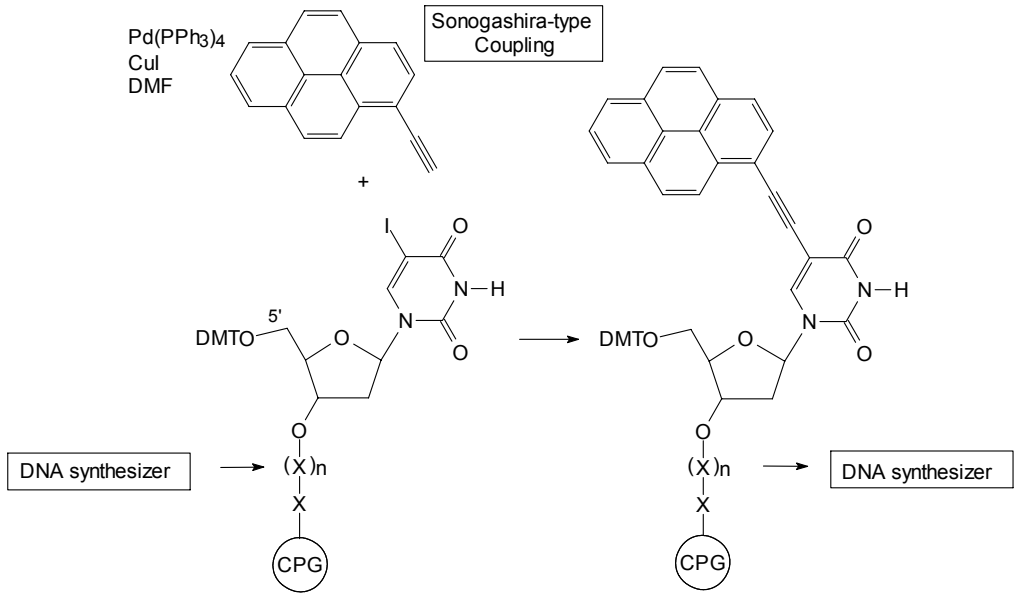

Figure 7-2. Schematic representation of the synthesis of pyrene-modified DNA. A DNA strand is synthesized and at the position of Py-≡-dU a 5-I-U is incorporated. Without deprotection of the 5'-OH the synthesizer is stopped, and the ethynylpyrene is coupled with a Sonogashira-type reaction off the synthesizer. Finally, the remaining bases of the sequence are added again using the DNA synthesizer.

The pyrene group of the new compound is located outside the base stack of a DNA duplex. In contrast to the Py-dU system previously described, the pyrene moiety is linked covalently to the uracil via an acetylene bridge. Thus, the distance between the pyrene group and the bases next to the uracil can be expected to be too large and too rigid for direct stacking interactions. Furthermore, it should not significantly interfere with the structure and stability of the duplex. Absorption spectra were recorded for the single stranded Py-≡-dU-labeled oligonucleotides in buffer and in DMSO (Figure 7-3). The spectra show two absorption maxima of the Py-≡-dU unit that are significantly red-shifted (378 and 402 nm) compared to the absorption of pyrene or the Py-dU group (~ 340 nm).

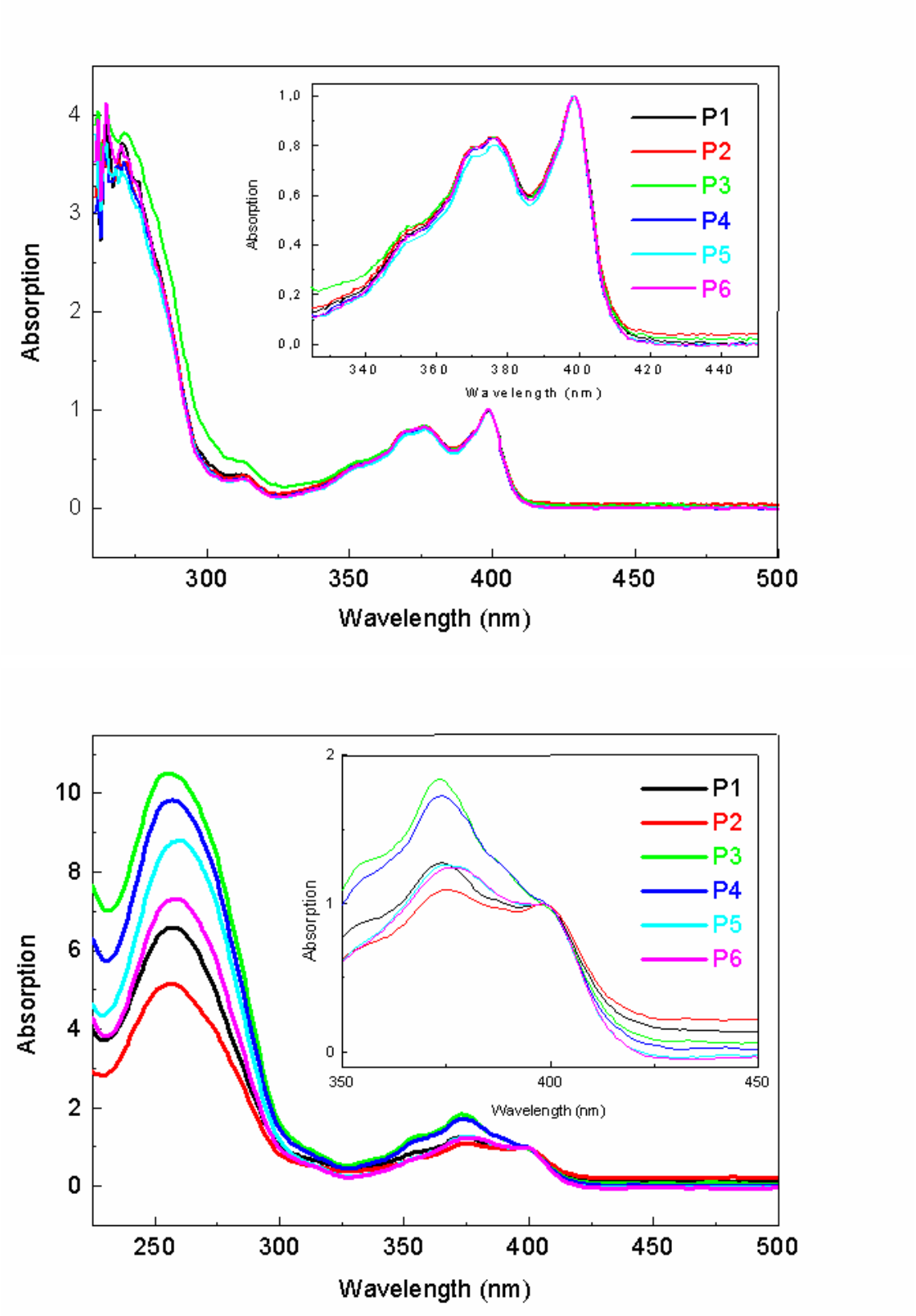

Figure 7-3. Absorption spectra of the pyrene-labeled DNA sequences in DMSO, normalized to the absorption at 398 nm (top), and in 10 mM Na-P_i buffer, pH 7.0 normalized, to the absorption at 402 nm (bottom).

DMSO is known to disrupt the secondary structure of nucleic acids.[286] Therefore UV/Vis spectra in DMSO were recorded to test the influence of base stacking on the Py-≡-dU absorption and to get an estimation of the extinction coefficient of Py-≡-dU at 260 nm to enable determination of DNA oligonucleotide concentration by measuring absorption at 260 nm.[287] Remarkably, in DMSO the absorption spectra of all six oligodeoxynucleotides exhibit the same shape and the same absorption maxima (374 and 398 nm, Figure 7-3). This provides evidence that in DMSO base-stacking interactions between the Py-≡-dU group and the adjacent bases are indeed interrupted, since in aqueous buffer the spectra are significantly different (Figure 7-3).

To find out if incorporation of the Py-≡-dU group perturbs DNA duplex structure, UV melts and CD spectra of the duplexes were measured. Determined melting temperatures are reported in Table 7-1 and compared with calculated T_m for duplexes containing T instead of the Py-≡-dU group as a reference. In general, melting temperatures of the Py-≡-dU containing duplexes are slightly higher than calculated T_m of reference duplexes. This slight increase of 2 to 3 °C can be attributed to the stabilization of DNA by the acetylene group.[84, 85]

Table 7-1. Comparison of measured melting temperatures of DNA duplexes containing Py-≡-dU versus calculated T_ms of reference duplexes.

DNA duplex	T_m exp [°C]	T_m calc [°C]
P1/C1	52.2	50.6
P2/C2	52.3	54.9
P3/C3	56.4	54.9
P4/C4	55.1	52.7
P5/C5	56.1	52.7
P6/C6	53.0	50.6

CD spectra recorded for all six duplexes confirmed B-form DNA structure. No Cotton effect was observed in the absorption range of the Py-≡-dU unit (330 to 420 nm) (Figure 7-4), providing evidence that the pyrene moiety is not stacked within the duplex.

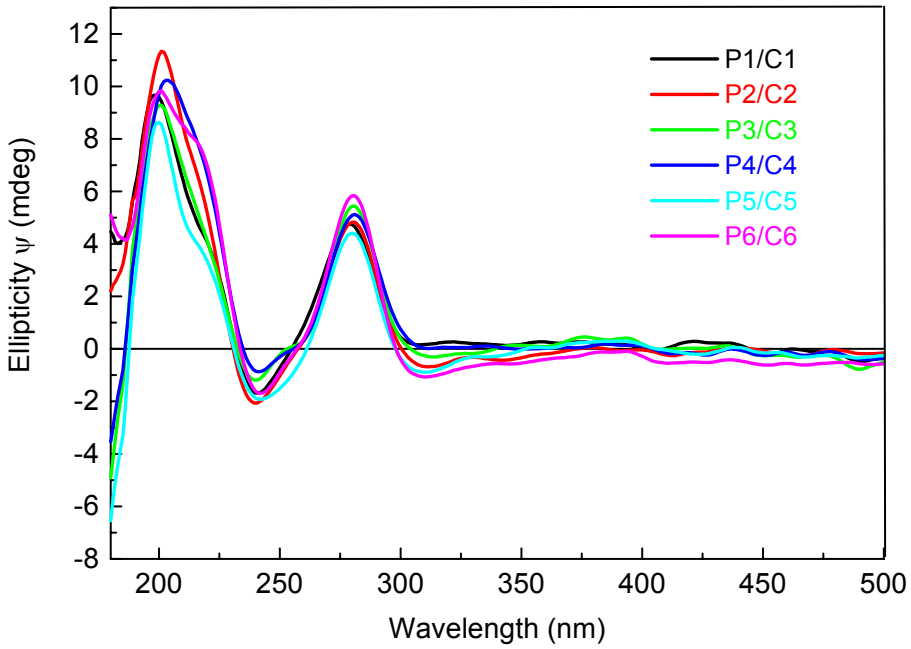

Figure 7-4. CD spectra of the six DNA duplexes (2.5 µM) in 10 mM NaPi buffer pH 7.0. All spectra are indicative for B-form DNA.

In summary, it can be concluded that the stability and structure of the duplexes are not significantly perturbed by the incorporation of the nucleotide base analog Py-≡-dU.

7.3 Results

Fluorescence emission spectra were recorded on single stranded DNA samples in buffer with identical optical densities at the excitation wavelength of 402 nm, and in DMSO with identical optical densities at the excitation wavelength of 398 nm to find out how the flanking bases effect the quantum yield of the Py-≡-dU group in duplex DNA.

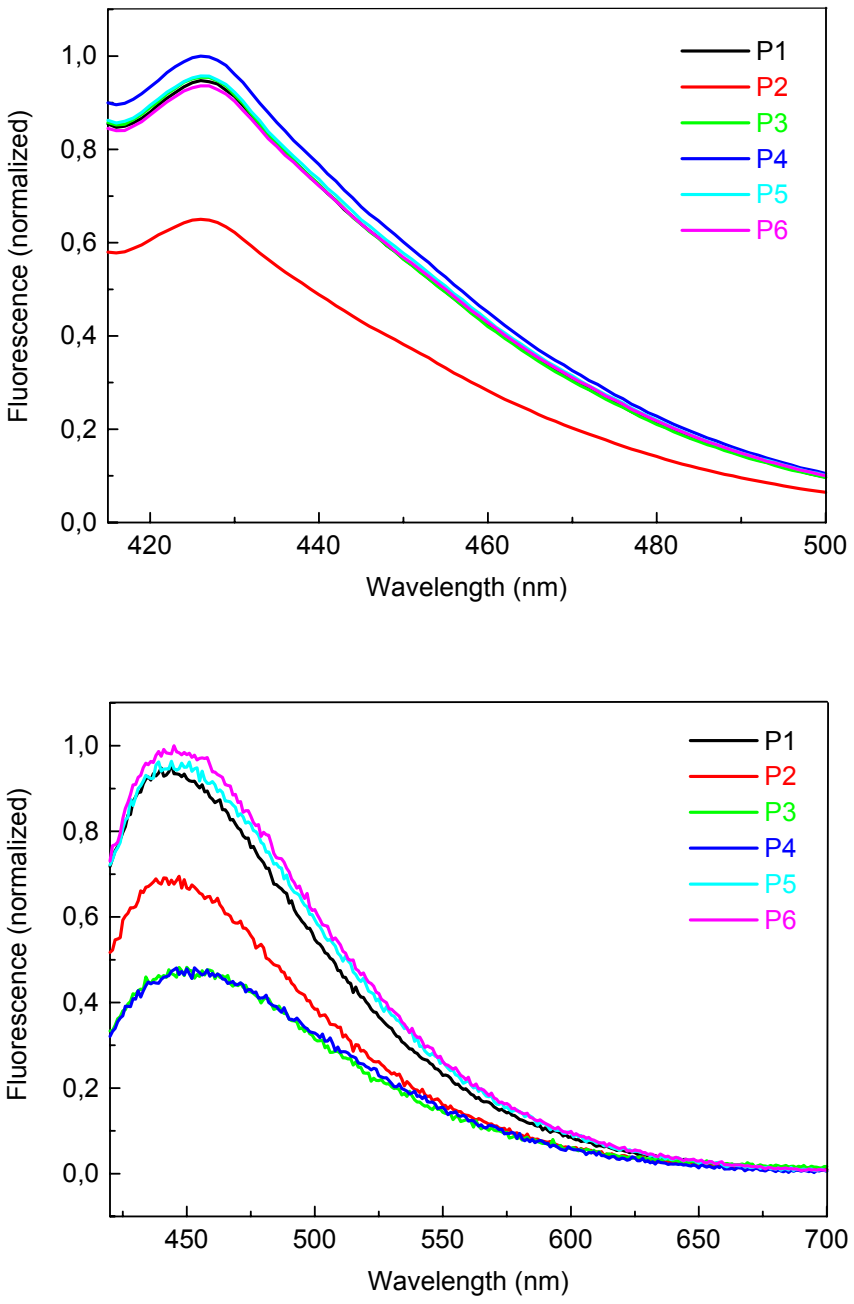

Figure 7-5. Fluorescence emission spectra of single stranded pyrene labeled DNA in DMSO (top) and 10 mM Na-P_i-buffer, pH 7.0 (bottom).

The emission intensities of the single strands in DMSO are virtually identical, whereas the fluorescence signals in buffer are significantly different (Figure 7-5), confirming again that stacking is interrupted in DMSO. However, there is one major exception: the DNA sequence **P2** with two gunanines flanking the Py-≡-dU group shows a substantially quenched

fluorescence signal in DMSO. This observation can be explained by the reports of *Saito et al.*[288, 289] who used cyanobenzochinone-modified uridines as hole donors for the investigation of DNA-mediated HT. They found that a G located on the complementary strand one base pair away from the modified U can act as a very efficient hole acceptor. Consequently, it can be assumed that a hole transfer process occurs here, too.

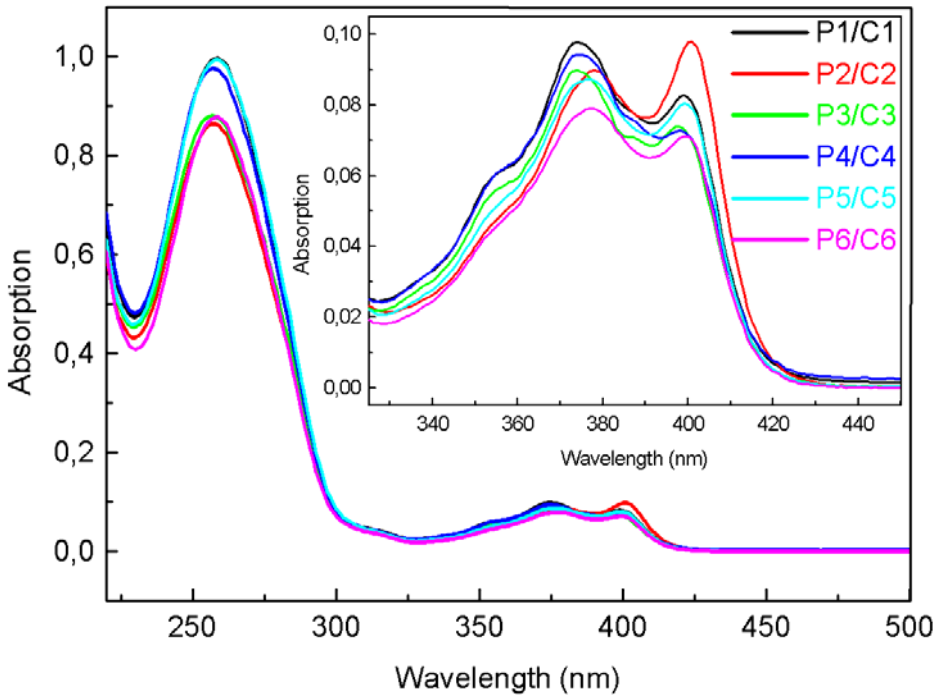

Figure 7-6. Absorption spectra of the six DNA duplexes (2.5 µM) in 10 mM Na-P_i buffer, pH 7.0, recorded at room temperature, with an excitation wavelength of 402 nm.

Subsequently, absorption and fluorescence emission spectra were measured for all DNA duplexes in buffer. Absorption spectra of duplexes with identical concentration show two major maxima of Py-≡-dU absorption with slightly varying peak positions and intensities (Figure 7-6). Fluorescence emission spectra were recorded at an excitation wavelength of 402 nm and are shown in Figure 7-7. It is important to compare the fluorescence spectra of the single strands in DMSO, where base-stacking is interrupted, with the spectra of the double strands in buffer solution. One can clearly see that, contrary to the measurements in DMSO, in aqueous buffer the emission intensities of the duplexes vary significantly depending on the bases flanking the Py-≡-dU and decrease in the following order: P1/C1 > P4/C4 ~ P3/C3 > P5/C5 ~ P6/C6 > P2/C2.

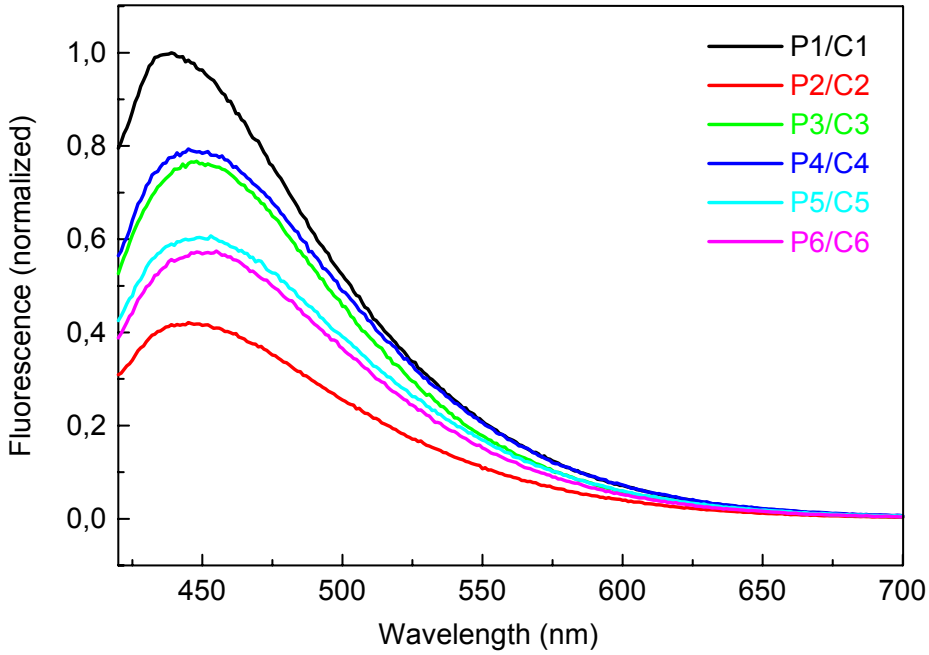

Figure 7-7. Fluorescence emission spectra of DNA duplexes (2.5 µM) in 10 mM Na-P_i-buffer, pH 7.0, recorded with an excitation wavelength of 402 nm and normalized to the absorbance at 402 nm.

Despite the uncertainty related to irreversible electrochemistry, the following trend for the reducibility of the nucleobases was established: T,U ≈ C >> A > G.[134] With respect to this trend, it can be expected that the U radical anion which is formed upon photoexcitation and subsequent intramolecular ET in the Py-≡-dU group should only be able to reduce adjacent pyrimidine bases, C or T (Figure 7-8).

In fact, the quantum yields follow the trend of the reducibility of nucleobases, except for the strand where G is located next to the Py-≡-dU group. As discussed for the comparably low emission of the corresponding single strand in DMSO, it is proposed that a hole is injected into G in this system, as suggested by the experiments by *Saito et al.*[288, 290], which results in the lower fluorescence intensity.

In duplex **P1/C1**, an ET from the Py-≡-dU group to the adjacent A is not expected because of thermodynamic reasons. In contrast, a significant quenching of the emission can be observed, when a T or C is placed adjacent to the Py-≡-dU group, as it is the case, for example, in **P6/C6**. This observation can be attributed to a base-to-base ET from the Py-≡-dU group to adjacent pyrimidines (Figure 7-8).

Based on the presented experiments one can conclude that Py-≡-dU is a very promising tool to study ET through DNA. It is able to inject an electron into the base stack, while simultaneously acting as a spectroscopic label to enable observation of the processes. Time-resolved experiments are currently performed in the group of Dr. T. Fiebig to study the dynamics of the electron injection and the base-to-base ET.

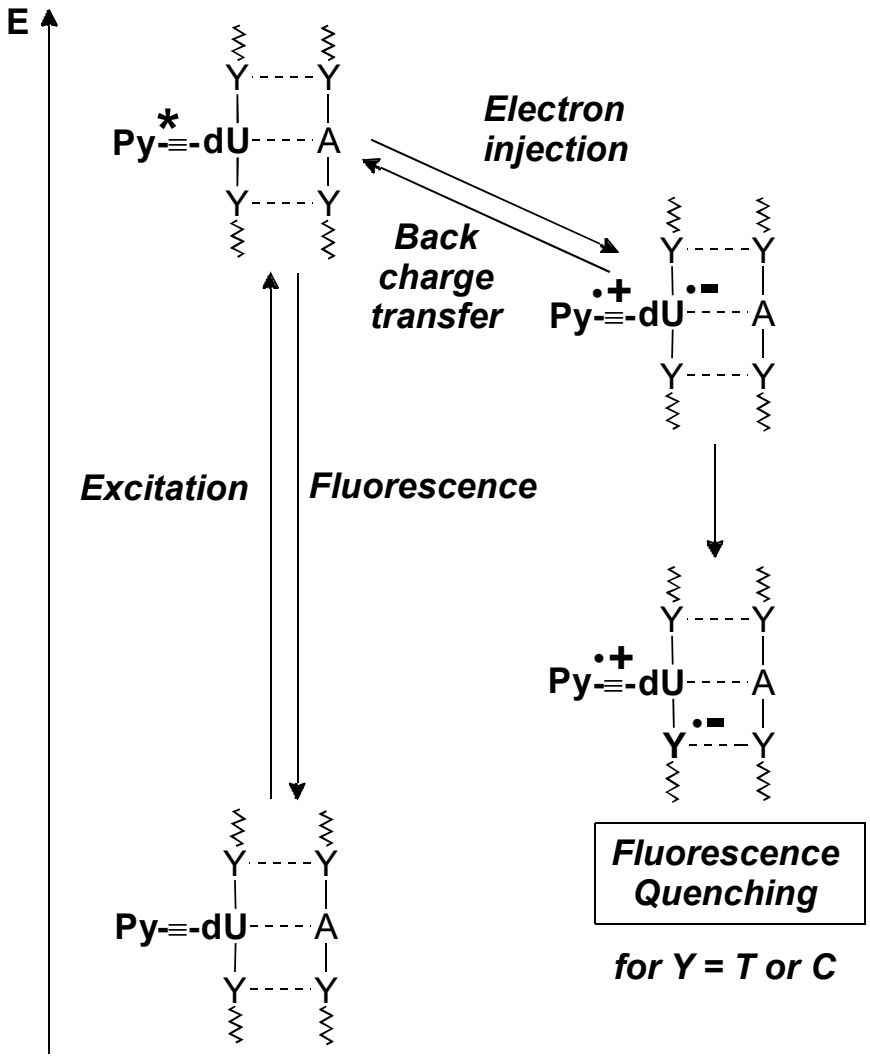

Figure 7-8. Reductive ET in pyrenylethynyl-modified DNA duplexes: Excitation of the Py-≡-dU group at 402 nm results in an ET yielding the $Py^{\bullet+}$-≡-$dU^{\bullet-}$ biradical, which is in equilibrium with the excited Py*-≡-dU. If ET to the adjacent DNA bases occurs as an alternative pathway, quenching of the Py* emission is observed.

8 Summary

In the presented thesis the fluorescent nucleoside base analogs 2-aminopurine and 5-(1-pyrenylethynyl)-2'-deoxyuridine were used to study the structure and dynamics of nucleic acids, their interactions and electronic properties.

The method of studying RNA loop-loop kissing interactions using fluorescence spectroscopy was validated by incorporating 2-AP into the loops of RNA hairpins taken from the intensely investigated *ColE1* plasmid replication system. By observing changes in the 2-AP fluorescence it was possible to determine equilibrium binding constants as well as on- and off-rates for kissing complex formation and a binding constant for the auxiliary protein Rom binding to the kissing complex. These results are in agreement with previous studies using other methods, hence, the fluorescence assay is validated. An advantage of the fluorescence spectroscopy in comparison to other applied methods, like native gel electrophoresis and filter binding assays, is the real-time kinetic resolution and the native like solution conditions. Thus, it was possible to derive a two-step binding model for the RNA loop-loop complex formation of R1 and R2 from the results of the kinetic studies. Additionally, the stringent divalent metal ion requirement for RNA loop-loop kissing complex formation could be studied in detail and apparent binding constants for the metal ions to the complex could be determined. The observed correlation of apparent metal ion binding constants with ionic radius and Lewis acidity lead to the conclusion that in the RNA complex there must be a structurally limited though somewhat flexible binding pocket for the divalent metal ions, since larger, more basic cations showed a weaker apparent binding constant than smaller, more acidic metals.

Transferring the experience with the now validated method to a new framework, a new RNA antisense system was investigated, namely the dimerization initiation site of HIV-1. With specifically designed heterodimeric samples the equilibrium binding constants, on- and off-rates of the kissing complex and the conversion to the extended mature duplex with the aid of the nucleocapsid protein could be investigated. In contrast to the bacterial system, the DIS hairpins were able to form a loop-loop kissing complex in the presence of divalent and monovalent cations or at millimolar concentrations, whereby the latter complexes have been found to be metastable and capable of spontaneously converting to the mature duplex form at an appreciable rate over time. Most importantly, based on these results the pathway of extended duplex formation was unequivocally confirmed, which proceeds from kissing

complex to mature duplex via a strand exchange, and the role of NCp7 in this structural isomerization was proposed to be the temporal control of the process.

After using changes in 2-AP fluorescence for the study of macromolecular interactions, it was reasonable to investigate the processes in more detail that can cause the observed fluorescence changes. Thus, the focus was shifted to the investigation of the electronic properties of 2-AP in DNA. Initially, the fate of the excitation energy of 2-AP was studied, and it was found that 2-AP can form excimers and exciplexes. A significant ground-state interaction of 2-AP and its neighboring bases was detected. This result can also be transferred to the stacking interactions of natural nucleic acid bases. Dynamic investigations revealed that stacking and destacking in DNA duplexes occur on the order of 5 ps.

Subsequently, the influence of neighboring bases on the fluorescence quenching by charge transfer was studied using dinucleotides composed of all natural DNA bases and inosine next to 2-AP. It was found that fluorescence intensities of these dinucleotides follow neither the trend for oxidizability nor reducibility of nucleobases and thus, photoexcited 2-AP is able to undergo both hole and electron transfer. It can be concluded that such charge transfer processes cause the quenching of the excited 2-AP within DNA or RNA.

Oxidative hole transfer has been studied extensively in the past decades, but very little is known about the mechanism of reductive electron transfer in DNA. Since 2-AP shows a behavior too complex to utilize for systematic studies, the reductive electron transfer properties were investigated in model DNA duplexes using a new fluorescent nucleside analog, Py-≡-dU. A new and improved synthetic method combining standard automated DNA synthesis and a Sonogashira-type cross coupling reaction on the solid phase was developed for the modification of DNA with the Py-≡-dU unit. Py-≡-dU was found to be a very promising electron injector, and it is proposed that charge can be transferred to adjacent C and T bases.

In summary, these results impressively demonstrate the wide range of questions that can be addressed using fluorescence spectroscopy.

9 Materials and Methods

9.1 Materials

Unless otherwise noted, all chemicals and reagents were purchased from Sigma, J. T. Baker, Life Technologies, ICN or Fluka, as ultra pure or ACS reagents. Distilled and deionized water (ddH_2O) was taken from a millipore unit, and if used for solutions of pure RNA it was either sterilized by autoclaving or treated with 0.01 % DEPC.

9.2 Frequently Used Buffers

1xTBM: 90 mM Tris, 90 mM boric acid, 1 mM $MgCl_2$
1xTBCa: 90 mM Tris, 90 mM boric acid, 1 mM CaCl
1/2xTBE: 45 mM Tris, 45 mM boric acid, 1 mM EDTA
standard buffer for RNA: 1 mM cacodylic acid, pH 6.5, 25 mM NaCl
standard buffer for DNA: 10 mM sodium phosphate (Na-P_i), pH 7.0

9.3 General Work Procedures

9.3.1 Denaturing Polyacrylamide Gel Electrophoresis (PAGE)

For denaturing minigels approximately 15 ml 20 % acrylamide (19:1 acrylamide: bisacrylamide) with 8 M urea and 1/2xTBE was mixed with 15 µl TEMED and 150 µl 10 % (w/v) APS to induce polymerization. After polymerization, gels were prerun in 1/2xTBE at room temperature (R.T.) at 10 W in a Hoefer Minigel apparatus. Samples were prepared with equal volumes of RNA or DNA solution and formamide and 1 µl of 1% (w/v) bromophenol blue solution, and heated to 90 °C for 1 min before loading samples on the gel. Gels were run at 10 W for approximately 45 min, and nucleic acids were visualized by ethidium bromide staining.

For preparative scale denaturing PAGE, 100 ml 20 % acrylamide (19:1) with 8 M urea and 1/2x TBE was mixed with 80 µl TEMED and 800 µl 10 % (w/v) APS to induce polymerization. After polymerization, gels were prerun in 1/2xTBE at R.T. at 40 W for about 15 to 30 min. Then wells were cleared from excess acrylamide and urea and samples from a

10 ml transcription reaction or a 1 µmole chemical synthesis was mixed with an equal volume of formamide and 1 µl of 10 % (w/v) bromophenol blue, denatured by heating to 90 °C for 1 min, loaded on the gel and run at 45 W for several hours. Nucleic acids were visualized by UV shadowing, and appropriate bands were cut out of the gel and stored at -20 °C until further treatment.

9.3.2 Native Polyacrylamide Gel Electrophoresis

- on RNA:

For native PAGE on RNA samples, per gel 15 ml of a 15 % acrylamide (75:1 acrylamide:bisacrylamide) solution containing either 1xTBM or 1/2xTBE were mixed with 15 µl TEMED and 150 µl 10 % (w/v) APS to cast the gels. Polymerized gels were preequilibrated for 30 min in the respective running buffer (1xTBM or 1/2xTBE) at 4 °C at 10 V/cm using a submarine minigel apparatus (BioRad). Then samples were loaded and run at 4 °C at 10 V/cm until the bromophenol blue reached the bottom of the gel. RNA was visualized by ethidium bromide staining.

In general, samples were prepared with 10 µM RNA hairpin or kissing complex in the respective running buffer, and 5 to 10 % loading dye (15 % glycerol, 1 mg/ml bromophenol blue in ddH_2O) was added before loading. Usually, 10 to 20 µl of the samples were loaded on the gels. To assay formation of complexes by R1inv and R2inv hairpins containing 2-aminopurine, and binding of these complexes by Rom, equal amounts (10 µM final concentration) of the complementary hairpins were mixed and incubated in 1xTBM for 5 to 10 min either with or without Rom in 5-fold excess. Before loading the samples on the gel, 5 to 10 % of loading dye was added, and 50 µL of samples were loaded. Samples were visualized by ethidium bromide staining.

- on DNA:

For native PAGE on DNA, 15 ml of a 15 % acrylamide (75:1 acrylamide:bisacrylamide) solution containing either 1xTBCa or 1/2xTBE were mixed with 15 µl TEMED and 150 µl 10 % (w/v) APS to cast the gels. The polymerized gels were preequilibrated for 15 to 30 min and run at room temperature at 10 V/cm in a Hoefer mini vertical electrophoresis unit. Samples were prepared essentially as with RNA, but at higher concentrations of DNA (23 µM). Samples were visualized by ethidium bromide staining or Py-≡-dU fluorescence.

9.3.3 High-Performance Liquid Chromatography (HPLC)

Synthesized DNA was purified by reverse-phase high-performance liquid chromatography (RP-HPLC) on a Waters 1525 HPLC system using a 25 cm x 10 mm Supelcosil LC-318 column (Supelco), preequilibrated with 100 % A (50 mM ammonium acetate buffer, pH 6.5). Usually DNA from a 1 µmole synthesis, dissolved in 300 µl ddH_2O was injected into the column and eluted with a gradient 0-15 % or 0-30 % B (acetonitrile) over 45 min.

9.3.4 Lyophilization

Aqueous solutions were frozen in dry ice or liquid nitrogen and lyophilized on a Christ Alpha-2-4 lyophilizer.

9.3.5 Annealing of RNA or DNA Duplexes

RNA or DNA duplexes were annealed by heating a solution of a 1:1 mixture of the single stranded complementary oligonucleotides to 85 to 90 °C for 5 min and cooling slowly to R. T. over a period of two to three hours.

9.3.6 Snap Cooling

Solutions of DIS RNA oligonucleotides were heated to 90 °C for 1min and quickly cooled on dry ice for 20 to 30 sec to force possibly aggregated RNA into monomeric hairpins.

9.3.7 MALDI-TOF Mass Spectroscopy

High-resolution MALDI-TOF mass spectra of DNA oligonucleotides were measured on a Bruker Biflex III spectrometer in a matrix containing 9 parts 50 mg/ml 3-hydroxypicolinic acid in ddH_2O:acetonitrile (50:50) and 1 part 50 mg/ml diammonium citrate in ddH_2O at a DNA concentration of 10 to 50 µM in linear negative mode.

9.3.8 UV/Vis Spectroscopy

Absorption spectra of RNA and DNA samples were measured on a Cary 50, Cary 100 or Cary 300 spectrophotometer (Varian Instruments, Palo Alto, CA) in ddH_2O, buffer or DMSO in 1 cm path length quartz cuvettes.

9.3.9 UV Melts

- on RNA:

Optical absorbance melting curves for RNA samples were measured on a Cary 300 spectrophotometer (Varian Instruments, Palo Alto, CA). Samples were prepared in melting buffer (10 mM sodium cacodylate, pH 6.5, 50 mM NaCl, 0.1 mM EDTA, with or without 5 mM $MgCl_2$, degassed by autoclaving or sparging with nitrogen for 15 min), so that the initial optical density at 260 nm was approximately 0.55-0.65 in quartz cuvettes with 1 cm path length. Temperature was controlled by a Cary temperature control unit, and was increased from 10 to 90 °C at a rate of 0.25 °C/min, and absorption at 260 nm was observed recording data every 1 °C. At temperatures below room temperature, the sample chamber was flushed with nitrogen.
Melting temperatures were determined by calculating the first derivatives of the melting curves and assuming the maximum in the derivative to be the melting temperature.

- on DNA:

Optical absorbance melting curves were measured on a Cary 100 (Varian). Samples were prepared in 10 mM sodium phosphate buffer, pH 7.0 with or without 250 mM NaCl, degassed by sparging with nitrogen for 15 min, with sample concentrations of 2.5 µM in 1 cm path length quartz cuvettes. Temperature was controlled by a Cary temperature control unit, and was increased from 10 to 60 or 90 °C at a heating rate of 0.25 or 1 °C/min for Py-≡-dU or excimer duplexes, respectively, recording absorption at 260 nm every 1 °C. At temperatures below room temperature, the sample chamber was flushed with nitrogen.
Melting temperatures were determined by calculating the first derivatives of the melting curves and assuming the maximum in the derivative to be the melting temperature.

9.3.10 Circular Dichroism Spectroscopy (CD)

CD spectra of DNA samples were recorded on a Jasco J-15 spectropolarimeter with a Jasco PTC-150J temperature control unit in a 1cm path length quartz glass cuvette. Samples were prepared in 10 mM Na-P_i, pH 7.0 with or without 250 mM NaCl in a total volume of 1 ml. Experiments were measured with a step resolution of 0.5 or 1 nm, scan speed of 500 or 1000 nm/min, and 2 nm bandwidth. Usually five spectra were averaged, and buffer blank spectra recorded with the same parameters were subtracted. Sample concentrations were 10 µM for the dinucleotides and 2.5 µM for all DNA duplexes. For dinucleotides, spectra

were recorded from 340 to 185 nm, for excimer samples, from 320 to 185 nm, for Py-≡-dU containing samples, the wavelength range was 450 to 200 nm.

9.4 Protein Preparations

9.4.1 T7 Polymerase

Affinity-tagged T7 polymerase was expressed and purified following a protocol elaborated by *T.E. Shrader*. *Escherichia coli* (*E. coli*) strain BL21 containing the plasmid pT7-911Q were plated on Luria agar containing 100 µg/ml ampicillin. 5 ml Luria agar base with 100 µg/ml ampicillin were inoculated with a single colony from the plate and incubated at 37 °C overnight. Of this starter culture 2 ml were used to inoculate 2 l LB broth with 100 µg/ml ampicillin. Cultures were shaken at 37 °C until the absorbance at 600 nm reached 0.4 - 0.6. Then cultures were induced for overexpression with 100 µM IPTG (GOLD Biotechnology, Inc) and shaken for 3 more hours at 37 °C. Cells were harvested by centrifugation at 7000 rpm for 15 min, and cell pellets were stored at -75 °C. The cell pellets were thawed at room temperature and resuspended in 25 ml lysis buffer (50 mM Tris, pH 8.0, 100 mM NaCl, 5 mM BME, 5 % glycerol) containing 1 mM imidazole. Cells were lysed by French pressing 2 - 3 times at 800 psi. Cell debris was removed from the lysate by centrifugation at 18000xg for 30 min. The cleared lysate (25 ml) was bound to 5 ml of Ni-NTA agarose resin (Qiagen) (10 ml resin + buffer) by gentle rocking for 30 min at 4 °C. After gently pelleting the resin in a clinical centrifuge, and discarding the supernatant, the resin was washed four times with 35 ml lysis buffer containing 1 mM imidazole, and four times with 35 ml lysis buffer containing 10 mM imidazole using batch method. T7 polymerase was eluted by washing the resin twice with 10 ml of lysis buffer containing 100 mM imidazole for 5 min at 4 °C. The eluted protein was concentrated in a Centriprep 30 concentrator (Millipore) to a concentration of approximately 6 mg/ml. Glycerol was added to a final concentration of 25 % and aliquots were stored at -20 °C (-75 °C for long term storage). Concentration was determined by measuring the absorption at 280 nm using the following relationship:
Abs 0.1 % (=1 g/l) at 280 nm = 1.344 (assuming all Cysteine residues to be single Cysteins)

9.4.2 Nucleocapsid Protein (NCp7)

Nucleocapsid protein (NCp7) from HIV-1 was expressed and purified in principle as described by *Lee et al*.[291] *E. coli* strain BL21(DE3) pLysE containing plasmid pRD2 were

plated on ZB[292] + agar (2 g Bacto Tryptone (Difco), 1 g NaCl, 3 g Bacto Agar (Difco) in 200 ml ddH_2O) with 100 µg/ml ampicillin and 34 µg/ml chloramphenicol and incubated overnight at 37 °C. 20 ml ZB broth[292] (2 g Bacto Tryptone, 1 g NaCl in 200 ml ddH_2O) containing 100 µg/ml ampicillin and 34 µg/ml chloramphenicol were inoculated with a single colony from the plate and incubated overnight in a shaker at 37 °C. 20 ml of this starter culture was used to inoculate 2 l M9ZB broth (20 g Bacto Tryptone, 10 g NaCl in 1.8 l ddH_2O + 200 ml M9salts: 2 g NH_4Cl, 6 g KH_2PO_4, 12 g $Na_2HPO_4x7H_2O$, 200 ml ddH_2O + 2 ml 1 M $MgSO_4$ + 40 ml 20 % glucose + 1 ml 0.2 M $ZnCl_2$) containing 100 µg/ml ampicillin and 34 µg/ml chloramphenicol, which was grown to an absorbance at 600 nm of 0.5 - 0.6, before it was induced with 1 mM IPTG. After three hours cells were harvested by centrifugation at 8000 rpm for 15 min. Cell pellet was resuspended in 30 ml lysis buffer (50 mM Tris, pH 8.0, 10 % (v/v) glycerol, 0.1 M NaCl, 0.1 mM $ZnCl_2$, 5 mM DTT, 2 mM EDTA) and stored at –70 °C. For lysis cells were thawed in ice-water, and 172 µl of 10 mM PMSF, 30 µl of 1 mg/ml pepstatin A, and 2.1 ml of 1 % (w/v) sodium deoxycholate were added, and cells were sonicated with 5 bursts of 20 seconds to reduce viscosity. Nucleic acids were precipitated by adding 4 % PEI, pH 7.9 dropwise to a final concentration of 0.4 %, and stirred for 15 min. The precipitate was pelleted by centrifugation at 23000xg for 30 min at 4 °C. The supernatant was collected, filtered (0.45 µm) and loaded at 1 ml/min onto a 20 ml Q-Sepharose and a 20 ml SP-Sepharose column connected in series and previously equilibrated with 200 ml of buffer A (50 mM Tris, pH 8.0, 10 % glycerol, 0.1 M NaCl, 0.1 mM $ZnCl_2$, 10 mM BME). The columns were washed with 60 ml buffer A, then the Q-Sepharose column was detached, and the SP-Sepharose column was washed with another 1.5 column volumes of buffer A. The protein was eluted with a ten column volume linear gradient from 40 % to 50 % buffer B (50 mM Tris, pH 8.0, 10 % glycerol, 1 M NaCl, 0.1 mM $ZnCl_2$, 10 mM BME). Then the protein was loaded (2 ml at a time, 11 shots) at a flow rate of 6 ml/min on a 60 cm x 21.5 mm TSK-GEL sizing column (Toso Haas), previously preequilibrated with two column volumes of buffer C (50 mM Tris, pH 7.0, 10 % glycerol, 0.1 M NaCl, 0.1 mM $ZnCl_2$, 10 mM BME). Collected protein fractions (about 160 ml) were concentrated using the SP-Sepharose column: the protein was loaded at 1 ml/min onto the column, which had previously been equilibrated with buffer C, and eluted with 50 % buffer B. The eluted protein (about 35 ml) was further concentrated down to 2-3 ml using centriprep 3 concentrators (Amicon), and was then dialyzed with a microdialysis chamber (Pierce Microsystems, Rockford, IL) into the storage buffer (25 mM sodium acetate, pH 6.5, 25 mM NaCl, 0.1 mM $ZnCl_2$, 0.1 mM BME, deoxygenated by sparging with nitrogen for 15 min), and stored at 4 °C. Concentration was

determined by measuring absorption using an extinction coefficient of 6.41 $mM^{-1}cm^{-1}$ at 280 nm.

9.5 Oligonucleotide Preparations

9.5.1 RNA Transcription and Purification

All unlabeled RNA hairpins (except DIS junction mutants) were synthesized by *in vitro* T7 polymerase run-off transcription using synthetic DNA oligonucleotide templates according to the method of Milligan and Uhlenbeck,[192, 293] after optimizing the reaction conditions, especially Mg^{2+} concentrations, in mini test reactions. DNA templates for R1inv and R2inv were purchased from Integrated DNA Technologies (Coralville, IA). All other DNA templates and primers were synthesized chemically on an Applied Biosystems 390 synthesizer (Perkin-Elmer, Forest City, CA) using standard phosphoramidite chemistry, and purified by preparative-scale denaturing PAGE. Nucleoside phophoramidites and controlled pore glass (CPG) columns were purchased from Glen Research (Sterling, VA).

In short, usually 10 ml transcription reactions were performed with reaction conditions as follows: 40 mM Tris, pH 8.3, 5 mM DTT, 0.01 % Triton X-100, 1 mM spermidine, 5 % (w/v) PEG-8000, 25 - 35 mM $MgCl_2$ (optimized for each template), 200 nM annealed template (primer and bottom strand), 4 mM each NTP (Pharmacia), 0.1 mg/ml T7 polymerase. The reaction mixture was incubated at 37 °C for at least 8 h or overnight. The reaction was stopped by adding the same concentration of EDTA, pH 8.0 as was Mg^{2+} in the reaction. RNA was precipitated with 1/10 volume 3 M sodium acetate, pH 5.5 and 3 volumes ethanol (200 proof) at -20 °C for at least 8 h or overnight. Precipitate was pelleted by centrifugation and supernatant discarded. Pellet was dried *in vacuo*, resuspended in ddH_2O and desalted by dialysis.

2-aminopurine 2'-O-methyl riboside containing RNA oligonucleotides (R1inv-9ap, R2inv-8ap, R2inv-3ap, DIS24GA-12ap, DIS24GA-4ap, DIS24GA(A9C)-12ap, DIS24GA(A9C)-4ap, DIS24GA(G10C)-12ap, DIS24GA(G10C)-4ap) and unlabeled DIS junction mutants were synthesized on an Applied Biosystems 390 synthesizer (Perkin-Elmer, Forest City, CA) using standard phosphoramidite chemistry.[294, 295] Nucleoside phosphoramidites and CPG columns were purchased from Glen Research (Sterling, VA). Post-synthesis base deprotection of the RNA oligonucleotides was carried out for 3 hours at 55 °C using a 3:1 mixture (v/v) of ammonia:methanol. The RNA oligonucleotides were then dried under

nitrogen, resuspended in 1 M solution TBAF in THF and stirred for 24 hours at room temperature for desilylation. Then, THF was evaporated under nitrogen, and the remaining solution desalted by dialysis.

All RNA oligonucleotides were purified using preparative-scale denaturing PAGE and recovered by electrophoretic elution using an electrophoresis chamber from Schleicher and Schuell. Eluted RNA was lyophilized to dryness, resuspended in 200 µl DEPC treated ddH_2O and desalted and exchanged into standard buffer (1 mM cacodylate [pH=6.5], 25 mM NaCl) by dialysis using a microdialysis system (Pierce Instruments, Rockford, IL). RNA concentrations were determined by measuring the absorption at 260 nm using extinction coefficients calculated by the biopolymer calculator of the Schepartz Laboratory at Yale University (URL: http://paris.chem.yale.edu/extinct.html).

9.5.2 DNA Synthesis and Purification

Unlabeled and 2-AP containing DNA oligonucleotides were synthesized on an Applied Biosystems Expedite 8909 synthesizer using standard solid phase protocols and deprotecting the 5'-OH. Phosphoramidites and CPG columns (1 µmol, 500 or 1000 Å) were purchased from ABI or Glen Research, synthesizer chemicals and reagents from ABI. CPG beads were transfered to eppendorff caps, and oligonucleotides were deprotected and cleaved off the CPG by treatment with 700 µl 25 % NH_3 at 60 °C for 10 h. DNA was dried, resuspended in 300 µl ddH_2O and purified by RP-HPLC using a gradient of 0-15 % acetonitrile over 45 min. Eluted DNA was lyophilized to dryness and resuspended in 100 µl ddH_2O.

Concentration of oligodeoxynucleotides was determined by measuring their absorption at 260 nm for unlabeled oligonucleotides, **A1** and **A2** and at 305 nm for 2-AP containing dinucleotides using extinction coefficients as follows:

A1: $\varepsilon_{260} = 119.86\ mM^{-1}cm^{-1}$

A2: $\varepsilon_{260} = 119.86\ mM^{-1}cm^{-1}$

C1: $\varepsilon_{260} = 185.2\ mM^{-1}cm^{-1}$

C2: $\varepsilon_{260} = 182.5\ mM^{-1}cm^{-1}$

C3: $\varepsilon_{260} = 190.4\ mM^{-1}cm^{-1}$

C4: $\varepsilon_{260} = 193.8\ mM^{-1}cm^{-1}$

C5: $\varepsilon_{260} = 193.8\ mM^{-1}cm^{-1}$

C6: $\varepsilon_{260} = 197.1\ mM^{-1}cm^{-1}$

dinucleotides ApX (with X = A, T, C, G, or I): ε_{305} = 7.2 $mM^{-1}cm^{-1}$[45]. Extinction coefficients for **A1**, **A2**, and **C1** through **C6** were calculated using pairwise extinction coefficients as described in *Puglisi and Tinoco*.[296]

9.5.3 5-(1-pyrenylethynyl)-2'-deoxyuridine Containing DNA: Synthesis and Purification

DNA oligonucleotides containing 5-(1-pyrenylethynyl)-2'-deoxyuridine (Py-≡-dU) were synthesized analogous to the protocol of *Khan and Grinstaff*,[285] where the ethynylpyrene moiety is attached off the synthesizer to a 2'-deoxy-5-iodouridine (5-I-dU), incorporated into a chemically synthesized DNA oligonucleotide, by a Pd(0) Sonogashira cross-coupling reaction.

All solid-phase syntheses were performed on a commercial ABI Expedite 8909 synthesizer using standard automated DNA synthesis protocols (1 µmol). Phosphoramidites and CPGs were purchased from Glen Research, all other synthesizer chemicals from ABI. In detail, solid-phase synthesis was performed in such a manner that the sequence was stopped after the incorporation of 5'-DMT-3'-cyanoethyl-N,N'-diisopropyl phosphoramidite-2'-deoxy-5-iodouridine (5-I-dU), without deprotecting the 5'-hydroxyl or cleaving the oligonucleotide from the resin. The column was subsequently removed from the synthesizer and dried *in vacuo*. Then the column was attached to a syringe and the reaction solution consisting of 60 µmol ethynylpyrene, 30 µmol $Pd(Ph_3P)_4$ and 30 µmol CuI in 0.5 ml dry DMF:TEA (3.5:1.5) was injected into the column and into another syringe, attached to the other end of the column. The reaction solution was moved back and forth between the two syringes through the column several times to ensure even distribution of reaction solution. After a coupling time of three hours at R. T., the reaction solution was discarded, the column washed with 10 ml DMF:TEA (9:1) and 40 ml dry acetonitrile, dried *in vacuo*, and reinstalled on the synthesizer. Solid-phase synthesis was resumed, and additional DNA bases were added. Deprotection, cleavage from resin and purification by HPLC was performed as described above, but the gradient for HPLC purification was run from 0-30 % acetonitrile in 45 min.

Concentrations of oligodeoxynucleotides containing Py-≡-dU were determined by measuring their absorption at 260 nm using the following extinction coefficients:

P1: ε_{260} = 219.3 $mM^{-1}cm^{-1}$

P2: ε_{260} = 212.6 $mM^{-1}cm^{-1}$

P3: ε_{260} = 204.7 $mM^{-1}cm^{-1}$

P4: ε_{260} = 206.0 $mM^{-1}cm^{-1}$

P5: ε_{260} = 206.0 $mM^{-1}cm^{-1}$

P6: ε_{260} = 207.4 $mM^{-1}cm^{-1}$

Extinction coefficients were determined by measuring absorption of **P1** through **P6** at 260 nm and 392 nm in DMSO to interrupt base stacking[286] and therefore allow estimation of the extinction coefficient of Py-≡-dU at 260 nm, which was calculated according to the following equation:[287]

$$\varepsilon_{260}(\text{Py-≡-dU}) = \varepsilon_{392}(\text{Py-≡-dU}) * A_{260}(P_n) / A_{392}(P_n) - \varepsilon_{260}(DNA_n) \quad (9.1)$$

where ε_{260}(Py-≡-dU) is the extinction coefficient of Py-≡-dU at 260 nm, ε_{392}(Py-≡-dU) is the extinction coefficient of Py-≡-dU at 392 nm, $A_{260}(P_n)$ is the absorbance at 260 nm of a pyrenylethynyl-modified DNA strand P_n (n = 1 - 6), A_{392} (P_n) is the absorbance at 392 nm of the same pyrenylethynyl-modified DNA strand P_n (n = 1 - 6), and $\varepsilon_{260}(DNA_n)$ is the extinction coefficient of the unmodified DNA_n. With an ε_{392}(Py-≡-dU) = 42 $mM^{-1}cm^{-1}$[284] the resulting ε_{260}(Py-≡-dU) was calculated to be 40 $mM^{-1}cm^{-1}$, which could then be used to calculate the $\varepsilon_{260}(P_n)$.

Masses of DNA strands P1 to P6 were determined by MALDI-TOF mass spectroscopy to confirm correct sequence and incorporation of Py-≡-dU. Results are shown in Table 9-1.

Table 9-1. Calculated and experimentally determined masses of pyrenyethynyl-modified DNA strands **P1** to **P6**.

DNA strand	calculated mass	measured mass
P1	6022	6025
P2	6054	6054
P3	5974	5976
P4	5989	5989
P5	5989	5989
P6	6004	6004

9.6 Fluorescence Experiments

9.6.1 Fluorescence Experiments on RNA

- *ColE1* samples R1inv and R2inv

Steady State Fluorescence Measurements of RNA Loop-Loop Complex Formation and Rom Binding. The fluorescence of RNA oligonucleotide samples selectively labeled with 2-aminopurine was measured at 25 °C on a SPEX Fluoromax-2 spectrofluorometer (Instruments SA, Edison, NJ) using a 0.3 cm square cuvette in 150 µl of standard buffer solution (25 mM NaCl and 1 mM cacodylate [pH 6.5]) with 5 mM $MgCl_2$ added. Emission spectra were recorded over the wavelength range of 330 to 450 nm with an excitation wavelength of 310 nm. The spectral band pass was 5 nm for spectra collected at 100 nM RNA concentrations and 7 nm for spectra collected at 25 nM RNA concentration.

The equilibrium dissociation constant for RNA loop-loop kissing formation was determined by following the decrease in fluorescence (F) at 371 nm as a fixed concentration (25 or 100 nM) of the fluorescent RNA hairpin was titrated with increasing amounts of its unlabeled complement. Approximately 10 points were recorded for every titration experiment in a range from zero to twice the starting concentration of the labeled hairpin. The RNA-RNA binding in each case was fitted using a single site equilibrium binding equation:

$$F = -\{\{F_0 - F_f\}/2 * [R - ap]_{tot}\}\{b - \sqrt{b^2 - (4[R]_{tot}[R - ap]_{tot})}\} + F_0 \qquad (9.2)$$

$$b = K_d + [R]_{tot} + [R\text{-}ap]_{tot}$$

where F_o and F_f are the initial and final fluorescence intensities, respectively, $[R\text{-}ap]_{tot}$ is the total concentration of the 2-AP labeled RNA hairpin, and $[R]_{tot}$ is the total concentration of the unlabeled complementary RNA hairpin.

To determine apparent binding constants for divalent metal ions binding to the RNA inverted loop-loop complex the decrease in fluorescence at 371 nm was monitored as a fixed concentration of R1inv-9ap and R2inv, mixed in 1:1 stoichiometry in standard buffer, was titrated with increasing amounts of the divalent metal ion. Metal binding, which induces RNA complex formation, was monitored indirectly by measuring 2-AP quenching associated with RNA loop-loop complex formation and fit using equation 9.3, which describes a single class of metal binding site(s).

$$F = -\{\{F_0 - F_f\}/2 * [R1inv - 9ap]_{tot}\}\{b - \sqrt{b^2 - (4[M^{2+}]_{tot}[R1inv - 9ap]_{tot})}\} + F_0 \quad (9.3)$$

$$b = K_{app} + [M^{2+}]_{tot} + [R1inv\text{-}9ap]_{tot}$$

where F_o and F_f are the initial and final fluorescence intensities, respectively, $[R1inv\text{-}9ap]_{tot}$ is the total R1inv-9ap concentration, which represents the total RNA complex concentration, and $[M^{2+}]_{tot}$ is the total concentration of divalent metal ion.

The dissociation of the loop-loop complex was measured at 25 and 35 °C by following the increase in 2-AP fluorescence of either R2inv-8ap • R1inv or R1inv-9ap • R2inv as the RNA complex dissociates. The reaction was carried out in standard buffer solution with 5 mM $MgCl_2$ and made irreversible by trapping either the free R1inv or R2inv, respectively, with a 20-fold excess of unlabeled complementary RNA hairpin added manually, thereby preventing rebinding of the dissociated hairpin to the 2-AP labeled complement. The time course was fitted using first order rate, $F_t = F_1[1\text{-}\exp(-k_1 t)] + C$, where k_1 is the observed off-rate for the complex.

The equilibrium dissociation constant K_D for Rom binding to the R1inv•R2inv loop-loop complex was determined by following the decrease in fluorescence at 371 nm as a fixed concentration of R1inv-9ap and R2inv, mixed in 1:1 stoichiometry in standard buffer containing 30 mM $SrCl_2$, was titrated with Rom. At this concentration of $SrCl_2$, 100 % RNA loop-loop complex was observed so that the binding data could be fitted using a single-site binding mode for Rom according to equation 9.4:

$$F = -\{\{F_0 - F_f\}/2 * [R2 \bullet R1\text{-}9ap]_{tot}\}\{b - \sqrt{b^2 - (4[Rom]_{tot}[R2 \bullet R1\text{-}9ap]_{tot})}\} + F_0 \quad (9.4)$$

$$b = K_d + [Rom]_{tot} + [R2 \bullet R1\text{-}9ap]_{tot}$$

where F_o and F_f are the initial and final fluorescence intensities, respectively, $[R2 \bullet R1\text{-}9ap]_{tot}$ is the total R2inv • R1inv-9ap concentration, and $[Rom]_{tot}$ is the total concentration of Rom protein.

Rom contains no tryptophan residues, therefore no correction had to be applied to remove a fluorescence contribution from the protein.

All emission spectra were corrected for Raman signals from buffer blanks.

Stopped-flow Measurement of Binding Kinetics. To determine the association rates of RNA loop-loop complex formation, stopped-flow fluorescence experiments were performed at 25 °C in standard buffer solution with 5 mM $MgCl_2$ using a Stopped-Flow device from Applied Photophysics (Surray, UK) in the two-syringe mode (dead time = 1.1 ms). In these experiments, the 2-AP containing RNA was excited at 310 nm, and the fluorescence was monitored using a 335 nm cut-off filter.

The kinetics of RNA complex formation was followed using pseudo-first order conditions, where the unlabeled hairpin was present at concentrations 20-fold greater than the labeled one. The time course of the decrease in 2-AP fluorescence (F_t) as a result of loop-loop complex formation showed two kinetic phases which suggests a two-step binding mechanism, and was fit to the double exponential expression, $F_t = F_1 \exp -k_1 t + F_2 \exp -k_2 t + C$ where F_1, F_2 and k_1, k_2 are the amplitudes and rate constants for the first and second kinetic phases, respectively, and C is a constant offset.

In experiments using R1inv-9ap as the labeled hairpin and R2inv in concentrations ranging from 5- to 25-fold R1inv-9ap concentration, one kinetic phase is found to be linearly dependent on complementary unlabeled RNA hairpin concentration, while a second phase follows approximately a hyperbolic dependence on unlabeled RNA hairpin concentration.

The concentration dependence of the observed rates of binding was fit using the simple two-step binding mechanism of equation 9.5:

$$\text{R1inv} + \text{R2inv} \underset{k_{-1}}{\overset{k_1}{\rightleftharpoons}} \text{R1inv•R2inv} \underset{k_{-2}}{\overset{k_2}{\rightleftharpoons}} \text{R1inv•R2inv*} \qquad (9.5)$$

The concentration dependent rates of the reaction, showing linear and hyperbolic dependent curves, were fitted using the program *KaleidaGraph* (Synergy Software). The linearly dependent rate was fit to the equation $k_{obs} = k_1[\text{R2inv}] + (k_{-1} + k_2 + k_{-2})$, with the slope defining the second order rate constant and the intercept giving an estimate of the overall dissociation rates, $k_{-1} + k_2 + k_{-2}$. The maximal rate ($k_{max} = k_2 + k_{-2}$) was estimated from the maximum of the hyperbolic dependent rate. Since ($k_{-1} + k_{-2}$) << k_2, k_2 was estimated by assuming k_{-1} and k_{-2} were equal to zero in these equations. Due to the extremely slow rates (estimated to be less than 10^{-2} s^{-1}), k_{-1} and k_{-2} could not be determined explicitly from fitting the curves. However, using the measured k_{off}, the product $k_{-2}k_{-1}$ could be determined from the

simplified equation $(k_{-2}k_{-1})/k_2$ and the equilibrium constant K_D^{calc} was calculated using k_2, k_1 and $k_{-2}k_{-1}$.

- HIV-1 DIS samples

Steady State Fluorescence Measurements of DIS Kissing Dimer Formation and Binding by NCp7. The fluorescence emission spectra of RNA oligonucleotide samples (100 nM) selectively labeled with 2-AP were measured at 25 °C on a SPEX Fluoromax-2 spectrofluorometer (Instruments SA, Edison, NJ) using a 0.3 cm square cuvette in 150 µl of standard buffer solution with 5 mM $MgCl_2$. Emission spectra were recorded over the wavelength range of 330 to 450 nm with an excitation wavelength of 310 nm and a spectral band pass of 5 nm.

The equilibrium binding constant (K_D) for DIS loop-loop kissing dimer formation was determined by following the decrease in fluorescence at 371 nm as a fixed concentration of the fluorescent DIS24(GA)-12ap was titrated with increasing amounts of either the DIS24(UC) or DIS23(HxUC) complement. The RNA-RNA binding in each case was fit using the single site equilibrium binding equation.

$$F = -\{\{F_0 - F_f\}/2 * [DIS(GA)]_{tot}\}\{b - \sqrt{b^2 - (4[DIS(UC)]_{tot}[DIS(GA)]_{tot})}\} + F_0 \qquad (9.6)$$

$$b = K_d + [DIS(UC)]_{tot} + [DIS(GA)]_{tot}$$

where F_o and F_f are the initial and final fluorescence intensities, respectively, $[DIS(GA)]_{tot}$ is the total DIS24(GA)-12ap concentration, and $[DIS(UC)]_{tot}$ is the total concentration of DIS24(UC) or DIS24(HxUC).

The K_Ds of the junction mutant samples (Figure 4-15) were measured and fit accordingly.

The dissociation kinetics of the DIS loop-loop kissing dimer was measured by following the increase in 2-AP fluorescence of DIS24(GA)-12ap as the DIS24(GA)-12ap•DIS23(HxUC) complex dissociates. The reaction was carried out at 35 °C using a DIS kissing dimer concentration of 100 nM, in standard buffer solution with 5 mM $MgCl_2$ and made irreversible by trapping the free DIS23(HxUC) with a 20-fold excess of unlabeled DIS24(GA) stem-loop added manually. For dissociation experiments carried out in the presence of NCp7, the DIS24(GA)-12ap•DIS23(HxUC) kissing dimer was preincubated with 500 nM protein. The time course of the dissociation of the DIS kissing dimer was fit using first order rate, $F_t = F_1[1\text{-}\exp(-k_1 t)] + C$, where F_1 and k_1 is the observed amplitude and off-rate, respectively, for the complex, and C is a constant offset.

The kinetics of RNA-RNA association was followed at 25 °C in standard buffer solution with 5 mM $MgCl_2$ using pseudo-first order conditions, where DIS23(HxUC) was present at concentrations of 20-fold greater than the DIS24(GA)-12ap. A DIS24(GA)-12ap concentration of 100 nM was used. For association experiments carried out in the presence of NCp7, the DIS23(HxUC) was preincubated with 500 nM protein and the two macromolecules were mixed simultaneously with DIS24(GA)-12ap. The time course of the decrease in 2-AP fluorescence (F_t) as a result of loop-loop complex formation was fit using an exponential expression, $F_t = F_1 \exp(-k_1 t) + C$ where F_1 and k_1 are the amplitude and apparent on-rate, respectively, for the complex and C is a constant offset.

To determine apparent binding constants for several mono- and divalent metal ions binding to the RNA inverted loop-loop complex the decrease in fluorescence at 371 nm was monitored as a fixed concentration of DIS24GA-12ap and DIS23HxUC, mixed in 1:1 stoichiometry in standard buffer, was titrated with increasing amounts of the mono- or divalent metal ions. Metal binding, which induces RNA complex formation, was monitored indirectly by measuring 2-AP quenching associated with RNA loop-loop complex formation and fit using equation 9.7, which describes a single class of metal binding site(s).

$$F = -\{\{F_0 - F_f\}/2 * [\text{DISGA-12ap}]_{tot}\}\{b - \sqrt{b^2 - (4[Me]_{tot}[\text{DIS24-12ap}]_{tot})}\} + F_0 \qquad (9.7)$$

$$b = K_{app} + [Me]_{tot} + [\text{DIS24-12ap}]_{tot}$$

where F_o and F_f are the initial and final fluorescence intensities, respectively, $[\text{DIS24-12ap}]_{tot}$ is the total DIS24GA-12ap concentration, which represents the total RNA complex concentration, and $[Me]_{tot}$ is the total concentration of mono- or divalent metal ion.

Binding of NCp7 to the DIS kissing dimer was followed by monitoring the quenching of tryptophan (Trp) fluorescence emission as a fixed concentration (250 or 500 nM) of NCp7 was titrated with increasing amounts of DIS kissing dimers, preformed in standard buffer with 5 mM $MgCl_2$. Trp fluorescence was measured at 25 °C on the SPEX Fluromax-2 using a 0.3 cm square cuvette in 150 µl standard buffer with 5 mM $MgCl_2$ and 0.4 % (w/v) freshly prepared PEG-20,000 added. Emission spectra were recorded over the wavelength range of 310 to 450 nm with an excitation wavelength of 295 nm and a spectral band pass of 5 nm. NCp7 binding was fit using equation 9.8, assuming two equivalent sites for NCp7 on the DIS kissing dimer as follows:

$$F = -\{\{F_0 - F_f\}/2 * [2 * DIS\,Kiss]_{tot}\}\{b - \sqrt{b^2 - (4[NCp7]_{tot}[2 * DIS\,Kiss]_{tot})}\} + F_0 \quad (9.8)$$

$$b = K_d + [NCp7]_{tot} + [2 * DIS\,Kiss)]_{tot}$$

where F_o and F_f are the initial and final fluorescence intensities, respectively, $[DIS\ Kiss]_{tot}$ is the total DIS(AG)•DIS(UC) complex concentration, and $[NCp7]_{tot}$ is the total concentration of NCp7 protein.

All emission spectra were corrected for Raman signals from buffer blanks.

Kinetic Measurement of NCp7 Catalyzed Structural Isomerization of the DIS dimer. Structural isomerization of DIS dimers was measured at 25 or 35 °C using the SPEX Fluoromax-2 spectrofluorometer by following the decrease in 2-AP fluorescence emission as a 1:1 mixture of DIS24(GA)-4ap and DIS24(UC) in standard buffer or a preformed DIS24(GA)-4ap•DIS24(UC) kissing complex in standard buffer containing 5 mM $MgCl_2$ is converted to the extended duplex by adding different concentrations of NCp7 or other 'conversion agents' like NaCl, denatured NCp7, or Rev peptide. To measure the conversion rates in the presence of short antisense oligodeoxynucleotides, 100 nM DIS24(GA)-4ap were mixed with 1 µM DNA oligo nucleotide in standard buffer with 5 mM $MgCl_2$. After adding a mixture of 100 nM DIS24(UC) and 250 nM NCp7 in standard buffer with 5 mM $MgCl_2$, the decrease in fluorescence was monitored. Conversion of junction mutants was measured by adding 250 nM NCp7 to a preformed kissing complex between a stem-labeled RNA hairpin with either the (A1C) or (G2C) mutation and complemenraty unlabeled hairpins with the corresponding mutations. The time course of the fluorescence decrease (F_t) as a result of extended duplex formation was fit using an exponential expression, $F_t = F_1 \exp(-k_1 t) + C$ where F_1 and k_1 are the amplitude and conversion rate, respectively, for the complex and C is a constant offset.

All emission spectra were corrected for Raman signals from buffer blanks.

Error Analysis. The reported errors are the standard uncertainties of the data from the best-fit theoretical curves. This method assumes that the standard uncertainty of the measurement is approximated by the standard deviation of the points from the fitted curve.[297]

9.6.2 Fluorescence Experiments on DNA

The fluorescence of DNA oligonucleotide samples was measured at 25 °C on a SPEX Fluoromax-3 spectrofluorometer (Instruments SA, Edison, NJ) using a 1 cm path length quartz cuvette in 1 or 2 ml of standard buffer solution (10 mM Na-P_i, pH 7.0) with or without 250 mM NaCl added.

Emission spectra of excimer samples labeled with 2-AP were measured in 1 ml standard buffer at a duplex concentration of 12.5 µM with excitation wavelengths varying from 310 to 350 nm recording emission over wavelength ranges varying from 330 to 600 nm to 360 to 600 nm accordingly. The spectral band pass was 2 nm. Excitation spectra were recorded on the same samples with emission wavelengths varying from 330 to 470 nm and excitation wavelength ranges varying from 250 to 320 nm to 250 to 440 nm, accordingly.

For dinucleotide samples containing 2-AP emission spectra were recorded in 2 ml standard buffer at a DNA concentration of 10 µM over the wavelength range of 330 to 500 nm with an excitation wavelength of 310 or 320 nm with a spectral bandpass of 2 nm. Excitation spectra on the same samples were recorded with an emission wavelength of 370 nm and an excitation wavelength range of 220 to 350 nm.

The fluorescence of single stranded DNA oligonucleotide samples containing Py-≡-dU was measured on the Fluoromax-3 spectrofluorometer in standard buffer using samples with the same optical density of approximately 0.02 at the excitation wavelength 402 nm, recording emission from 420 to 700 nm, and in DMSO using samples with the same optical density of 0.04 at the excitation wavelength of 398 nm, recording emission from 415 to 500 nm. The spectral bandpass in all experiments was 2 nm. Fluorescence of 2.5 µM duplex DNA was measured in 10 mM Na-P_i, pH 7.0 with an excitation wavelength of 378 or 402 nm and an emission wavelength range of 400 to 700 nm or 420 to 700 nm, respectively, with a spectral band pass of 2 nm.

All excitation spectra were corrected for the excitation correction file included in the instrument software to correct for lamp fluctuations.

All emission spectra were corrected for Raman signals of buffer blanks.

10 Literature

[1] E. Ennifar, M. Yusupov, P. Walter, R. Marquet, B. Ehresmann, C. Ehresmann, P. Dumas, *Structure with Folding & Design* **1999**, *7*, 1439.

[2] N. Amann, E. Pandurski, T. Fiebig, H. A. Wagenknecht, *Chemistry-a European Journal* **2002**, *8*, 4877.

[3] J. R. Lakowicz, *Principles of Fluorescence Spectroscopy*, Kluwer Academic/Plenum, New York, **1999**.

[4] A. Sharma, R. G. Shulman, *Introduction to Fluorescence Spectroscopy*, John Wiley and Sons, Inc., New York, NY, **1999**.

[5] G. J. Kavarnos, *Fundamentals of Photoinduced Electron Transfer*, VCH, New York, NY, **1993**.

[6] IUPAC Comission on Photochemistry, *Pure and Applied Chemistry* **1996**, *68*, 2223/2286.

[7] G. G. Stokes, *Philosophical Transactions of the Royal Society of London* **1852**, *142*, 463.

[8] M. Kasha, *Discussions of the Faraday Society* **1950**, *9*, 14.

[9] R. I. Cukier, D. G. Nocera, *Annual Review of Physical Chemistry* **1998**, *49*, 337.

[10] C. Tommos, G. T. Babcock, *Accounts of Chemical Research* **1998**, *31*, 18.

[11] M. Y. Okamura, G. Feher, *Anoxygenic Photosynthetic Bacteria*, Kluver, Dordrecht, **1995**.

[12] S. Ferguson-Miller, G. T. Babcock, *Chemical Reviews* **1996**, *96*, 2889.

[13] V. Y. Shafirovich, S. H. Courtney, N. Q. Ya, N. E. Geacintov, *Journal of the American Chemical Society* **1995**, *117*, 4920.

[14] M. J. Rist, J. P. Marino, *Current Organic Chemistry* **2002**, *6*, 775.

[15] T. Förster, *Ann. Phys. (Leipzig)* **1948**, 55.

[16] L. Stryer, *Annu. Rev. Biochem.* **1978**, *47*, 819.

[17] P. Vigny, *Comptes Rendus Hebdomadaires Des Seances De L Academie Des Sciences Serie D* **1971**, *272*, 3206.

[18] D. Voet, W. B. Gratzer, R. A. Cox, P. Doty, *Biopolymers* **1963**, *1*, 193.

[19] D. N. Nikogosyan, D. Angelov, B. Soep, L. Lindqvist, *Chemical Physics Letters* **1996**, *252*, 322.

[20] T. Haupl, C. Windolph, T. Jochum, O. Brede, R. Hermann, *Chemical Physics Letters* **1997**, *280*, 520.

[21] L. Alaverdian, S. Alaverdian, O. Bilenko, I. Bogdanov, E. Filippova, D. Gavrilov, B. Gorbovitski, M. Gouzman, G. Gudkov, S. Domratchev, O. Kosobokova, N. Lifshitz, S. Luryi, V. Ruskovoloshin, A. Stepoukhovitch, M. Tcherevishnick, G. Tyshko, V. Gorfinkel, *Electrophoresis* **2002**, *23*, 2804.

[22] G. Xue, E. S. Yeung, *Electrophoresis* **2002**, *23*, 1490.

[23] C. Lee, E. Lemyre, P. M. Miron, C. C. Morton, *Current Opinion in Pediatrics* **2001**, *13*, 550.

[24] C. Fauth, M. R. Speicher, *Cytogenetics and Cell Genetics* **2001**, *93*, 1.

[25] R. Amann, B. M. Fuchs, S. Behrens, *Curr. Opin. Biotech.* **2001**, *12*, 231.

[26] J. Pernthaler, F. O. Glockner, W. Schonhuber, R. Amann, *Methods in Microbiology* **2001**, *30*, 207.

[27] E. A. Mothershed, P. K. Cassiday, K. Pierson, L. W. Mayer, T. Popovic, *Journal of Clinical Microbiology* **2002**, *40*, 4713.

[28] N. Li, W. G. Tan, R. Y. Tsang, D. L. J. Tyrrell, N. J. Dovichi, *Analytical and Bioanalytical Chemistry* **2002**, *374*, 269.

[29] A. E. Remmers, R. R. Neubig, *Journal of Biological Chemistry* **1996**, *271*, 4791.

[30] Y. P. Jia, S. S. Patel, *Journal of Biological Chemistry* **1997**, *272*, 30147.

[31] M. R. Otto, L. B. Bloom, M. F. Goodman, J. M. Beechem, *Biochemistry* **1998**, *37*, 10156.

[32] R. P. Bandwar, S. S. Patel, *Journal of Biological Chemistry* **2001**, *276*, 14075.

[33] J. T. Stivers, K. W. Pankiewicz, K. A. Watanabe, *Biochemistry* **1999**, *38*, 952.

[34] B. W. Allan, J. M. Beechem, W. M. Lindstrom, N. O. Reich, *Journal of Biological Chemistry* **1998**, *273*, 2368.

[35] B. W. Allan, N. O. Reich, J. M. Beechem, *Biochemistry* **1999**, *38*, 5308.

[36] J. J. Sullivan, K. P. Bjornson, L. C. Sowers, P. L. deHaseth, *Biochemistry* **1997**, *36*, 8005.

[37] Y. P. Jia, A. Kumar, S. S. Patel, *Journal of Biological Chemistry* **1996**, *271*, 30451.

[38] K. P. Bjornson, K. J. M. Moore, T. M. Lohman, *Biochemistry* **1996**, *35*, 2268.

[39] D. Klostermeier, D. P. Millar, *Methods* **2001**, *23*, 240.

[40] S. R. Kirk, N. W. Luedtke, Y. Tor, *Bioorganic & Medicinal Chemistry* **2001**, *9*, 2295.

[41] F. Walter, A. I. H. Murchie, J. B. Thomson, D. M. J. Lilley, *Biochemistry* **1998**, *37*, 14195.

[42] P. Z. F. Qin, A. M. Pyle, *Biochemistry* **1997**, *36*, 4718.

[43] G. S. Bassi, N. E. Mollegaard, A. I. H. Murchie, D. M. J. Lilley, *Biochemistry* **1999**, *38*, 3345.

[44] D. G. Xu, T. M. Nordlund, *Biophysical Journal* **2000**, *78*, 1042.

[45] M. Kawai, M. J. Lee, K. O. Evans, T. M. Nordlund, *Journal of Fluorescence* **2001**, *11*, 23.

[46] C. Z. Wan, T. Fiebig, O. Schiemann, J. K. Barton, A. H. Zewail, *Proceedings of the National Academy of Sciences of the United States of America* **2000**, *97*, 14052.

[47] T. Fiebig, C. Z. Wan, A. H. Zewail, *Chemphyschem* **2002**, *3*, 781.

[48] M. A. O'Neill, J. K. Barton, *Journal of the American Chemical Society* **2002**, *124*, 13053.

[49] D. C. Ward, E. Reich, L. Stryer, *J. Biol. Chem.* **1969**, *244*, 1228.

[50] J. A. Secrist, e. al., *Biochemistry* **1972**, *11*, 3499.

[51] J. A. Secrist, J. R. Barrio, N. J. Leonard, *Science* **1972**, *175*, 646.

[52] M. E. Hawkins, W. Pfleiderer, F. M. Balis, D. Porter, J. R. Knutson, *Analytical Biochemistry* **1997**, *244*, 86.

[53] M. E. Hawkins, W. Pfleiderer, O. Jungmann, F. M. Balis, *Anal. Biochem.* **2001**, *298*, 231.

[54] M. E. Hawkins, W. Pfleiderer, A. Mazumder, Y. G. Pommier, F. M. Falls, *Nucleic Acids Research* **1995**, *23*, 2872.

[55] R. X. F. Ren, N. C. Chaudhuri, P. L. Paris, S. Rumney, E. T. Kool, *Journal of the American Chemical Society* **1996**, *118*, 7671.

[56] C. Strassler, N. E. Davis, E. T. Kool, *Helv. Chim. Act.* **1999**, *82*, 2160.

[57] F. Godde, J. J. Toulme, S. Moreau, *Biochemistry* **1998**, *37*, 13765.

[58] F. Godde, *Antisense & Nucleic Acid Drug Development* **1998**, *8*, 469.

[59] F. Godde, J. J. Toulme, S. Moreau, *Nucl. Acids Res.* **2000**, *28*, 2977.

[60] L. M. Wilhelmsson, A. Holmen, P. Lincoln, P. E. Nielson, B. Norden, *Journal of the American Chemical Society* **2001**, *123*, 2434.

[61] P. Rao, S. A. Benner, *J. Org. Chem.* **2001**, *66*, 5012.

[62] A. Broo, *Journal of Physical Chemistry A* **1998**, *102*, 526.

[63] D. P. Millar, *Current Opinion in Structural Biology* **1996**, *6*, 322.

[64] L. C. Sowers, G. V. Fazakerley, R. Eritja, B. E. Kaplan, M. F. Goodman, *Proc. Natl. Acad. Sci. USA* **1986**, *83*, 5434.

[65] L. C. Sowers, B. R. Shaw, M. L. Veigl, W. D. Sedwick, *Mutation Research* **1987**, *177*, 201.

[66] L. C. Sowers, Y. Boulard, G. V. Fazakerley, *Biochemistry* **2000**, *39*, 7613.

[67] T. M. Nordlund, M. Kawai, M. J. Lee, K. O. Evans, *Biophys. J.* **2000**, *78*, 1822Pos.

[68] J. M. Jean, K. B. Hall, *Proceedings of the National Academy of Sciences of the United States of America* **2001**, *98*, 37.

[69] E. L. Rachofsky, R. Osman, J. B. A. Ross, *Biochemistry* **2001**, *40*, 946.

[70] E. L. Rachofsky, J. B. A. Ross, M. Krauss, R. Osman, *Journal of Physical Chemistry A* **2001**, *105*, 190.

[71] S. S. Sastry, B. M. Ross, *Biochemistry* **1996**, *35*, 15715.

[72] M. Menger, T. Tuschl, F. Eckstein, D. Porschke, *Biochemistry* **1996**, *35*, 14710.

[73] A. Ujvari, C. T. Martin, *Biochemistry* **1996**, *35*, 14574.

[74] J. T. Stivers, *Nucleic Acids Research* **1998**, *26*, 3837.

[75] M. J. Rist, J. P. Marino, *Nucleic Acids Research* **2001**, *29*, 2401.

[76] K. A. Lacourciere, J. T. Stivers, J. P. Marino, *Biochemistry* **2000**, *39*, 5630.

[77] J. M. Beechem, M. R. Otto, L. B. Bloom, R. Eritja, L. J. Reha-Krantz, M. F. Goodman, *Biochemistry* **1998**, *37*, 10144.

[78] Y. V. R. Reddy, D. N. Rao, *Journal of Molecular Biology* **2000**, *298*, 597.

[79] B. Mennucci, A. Toniolo, J. Tomasi, *Journal of Physical Chemistry A* **2001**, *105*, 4749.

[80] J. M. Jean, K. B. Hall, *Journal of Physical Chemistry A* **2000**, *104*, 1930.

[81] A. Holmen, B. Norden, B. Albinsson, *Journal of the American Chemical Society* **1997**, *119*, 3114.

[82] A. Holmen, A. Broo, B. Albinsson, B. Norden, *Journal of the American Chemical Society* **1997**, *119*, 12240.

[83] A. D. Malakhov, E. V. Malakhova, S. V. Kuznitsova, I. V. Grechishnikova, I. A. Prokhorenko, M. V. Skorobogatyi, V. A. Korshun, Y. A. Berlin, *Bioorganicheskaya Khimiya* **2000**, *26*, 39.

[84] A. Demesmaeker, R. Haner, P. Martin, H. E. Moser, *Accounts of Chemical Research* **1995**, *28*, 366.

[85] S. M. Freier, K. H. Altmann, *Nucleic Acids Research* **1997**, *25*, 4429.

[86] D. P. Weicherding, Dissertation thesis, (München), **2000**.

[87] H. M. Weintraub, *Scientific American* **1990**, *262*, 40.

[88] P. J. Green, O. Pines, M. Inouye, *Annual Review of Biochemistry* **1986**, *55*, 569.

[89] K. Nordstrom, S. Molin, J. Light, *Plasmid* **1984**, *12*, 71.

[90] K. Nordstrom, E. G. H. Wagner, *Trends in Biochemical Sciences* **1994**, *19*, 294.

[91] C. Hélène, J. J. Toulme, *Oligodeoxynucleotides: Antisense Inhibitors of Gene Expression*, McMillan Press, London, **1989**.

[92] P. O'neill, E. M. Fielden, *Advances in Radiation Biology, Vol 17* **1993**, *17*, 53.

[93] D. Wang, D. A. Kreutzer, J. M. Essigmann, *Mutation Research-Fundamental and Molecular Mechanisms of Mutagenesis* **1998**, *400*, 99.

[94] J. H. J. Hoeijmakers, *Nature* **2001**, *411*, 366.

[95] M. W. Grinstaff, *Angewandte Chemie-International Edition* **1999**, *38*, 3629.

[96] M. Gueron, R. G. Shulman, J. Eisinger, *Proceedings of the National Academy of Sciences of the United States of America* **1966**, *56*, 814.

[97] J. Eisinger, M. Gueron, R. G. Shulman, T. Yamane, *Proceedings of the National Academy of Sciences of the United States of America* **1966**, *55*, 1015.

[98] T. M. Garestie, C. Helene, Michelso.Am, *Biochimica Et Biophysica Acta* **1969**, *182*, 342.

[99] J. P. Morgan, M. Daniels, *Photochemistry and Photobiology* **1980**, *31*, 207.

[100] S. Georghiou, S. Zhu, R. Weidner, C. R. Huang, G. Ge, *Journal of Biomolecular Structure & Dynamics* **1990**, *8*, 657.

[101] S. Georghiou, S. M. Kubala, C. C. Large, *Photochemistry and Photobiology* **1998**, *67*, 526.

[102] P. T. Henderson, E. Boone, G. B. Schuster, *Helvetica Chimica Acta* **2002**, *85*, 135.

[103] B. Bouvier, T. Gustavsson, D. Markovitsi, P. Millie, *Chemical Physics* **2002**, *275*, 75.

[104] J. M. L. Pecourt, J. Peon, B. Kohler, *Journal of the American Chemical Society* **2001**, *123*, 5166.

[105] J. M. Pecourt, B. Kohler, *Abstracts of Papers of the American Chemical Society* **2000**, *220*, 148.

[106] J. M. L. Pecourt, J. Peon, B. Kohler, *Journal of the American Chemical Society* **2000**, *122*, 9348.

[107] A. Reuther, H. Iglev, R. Laenen, A. Laubereau, *Chemical Physics Letters* **2000**, *325*, 360.

[108] J. D. Watson, F. H. C. Crick, *Nature* **1953**, *171*, 737.

[109] D. D. Eley, D. I. Spivey, *Transactions of the Faraday Society* **1962**, *58*, 411.

[110] Y. A. Berlin, A. L. Burin, M. A. Ratner, *Superlattices and Microstructures* **2000**, *28*, 241.

[111] S. Priyadarshy, S. M. Risser, D. N. Beratan, *Journal of Physical Chemistry* **1996**, *100*, 17678.

[112] B. Armitage, *Chemical Reviews* **1998**, *98*, 1171.

[113] S. O. Kelley, J. K. Barton, *Metal Ions in Biological Systems, Vol 36* **1999**, *36*, 211.

[114] C. J. Burrows, J. G. Muller, *Chemical Reviews* **1998**, *98*, 1109.

[115] E. M. Boon, J. E. Salas, J. K. Barton, *Nature Biotechnology* **2002**, *20*, 282.

[116] G. Hartwich, D. J. Caruana, T. de Lumley-Woodyear, Y. B. Wu, C. N. Campbell, A. Heller, *Journal of the American Chemical Society* **1999**, *121*, 10803.

[117] N. M. Jackson, M. G. Hill, *Current Opinion in Chemical Biology* **2001**, *5*, 209.

[118] A. R. Pike, L. H. Lie, R. A. Eagling, L. C. Ryder, S. N. Patole, B. A. Connolly, B. R. Horrocks, A. Houlton, *Angewandte Chemie-International Edition* **2002**, *41*, 615.

[119] F. Patolsky, Y. Weizmann, I. Willner, *Journal of the American Chemical Society* **2002**, *124*, 770.

[120] C. D. Mao, W. Q. Sun, Z. Y. Shen, N. C. Seeman, *Nature* **1999**, *397*, 144.

[121] H. W. Fink, C. Schonenberger, *Nature* **1999**, *398*, 407.

[122] C. M. Niemeyer, *Angewandte Chemie-International Edition* **2001**, *40*, 4128.

[123] D. Porath, A. Bezryadin, S. de Vries, C. Dekker, *Nature* **2000**, *403*, 635.

[124] M. Ratner, *Nature* **1999**, *397*, 480.

[125] E. K. Wilson, *Chemical & Engineering News* **1998**, *76*, 51.

[126] R. E. Holmlin, P. J. Dandliker, J. K. Barton, *Angewandte Chemie-International Edition* **1997**, *36*, 2715.

[127] D. B. Hall, S. O. Kelley, J. K. Barton, *Biochemistry* **1998**, *37*, 15933.

[128] R. A. Marcus, N. Sutin, *Biochimica Et Biophysica Acta* **1985**, *811*, 265.

[129] B. Paulson, K. Pramod, P. Eaton, G. Closs, J. R. Miller, *Journal of Physical Chemistry* **1993**, *97*, 13042.

[130] M. R. Wasielewski, *Chemical Reviews* **1992**, *92*, 435.

[131] J. R. Winkler, H. B. Gray, *Chemical Reviews* **1992**, *92*, 369.

[132] M. E. Nunez, J. K. Barton, *Current Opinion in Chemical Biology* **2000**, *4*, 199.

[133] S. Steenken, S. V. Jovanovic, *Journal of the American Chemical Society* **1997**, *119*, 617.

[134] C. A. M. Seidel, A. Schulz, M. H. M. Sauer, *Journal of Physical Chemistry* **1996**, *100*, 5541.

[135] M. Bixon, B. Giese, S. Wessely, T. Langenbacher, M. E. Michel-Beyerle, J. Jortner, *Proceedings of the National Academy of Sciences of the United States of America* **1999**, *96*, 11713.

[136] F. D. Lewis, X. Y. Liu, J. Q. Liu, S. E. Miller, R. T. Hayes, M. R. Wasielewski, *Nature* **2000**, *406*, 51.

[137] S. Steenken, *Chemical Reviews* **1989**, *89*, 503.

[138] H. A. Wagenknecht, *Chemie in Unserer Zeit* **2002**, *36*, 318.

[139] P. Fromherz, B. Rieger, *Journal of the American Chemical Society* **1986**, *108*, 5361.

[140] A. M. Brun, A. Harriman, *Journal of the American Chemical Society* **1992**, *114*, 3656.

[141] C. J. Murphy, M. R. Arkin, Y. Jenkins, N. D. Ghatlia, S. H. Bossmann, N. J. Turro, J. K. Barton, *Science* **1993**, *262*, 1025.

[142] T. J. Meade, J. F. Kayyem, *Angewandte Chemie-International Edition in English* **1995**, *34*, 352.

[143] F. D. Lewis, T. F. Wu, Y. F. Zhang, R. L. Letsinger, S. R. Greenfield, M. R. Wasielewski, *Science* **1997**, *277*, 673.

[144] S. O. Kelley, R. E. Holmlin, E. D. A. Stemp, J. K. Barton, *Journal of the American Chemical Society* **1997**, *119*, 9861.

[145] K. Fukui, K. Tanaka, *Angewandte Chemie-International Edition* **1998**, *37*, 158.

[146] C. Z. Wan, T. Fiebig, S. O. Kelley, C. R. Treadway, J. K. Barton, A. H. Zewail, *Proceedings of the National Academy of Sciences of the United States of America* **1999**, *96*, 6014.

[147] F. D. Lewis, Y. F. Zhang, X. Y. Liu, N. Xu, R. L. Letsinger, *Journal of Physical Chemistry B* **1999**, *103*, 2570.

[148] S. O. Kelley, J. K. Barton, *Science* **1999**, *283*, 375.

[149] V. Shafirovich, A. Dourandin, W. D. Huang, N. P. Luneva, N. E. Geacintov, *Physical Chemistry Chemical Physics* **2000**, *2*, 4399.

[150] W. B. Davis, S. Hess, I. Naydenova, R. Haselsberger, A. Ogrodnik, M. D. Newton, M. E. Michel-Beyerle, *Journal of the American Chemical Society* **2002**, *124*, 2422.

[151] M. Pascaly, J. Yoo, J. K. Barton, *Journal of the American Chemical Society* **2002**, *124*, 9083.

[152] B. Giese, J. Amaudrut, A. K. Kohler, M. Spormann, S. Wessely, *Nature* **2001**, *412*, 318.

[153] M. E. Nunez, D. B. Hall, J. K. Barton, *Chemistry & Biology* **1999**, *6*, 85.

[154] M. R. Arkin, E. D. A. Stemp, S. C. Pulver, J. K. Barton, *Chemistry & Biology* **1997**, *4*, 389.

[155] G. B. Schuster, *Accounts of Chemical Research* **2000**, *33*, 253.

[156] H. Ikeda, I. Saito, *Journal of the American Chemical Society* **1999**, *121*, 10836.

[157] B. Giese, *Annual Review of Biochemistry* **2002**, *71*, 51.

[158] R. F. Anderson, G. A. Wright, *Physical Chemistry Chemical Physics* **1999**, *1*, 4827.

[159] A. Messer, K. Carpenter, K. Forzley, J. Buchanan, S. Yang, Y. Razskazovskii, Y. L. Cai, M. D. Sevilla, *Journal of Physical Chemistry B* **2000**, *104*, 1128.

[160] Y. Razskazovskii, S. G. Swarts, J. M. Falcone, C. Taylor, M. D. Sevilla, *Journal of Physical Chemistry B* **1997**, *101*, 1460.

[161] Z. L. Cai, Z. Y. Gu, M. D. Sevilla, *Journal of Physical Chemistry B* **2000**, *104*, 10406.

[162] Z. L. Cai, M. D. Sevilla, *Journal of Physical Chemistry B* **2000**, *104*, 6942.

[163] Z. L. Cai, X. F. Li, M. D. Sevilla, *Journal of Physical Chemistry B* **2002**, *106*, 2755.

[164] X. F. Li, Z. L. Cai, M. D. Sevilla, *Journal of Physical Chemistry B* **2001**, *105*, 10115.

[165] M. G. Debije, M. T. Milano, W. A. Bernhard, *Angewandte Chemie-International Edition* **1999**, *38*, 2752.

[166] S. Steenken, J. P. Telo, H. M. Novais, L. P. Candeias, *Journal of the American Chemical Society* **1992**, *114*, 4701.

[167] A. Schwogler, L. T. Burgdorf, T. Carell, *Angewandte Chemie-International Edition* **2000**, *39*, 3918.

[168] C. Behrens, L. T. Burgdorf, A. Schwogler, T. Carell, *Angewandte Chemie-International Edition* **2002**, *41*, 1763.

[169] A. Schwogler, T. Carell, *Organic Letters* **2000**, *2*, 1415.

[170] T. Carell, L. T. Burgdorf, L. M. Kundu, M. Cichon, *Current Opinion in Chemical Biology* **2001**, *5*, 491.

[171] F. D. Lewis, X. Y. Liu, S. E. Miller, R. T. Hayes, M. R. Wasielewski, *Journal of the American Chemical Society* **2002**, *124*, 11280.

[172] N. Amann, H. A. Wagenknecht, *Synlett* **2002**, 687.

[173] T. L. Netzel, M. Zhao, K. Nafisi, J. Headrick, M. S. Sigman, B. E. Eaton, *Journal of the American Chemical Society* **1995**, *117*, 9119.

[174] N. Amann, E. Pandurski, T. Fiebig, H. A. Wagenknecht, *Angewandte Chemie-International Edition* **2002**, *41*, 2978.

[175] M. Raytchev, E. Mayer, N. Amann, H. A. Wagenknecht, T. Fiebig, *Journal of the American Chemical Society* **2003**, *submitted*.

[176] F. D. Lewis, Y. S. Wu, R. T. Hayes, M. R. Wasielewski, *Angewandte Chemie-International Edition* **2002**, *41*, 3485.

[177] E. M. Boon, J. K. Barton, *Current Opinion in Structural Biology* **2002**, *12*, 320.

[178] B. Giese, *Current Opinion in Chemical Biology* **2002**, *6*, 612.

[179] J. Tomizawa, in *Mol.Biology of RNA, New Perspectives* (Ed.: M. D. Inouye, B. S.), Academic Press, New York, **1987**, pp. 249.

[180] Y. Eguchi, T. Itoh, J. Tomizawa, *Annu. Rev. Biochem.* **1991**, *60*, 631.

[181] J. Tomizawa, *Cell* **1984**, *38*, 861.

[182] J. Tomizawa, *Cell* **1985**, *40*, 527.

[183] J. Tomizawa, *Cell* **1986**, *47*, 89.

[184] J. Tomizawa, *J. Mol. Biol.* **1990**, *212*, 683.

[185] Y. Eguchi, J. Tomizawa, *Cell* **1990**, *60*, 199.

[186] J. Tomizawa, *J. Mol. Biol.* **1990**, *212*, 695.

[187] Y. Eguchi, J. Tomizawa, *Journal of Molecular Biology* **1991**, *220*, 831.

[188] R. S. Gregorian, D. M. Crothers, *Journal of Molecular Biology* **1995**, *248*, 968.

[189] G. del Solar, M. Espinosa, *Molecular Microbiology* **2000**, *37*, 492.

[190] J. P. Marino, R. S. Gregorian, G. Csankovszki, D. M. Crothers, *Science* **1995**, *268*, 1448.

[191] A. Lee, D. Crothers, *Structure* **1998**, *6*, 993.

[192] J. F. Milligan, O. C. Uhlenbeck, *Methods in Enzymology* **1989**, *180*, 51.

[193] D. W. Banner, M. Kokkinidis, D. Tsernoglou, *Journal of Molecular Biology* **1987**, *196*, 657.

[194] W. Eberle, W. Klaus, G. Cesareni, C. Sander, P. Rosch, *Biochemistry* **1990**, *29*, 7402.

[195] K. A. Johnson, *The Enzymes, Vol. XX*, Academic Press, Orlando, FL., **1992**.

[196] K.-Y. Chang, I. Tinoco, *J. Mol. Biol.* **1997**, *269*, 52.

[197] J. L. Clever, Wong, M. L., Parslow, T. G., *Journal of Virology* **1996**, *70*, 5902.

[198] J. C. Paillart, E. Westhof, C. Ehresmann, B. Ehresmann, R. Marquet, *Journal of Molecular Biology* **1997**, *270*, 36.

[199] P. F. Predki, L. M. Nayak, M. B. C. Gottlieb, L. Regan, *Cell* **1995**, *80*, 41.

[200] B. Holz, S. Klimasauskas, S. Serva, E. Weinhold, *Nucleic Acids Research* **1998**, *26*, 1076.

[201] M. W. Frey, L. C. Sowers, D. P. Millar, S. J. Benkovic, *Biochemistry* **1995**, *34*, 9185.

[202] L. A. Marquez, L. J. RehaKrantz, *Journal of Biological Chemistry* **1996**, *271*, 28903.

[203] A. M. Parrott, H. Lago, C. J. Adams, A. E. Ashcroft, N. J. Stonehouse, P. G. Stockley, *Nucleic Acids Research* **2000**, *28*, 489.

[204] M. Menger, F. Eckstein, D. Porschke, *Nucleic Acids Research* **2000**, *28*, 4428.

[205] J. A. Levy, A. D. Hoffman, S. M. Kramer, J. A. Landis, J. M. Shimabukuro, *Science* **1984**, *225*, 840.

[206] R. C. Gallo, S. Z. Salahuddin, M. Popovic, G. M. Shearer, M. Kaplan, B. F. Haynes, T. J. Palker, R. Redfield, J. Oleske, B. Safai, G. White, P. Foster, P. D. Markham, *Science* **1984**, *224*, 505.

[207] F. Barresinoussi, J. C. Chermann, F. Rey, M. T. Nugeyre, S. Chamaret, J. Gruest, C. Dauguet, C. Axlerblin, F. Vezinetbrun, C. Rouzioux, W. Rozenbaum, L. Montagnier, *Science* **1983**, *220*, 868.

[208] A. D. Frankel, J. A. T. Young, *Annual Review of Biochemistry* **1998**, *67*, 1.

[209] B. G. Turner, M. F. Summers, *Journal of Molecular Biology* **1999**, *285*, 1.

[210] W. Fu, R. J. Gorelick, A. Rein, *Journal of Virology* **1994**, *68*, 5013.

[211] J. C. Paillart, R. Marquet, E. Skripkin, C. Ehresmann, B. Ehresmann, *Biochimie* **1996**, *78*, 639.

[212] H. J. Kim, K. Lee, J. J. Orear, *Virology* **1994**, *198*, 336.

[213] E. Skripkin, J. C. Paillart, R. Marquet, B. Ehresmann, C. Ehresmann, *Proceedings of the National Academy of Sciences of the United States of America* **1994**, *91*, 4945.

[214] M. Laughrea, L. Jette, *Biochemistry* **1994**, *33*, 13464.

[215] B. Berkhout, J. L. B. vanWamel, *Journal of Virology* **1996**, *70*, 6723.

[216] M. Laughrea, L. Jette, *Biochemistry* **1996**, *35*, 1589.

[217] G. Miele, A. Mouland, G. P. Harrison, E. Cohen, A. M. L. Lever, *Journal of Virology* **1996**, *70*, 944.

[218] J. C. Paillart, E. Skripkin, B. Ehresmann, C. Ehresmann, R. Marquet, *Proceedings of the National Academy of Sciences of the United States of America* **1996**, *93*, 5572.

[219] M. Laughrea, L. Jette, J. Mak, L. Kleiman, C. Liang, M. A. Wainberg, *Journal of Virology* **1997**, *71*, 3397.

[220] M. Laughrea, N. Shen, L. Jette, M. A. Wainberg, *Biochemistry* **1999**, *38*, 226.

[221] J. C. Paillart, L. Berthoux, M. Ottmann, J. L. Darlix, R. Marquet, B. Ehresmann, C. Ehresmann, *Journal of Virology* **1996**, *70*, 8348.

[222] E. Skripkin, J. C. Paillart, R. Marquet, M. Blumenfeld, B. Ehresmann, C. Ehresmann, *Journal of Biological Chemistry* **1996**, *271*, 28812.

[223] F. Jossinet, J. C. Paillart, E. Westhof, T. Hermann, E. Skripkin, J. S. Lodmell, C. Ehresmann, B. Ehresmann, R. Marquet, *Rna-a Publication of the Rna Society* **1999**, *5*, 1222.

[224] J. S. Lodmell, J. C. Paillart, D. Mignot, B. Ehresmann, C. Ehresmann, R. Marquet, *Antisense & Nucleic Acid Drug Development* **1998**, *8*, 517.

[225] J. S. Lodmell, C. Ehresmann, B. Ehresmann, R. Marquet, *Rna-a Publication of the Rna Society* **2000**, *6*, 1267.

[226] J. S. Lodmell, C. Ehresmann, B. Ehresmann, R. Marquet, *Journal of Molecular Biology* **2001**, *311*, 475.

[227] D. Muriaux, H. DeRocquigny, B. P. Roques, J. Paoletti, *Journal of Biological Chemistry* **1996**, *271*, 33686.

[228] Y. X. Feng, T. D. Copeland, L. E. Henderson, R. J. Gorelick, W. J. Bosche, J. G. Levin, A. Rein, *Proceedings of the National Academy of Sciences of the United States of America* **1996**, *93*, 7577.

[229] D. Muriaux, Fossé, P., Paoletti, J., *Biochemistry* **1996**, *35*, 5075.

[230] K. I. Takahashi, S. Baba, P. Chattopadhyay, Y. Koyanagi, N. Yamamoto, H. Takaku, G. Kawai, *Rna-a Publication of the Rna Society* **2000**, *6*, 96.

[231] K. Takahashi, S. Baba, Y. Koyanagi, N. Yamamoto, H. Takaku, G. Kawai, *Journal of Biological Chemistry* **2001**, *276*, 31274.

[232] A. Rein, L. E. Henderson, J. G. Levin, *Trends in Biochemical Sciences* **1998**, *23*, 297.

[233] E. Remy, H. de Rocquigny, P. Petitjean, D. Muriaux, V. Theilleux, J. Paoletti, B. P. Roques, *Journal of Biological Chemistry* **1998**, *273*, 4819.

[234] B. D. Chan, K. Weidemaier, W. T. Yip, P. F. Barbara, K. Musier-Forsyth, *Proceedings of the National Academy of Sciences of the United States of America* **1999**, *96*, 459.

[235] X. G. Li, Y. D. Quan, E. J. Arts, Z. Li, B. D. Preston, H. deRocquigny, B. P. Roques, J. L. Darlix, L. Kleiman, M. A. Parniak, M. A. Wainberg, *Journal of Virology* **1996**, *70*, 4996.

[236] T. Y. Wu, J. H. Guo, J. Bess, L. E. Henderson, J. G. Levin, *Journal of Virology* **1999**, *73*, 4794.

[237] M. C. Williams, R. J. Gorelick, K. Musier-Forsyth, *Proceedings of the National Academy of Sciences of the United States of America* **2002**, *99*, 8614.

[238] J. H. Guo, T. Y. Wu, B. F. Kane, D. G. Johnson, L. E. Henderson, R. J. Gorelick, J. G. Levin, *Journal of Virology* **2002**, *76*, 4370.

[239] J. H. Guo, T. Y. Wu, J. Anderson, B. F. Kane, D. G. Johnson, R. J. Gorelick, L. E. Henderson, J. G. Levin, *Journal of Virology* **2000**, *74*, 8980.

[240] J. H. Guo, L. E. Henderson, J. Bess, B. Kane, J. G. Levin, *Journal of Virology* **1997**, *71*, 5178.

[241] F. Girard, F. Barbault, C. Gouyette, T. Huynh-Dinh, J. Paoletti, G. Lancelot, *Journal of Biomolecular Structure & Dynamics* **1999**, *16*, 1145.

[242] A. Mujeeb, J. L. Clever, T. M. Billeci, T. L. James, T. G. Parslow, *Nature Structural Biology* **1998**, *5*, 432.

[243] A. Mujeeb, T. G. Parslow, A. Zarrinpar, C. Das, T. L. James, *Febs Letters* **1999**, *458*, 387.

[244] E. Ennifar, P. Walter, B. Ehresmann, C. Ehresmann, P. Dumas, *Nature Structural Biology* **2001**, *8*, 1064.

[245] J. L. Clever, M. L. Wong, T. G. Parslow, *Journal of Virology* **1996**, *70*, 5902.

[246] J. C. Paillart, R. Marquet, E. Skripkin, B. Ehresmann, C. Ehresmann, *Journal of Biological Chemistry* **1994**, *269*, 27486.

[247] E. G. H. Wagner, R. W. Simons, *Annu. Rev. Microbiol.* **1994**, *48*, 712.

[248] R. Marquet, F. Baudin, C. Gabus, J. L. Darlix, M. Mougel, C. Ehresmann, B. Ehresmann, *Nucleic Acids Research* **1991**, *19*, 2349.

[249] A. C. Prats, C. Roy, P. Wang, M. Erard, V. Housset, C. Gabus, C. Paoletti, J. L. Darlix, *Journal of Virology* **1990**, *64*, 774.

[250] D. Muriaux, P. Fosse, J. Paoletti, *Biochemistry* **1996**, *35*, 5075.

[251] H. Derocquigny, C. Gabus, A. Vincent, M. C. Fourniezaluski, B. Roques, J. L. Darlix, *Proceedings of the National Academy of Sciences of the United States of America* **1992**, *89*, 6472.

[252] Y. Mély, H. DeRocquigny, N. Morellet, B. P. Roques, D. Gérard, *Biochemistry* **1996**, *35*, 5175.

[253] C. Vuilleumier, E. Bombarda, N. Morellet, D. Gerard, B. P. Roques, Y. Mely, *Biochemistry* **1999**, *38*, 16816.

[254] E. Bombarda, A. Ababou, C. Vuilleumier, D. Gerard, B. P. Roques, E. Piemont, Y. Mely, *Biophysical Journal* **1999**, *76*, 1561.

[255] M. A. Urbaneja, B. P. Kane, D. G. Johnson, R. J. Gorelick, L. E. Henderson, J. R. Casas-Finet, *Journal of Molecular Biology* **1999**, *287*, 59.

[256] R. L. Karpel, L. E. Henderson, S. Oroszlan, *Journal of Biological Chemistry* **1987**, *262*, 4961.

[257] R. N. De Guzman, Z. R. Wu, C. C. Stalling, L. Pappalardo, P. N. Borer, M. F. Summers, *Science* **1998**, *279*, 384.

[258] G. Myers, B. Korber, B. H. Hahn, K.-T. Jeang, J. W. Mellors, F. E. McCutchan, L. E. Henderson, G. N. Pavlakis, in *Human Retroviruses and AIDS*, Los Alamos National Laboratory, Los Alamos, New Mexico, USA, **1995**.

[259] P. B. Hackett, M. W. Dalton, D. P. Johnson, R. B. Petersen, *Nucleic Acids Research* **1991**, *19*, 6929.

[260] R. L. Alford, S. Honda, C. B. Lawrence, J. W. Belmont, *Virology* **1991**, *183*, 611.

[261] V. Theilleux-Delalande, F. Girard, T. Huynh-Dinh, G. Lancelot, J. Paoletti, *European Journal of Biochemistry* **2000**, *267*, 2711.

[262] H. Huthoff, B. Berkhout, *Biochemistry* **2002**, *41*, 10439.

[263] R. Khan, D. P. Giedroc, *Journal of Biological Chemistry* **1992**, *267*, 6689.

[264] F. Dibhajj, R. Khan, D. P. Giedroc, *Protein Science* **1993**, *2*, 231.

[265] J. C. You, C. S. McHenry, *Journal of Biological Chemistry* **1993**, *268*, 16519.

[266] V. Tanchou, C. Gabus, V. Rogemond, J. L. Darlix, *Journal of Molecular Biology* **1995**, *252*, 563.

[267] J. C. You, C. S. McHenry, *Journal of Biological Chemistry* **1994**, *269*, 31491.

[268] R. D. Berkowitz, A. Ohagen, S. Hoglund, S. P. Goff, *Journal of Virology* **1995**, *69*, 6445.

[269] Y. X. Feng, S. Campbell, D. Harvin, B. Ehresmann, C. Ehresmann, A. Rein, *Journal of Virology* **1999**, *73*, 4251.

[270] A. S. Davydov, *Theory of Molecular Excitons*, McGraw-Hill, New York, NY, **1962**.

[271] A. L. Sobolewski, W. Domcke, C. Dedonder-Lardeux, C. Jouvet, *Physical Chemistry Chemical Physics* **2002**, *4*, 1093.

[272] N. J. Kim, G. Jeong, Y. S. Kim, J. Sung, S. K. Kim, Y. D. Park, *Journal of Chemical Physics* **2000**, *113*, 10051.

[273] E. Nir, K. Kleinermanns, L. Grace, M. S. de Vries, *Journal of Physical Chemistry A* **2001**, *105*, 5106.

[274] A. A. Voityuk, K. Siriwong, N. Rosch, *Physical Chemistry Chemical Physics* **2001**, *3*, 5421.

[275] H. Y. Yi-Brunozzi, O. M. Stephens, P. A. Beal, *Journal of Biological Chemistry* **2001**, *276*, 37827.

[276] R. A. Hochstrasser, T. E. Carver, L. C. Sowers, D. P. Millar, *Biochemistry* **1994**, *33*, 11971.

[277] M. A. O'Neill, J. K. Barton, *Proceedings of the National Academy of Sciences of the United States of America* **2002**, *99*.

[278] H. Kang, P. J. Chou, W. C. Johnson, D. Weller, S. B. Huang, J. E. Summerton, *Biopolymers* **1992**, *32*, 1351.

[279] C. R. Cantor, M. M. Warshaw, H. Shapiro, *Biopolymers* **1970**, *9*, 1059.

[280] N. S. Hush, A. S. Cheung, *Chemical Physics Letters* **1975**, *34*, 11.

[281] V. Shafirovich, A. Dourandin, N. P. Luneva, N. E. Geacintov, *Journal of the Chemical Society-Perkin Transactions 2* **2000**, 271.

[282] M. Enescu, L. Lindqvist, *Journal of Physical Chemistry* **1995**, *99*, 8405.

[283] S. D. Wetmore, R. J. Boyd, L. A. Eriksson, *Chemical Physics Letters* **2000**, *322*, 129.

[284] V. A. Korshun, E. V. Manasova, K. V. Balakin, I. A. Prokhorenko, A. G. Buchatskii, Y. A. Berlin, *Bioorganicheskaya Khimiya* **1996**, *22*, 923.

[285] S. I. Khan, M. W. Grinstaff, *Journal of the American Chemical Society* **1999**, *121*, 4704.

[286] P. Koenig, S. A. Reines, C. R. Cantor, *Biopolymers* **1977**, *16*, 2231.

[287] R. Kierzek, Y. Li, D. H. Turner, P. C. Bevilacqua, *Journal of the American Chemical Society* **1993**, *115*, 4985.

[288] K. Nakatani, C. Dohno, I. Saito, *Journal of the American Chemical Society* **2001**, *123*, 9681.

[289] K. Nakatani, C. Dohno, I. Saito, *Journal of the American Chemical Society* **1999**, *121*, 10854.

[290] K. Nakatani, C. Dohno, A. Ogawa, I. Saito, *Chemistry & Biology* **2002**, *9*, 361.

[291] B. M. Lee, R. N. De Guzman, B. G. Turner, N. Tjandra, M. F. Summers, *Journal of Molecular Biology* **1998**, *279*, 633.

[292] F. W. Studier, A. H. Rosenberg, J. J. Dunn, J. W. Dubendorff, *Methods in Enzymology* **1990**, *185*, 60.

[293] J. F. Milligan, D. R. Groebe, G. W. Witherell, O. C. Uhlenbeck, *Nucleic Acids Research* **1987**, *15*, 8783.

[294] S. L. Beaucage, M. H. Caruthers, *Tetrahedron Lett.* **1981**, *22*, 1859.

[295] M. H. Caruthers, A. D. Barone, S. L. Beaucage, D. R. Dodds, E. F. Fisher, L. J. McBride, M. Matteucci, Z. Stabinsky, J. Y. Tang, *Methods in Enzymology* **1987**, *154*, 287.

[296] J. D. Puglisi, I. Tinoco, *Methods in Enzymology* **1989**, *180*, 304.

[297] B. P. Flannery, S. A. Teukolsky, V. W. T., *Numerical Recipes in Fortran*, 2nd ed., Cambridge University Press, Cambridge, **1992**.